Saurashtra University

Re – Accredited Grade 'B' by NAAC
(CGPA 2.93)

Parekh, Bharatkumar B., 2005, *"Growth and Characterization of some Bio-material Crystals",* thesis PhD, Saurashtra University

http://etheses.saurashtrauniversity.edu/id/861

GROWTH AND CHARACTERIZATION OF SOME BIO-MATERIAL CRYSTALS

THESIS SUBMITTED TO THE

SAURASHTRA UNIVERSITY

RAJKOT

FOR THE DEGREE OF

Doctor of Philosophy

IN

PHYSICS

BY

PAREKH BHARATKUMAR B.
M.Sc.

GUIDE
DR. MIHIR J. JOSHI
M.Sc., Ph.D.

DEPARTMENT OF PHYSICS

SAURASHTRA UNIVERSITY

RAJKOT-360 005.

INDIA

DECEMBER 2005

Statements Under O.Ph.D.7 of Saurashtra University

The contents of this thesis is my own work carried out under the supervision of *Dr. M. J. Joshi* and leads to some contributions in Physics supported by necessary references.

(Bharat B. Parekh)

This is to certify that the present work submitted for Ph. D. Degree of the Saurashtra University, Rajkot, by *Shri Bharat kumar Balkrishna Parekh* has been the result of about three years of work under my supervision and is a valuable contribution in the field of "Solid State Physics and Materials Science".

(Dr. M. J. Joshi)
Department of Physics
Saurashtra University
Rajkot-360 005.
INDIA.

ACKNOWLEDGEMENT

Bharatkumar B. Parekh

Rajkot

29th December, 2005

Abstract

The recent advances in science and technology have brought a great demand of various crystals with numerous applications. A field of multidisciplinary nature in science and technology has been emerged, known as crystal growth, which deals with the crystal growth methods, crystals characterizations and crystal growth theories. There are different kinds of crystals having various applications grown by different techniques. Broadly speaking, there are three main categories of crystal growth processes. (I) $S \rightarrow S$, process involving solid-solid phase transitions, (II) $L \rightarrow S$, process involving liquid-solid phase transitions, and (III) $V \rightarrow S$, process involving gas-solid phase transitions.

Bio-crystallizations are very important phenomena in which crystal growth of specific bio-material compounds occur in a body of living organisms like, animals and plants. There are many reasons and theories proposed for this. In human body, certain types of bio-crystallizations and bio-mineralizations are considered to be responsible to different ailments, which are arthritis, urinary stones, cholesterol deposition in blood vessels, gall stones, cataract, etc.

Gel growth is the most suitable method for growth as well as for the growth inhibition study of bio-material crystals. Gel growth technique is very simple technique, which requires only some common laboratory glasswares and chemicals and provides comparatively good crystals at ambient temperatures. In the present investigation, hydroxyapatite, monosodium urate monohydrate, calcium pyrophosphate tetrahydrate, calcium hydrogen phosphate dihydrate, and sodium oxalate crystals have been grown using gel growth technique and sodium pyrophosphate and organic crystal of 4-(2-hydroxy-phenylamino)-pent-3-en-2-one, have been grown using the solution growth technique.

The thesis consists of ten chapters as follows.

Chapter I gives a general introduction to the subject and tries to justify the present investigation. This chapter also presents a brief history of bio-crystallization of various substances, which are responsible for various ailments, as well as the etiology and economical aspects of the bio-crystallization. It also covers the aim of the study.

Chapter II gives a brief review on the two prime bio-mineralization and bio-crystallization processes, i.e., arthropathy and urinary stones. The role of different crystals in arthritis, gout and urinary crystals is discussed. This chapter helps to understand the mechanisms of crystal formation in our body and how to tackle this problem.

Chapter III deals with crystal growth techniques employed to grow the crystals of interest. This chapter also gives the general picture of crystal growth methodologies and focuses the attention on the gel and solution growth techniques. The gel growth technique is advantageous to mimic the body tissues and serves as a good *in vitro* model to study the growth of bio-materials crystals. Different types of gels, gel structures, gelling mechanisms and gel properties are explained in brief. Solution growth is also an important technique to grow crystals, which are also dealt with in a brief manner. The advantages and disadvantages of these techniques are explained.

Altogether, in this chapter, modified gel growth technique has been described to grow micro crystals. This technique is useful as a rapid screening test for *in vitro* crystallizations of bio-materials.

Chapter IV chiefly describes different experimental techniques used to characterize the grown crystals. These techniques are powder X-ray diffraction (XRD), Thermo-gravimetry Analysis (TGA), Fourier Transform Infrared Spectroscopy (FT-IR), Dielectric study, Photoconductivity study and powder Kurtz technique for

measurement of efficiency of second harmonic generation of nonlinear optical (NLO) materials. Herbal extracts preparations are also given in this chapter.

Chapter V deals with the growth, characterization and inhibition study of hydroxyapatite (HA) crystals. The crystals of HA were grown by using the single diffusion reaction type gel growth technique in silica gel. The gel was set by adding orthophospheric acid to sodium meta-silicate solution of 1.06 specific gravity in such a manner that 6.0 pH was obtained. After setting the gel, 20ml of 1 M calcium chloride solution was poured on the gel as a supernatant solution. Large numbers of Liesegang rings were observed. These Liesegang rings were made up of HA crystals.

The crystals were characterized by various experimental techniques, viz. powder XRD, FTIR, dielectric studies and particle size measurements. From the powder XRD study it was confirmed that the crystals have monoclinic system with the unit cell parameters as; *a =9.432 , b=18.843 , C =6.923 , á = â =90.010* and *ã = 119.050,* which is only observed at the lower temperature crystal growth of hydorxyapatite crystals. FT-IR spectrum confirms the presence of the O-P-O bending, P-O symmetric and asymmetric stretching, O-H bending and stretching and oxygen-metal bonds. Initially, the dielectric constant decreases rapidly with increasing frequency and then decreases very slowly, indicating higher space charge polarizability of the material in the low frequency region and a relaxation type behaviors.

The inhibitive effect of herbal extracts of *Boswellia Serrata* gum resin*, Tribulus terrestris* fruit*, Rotula aquatica* root*, Boerhaavia diffusa* root, *Commphora wighitii,* and *Aerva Lanata,* has been studied on the growth of HA. This inhibition study was divided into two parts, (1) effect of the herbal extracts on the growth of the

HAP crystals and (2) the effect of the herbal extracts on the already grown HA crystals.

The effects of herbal extracts on the growth of HA crystals were studied by measuring the number of Liesegang rings, their width and spacing between them. From all these parameters the inhibitive nature was decided for different extracts. *Rotula aquatica* and *Aerva Lanata* extracts were found to be quite potent to inhibit the growth of HA crystals. No effect of herbal extracts on the already grown HA crystals have been observed. In this study, both ethanolic and hydro-ethanolic extracts were used. In the case of ethanolic extracts the numbers of rings were less. All ethanolic extracts showed delayed nucleation with comparison to that of the aqueous ones. For hydro-ethanolic extracts, the thick bands were obtained and it was not possible to measure the spacings and other parameters. However, the particle size increased with comparison to previous ethanolic extracts.

To confirm the significance of results, a statistical analysis, i.e., single factor ANOVA was applied, which showed high correlations. To understand the diffusion mechanism in the gel, diffusion coefficients were also calculated using various theories.

Chapter VI covers the growth, characterization and inhibition study of monosodium urate monohydrate (MSUM) crystals. The MSUM crystal growth was carried out using the gel growth technique as well as the wet chemical process. In the wet chemical process the aqueous solution of 0.2 M, NaOH was stirred well and heated up to 70 ^{0}C. After achieving the required temperature, uric acid was added to make its suspension into the NaOH solution. After some times fine particles of MSUM crystals were found at the bottom of the beaker, which were in coagulated form and looked

like amorphous porous material. The powder XRD confirmed that it was a well crystalline material. Probable reaction is as follows.

$$NaOH + C_5H_4N_4O_3 \quad NaHC_5H_2N_4O_3 \cdot H_2O$$

These crystals were characterized by various experimental techniques such as, powder XRD, FTIR, dielectric study and TGA. From the TGA study it confirmed that MSUM crystals were thermally unstable and started losing water of hydration 170 ^{0}C. At 240 ^{0}C, water molecules were completely removed. The crystal was decomposing through two stages. Subsequently, the sample lost nearly 75 to 80 % of original mass and finally it was converted into Na_2O, which remained stable up to the end of the analysis. One water molecule was associated with the compound. Coats and Redfern relation was applied to evaluate the kinetic parameters. The order of reaction and the activation energy was found to be ¼ and 120.324 kJmol^{-1}, respectively. The thermodynamic parameters were also evaluated. The FT-IR spectrum confirms the presents of O-H stretching N-H rocking and stretching, C = C bond, C= O carbonyl group (keton group), and C – N bond. There was no standard crystalline data of MSUM crystals available for the matching with the powder XRD pattern. The dielectric study suggested that higher space charge polarizability in the low frequency region and a relaxation type behavior.

As this crystal is associated with much painful gout, therefore, inhibition studies have been carried out using various herbal extracts, *Boswellia serrata* gum resin, *Aerava lanata*, *Rotula aquatica* root and *Boerhaavia diffusa* root. *R. aquatica* and *A. lanata,* 1% aqueous extract solutions gave significant inhibition of MSUM crystals. Till today there is no remedy to dissolve the MSUM crystal in synovial fluid, which is responsible for gout. This study may help the prevention or cure of gout.

Chapter VII explains the growth and characterization of calcium pyrophosphate crystals (CPP). The CPP crystals were grown by the single diffusion gel growth technique and also by the wet chemical process. Gel solution was prepared from the mixture of sodium meta-silicate solution of 1.05 specific gravity and sodium pyrophosphate dodecahydrate solution. This mixture was acidified with the solution of 2N acetic acid to obtain 4.5 pH. The gel was set within three days. On the set gel, 0.25 M, $Ca(NO_3)_2$ solution was poured. Two days after pouring the solution, some Liesegang rings started to appear. Some small, transparent, round shaped single crystals of CPP were grown within the gel. These crystals were characterized by various experimental techniques, i.e. powder XRD, TGA, FT-IR, and dielectric study. The CPP crystals showed very high thermal stability after losing the associated water molecules at 110 ^{0}C and after dehydration remain stable up to 900 ^{0}C. From the calculation, it was noticed that four water molecules were associated with the crystals. Hence it is calcium pyrophosphate tetrahydrate (CPPT). Coats and Redfern relation was applied to the dehydration stage of the thermogram to evaluate the kinetic parameters. The values of order of reaction and activation energy were found to be 5/2 and 72.214 kJ Mol^{-1}, respectively. The thermodynamic parameters were also evaluated. The dielectric study suggested the same behavior as for the hydroxyapaptite and MSUM.

These crystals grow in the synovial fluid and cause inflammation in soft tissue with terrific pain. This is also known as pseudo-gout. Due to this reason, a growth inhibition study was also carried out using various herbal extracts to identify the potent inhibitor. The three aqueous extracts studied, namely, *R. aquatica, B. diffusa* and *C.wightti,* for inhibition study. *C. wightti* shows the best inhibition results for CPPT crystals, which was followed by *R. aquatica, B. diffusa*.

Chapter VIII gives details of the growth and inhibition study of macro and micro crystals of CHPD (brushite). The single diffusion gel growth technique was employed to grow macro level CHPD crystals. Tartaric acid and citric acid were used for growth inhibition studies. For low concentrations they exhibited inhibition of growth, but for higher concentrations they dissolved the grown crystals. Both were found to be potent inhibitors.

For micro level CHPD crystals a modified gel growth technique was used and different concentration of citric acid were used for the inhibition study. The growth of micro-crystals and the inhibition study is advantageous in many respects. This experiment gave very interesting and rapid results.

Chapter IX gives details of the growth and characterization of some crystal of special interest. Various oxalates are found in different systems of human body. It is also expected to be responsible for calcium oxalate crystallization in urinary system. It was expected when oxalic acid solution was poured on the gel, the crystals of oxalic acid would grow, but the sodium ion present due to sodium meta-silicate reacted with the oxalate ion of diffusing oxalic acid and grew sodium oxalate crystals. Sodium oxalate crystals were grown by the solubility reduction gel growth method and characterized by various experimental techniques such as TGA, FT-IR and dielectric study. The thermo-gravimetry analysis suggested that the crystals were decomposed in three different stages, losing 60 % of its original weight and Na_2O was the end product, which was stable up to 900 ^{0}C. From the thermogram kinetic parameters as well as the thermodynamic parameters were also evaluated. FT-IR spectrum confirmed the presences of, C=O bond, C-C bond and O-H bending. Dielectric study suggested that the dielectric constant of the sodium oxalates crystals was very less responsive to the frequency change.

Sodium pyrophosphate crystals were grown from the solution growth technique using indigenously made solution growth set-up. Single crystals of sodium pyrophosphate were characterized by various experimental techniques. P-O symmetric and asymmetric stretching, O-P-O bending, O-H bending and stretching and metal-oxygen bonds were confirmed from the FT-IR spectrum and the dielectric study suggested a high polarizability of the material in the low frequency region.

In this chapter, also the organic crystal of 4-(2-hydroxy-phenylamino)-pent-3-en-2-one (HPAP) has been grown with the help of slow evaporation solution growth technique. The crystals were characterized by various experimental techniques such as FTIR, TGA, single crystal XRD and dielectric study. From the single crystal XRD it was confirmed that the HPAP crystal having orthorhombic crystal structure and space group $P2_12_12_1$. The cell parameters are as follows,

$a = 8.839(3)$, $b = 10.517(2)$, $C = 11.223(3)$, $á = â = ã = 90.00$

HPAP crystals show very poor thermal stability, at 350 ^{0}C it decomposes completely. Various bond such as, C=O, C=C, C-N, N-H stretching and rocking, O-H bond and ring skeleton were confirmed from the FT-IR spectrum. Dielectric constant was very less responsive to the frequency change. The crystal exhibited photo-conducting nature and shows the positive photoconductivity, while HPAP crystal exhibited very poor second harmonic generation (SHG) efficiency almost one tenth efficiency with comparison to the well known NLO material, potassium dihydrogen phosphate (KDP).

Chapter X gives the general conclusion, explains the results in terms of relevant theories and compares with those of reported earlier by citing literature. Scope of the future work is also described.

CONTENTS

Chapter I

General Introduction

Apagatamale hi mansi

Sphatikamaòâviva |

Rajanikaragabhastayah sukham

Pravisantyupadǽíaguòâh ||

(Kâdambarî)

Famous Sanskrit poet *Bâna* in his epic *Kâdambarî* compares nicely the optical property of crystals with virtues in the above mentioned couplets as, "Just as the rays of the Moon can easily enter into a crystal (jewel); similarly the virtues of good advice- preaching- can easily enter into a mind from which impurity-ignorance-is removed." In the ancient Sanskrit literature there are many references available on crystals; for instance, in *Bhâgavata Purâòa* a crystal wall is referred to as *Sphaþika-kudya*, the great Sanskrit poet Kâlidâsa in his classic work *Kumâra-Sambhava* narrates crystal rosary as *Sphaþikâksha Mâlikâ*.

Crystals have always been appreciated for their transparency and perfections, perhaps, due to this a phrase in English, *as clear as crystal,* as well as in Sanskrit, *Sphatika-Prabhâ,* for glittering crystals have become common in practice. In Sanskrit language the crystals are known as *Sphatika*. Earlier Greeks were calling crystals as *Krystallos*-means clear ice. However, it was applied not only to ice, but also to transparent minerals such as quartz and other rock crystals. Nevertheless, the Bible

also uses the transparency and optical properties of crystals in several narrations, for example,

The city shone like a precious stone, like jasper, clear as crystal. (Revelation. 21:11).

However, the word "crystal", as used in every day life, brings up a variety of mental impressions; one thinks of the glistening grains in certain types of rocks; of "rock crystals" and sculptured figures in museums; of sugar, especially the kind with large curiously shaped grains; of cut-glass vases for decoration; of diamonds, rubies and sapphire; of the simple "crystal and cat whiskers" type of radio, or even of the fortune teller's "crystal sphere". As per the modern scientific definition of the crystal, not all of these crystals could be recognized as a true crystal. However, our mental pictures roused by all of them include impression of light- the scintillating reflections from rocks or sugar crystals, the radiant flashing beauty of diamonds, and the more mysterious light effects within transparent objects.

In majority of the cases, the reflections of light and the transparency of the medium lead the user to adopt the word crystal for many objects. Today the law and order in crystals manifest themselves form of regular patterns of arrangements of particles in space, where these particles are the atoms or groups of atoms or molecules of which all matters are composed.

It was a great question before human being that how crystals were formed in the rocks. The freezing of water suggested that the crystals in rocks might have been formed in a similar way, i.e. by freezing of material, which was at one time in a molten state. But this was not the only way in which the crystals were formed; in fact, many finest crystals found in nature, such as the quartz crystal, have been grown from solutions. However, it is possible for a crystal to be formed directly from a gas

without passing through the liquid state; examples are hoarfrost, i.e. ice crystals which are grown from water vapor in the air; a few mineral substances which are mainly found around volcanoes, where sulphur and ammonium chloride crystals are formed from gases emitted during eruptions. A number of large natural salt crystals are grown from constant evaporation of sea water since ages nearby the Dead Sea in Israel.

Notwithstanding, from the astrological point of view, the crystals of particular colors play an important role to strengthen the position of the respective planets in the horoscope, for example, a topaz with yellow tinge is believed to be useful for strengthening Jupiter. In the metaphysics, however, the applications of different crystals are found since ages. All modern physical properties have counterparts in the mental or *psychic world;* as per beliefs, for example, amplification, in which crystals amplify body energy and thoughts and enable thoughts to be more effective; transformation, it purifies and transforms the molecular composition of matter; storage, crystals can be charged with energy which will store it for use; focus, focusing energy of thoughts with crystals for healing; and transference, the energy can enable to transfer to someone who is at distant place, that is, telepathy. Today crystals are active elements of immense potentials in science, technology and industry. The crystalline property has applications in devices such as; laser resonators, acoustoptic modulators, phase decay plates, polarizers, pyro-electric detectors, piezo-electric devices, crystal x-ray monochromaters, scintillation detectors, holographic devices, membranes of iron selective electrodes and substrate for thin films.

Today, the growths of crystals do not remain the phenomena only occurring in nature, but have become well advanced as well as widely used techniques in the laboratories and industries. There always has been a requirement of good quality crystals for various applications in science and technology; hence various growth

techniques developed to grow suitable crystals. The world crystal production has been estimated more than 20,000 tones per year. Out of that the largest share of about 60% is from semiconductor materials, for instance, silicon, gallium arsenide, indium phosphide, gallium phosphide, cadmium telluride and its alloys.
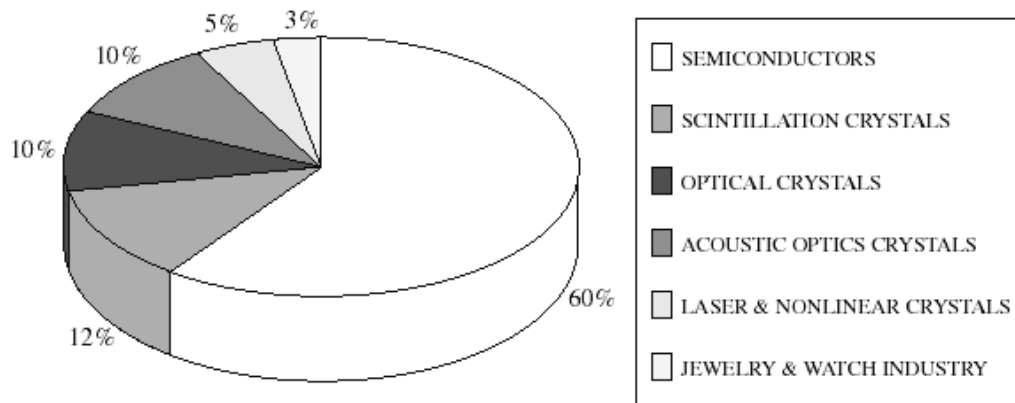
Figure (1.1): Estimated shares of world crystal production in 1999 [1]

One can notice from the figure (1.1) that the optical crystals, scintillator crystals and acousto-optic crystals have about equal shares of 10% each. However, laser and nonlinear optical crystals and for jewelry and watch industry shares only a few per cent. This has been reviewed by Scheel [1]. Moreover, Santhana Raghavan and Ramasamy [2] have reviewed the recent trends in crystal growth technology in terms of the world wide production of different technologically important crystals. As per one survey, the North American market of piezo-electric crystals and devices was estimated $ 1.15 billion in 2001. It is, further, expected to grow $1.86 billion by 2006 at an Annual Average Growth Rate (AARG) of 10%. Piezo-electric quartz crystal devices, notwithstanding, comprises largest market segment due to the recent boom in the wireless and mobile technologies [3].

The designing and development of various crystal growth techniques of the present day is a result of continuous and fruitful modifications occurring since last

several decades and, till today, the modifications in processes are continuing. The crystal growth requires emphasis on the following three aspects, (I) Theory of nucleation and growth, (II) Experimental crystal growth, and (III) Characterization of crystals

Schieber [4] has well explained this in a schematic representation, which is shown in figure (1.2).

Theory of nucleation and growth 1   Experimental crystal growth 2   Characterization of crystals 3

INTERFACE V/S DIFFUSION PROCESS

MELTGROWTH OF SEMICONDUCTORS

ELECTRONICS

SOLIDSTATE PHYSICS

MATHEMETICAL GROWTH OF CRYSTALS

HIGH-PRESSURE GORWTH

PERFECTION OF CRYSTALS

KINETICS OF GROWTH

VAPOR GROWTH OF SAPHIRE

PROPERTIES OF CRYSTALS

STRAIN ANNEAL GROWTH OF METALS

SEGREGATION COEFFICIENTS

MORPHOLOGICAL STABILITY CRITERIA

THREE DIMENTIONAL NUCLEATION

STOICHIOMETRY MAGNETISM PURITY

FLUX GROWTH OF FERRITES

ZONE MELTING OF ORGANIC CRYSTALS

CRYSTALOGRAPHY OF STRUCTURE

PERTURBATION BY IMPURITY FLOW

AUTOMATIC PLASMA TORCH-VERNEUIL

Figure (1.2): Three aspects of crystal growth

Altogether, the modern as well as the next generation crystal growth requires multi-directional development in various field and their interconnections, which has been described in a schematic representation in figure (1.3) by Prasad [5].
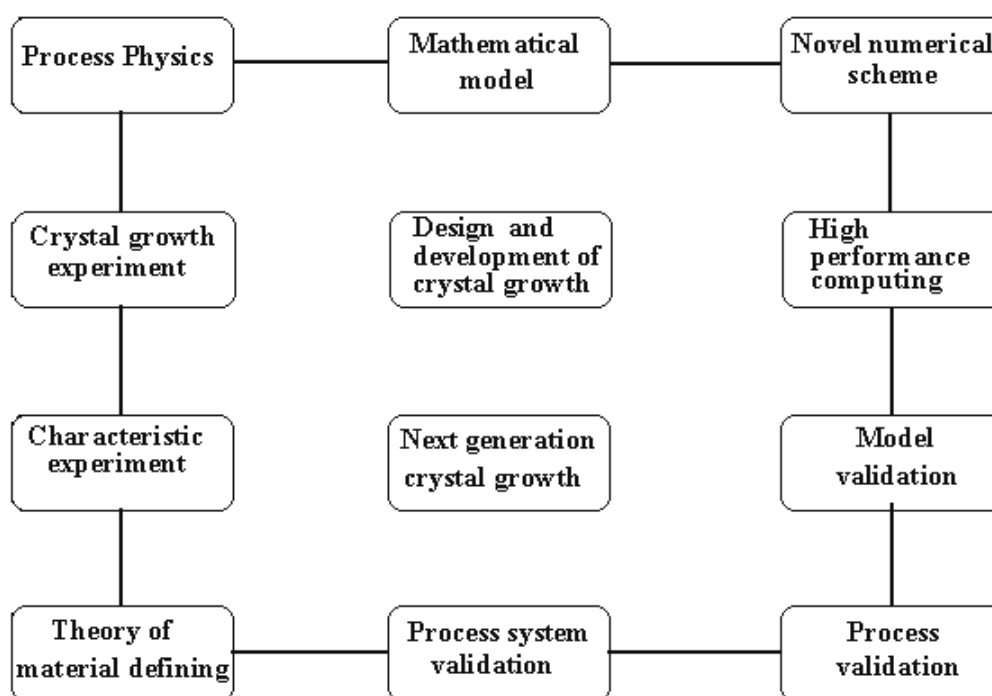
Figure (1.3): Multi-dimensional needs of crystal growth

In fact, the crystal growth deals with a tremendous complexity of interdisciplinary nature. It has been postulated by Scheel [6] that for a specific crystal of defined size and perfection, there is only one optimum and economic growth technology considering the thermodynamics, growth kinetics and economic factors. The crystal performance, the crystal size, the efficiency of growth method and the prize of crystals are correlated by him. However, practical work is needed in order to understand and appreciate the complexity of crystal growth process in view to involve phase transformations, of the many parameters that have to be compromised and optimized, and in view of the scaling problems, which hampers realistic numerical.

Crystal growth has been discussed by many authors in detail [7-9]. This has been correctly quoted in a different manner by Gilman [10] in his edited book "The *Arts and Science of Growing Crystals*" as, "The Systematic production of artificial

Crystals might be viewed as a new "*agriculture*" that has began to flourish. It differs from true agriculture in that its products are mostly inorganic at present, but it has many features common with normal agriculture and promises to have a somewhat comparable effect on society. The new agriculture consists of "growing" solid crystals from a "nutrient" phase (gas, liquid or solid). To start the growth process, the nutrient is often "seeded" with small crystal to be grown, and some workers speak of "reaping the harvest" after a certain length of time".

There are many well-written books available on subjects like fundamentals of crystal growth [11]; different crystal growth techniques and their theories, characterization, applications [10, 12, 13, 14-18]; and understanding the Growth mechanism [19]. Recently, a handbook of Crystal Growth is also published [20]. Even book is available with wonderful photographs of grown crystals [21]. Whereas, the authors Stangl and Stang [22] in their book, entitled "*Crystals and Crystal Gardens You can Grow*", have considered the growth of a variety of beautiful crystals as the growth of flowers in a garden which one can do, thereby, they have agreed to the concept of Gilman [10] of "agriculture". Recently, two books have been published on crystal growth dealing with the progress in crystal growth. For the first time a complete survey of interdisciplinary fields of crystal growth, technologies and fabrication of crystal machining are claimed to be included [23]**.** In another book, 50 years progress in crystal growth has been covered in various contributed articles by the crystal growth pioneers [24].

Bio-crystallization is an important phenomenon occurring in various parts of living body of humans, animals as well as plants. This has raised considerable interests amongst crystal growers, biochemists and doctors. The understanding of biocrystallizations may lead to develop processes which can modify or control them,

which may also prove to be very significant in the treatment of several disease and ailments. Figure (1.4) is a schematic representation of the process involved in mineralization indicating the role of organic matrix in the biological system. Beside this, figure (1.5) is the schematic representation of the crystal growth process in biological system.

```
                          ┌───────────────┐
                          │  Environment  │
                          └───────┬───────┘
              ┌───────────────────┴────────────────────┐
      ┌───────────────┐                         ┌───────────────┐
      │   Inorganic   │                         │   Biological  │
      └───────┬───────┘                         └───────┬───────┘
      ┌───────────────┐              ┌──────────────────┴──────────────────┐
      │ Physicochemical│            ┌───────────────┐          ┌─────────────────┐
      └───────┬───────┘            │  Biochemical  │          │ Physicochemical │
      ┌──────────────────┐        └───────────────┘          └─────────────────┘
      │ Geological Minerals│            └──────┌───────────────┐──────┘
      └──────────────────┘                     │ Organic Matrix │
                                               └───────┬───────┘
                                   ┌───────────────────┴────────────────┐
                          ┌─────────────┐                    ┌──────────────┐
                          │  Controlled │                    │   Induced    │
                          │Mineralization│                   │Mineralization│
                          └──────┬──────┘                    └──────────────┘
              ┌──────────────────┼──────────────────┐
      ┌─────────────┐    ┌─────────────┐     ┌──────────────┐
      │   Spatial   │    │  Structural │     │ Stereochemcial│
      └─────────────┘    └─────────────┘     └──────────────┘
```
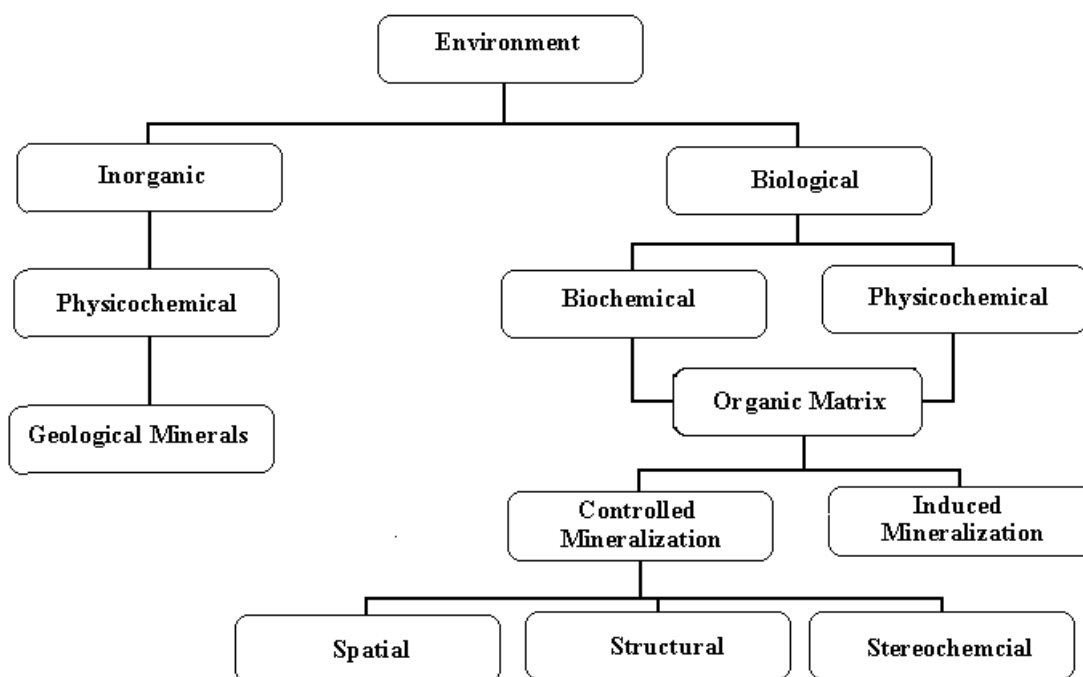
Figure (1.4): Various mineralization processes in different environments

Many multi-cellular organisms produce hard tissues as bones, shells, skeletal units, and spicules [25], which are the examples of bio-mineralization processes. These hard tissues are bio-composites and incorporate both structural macromolecules (lipids, proteins and polysaccharides) and minerals of, perhaps, sixty different kinds, including hydroxyapaite, calcium carbonate and silica. Interestingly, many single celled organisms, such as bacteria and algae, also produce inorganic materials either inter-cellularly or extra-celullarly [26].
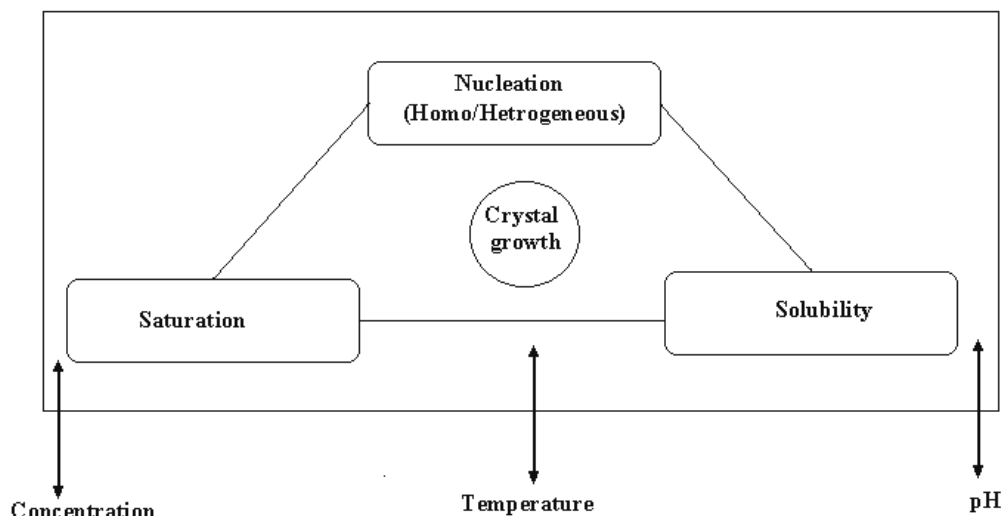
Figure (1.5): Factors affecting the growth of crystals

There are several examples of micro-organisms, which include magnetotactic bacteria synthesizing magnetite [27]; chrysophytes [28], diatoms and actinopoda synthesizing siliconous materials and S.layer bacteria synthesizing gypsum and calcium carbonate surface layers [29]. Normally, hard tissues are mechanical devices (for example, skeletal, cutting and grinding), or they serve a physical function (for example, magnetic, optical, piezoelectric). Bio-inorganics are also ion sources that are vital for physical activities and, therefore, integral part of the organism. A very interesting survey of biomimatics as well as materials fabrication through biology and bio-mineralization is given by Sarikaya [29].

There are numerous bio-materials which are synthesized *in vitro*. These synthetic bio-materials have numerous applications and great demands. Therefore, the world market is continuously growing with the demand of various novel bio-materials. In 1998, the world-wide value of biomaterials market was estimated to be some 25 billion euros, with a predicted growth rate of 12% per year. Almost one third of this world market, about 7 billion euros, was in Europe, with the US biomaterials market somewhat larger at around 10 billion euros. It is worth noting that the 20%

annual growth rate in US biomaterials outstrips all other sectors of the medical device industry. With strong report from the European Commission's Fifth Frame Work Program and Research and Development, Europe is rapidly growing sector in bio-materials whose world market is worth over 25 billion euros annually [30].

Cholesterol crystals are believed to be the main culprit for the cardiac problems. Altogether, it is very important bio-material with startling properties. Therefore, it is termed as the Jekyll and Hyde molecule in the elaborative review by Wrenn [31]. In the case of gall stones, the vesicles and micelles transport cholesterol in the bile; whereas the spherical type lipoproteins transport cholesterol in the blood stream. Actually, LDL (Low Density Lipoprotein) delivers cholesterol to the cells and HDL (High Density Lipoprotein) is involved in the reverse transport of cholesterol from the cells. Inasmuch as crystalline cholesterol, which contributes to atherosclerosis, originates from LDL, cholesterol. As per one survey, cardiovascular diseases (CVD) heart disease and stroke- topping the list for death and disability. Globally, 17 million people died of all CVD in 2001. In 1986, coronary artery bypass grafting (CABG) accounted less than 10% of all cardiac surgeries in India, today it accounts 60% [32]. Gall stone disease is also quite common worldwide. Gall stone disease afflicts 12% of USA population [31].

Apart from the bio-mineralization, the bio-crystallization is also a root cause of many ailments for the humans. One of the common ailments is the cataract, which is caused by certain crystals. Brooks et al. [33] reported that face centered cubic (F.C.C.) type ferritin crystals in cataracts play important role in light diffraction. Kmoch et al. [34] have reported the cataracts caused by protein crystallization in the lens. Moreover, attempt is made to link human genetic cataracts with mutations in the *gamma D crystalline* gene [35]. It has been suggested that the opacity occurs because

of the spontaneous crystallization of the mutant proteins. Measurements of the solubility curves of crystals, particularly, of the *Arg-58* to *His* and *Arg-36* to *Ser* mutants of *gammaD crystalline,* show that the mutations dramatically lower the solubility of the protein, which results into crystallizations.

Moreover, many people in this world are suffering from the problems of painful joints, which are commonly termed as gout or arthritis depending upon the conditions of their afflictions. This is also commonly termed as arthropathy (joint disease). Arthrpathy is also regarded as the crystal induced ailment, which is due to the deposition of hydroxyapatite, monosodium urate, uric acid or calcium pyrophosphate di-hydrate crystals in the joints. This problem is found not only in humans but also in several types of animals, such as, reptiles, mammals and birds. Recently, from the fossil study, it has been found that the arms and legs of the most ferocious carnivore dinosaur *Tyrannosaurus Rex* had collection of urate crystals, which ultimately might have led to gout. Studies conducted for three decades in the *Third World* countries have confirmed that the rheumatoid arthritis occurs throughout the world. This also depends on the potential biases resulting from the socio-economic, demographic and health care conditions in these countries. In India, the prevalence of rheumatoid arthritis (0.75%) is similar to that in the West. In China, Indonesia, and the Philippines, in contrast, rheumatoid arthritis appears rare (prevalence below 0.4%), in both urban and rural settings. The rarity of rheumatoid arthritis in rural Africa contrasts with the high prevalence of the disease in Jamaica, where over 2% of the adult population is affected. In a study in Latin America, rheumatoid arthritis was the reason for seeking medical advice in 22% of rheumatology clinic patients [36]. Musculoskeletal (pertaining to the muscular and skeletal systems) conditions are major burden on individuals, health systems, and

social care systems, with indirect costs being predominant. This burden has been recognized by the United Nations and WHO, by endorsing the *Bone and Joint Decade 2000-2010*. Osteoarthritis, which is characterized by loss of joint cartilage that leads to pain and loss of function primarily in the knees and hips, affects 9.6% of men and 18% of women aged >60 years. Increase in life expectancy, the ageing populations are expected to make osteoarthritis the fourth leading cause of disability by the year 2020. Joint replacement surgery, where available, provides effective relief. Rheumatoid arthritis is an inflammatory condition that usually affects multiple joints. It affects 0.3-1.0% of the general population and is more prevalent among women in developed countries. Persistent inflammation leads to joint destruction, but the disease can be controlled with drugs. The incidence may be on the decline, but the increase in the number of older people in some regions makes it difficult to estimate future prevalence [37]. Therefore, it is always desired to develop therapies to either dissolve the crystals responsible for arthropathies or inhibit their growth.

Looking at the great heritage of traditional knowledge of different herbs, there is a great demand of herbal medicine in the world. It is note worthy that the herbal medicine is still the mainstay of about 75-80 % of the world population, mainly, developing countries. In France and Germany, nevertheless, many herbs and herbal extracts are used as prescription drugs and the sale has increased from $ 6 billion to $ 20 billion from 1991 to 2000. In India the herbal market is of about $ 1 billion and export is around $ 80 million annually. A detailed review has been written by Kamboj [38] pertaining to the importance of major traditional herbal medicine in India, the role of WHO in the herbal medicine and the standardization of herbal medicines. On the basis of traditional knowledge of Ayurveda, the theory proposed by Patwardhan et al. [39] on the reverse pharmacology, the present author, hereby, deals with the *in*

vitro inhibition and dissolution of different crystals, namely, monosodium urate, hydroxyapatite and calcium pyrophosphate, responsible for arthropathies by different herbal extracts. This may prove to be a good screening model for the *in vivo* studies and animal models. It is also important to develop an *in vitro* model for the growth and inhibition of these crystals at either the room temperature or the body temperature. Generally, these crystals are difficult grow at room temperatures. Because of the very low solubility of uric acid in water at room temperature the MSUM crystals are difficult to grow [40]. The most stable nature of hydroxyapatite at very high temperatures usually requires high temperature techniques like hydrothermal method and the sol-gel method [41] as well as the decomposition calcium phosphate compounds provides calcium pyrophosphate at high temperatures [42], which all forbid growing these compounds at room temperatures. This, somewhat, difficult task was taken up and these crystals were successfully grown at the body temperatures or at the room temperatures. The growth and inhibition in the presence of various herbal extracts as well as characterization of the crystals would provide valuable information for the formulation of drug for the arthropathies in a collaborative manner after *in vivo* and animal studies.

Urinary stone problem is one of the oldest and the wide spread afflictions of human beings. As per one estimate, around 2 million people are treated world wide with Extra Corporal Shock Wave Lithotripsy (ESWL) [43]. Around 12% of population in the European Union suffers at least one process related to urolithaisis [44]. About one adult in 1000 is hospitalized annually in the USA because of urinary calculi [45]. In India, 12% of the population is expected to have urinary stones, out of which 50% may end up with loss of kidneys or renal damage. Moreover, nearly 15% of the population of northern India suffers from kidney stones [46]. Saurashtra region

of Gujarat state is also well-known for the high incidences of urinary stones. As per one study conducted by Joshi [47] that out of 3405 patients treated in the Kidney Hospital, 37.33 % were urinary calculi patients and out of them nearly 76 % were males as well as out of them 47.4% of patients were in the age group of 21 to 40 years, that is, the prime working age. This is really alarming to Saurashtra region. Therefore, it is also important to study the growth and inhibition of urinary type crystals *in vitro* and identify the potent inhibitors. The predecessors of the present author [48, 49] have significantly contributed in this direction. However, the present author aims to develop comparatively new, faster, time saving, material and chemical saving technique of microcrystal growth and study the growth, inhibition, alteration in morphology *in situ* under optical microscope. In the present thesis emphasis is made on brushite crystals. The growth inhibition of brushite (Calcium hydrogen phosphate dihydrate-CHPD) crystals by weak acids like tartaric acid and citric acid, commonly found in fruits, is carried out to find the potential applications.

Some spin off studies, related to the present study, are also aimed by the author. Sodium pyrophosphate crystal growth and characterization is taken up in the spin off study in order to understand the availability and the role of pyrophosphate salts in human body. Similarly, the oxalic acid metabolism is very important in the body, since it is expected to supply anions to the growing calculi in the urinary system. Therefore, water soluble salt of oxalic acid, that is, sodium oxalate, is aimed to be studied. Crystals of sodium oxalate are grown by the gel growth technique and characterized. Apart from these, organic crystal 4-(2-hydroxy-phenylamino)-pent-3-en-2-one (HPAP) is grown because of its possible pharmaceutical, photo-conducting and nonlinear optical applications.

This is a humble effort to clasp various disciplines of science on the common platform. It brings chemistry, biology, phyto-chemistry, Ayurveda, crystallography and, of course, physics on a common platform at present and, further, it expects to be joined by pharmacy, toxicology, pharmacology, medicine and probably the life science at the end.

References:

[1]   H. J. Sheel; *J. Cryst . Growth,* **211** (2000) 1.

[2]   P. Santhana Raghavan and P. Ramasamy; *PINSA*, **68** (2002) 235.

[3]   M. Rajan; Business Communication Co., Oct.2001,

        http://bccresearch .com/press.

[4]   M. Schieber; *"Introductory Remarks" in "Techniques of Crystal Growth"*,
        Proc.Int. Conference on Crystal Growth, Boston, (1966), Pergamon Press,
        Oxford.

[5]   V. Prasad; *"Role of Modeling in Process and System Development for Crystal
        Growth"*, Invited Talk, P.C.S.C.,2001, N.P.L., New Delhi, 26-28, February,
        2001, India.

[6]   H. J. Scheel, *Plenary Lecture* at Second Asian Conference on Crystal Growth
        and Crystal Technique, CGCT-2, Aug. 28-31, 2002, Seoul, Korea.

[7]   A. R. Verma; *"Crystal Growth and Dislocations"*, Butterworths, London,
        (1953).

[8]   K. A. Jackson; *"Growth and Perfection of Crystals"*, Eds. R. H. Doremus, B.
        W. Roberts, D. Turnbull, Wiley, New York, (1958).

[9]   W. A. Tiller; *Acta. Met*., **5**(1957) 565.

[10]   J. J. Gilman; *"The Arts and Science of Growing Crystals"*, John Wiley, New
        York, (1963).

[11]   J. P. van der Eerden; *"Fundamentals of Crystal Growth"*, World Scientific
        Publishing, (1993).

[12]   R. A. Laudise; *"Crystal Growth", in "Techniques of Crystal Growth"*, Proc.
        Int. Conference on Crystal Growth, Boston (1966).

[13]   B. R. Pamplin; *"Crystal Growth"*, Pergamon Press (1975).

[14]   B. Chalmers; *Principles of Solidification*", John Wiley, New York, (1964).

[15]   N. Bardsley, D. T. J. Hurle and J. B. Mullin; *Crystal Growth*: *A Tutorial Approch*", North- Holland Series in Crystal Growth, Vol-2, Amstredam, (1979).

[16]   A. V. Shubnikov, A. A. Chernov, N. N. Sheftal; "*Growth of Crystals*", Kluwar Academic, (1979)

[17]   A. Majchrowski; "*Single Crystal Growth, Characterization and Applications*", Ed. J. Zielinski, SPIE-International Society for Optical Engineering, (1999).

[18]   K. Byrappa and T. Ohachi, Eds.; *Crystal Growth Technology: Characterization and Applications,* Noyes Publication, (2001).

[19]   K. Nishioka, J. Harda, A. Sasaki, H. Teiki; "*Advaces in Understanding of Crystal Growth Mechanism*", Elsevier Science, (1997).

[20]   D. T. J. Hurle; *Handbook of Crystal Growth*, Vols.-1 to 3, Elsevier Science, (1999-2000).

[21]   A. Holden and P. S. Morison; "*Crystal and Crystals Growing*", Amazon

[22]   J. Stangl and J. Stang; "*Crystals and Crystal Gardena You Can Grow*", Horn Book, (1990).

[23]   H. J. Scheel and T. Fakuda; *Crystal Growth Technology,* Wiley, New York, (2004)

[24]   R. A. Feigelson; *50 Years Progress in Crystal Growth,* Elsevier, New York, (2004)

[25]   H. A. Lowenstam; *Science,* **211** (1981) 1131.

[26]   K. Simkiss and K. M. Wilbur in *Biomineralization*, Academic, New York, (1989).

[27]   R. B. Frankel and R. P. Blakemore, eds, in *Iron Biominerals*, Plenum, New York, (1991).

[28]   J. Kristiansen and R. A. Andersen, Eds, in *Chrysophytes Aspects and Problems,*Cambridge Univ. Press, Cambridge, (1986).

[29]   M. Sarikaya, *Proc. Natl. Acad. Sci. USA*, **B96** (1999) 14183.

[30]   http:// eropa.eu.int/common/dg12/fps.html

[31]   S. P. Wrenn; *"Engineering Approaches to Cholesterol-Linked Diseases "*, (2001).

[32]   S. Padmavati, *Prevention of Heart Disease in India in the 21st Century, Need for a Concentrated Effort,* National Heart Institute, New Delhi.

[33]   D. G. Brooks, K. Manova-Todorova, J. Farmer, L. Lobmayr, R. B. Wilson, R. C. Eagle, Jr., T. G. St. Pierre and D. Stambolian, *Invest. Ophthalmol. Vis. Sci.,* **43**(2002)1121.

[34]   S. Kmoch, J. Brynda, B. Asfaw, K. Bezouska, P. Novak, P. Rezakova, L. Ondrova, M. Filipec, J. Sedlacek and M. Elleder, *Hum. Mol. Genet.,* **9** (2000) 1779.

[35]   A. Pande, J. Pande, N. Asherie, A. Nomakin, O. Ogun, J. King and G. B. Benedek, *Proc. Natl. Acad. Sci. USA,* **98** (2001) 6116.

[36]   M. Mijiyawa, *Rev. Rhum. Engl. Ed*., 62 (1995) 121.

[37]   A. D. Woolf and B. Pfleger, *Bull. World Health Org*., **81**(2003**)** 646.

[38]   V. P. Kamboj, *Curr. Sci*., **78** (2002) 35.

[39]   B. Patwardhan, A. D. B. Vaidya and M. Chorghade, *Curr. Sci*., **86** (2004) 789.

[40]   Kirk Othmer, *"Encyclopedia of Chemical Technology",* 2nd Ed., Vol.21, Interscience, Division of John Willey & Sons Inc. (1970) p-107.

[41] K. Yanagisawa, H. Toya, Qi Feng, N. Yamasaki, *Phosphorus Res. Bulletin,* **5** (1995) 43.

[42] Kirk Othmer, *"Encyclopedia of Chemical Technology",* 2nd Ed., Vol.17, Interscience, Division of John Willey & Sons Inc. (1970) p- 456.

[43] J. Alcover, A. Rousald, F. J. Ruiz-Marcellan and R. Serrate; *LVII Congreso Nacional de Urologia,* ENE Ediciones S. A., Madrid, (1982).

[44] H. J. Schneider, *Urolothiasis, Etiology, Diagnosis*, Hand book of Urology, Vol. 1,Springer-Verlag, Heidelberg, (1985) 137.

[45] The Merck Manual of Diagnosis and Therapy, Section 17, Genito-urinary Disorder, Chapter 22, Urinary calculi.

[46] K. C. Joseph, B.B. Parekh and M.J. Joshi, *Curr. Sci.,* **88 (8)** (2005) 1232.

[47] Vivek Joshi, *Urinary Calculus Disease: A preliminary Study,* B. T. Savani Kidney Hospital, Rajkot, (2005), Private Communication.

[48] V. S. Joshi: *Ph.D. Thesis,* Saurashtra University, Rajkot (2001).

[49] K. C. Joseph: *Ph.D. Thesis,* Saurashtra University, Rajkot (2005).

Chapter II

Brief Review on Bio-crystallization Induced Ailments

2.1   Introduction:

Bio-crystallizations and bio-mineralizations are very important phenomena in which crystal growth of specific bio-material compounds occur in body of living organisms. These phenomena are observed in animals and plants, which are discussed in the Chapters I and X. There are many reasons and theories proposed for this. In a human body, certain bio-crystallizations and bio-mineralization phenomena are considered to be responsible to different ailments, which can be broadly categorized as;

(1) Crystallization responsible for arthritis, gout and other related problems

(2) Crystallization responsible for urinary stone problems

(3) Crystallization of cholesterol in blood vessels leading to heart problems

(4) Crystallization of cholesterol in gall bladder stones

(5) Crystallization responsible to cataracts.

There are hosts of references available on the phenomena of bio-mineralization and bio-crystallization. The growth of bio-molecules has great impact on study of the root of ailments and find out the newer approaches engineered by the molecules for the drug delivery systems. The growth of organic macro-molecules such as proteins, nucleic acid or their complexes and viruses are reported by many authors. This is very essential to understand the growth of these crystals, which has been recently explored by well-known crystal growers Chernov [1, 2] and Veesler [3].

Crystals play important role in the life of human beings. An interesting article has been written by Addadi and Weiner [4] on crystal asymmetry and life. Moreover, in the race towards developing the nano-structured materials, recently, the biomaterials have also entered into the fray [5-7].

These bio-crystallizations and bio-mineralizations have deep social as well as economic impact. A large number of people are suffering from different ailments related to the bio-mineralization and bio-crystallization phenomenon. Occurrences of bio-mineralization in the form of crystals in to living tissues cause severe inflammation and pain. These ailments can be dealt with by considering the three main aspects, i.e., prevention, relief, and cure.

The aim of the present author is to grow various bio-material crystals responsible to *arthropathies* (joint disease) and urinary stones *in vitro,* characterize them and try to find the inhibition of growth or dissolution by using different herbal extracts. The results of inhibition studies *in vitro* are followed by macrophage response studies and animal model studies for final formulation by the collaborators. This overall collaborative work is expected to bring some formulations of herbal extract to deal with the arthropathies.

2.2   Crystal Associated Arthropathies:

Mankind has, in all possibility, suffered from arthropathies for many thousand of years. The hand of Egyptian mummy, dating about 1500 BC, shows osteoarthritis. Although artistes have seldom depicted the deformities of the rheumatoid hand, one well-known exception is the self-portrait of Augus Renoir, famous French painter, drawn in 1914. He shows himself painting with severely crippled hand [8]. Various types of crystals are associated with the arthropathies [9], the main crystals are briefly summarized in table (2.1).

Table (2.1)

Crystals associated with arthropathies [9]

Type of crystal usually involved	Condition	Condition also known as
Hydroxyapatite	Calcific tendinitis	-
Hydroxyapatite	Acute calcific tendinitis	Acute periarthritis
Calcium pyrophosphate	Chondrocalcinosis	Cartilage calcification
Calcium pyrophosphate	Pseudogout	Acute pyrophosphate arthritis
Calcium pyrophosphate (and sometimes apatite)	Osteoarthritis with crystals	Chronic pyrophosphate arthritis
Urate	Gout	-

However, the main three types of crystals, namely, hydroxyapatite (HA), calcium pyrophopsphate dihydrate (CPPD) and monosodium urate monohydrate (MSUM), are dealt with in details in the present thesis.

2.2.1. Hydroxyapatite Related Arthropathy:

Human *cortical* (dense) bone consists of *ostenos* (cylindrical channels) that are held together by a frame-work of hard tissues, mainly natural hydroxyapatite. The major phase found in bone is hydroxyapatite (HA, $Ca_{10}(PO_4)_6(OH)_2$). The other commonly known calcium phosphate phases are octacalcium phosphate (OCP, $Ca_8H(PO_3)OH$), tricalcium phosphate (TCP, $Ca_3(PO_4)_2$), calcium hydrogen phosphate dihydrate, (CHPD, $CaHPO_4 . 2H_2O$) and dicalcium phosphate (DCP, $Ca_2P_2O_7$) [10]. The HA is not only a bio-compatible but also a bioactive material. It directly bonds to the bones and favors the implant fixation. The bone replacement is an important subject in the field of reparative medicine and the most studied material is the porous HA. Development and characterization of 3-D HA bone tissue engineering scaffolds are reported [11]. The HA and calcium deficient HA was precipitated from aqueous

solution [12, 13].This compound has been used to study the hard tissue calcifications such as bone, teeth and many undesirable cases of pathological mineralization of the articular (pertaining to joints) cartilage [14, 15], cardiac valves [16, 17] and kidney stones [18]. Apart from these, HA have many other diverse applications, for example, in chromatography [19], in solid state ionics [20, 21], in catalysis [22], in drug delivery systems [23], in fuel cells [24], and in gas sensing [25]. As already mentioned earlier, the HA and other phosphates are the main constituents of the human bones. In healthy adults, apatite occurs mainly in bones and teeth. Sometimes, however, calcium crystals form in other body tissues, for example, apatite can form in *tendons* (the fibrous cords that attach muscles to bones). This condition is called *'calcific tendinitis'*. The usual site for this is the shoulder, in the tendon of the supraspinatus muscle that helps move the shoulder joint, as described in figure (2.1). Apatite crystal deposition induced inflammation is a common finding in bursitis and periarthritis.
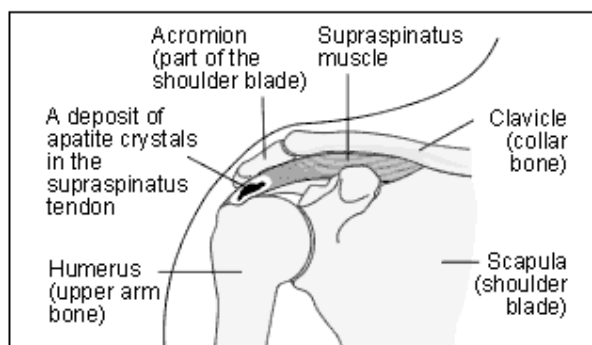
Figure (2.1): Calcific tenditinitis of the shoulder [26]

Apatite also occurs in some otherwise unexplained acute arthritis and, like CPPD, is common in osteo-arthritic joint effusions. Most joints or bursae (A fibrous sac lined with sinovial membrane containing sinovial fluids) can be involved, with more common sites including shoulders, hips, knees, and digits (human fingers). Joint or

periarticular inflammation can be acute or chronic. An extremely destructive arthritis has been noted especially at shoulders ("Milwaukee shoulder"), hips, and knees. X-rays can also show soft tissue calcifications with or without bony erosions, which is shown in figure (2.2) Apatite deposition can also be associated with scleroderma (a disease in which localized oedema of a skin is followed by hardening, atrophy,etc) and the other connective tissue diseases like osteoarthritis and erosive arthritis (See Table(2.1) [27] and with high-dose vitamin D therapy. Serum studies are generally normal except that phosphate levels are often elevated in renal dialysis patients who are at high risk of apatite deposition. In most instances the cause of soft tissue apatite deposition is not known.
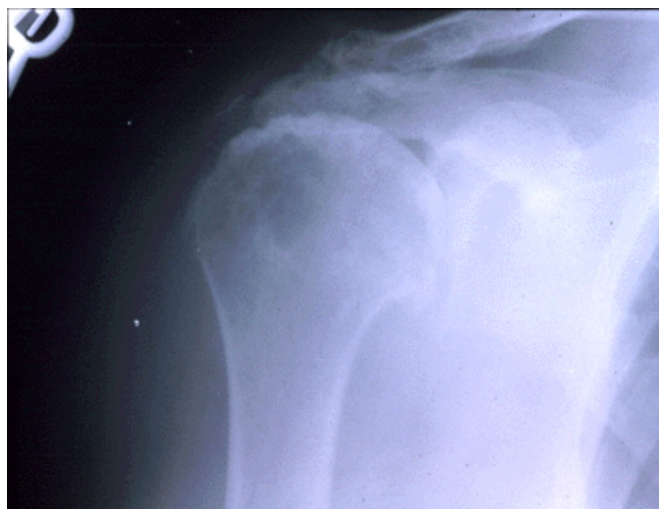
Figure (2.2): **X-ray of the damaged shoulder due to crystal formation**

Common areas of involvement include the shoulder, greater trochanter of the hip, lateral epicondyle of the elbow, tendons about the wrist, and tendon attachments at the medial and lateral aspects of the knee, but tendons around the hip, hand, or occasionally other places in the body can also be affected [26].

Another form of apatite crystal-induced inflammation has been observed in patients undergoing haemodialysis (a blood dialysis in which waste products are

removed and replaced by useful ones) for chronic renal failure [28, 29]. The inflammation is appeared to be related to the calcific deposits of apatite crystals found in and around involved joints. Studies suggest that calcification in these patients is related to elevated serum phosphorus concentration. Increased frequency and efficiency of dialysis to maintain normal serum phosphate levels, coupled with regular use of aluminum hydroxide to bind phosphate in the gastrointestinal tract, which has led to prevention and control of these crystal related symptoms.

The role of apatite in the etiopathogenesis of the lesions is still somewhat contested. It has suggested that HA crystals, phagocytosed (engulfing foreign bodies by cells) by synovial macrophage like cells, activate collagenase and neutral protease enzymes. [30, 31]. Active enzymes then lead to joint destruction, "*enzymatic strip-mining",* and release of additional crystals and particulate collagen into the joint space, thereby, augmenting the destructive response. This hypothesis is supported by experimental investigations that demonstrated increased collagenase and neutral protease activities following the addition of hydroxyapatite crystals to cultured synovial cells [31], release of prostaglandin PGE_2 in a dose-related fashion [32] and a mitogenic (cell division producing) response of synovial cells to calcium-containing crystals [33]. The blocking crystal dissolution inhibited the mitogenic effect of HA crystals but did not inhibit collagenase synthesis.

The detailed metabolism of HA deposition in the body is still not fully understood to the best of the present author's knowledge. On the other hand, in case of other crystals responsible for the arthropathy, it is well documented. However, the alterations in calcium and phosphorus metabolism are generally not observed in patients with BCP or HA disease, other than in those with underlying associated

disease, such as uraemic syndrome (renal failure- disturbs biochemical balance), who are undergoing dialysis therapy.

The HA crystals are identified in synovial fluid in different ways. Multiple filling defects on arthro-graphy were seen at times, consistent with *osteochondromatosis* (benign tumor of cartilage or bone). Studies of synovial fluids revealed micro-spheroids containing crystals first described as HA. Further studies suggested that crystal population associated with these disorders were not pure apatite but rather a heterogeneous mixture of crystals, including partially carbonate-substituted HA, octa-calcium phosphate, and tri-calcium phosphate [34]. However, the specific identification of BCP crystals in the synovial fluid by light microscopy is difficult, owing to their small size (less than 1 ìm in length). But shiny, non-bifringent, irregular cytoplasmic (living material of the cell external to nucleus) inclusions that may result from clumps of crystals have been reported [35]. When seen extra-cellularly, they take on the appearance of "shiny coins". Similarly, purplish cytoplasmic inclusions can be seen on Wright-stained smears. Moreover, the clumps of crystals stain strongly with Alizarin red [36] or von Kossa stains.

As in all forms of sub-acute and chronic arthritis, appropriate attention to physical therapy programs, including heat and exercise, is important in maintaining joint range of motion and providing further symptomatic relief. Otherwise large periarticular deposits of crystals may occasionally require surgical excision.

It is worth noting that different techniques have been employed by various researchers to obtain HA. Hydroxyapatite and calcium deficient HA was precipitated from aqueous solution [12, 13]. Generally, HA crystals were grown by hydrothermal methods at elevated temperatures and pressures [37]. Altogether, many other authors have attempted to obtain HA, for example, flux growth of HA whiskers [38], high

temperature sintering [39], HA bio-ceramic by wet chemical process [40] and microwave irradiation synthesis of HA ceramic [25]. There are certain experiments performed at the synthetic body fluid (SBF) conditions, which includes, synthesis of bio-mimetic HA powders at 37 ^{0}C in SBF [41] and HA coating by bio-mimetic method on titanium alloy using SBF [42]. In this bandwagon of HA crystal growth and synthesis, the latest to join are nano-size HA. The template-assisted synthesis of HA nano-wires [43] and physico- chemical properties of nano-crystalline apatites [45] have been recently reported.

It is important to study the growth inhibition of HA. In this direction certain efforts have been made, which are the effects of various amino acids on the growth of HA [44-48] and the effect of certain drugs on the growth and dissolution of HA [49-51]. Nevertheless, no major efforts are made on the growth inhibition study of HA crystals in the presence of different herbal extracts.

Hydroxyapatite ($Ca_{10}(PO_4)_6(OH)_2$) crystals have been grown by the present author employing the gel growth technique. The growth and characterization of HA as well as inhibition study under the influence of different herbal extracts are important aspects of the present study, which are discussed in detail in Chapter-V.

2.2.2. Monosodium Urate Monohydrate Crystal-Associated Arthropathy:

Deposition of monosodium urate monohydrate (MSUM) crystals or urate crystals in a joint causes inflammatory arthritis known as gout [52]. Gout is a term represents a heterogeneous group of diseases found exclusively in man. Due to its peculiarity, gout is known as the *king of diseases* and the *disease of kings*. Several excellent narrative and pictorial histories of gout have appeared [53-74]. The major events in the history of gout are summarized in table (2.2).

Table (2.2)

Major events in the history of Gout [53-74]

Date	Event	Author(s)
5th Century B.C.	Aphorisms on gout	Hippocrates
1st Century A.D	Familial nature	Seneca et al.
3rd Century	Tophi described	Galen
13th Century	The term gout originated	de Vielehardouin et al.
1679	Crystals in gouty tophi	van Leeuwenhoek et al.
1776	Uric acid in stones	Scheele
1797	Urate in Tophi	Wollaston
1814	Specificity of colchicine in acute gout	Want
1848	Hyperuricemia in gout	Garrod
1899	Urate crystals cause gouty arthritis	Freudweiler
1950	Introduction of effective uricosuric agents	Talbot, Gutmann and YU et al.
1963	Introduction of alloupurinol	Rundles et al.
1967	First specific enzyme defect described in patients with gout	Kelly et al

In general, gout in its full development is manifest by the following important points [75]:

(a)   An increase in the serum urate concentration.

(b)   Recurrent attacks of a characteristic type of acute arthritis, in which crystals of MSUM are demonstrable in leukocytes of synovial fluid.

(c)   Aggregated deposits of MSUM (tophi) occurring chiefly in and around the joints of the extremists and sometimes leading to severe crippling and deformity.

(d)   Renal disease involving glomerular, tubular and interstitial tissues and blood vessels.

(e)   Uric acid urolithiasis.

However, these manifestations can occur in different combinations.

Gouty arthritis is the most common form of inflammatory joint disease in men older than 40 years [74]. Recently, a mechanism of inflammation in gout is discussed by Dalbeth and Haskard [76]. The prevalence of gout seems to increase substantially with age and increasing serum urate concentration [77, 78]. For example, the prevalence was 15 per 1000 in males in the age group from 35 to 44 years [79]. The annual incidence rate of gout is 4.9 percent for urate levels greater than 9 mg per dl, 0.5 percent for urate levels 7.0 to 8.9 mg per dl and 0.1 percent for the values less than 7.0 mg per dl. [79].

Broadly speaking, gout can be divided in four different stages termed as, (a) asymptomatic hyperuricemia (excess uric acid in blood), (b) acute gouty arthritis, (c) inter-critical gout and (d) chronic tophaceous gout.

(a)   Asymptomatic Hyperuricemia:

Asymptomatic hyperuricemia is the term for an abnormally high serum urate level, without gouty arthritis or nephrolithiasis. Hyperuricemia is defined as a serum urate concentration greater than 7 mg/dl (416 μmol/l), the approximate level at which urate is supersaturated in plasma [80].

Hyperuricemia predisposes patients to both gout and nephrolithiasis, but therapy is generally not needed in the asymptomatic patient. However, hyperuricemia in the asymptomatic patient provides the physician with an opportunity to modify or correct underlying acquired causes of hyperuricemia , which are summarized in table (2.3).

Table (2.3)

Acquired Causes of Hyperuricemia

Increased urate production	
Cause	
Nutritional	Excess purine, ethanol and fructose consumption
Hematologic	Myeloproliferative and lymphoproliferative disorders, polycythemia
Drugs	Ethanol, cytotoxic drugs, vitamin B_{12} (treatment of pernicious anemia)
Miscellaneous	Obesity, psoriasis, hypertriglyceridemia
Decreased renal excretion of urate	
Cause	
Drugs	Ethanol, cyclosporine (Sandimmune), thiazides, furosemide (Lasix) and other loop diuretics, ethambutol (Myambutol), pyrazinamide, aspirin (low-dose), levodopa (Larodopa), nicotinic acid (Nicolar)
Renal	Hypertension, polycystic kidney disease, chronic renal failure (any etiology)
Metabolic/endocrine	Dehydration, lactic acidosis, ketosis, hypothyroidism, hyperparathyroidism
Miscellaneous	Obesity, sarcoidosis, toxemia of pregnancy

The phase of asymptomatic hyperuricemia ends with the first attack of gouty arthritis or of urolithiasis. In most instances gout comes first and usually after at least 20 to 30 years of sustained hyperuricemia.

(b)   Acute Gouty Arthritis:

Acute gout is characterized by the sudden onset of pain, *erythema* (reddening of skin), limited range of motion and swelling of the involved joint. The peak incidence of acute gout occurs between 30 and 50 years of age [81]. Approximately 90 percent of the first attacks are *mono-articular* (pertaining to single joint). In more than one half of patients with acute gout, the first *metatarsophalangeal* (pertaining to metatarsus -five bone of foot between ankle and toes- and phalanges -small bones of fingers and toes) joint is the initial joint involved. Joint involvement (in order of decreasing frequency) includes the metatarsophalangeal joint, the instep/forefoot,

ankle, knee, wrist and fingers. Different interesting surveys and reports are published. Women develop gout at an older age than men and have twice the prevalence of hypertension, renal insufficiency and exposure to diuretics [82]. The onset of gout before 30 years of age in men or before menopause in women is a typical one and raises concern about an associated inherited enzyme defect or renal disease.

(c)   Inter-critical Gout:

Following the recovery from acute gouty arthritis, the patient reenters an asymptomatic phase of the disease. This phase is referred to as *inter-critical gout*. It is during this inter-critical phase, the physician should focus on secondary causes of hyperuricemia. Medications should be assessed to identify those that may aggravate the patient's condition (e.g., diuretics) and dietary education regarding purine-rich foods (which contribute to higher serum uric acid levels) should be provided to the patient at this time. The patient should also be counseled about limiting alcohol consumption and gradually losing weight, if obese.

(d)   Chronic Tophaceous Gout:

Tophi are chalky deposits of sodium urate that are large enough to be seen on radiographs, may occur at virtually any site. The most common sites include the joints of the hands or feet. The helix of the ear, the olecranon (point of elbow) bursa and the Achilles tendon (tendinous termination in to the heel bone) are classic, albeit less common, locations for tophi. Articular tophaceous gout can result in a destructive arthropathy and chronic secondary osteoarthritis. The duration of time between the first gouty attack and recognizable tophaceous disease is highly variable and may range from three to 42 years (mean: 11.6 years) [83]. The rate of urate deposition and, consequently, the rate of tophi formation correlate with the duration and severity of hyperuricemia [84]. Tophaceous disease is more likely to occur in patients having; a

polyarticular presentation, a serum urate level higher than 9.0 mg / dl (535 μmol/l) at a younger age at disease onset, i.e., 40.5 years or younger [85].

Pathogenesis of Gout:

The biochemical hallmark and prerequisite of gout is *hyperuricemia*. The concentration of uric acid in body fluids is determined by the balance between rates of production and elimination of urate. The development of hyperuricemia may be due to an excessive rate of uric acid production, a decrease in the renal excretion of uric acid, or a combination of both events.

Hyperuricemia and gout may be classified as a primary, a secondary, or an idiopathic. Primary hyperuricemia or gout refers to those cases that appear to be innate, that are neither secondary to another acquired disorder nor a subordinate manifestation of an inborn error that leads initially to a major disease unlike gout. Secondary hyperuricemia or gout refers to those cases that develop in the course of another disease or as a consequence of drugs. Finally, idiopathic hyperuricemia or gout represents those cases in which a more precise classification cannot be assigned.
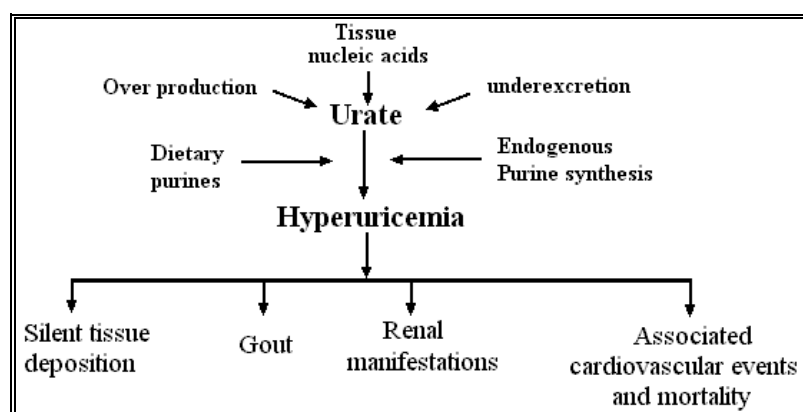
Figure (2.3): The hyperuricemia cascade

The deposition of MSUM crystals in the tissues is the resultant of the raised level of uric acid (urate) in blood and other body fluids, which is called hyperuricemia. Hyperuricemia, as it is already referred quite frequently earlier in this

discussion, is a serum urate concentration in excess of urate solubility (6.8 mg/dl) [86]. The following figure (2.3) shows the cascade of hyperuricemia, and table (2.3) presents the acquired causes of hyperuricemia.

From figure (2.3) one can notice that achieving hyperuricemia is a quite complex process and there are diverse reasons and sources such as, dietary purines, tissue nucleic acids, and endogenous purine synthesis. The over production of dietary purines or under-excretion of endogenous purine synthesis leads to hyperuricemia and, ultimately, leads to many disorders.

Purine Metabolism:

The role of purines in human diseases recognized with the observation that uric acid, the end product of purine metabolism, was a component of some renal calculi [66] and its salt MSUM was present in crystalline form in synovial fluid during the acute attack of gouty arthritis [69].

It is interesting to understand the molecular structure of the parent purine compound. The purine is composed of a six-member pyrimidine ring fused to the five member imidazole ring.
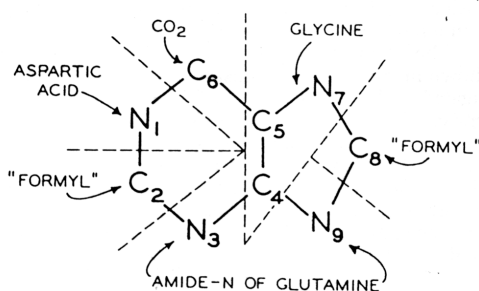
Figure (2.4): Origins of atoms of the purine ring

The origins of individual atoms of the purine ring are as follows.: carbon atoms 4 and 5 and nitrogen atom 7 come from glycine [87-89], carbon atoms 2 and 8 come from formate [89-90], carbon atom 6 comes from CO_2 [88, 91], nitrogen atoms 3 and 9

come from the amide nitrogen of glutamine [92-94], and finally, nitrogen atom 1

comes from aspartic acid [93]. These precursor-product relationships are shown in

figure (2.4).
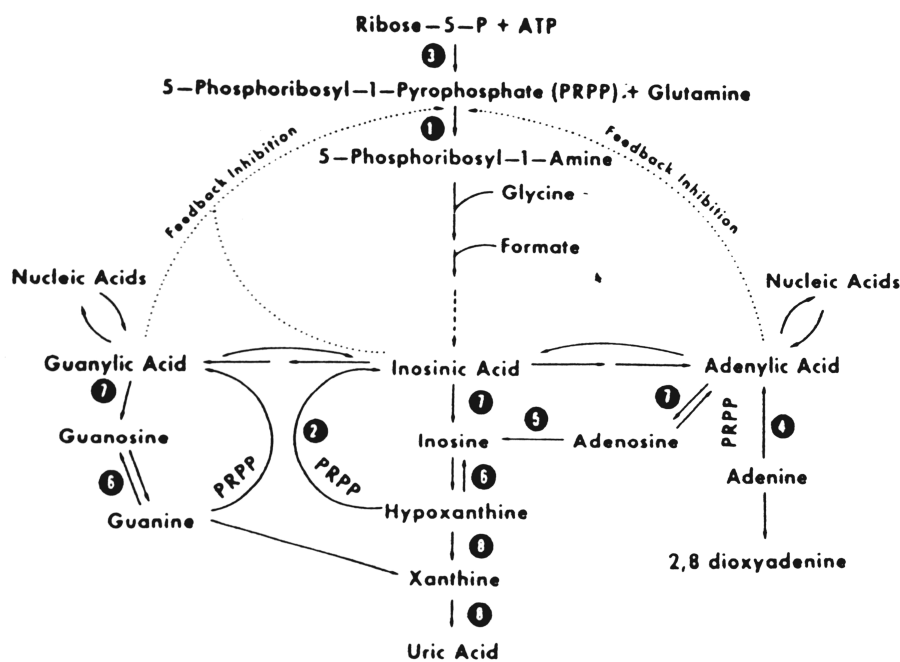
Figure (2.5): Purine metabolism: (1) Amidophosphoribosyltransferase; (2) hypoxanthine- guanine phosphoribosyl transferase; (3) PRPP synthetase (4) adenine phosphoribosyltranferase (5) adenosine deminase (6) purine nucleoside phosphorylase (7) 5'-nucleotidase; (8) xanthine oxidase (From: Seegmiller, J.E. et al.: Science 155 (1967) 1682.)

The purine metabolism and the production of uric acid is quite complex. This

has been presented in the flow chart of figure (2.5). The detailed discussion is avoided

in the present thesis; however, the elaborative discussion is available elsewhere [95].

In about two-third of daily purine load is generated endogenously form turnover of

cells, while one third is delivered from the diet.

Two different mammalian purine phosphoribosyltransferase (formly termed

rebonucleotied Pyrophosphorylases) have been identified: one is adenine

phosphoribosyltransferase (APRT) acting on 4(5)-amino-5(4)-imidazolecarboxamide

AIC and adenine (Reaction-4 in figure (2.5)) [96, 97], and the other one is

hypoxanthine-guanine phosphoribosyltransferase (HPRT) acting on hypoxanthine and guanine (Reaction-2 Figure (2.5)) [98, 99].

Since purine nucleoside phosphorylase acts most readily on inosine and guanosine [100], the major bases generated are very likely hypoxanthine and guanine. Guanine is deaminated to xanthine by guanase as shown in figure (2.5). Hypoxanthine is oxidized to xanthine by xanthine oxidase and then further oxidized to uric acid by the same enzyme (Reation-8). It is the D-form of xanthine oxidase that is responsible for the formation of uric acid as the final metabolic product in human purine metabolism. The enzymes, which convert hypoxanthine to xanthine and, finally, xanthine to uric acid, are shown in figure (2.5) by Reaction-8.

Hypoxanthine + H_2O + 2 O_2 Xanthine + 2O $^{2-}$ + 2H$^+$

Hypoxanthine + H_2O + O_2 Xanthine + H $_2O_2$

Xanthine + H_2O + 2 O_2 Uric acid + 2O $_2-$ + 2H$^+$

Xanthine + H_2O + O_2 Uric acid + H $_2O_2$
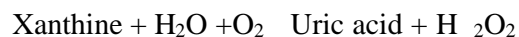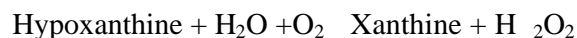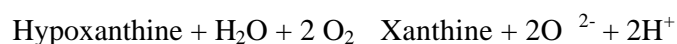
The compounds, O^{2-}, H_2O_2, and OH^{1-} are important mediators of inflammation and tissue destruction.

Treatments and Preventions of Gout:

About 300 years ago, John Locke, a philosopher, proposed a diet, which was low in meat and high in milk, dairy products and herbs as a means to prevent gout [101, 102]. Purine rich food includes animal meats, sea foods and certain plants. By contrast, dairy products, grains and their products, vegetables, fruits, nuts, sugars are low in purines. There are several remedies based on plants such as cherries [103], leaves of *Lagerstroemia speciosa* [104] and certain Northeastern North American plants [105]. A very good editorial has been written recently, by A.G. Fam [106], editor of the Journal of Rheumatology, entitled "Gout: Excess calories, purines and

alcohol intake and beyond response to a urate lowering diet". In this editorial he has discussed critically all the aspects related to gout from the dietary habits, causes to the prevention of gout. Is that the gout is affecting to the gourmands who love rich food, connoisseur of alcohol and sedentary life? A large debate is going on this. Nowadays it is believed that if the attention is paid on to achieving a good diet and regular mild exercise then it is helpful in gout and arthritis [107].

A large number of literatures are available on gout [97, 108-109]. The authors deal with various aspects of gouts and how to tackle it. Hence the detailed discussion is avoided here. However, the *in vitro* growth, characterization and growth inhibition of gout, related MSUM crystals in different herbal extracts solutions will be discussed in Chapter-VI. This inhibition study may be helpful to either prevent or cure the MSUM induced gouty arthritis.

The therapeutic aims in the case of gout are, (1) to terminate the acute attack as promptly as possible, (2) to prevent recurrences of acute gouty arthritis, (3) to prevent or reserve complications of the disease resulting form deposition of sodium urate and /or uric acid crystals in joints, kidneys, or other sites and (4) to prevent or reverse associated features of the illness that are also deleterious such as obesity, hypertriglyceridemia, or hypertention.

Treating gout is also a major challenge. The four treatment options are available for the acute gouty attack, which are NSAIDs, (Non-Steroidal Anti-Inflammatory Drugs), colchicine, corticosteroids and analgesics. Usually, NSAIDs are the preferred therapy for the treatment of patients without complications. Indomethacin (Indocin) was the first NSAID used for gout, but other NSAIDs, including ibuprofen (Motrin), naproxen (Naprosyn), sulindac (Clinoril), piroxicam (Feldene) and ketoprofen (Orudis), are also effective in the treatment of acute gout

[110]. The use of low-dose colchicine as prophylaxis for the prevention of gouty arthritis was first described in 1936 by Cohen [111]. It is common practice among rheumatologists to administer prophylactic or low-dose colchicine (from 0.6 mg to 1.2 mg) and at the same time urate-lowering drug therapy is initiated, but this regimen has not been widely embraced by primary care physicians [112, 113].

After the gouty attack is treated and prophylactic therapy is initiated, the issue of ongoing urate deposition should be addressed. A common practice is not to initiate drug therapy aimed at lowering urate levels after the initial attack. Rather, most clinicians prefer to aggressively correct or reverse sources of hyperuricemia in hopes of lowering the serum urate level without the use of medication. Sulfinpyrazone (Anturane), Probenecid (Benemid) and Allopurinol (Zyloprim) are well established indications for the use of urate-lowering agents.

However, it is worthy to mention that colchicines has draw backs, which includes slow on set of action, narrow ratio of benefit to toxicity and reduced efficiency when used for more than 24 hrs. After the attack begins, conventional NASAIDs exerts their anti-inflammatory effects mainly through inhibition of the enzymes Clyclo-oxygenase, which catalyses the conversion of arachidonic acid to pro-inflammatory prostaglandins particularly prostaglandin E_2. Conventional NASIDs inhibits both cyclo-oxygnase-1 (COX_1) and cyclo-oxygenase-2 (COX_2). Their anti-inflammatory effects are largely due to suppression of COX_2, and most adverse effects, particularly gastrointestinal toxicity, results from inhibition of cyclo-oxygenase-1 (COX_1). New NASIDS such as celecoxib, refecoxib, valdecoxib, etc. are highly COX_2 selective [114]. Very recently, the prophylactic effect of highly selective COX_2 inhibition in acute MSU crystal induced inflammation in the rat subcutaneous (beneath the skin) air pouch has been reported by Nalbant et al [115].

Nevertheless, the present authors has grown and characterized MSUM crystals and studied the *in vitro* growth inhibition of the crystals in the presences of different herbal extracts. Further, the collaborators have adopted, more-or-less, the same technique as reported by Nalbant [115] to study the prophylactic use of these herbal extracts on animals to find out the pre-clinical formulations. This has been reported elsewhere [116]. The *in vitro* growth inhibition of MSUM crystals will be discussed in chapter- VI.

2.2.3. Calcium Pyrophosphate Crystal-Associated Arthropathy:

With the use of skeletal radiography, it became apparent that articular (pertaining to joints) cartilage calcification (chndrocalcinosis-CC) was a common phenomenon occurring either alone or in association with arthritis. Clinical and pathologic diversity was first emphasized by Mandl in 1927 [117]. The major milestone was achieved to identify urate crystals in gout, using compensated polarized microscopy, by McCarty and Hollander [118] in 1961. Within a year McCarty and colleagues [119] discovered the non-urate crystals, identified by X-ray diffraction as calcium pyrophosphate dihydrate (CPPD) ($Ca_2P_2O_7 \cdot 2H_2O$), in the knee fluids from patients with acute synovitis (inflammation of synovial membrane) and CC. However, the clinical similarity to gout prompted the term *pseudogout*. Cadaveric studies subsequently established CPPD as the most common but not exclusive cause of knee CC. However, CPPD is also associated with the subacute and chronic arthritis. To make this simple, McCarty [120] designated the total disease state associated with CPPD crystal deposition as calcium pyrophosphate deposition disease (CPDD). The term *chondrocalcinosis* is still widely used, although it lacks the specificity of nomenclature defined on the basis of crystal type. Pyrophosphate arthropathy (PA) is

a nosologically attractive term that can be modified to define acute and chronic disease manifestation [121]. The following definitions are used nowadays [122]:

- **Chondrocalcinosis** – the calcification of articular fibro- or hyaline (transparent) cartilage.

- **Pyrophosphate arthropathy** – the structural cartilage and bone abnormality (identical to osteoarthritis-OA) associated with intra-articular CPPD deposition.

- **Pseudogout** - the clinical syndrome of acute synovitis associated with intra-articular CPPD deposition.

The CPPD crystal deposition disease is usually idiopathic (spontaneous origin) and presents as sporadic episodes in the majority of patients. There are rare familial forms of the disease and its association with some metabolic disorders-such as hyperparathyroidism (over action of the parathyroid glands with increase in serum calcium level), haemochromatosis (a congenital error in iron metabolism with increased iron deposition in tissues), hypercalcaemia (and perhaps other hypercalcaemic states), diabetes mellitus (a condition characterized by hyperglycaemia due to deficiency of insulin) and hypomagnesaemia (decreased magnesium in the blood) [123, 124]. It has been noted that the treatment of osteoarthritis (OA) of the knee with intra-articular injections of hyaluronic acid preparations (such as Hylan GF-20) are associated with triggering of an acute attack of pseudo gout [125].

The CPPD crystal associated disease is clinically heterogeneous and may cause both an acute or chronic arthritis.

Acute Synovitis (Pseudogout):

Generally, CPPD deposition disease presents early onset (<50 yrs) with acute presentation. The knee is by far the commonest site followed by wrist, shoulder, ankle and elbow. A typical attack develops rapidly with severe pain, stiffness and swelling, maximum within 6-24 hours of onset. Overlying erythema is common and examination reveals a tender joint held in the loose pack position with signs of marked synovitis. Acute attacks are usually self-limiting and resolve within one to three weeks. The most pseudogout episodes are developed spontaneously.

Chronic Pyrophospahte Arthropathy:

This common condition is generally belongs to elderly (<50 yrs) male and female. Large and medium size joints are mainly affected, again the knee being most common, followed by wrists, shoulders, elbows, hips and mid-tarsal joints. In hand, the metacarpophalangeal joints, particularly the second and the third, are the most common and most severely affected. Presentation is usually with chronic pain, inactivity, stiffness, limitation of movement, and functional impairment. Affected joints usually reveal signs of OA (bony swelling, crepitus, restricted movement) with
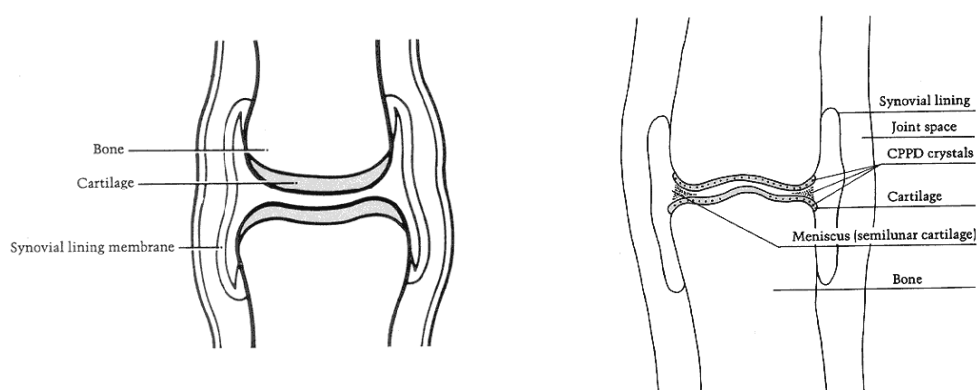
Figure (2.6): (a) Normal Joints and (b) after deposition of CPPD crystals [126]

varying degrees of synovitis. Typically, knees show bi or tri-compartmental disease with marked or predominant patella (knee cap bone)-femoral (thigh bone) involvement.

Tophaceous CPPD deposition is very rare, but reported in intra-or peri-articular (surrounding joints) sites that include the elbow, finger joints, acromio-clavicular joint (joint of summit of shoulder and collar bone) and hip. Most commonly it arises at sites of chondroid metaplasis in subjects with no CC, elsewhere. CC is one of a family of conditions associated with ectopic (mal-position of organ) mineralization. This family also includes disorders of mineralization of bone, spinal and other ligaments and vascular calcification. The key role of transport and metabolism of inorganic pyrophosphate (PPi) in control of mineralization has the likely explanation for the association of a variety of genetic variants with CC and ectopic mineralization. Genetic study of CC has been reported by Zhang and Brown [127] very recently.

Factors Affecting Etiology of CPDD:

There are several factors affecting the etiology of CPPD related disease or CC. These factors are summarized as follows.

Ageing

Ageing is a major predisposing factor to CC. The synovial fluid from normal knees shows no increase in inorganic pyrophosphate (PPi) levels with age, therefore, favoring age-related alterations in cartilage matrix poses as the principal cause [128].

Familial Predisposition

A primary cartilage abnormality (reduction in proteoglycan, increase in phospholipid) is suggested by histological (microscopic study of tissues) studies of Swedish and Japanese families [129, 130]. A generalized abnormality of PPi

metabolism is reported in French and American kindred [131]. Genetic linkage to chromosome 5p has been identified in one UK family [132]. It seems likely that different mechanisms operate in different families, resulting in wide variations in phenotypic expressions.

Metabolic Predisposition

The PPi metabolism has important role to play. Associations with metabolic disease can be rationalized through effects on PPi metabolism as briefly mentioned in the following points:

- Reduced breakdown of PPi by alkaline phosphatase (enzyme) due to reduced levels (or hypophosphatasia), presence of inhibitory ions (calcium, iron or copper in hyperparathyroidism, haemochromatosis and Wilson's disease, respectively) and impaired complexing with magnesium (hypomagnesaemia).

- Enhanced nucleation of CPPD crystals by increased iron (haemochromatosis), or copper (Wilson's disease)

- Increased PPi production through para-thyroid hormone (PTH) stimulation of adenylate cyclase (hyperparathyroidism).

This has been discussed in detail by Wright and Doharty [133] elsewhere.

Mechanisms of CPPD Crystal Formation

It is already discussed that the PPi metabolism is very crucial for the CPPD crystals. This PPi is produced as a byproduct of multiple intra-cellular biosynthetic reactions throughout the body [131]. Despite a very high turnover, both intra- and extra-articular concentrations are maintained at, generally, low levels by ubiquitous pyrophosphatases which metabolize PPi (complexed to magnesium) to orthophosphates. Numerous biological roles for PPi are now recognized [128] and an

important role in locomotors tissues (tissues used in movement) is modulation of mineralization (principally apatite).
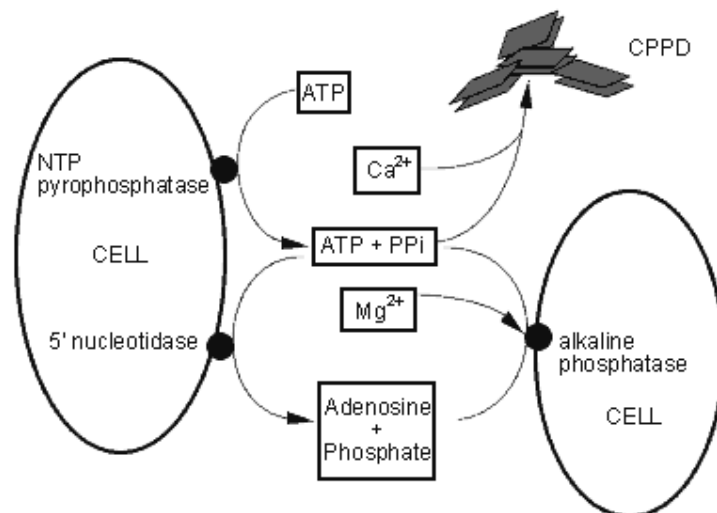
Figure (2.7): Outline of main factors relating to extra cellular pyrophosphate

metabolism

By and large the source of extra-cellular PPi still remains uncertain. Since the substrates for its formation are nucleoside triphosphates (NTP), virtually all PPi derived from NTP-dependent biosynthetic reactions. Probably, it originates extra-cellularly as PPi, being a phosphate ester, cannot cross cell membranes. No active or facilitative transport mechanism for PPi has been demonstrated at the cell surface, although some NTP may reach the extra-cellular space during cell division and injury. Several cells, including chondrocytes, possess ecto-enzymes (NTP pyrophosphatase) that convert leaked NTP to nucleosides and the extra-cellular PPi. The extra-cellular PPi, complexed with magnesium, is then rapidly broken down to orthophosphate, which crosses cell membranes by surface alkaline phosphatase. An outline of the main factors relating to extra-cellular pyrophosphate metabolism is shown in figure (2.7). The extra-cellular ATP, a major substrate for PPi, has been confirmed in

synovial fluid, with higher levels in pyrophosphate arthropathy than OA or rheumatoid arthritis [131]. Chondrocytes appear to be the principal source of increased intra-articular PPi.
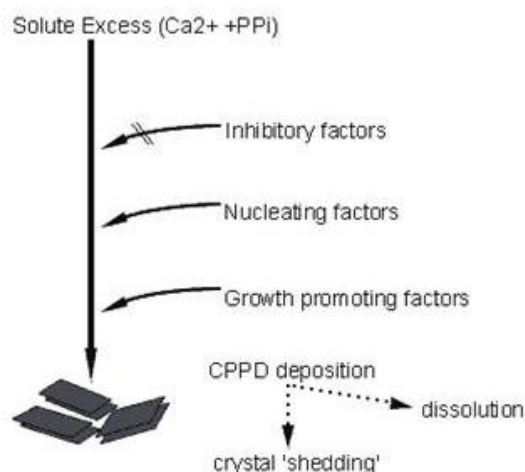
Figure (2.8): Factors influencing the CPPD crystal formation

The CPPD formation appears to be restricted principally to fibro and hyaline cartilages and less commonly to capsule or tendon. The factors likely to affect the formation, growth and dissolution of CPPD crystals are outlined in figure (2.8). Unlike urate crystals, they require exact physiochemical conditions for the formation and the current knowledge is derived from the model systems and the following generalities appear to be true. Many models have been proposed and most knowledge derives from model systems employing gels (non-biological, gelatin or native collagen gels). From these the general remarks can be made as follows [133].

- In addition to the product, $Ca2^+$ x PPi, local magnesium concentration is important and influences CPPD deposition by inhibiting nucleation and growth, and enhancing dissolution. Orthophosphate, chondrotin sulphate, and proteoglycan are inhibiting the nucleation and growth. With proteoglycan this effect depends on the spatial arrangement of carboxylate ligands, which may operate via calcium

binding or spatial regulation of Mg^{++}, phosphate or unidentified small molecular weight promoters and inhibitors.

- Conversely, nucleating and growth promoting factors include ions ($Fe^{+3} > Fe^{+2}$) and seeded MSUM crystals. However, seeded apatite has little epitaxial effect but it efficiently traps PPi leading to more stable CPPD growth. Moreover, a possible promoting role of collagens and acidic phospholipids requires further study and confirmations.

- Formation CPPD crystal is slow, usually, occurring via intermediate crystal species, that transform in to the more triclinic.

Histological studies suggest that CPPD crystals form in peri-cellular sites, principally, in phospholipid-rich articular chondrocyte vesicles (akin to matrix vesicles of immature cartilage) in the mid-zone of fibro- and hyaline cartilage [130]. A close association is reported with hypertrophic (increase in the size of tissue or structures) or metaplastic chondrocytes, the surrounding matrix often being proteoglycan depleted and degenerative. These findings support the importance of tissue (*soil*) factors, implying that reduction of inhibitors (e.g. proteoglycan) and increase in promoters (e.g. lipid) combine to co-promote CPPD crystal formation. Conversely, elevation of synovial fluid PPi, consequent upon increased release and breakdown of NTP from the hypertrophic metabolically active chondrocytes, favors a *seed* component. The relative importance of these multiple factors will vary in different clinical settings.

Concurrent deposition of CPPD and apatite crystals is common. This is probably explained by epitaxial growth (one type of crystal seeding and growth of another on its active surface) and the fact that modest increase in PPi concentration

stimulates apatite formation; although, paradoxically, very high concentrations of PPi inhibit apatite formation and growth.

'Crystal shedding' is the mechanism which appears to explain the occurrence of CPPD within synovial fluid [134]. Shedding occurs due to reduction in crystal size, fissuring of cartilage, or alterations in cartilage matrix that facilitate crystal escape. Direct evidence of shedding comes from reduction in radiographic CC during pseudo-gout attacks and during follow-up of chronic pyrophosphate arthropathy patients [135]. Shedding from cartilage deposits may expose previously protected, but now *naked* (non-protein coated) crystals to soluble inflammatory mediators and cells, thereby, triggering acute attacks.

Treatments:

The aims of management are identical to those for osteoarthritis, specifically, (1) to educated the patient, (2) to reduce pain and stiffness and (3) to maintain or improve function.

Management of Acute Pseudo-gout:

For the management of pseudo-gout, NSAIDs may be helpful to reduce symptoms but should be used with caution in elderly and medically unfit patients; simple analgesics are often adequate. Oral colchicine is also effective but rarely required.

Chronic Pyrophosphate Arthropathy:

Unlike gout, there is no specific therapy. Simple analgesics and topical NSAIDs are safe and often effective and they should be tried first; moreover, combined analgesics and oral NSAIDs may be more effective but their use is limited by side-effects. Intra-articular steroid injection may temporarily improve symptoms. Intra-articular radio-colloid may be considered in patients with troublesome knee or

shoulder synovitis who show definite but temporary improvement following steroid injection; however, the benefit may last months rather than just weeks. Patients with progressive or destructive large joint arthropathy appear to derive benefit from surgery equal to the patients with uncomplicated OA.

Several attempts have been made to study the dissolution of CPPD crystals, which are very important to design various drugs to dissolve crystals. Shinozaki and K.P. Pritzker [136] reported that polyamines enhanced CPPD crystal dissolution. They found that alkaline phosphatase (ALP), an enzyme, with pyrophosphatase actively dissolved CPPD crystals. Earlier, Xu et al. [137] already studied the effect of pyrophosphatase on dissolution of CPPD crystals. In comparatively recent study, Cini et al. [138] have reported dissolution of calcium pyrophosphate crystals by polyphosphates *in vitro* and *ex vivo* study. Linear potassium triphosphate, cylic trisodium metaphosphate and polymeric sodium exhibited ability to dissolve synthetic CPPD and crystalline aggregates of menisci from patients with CC. They concluded that polyphosphates were effective in dissolving CPPD. However, no major work is reported on dissolving CPPD crystals using herbal extrects.

There is good number of review articles and monograms on CPPD induced arthropathies. Update on pathogenesis, clinical features and therapy for CPPD induced arthropathies are reported by Hang-Korng and Liote [139]. An overview on crystal induced arthritis by Gupta [9] includes detailed accounts of CPPD induced arthritis. Wheeless textbook on orthopaedics [140], the Merck manual [141] and crystal related arthropathies [133] also deal with CPPD induced arthropathy in detail.

In the present study, the calcium pyrophosphate (CPP) crystals have been grown by using the single diffusion gel growth technique and characterized by various techniques. Several herbal extracts were used to study the inhibitive effect on the

growth of CPP crystals. This will be discussed in Chapter-VII. The author, hereby, focuses on the other crystal related ailment in the following part of this chapter, which are the urinary stone problems.

2.3   Urinary Stone Problems:

The urinary stones, usually known as renal calculi, kidney stones, nephrolithiasis, urolithiasis, concentration or concernments, are solid masses of sediments formed in some part of the urinary tract. The urinary calculi are among the oldest afflictions of man [10] and even of animals [142]. A first bladder stone was found in an Egyptian mummy, which was first reported by Elliot [143]. The mummy was of sixteen-year-old boy who probably lived seven thousand years ago. In India, the earliest Sanskrit documents like the *Vedas*, the *Puraòas* and the *Samhitâs* also described urinary stone and their remedies [144]. The *Charak Samhitâ* contains sufficient but scattered matter pertaining to anatomy, physiology and pathology of *Mutrava ha aºmari* as well as the diagnosis and treatment of its disorders. The *Susruta Samhitâ* is the pioneer text in surgery and it contains more descriptive explanations as far as the anatomy and physiology of *Mutrava ha aºmari* is concerned. The *Aºamari Nidâna* chapter provides a scientific description.

Nowadays, urinary calculi are common in all regions of the world, and the occurrence in some areas is so alarming that they are known as "stone belts" [145]. There are many areas of high incidence of urinary calculi which include British Isles, Scandinavian countries, Northern Australia, central Europe, northern India, Pakistan and Mediterranean countries [10]. Saurashtra region of Gujarat state has higher prevalence of urinary stones.

Calcium stones are the most common comprising of 75% of all urinary stones and majority of them are of calcium oxalate monohydrate (COM or *whwellite*) or

calcium oxalate dihydrate (COD or *weddelite*). Generally, urinary stones are formed as pure calcium oxalate (50%) and pure calcium phosphate (5%), or as mixtures of calcium oxalate and calcium phosphate (45%). Usually, oxalate, phosphate, uric acid and urate crystals are found in urinary stones [10], which are compiled in Table (4).

Table (2.4)

The crystalline components of urinary stone [10]

Compounds		Mineralogic Name	Formula
Oxalates	Calcium Oxalate Monohydrate	Whewellite	$CaC_2O_4 \cdot H_2O$
	Calcium Oxalate Dihydrate	Weddellite	$CaC_2O_4 \cdot 2H_2O$
Phosphates	Hydroxyapatite	Hydroxyapatite	$Ca_{10}(PO_4)_6(OH)_2$
	Calcium Hydrogen Phosphate Dihydrate	Brushite	$CaHPO_4 \cdot 2H_2O$
	Tricalcium Phosphate	Whitlockite	$Ca_3(PO_4)_2$
	Magnesium Ammonium Phosphate Hexahydrate	Struvite	$MgNH_4PO_4 \cdot 6H_2O$
	Magnesium Hydrogen Phosphate Trihydrate	Newberyite	$MgHPO_4 \cdot 3H_2O$
	Carbonate Apatite	Carbonate apatite	$Ca_{10}(PO_4,CO_3,OH)_6(OH)_2$
	Octacalcium Phosphate	-	$Ca_4H(PO_4)_3 \cdot 2.5 H_2O$
Uric Acid	Uric Acid Anhydrous	-	$C_5H_4N_4O_3$
	Uric Acid Dihydrate	-	$C_5H_4N_4O_3 \cdot 2H_2O$
Urates	Ammonium Acid Urate	-	$C_5H_3N_4O_3NH_4$
	Sodium Acid Urate Monohydrate		$C_5H_3N_4O_3Na \cdot H_2O$

2.3.1   Etiology of Urolithiasis:

Many investigators tried to understand the causes of stone formation. Generally, the etiology or aetiology (study of causes of disease) of urinary stones is categorized as follows [10]:

(1) Age, (2) Genetic disorder, (3) Occupation, (4) Climate, (5) Metabolic disturbances, (6) Presence of infections, (7) Dietary Patterns, and (8) Amounts of water consumed.

The age and sex of the patients is found to be important in the stone formation. As per one study, the peak incidence of urinary calculi occurs in the twenties to forties [146-149]. Several disorders that cause renal stones are hereditary. Familial *renal tubular acidosis* (RTA) is associated with nephrolithiasis and *nephrocalcinosis* in almost 70% of patients [150].

Water intake and dietary patterns also play an important role in formation of urinary stones. Water diuresis reduces the average time of residence of free crystal, particles in urine and dilutes the components of urine that may crystallize. Finlayson [145] conclude that the dilution effects of water diuresis out-weigh the changes in ion activity and, therefore, do help to prevent stone formation. Sierakowski et al. [151] state that excessive water hardness causes a greater incidence of stone disease. Dietary intake of various foods and fluids that result in greater urinary excretion of substance that produce stones has a significant effect on the incidence of urinary calculi. Ingestion of excessive amounts of purines [152], oxalates [153], calcium phosphate and other elements often results in excessive excretion of these components in urine. This is ultimately expected to affect the probability of incidence of urinary calculi.

2.3.2 Theories of Growth of Urinary Calculi:

In general, stone formation requires supersaturated urine. Super-saturation depends on urinary pH, ionic strength, solute concentration and complexation. Ionic strength is determined primarily by the relative concentration of mono-valent ions. As ionic strength increases, the activity coefficient decreases. The activity coefficient

indicates the availability of a particular ion. The greater the concentration of two ions, the more likely they are to precipitate. Low ion concentrations result in under-saturation and increased solubility. Other factors also play major roles in the development of urinary calculi, which includes complexation. Complexation influences the availability of specific ions. Crystal formation is modified by a variety of other substances found in the urinary tract including magnesium, citrate, pyrophosphate and a variety of trace metals. These may act at the active crystal growth sites or as inhibitors in solution. The nucleation theory suggests that urinary stones originate from crystals or foreign bodies immersed in supersaturated urine. This theory has some drawbacks. Stones do not always form in patients who are hyper-excretors or who are at risk for dehydration.

While, the crystal inhibitor theory proposes that calculi form due to the absence or low concentration of natural stone inhibitors including magnesium, citrate, pyrophosphate, glycoprotein and a variety of trace metals. This theory, however, does not have absolute validity since many people lacking such inhibitors may never form stones and others with abundance of inhibitors may, paradoxically, form them.

Broadly speaking, multiple steps are involved in crystal formation, including nucleation, growth and aggregation. Nucleation initiates the stone process and may be induced by a variety of substances including proteinaceous matrix, crystals, foreign bodies and other particulate tissues. This *Heterogeneous nucleation* requires less energy and may occur in less saturated urine, which is a common theme in stone formation. A crystal of one type, thereby, serves as a nidus for the nucleation of other types with a similar crystal lattice [154].

An attractive theory for the origin of primary renal calculi was proposed by Randall [155]. Randall's plaque theory is based upon a submucosal lesion (below

mucous membrane) of unknown nature in the renal papilla that is exposed to urine by erosion of the overlying epithelium, urinary salts are deposited on the resultant plaque and augmented by accretion. The deposit eventually breaks away as a free calculus. Such a calculus has a definite indentation where it has grown, as if molded over the papilla. A small, shallow, rough depression near the center of the indentation is indeed often seen and is the point of attachment according to Randall's theory.

In normal urine, the concentration of calcium oxalate is four times higher than its solubility. Low urinary volumes, high rates of calcium oxalate, phosphate or urate excretion and low citrate and magnesium excretion all increase calcium oxalate super-saturation. Ones calcium oxalate concentration becomes more than the critical super-saturation, K_{sp}, the crystallization takes place. Because of inhibitors and other molecules, calcium oxalate precipitation in urine occurs only when its super-saturation is seven to eleven times its solubility. The process, where nuclei form in pure solution, is known as *homogeneous nucleation*. The crystals grow further on these nuclei. This will be discussed in somewhat details in Chapter- VIII.

Another concept developed to understand the genesis of urinary calculi is of aggregation. Crystal nuclei can not grow large enough to attach to and occlude renal tubular lumens within the five to seven minutes, that it takes them to pass through tubules and enter the renal pelvis. Nevertheless, they can aggregate into large lumps within a minute [156]. Therefore, the crystal growth alone cannot explain clinical stone diseases, a combination of *growth and aggregation* both are needed. Magnesium and citrate are expected to inhibit crystal aggregation. Nephrocalcin, an acidic glycoprotein of renal origin, also inhibits calcium oxalate nucleation, growth and aggregation [157, 158]. Interference with crystal growth and aggregation is a major therapeutic strategy for the prevention of recurrent stone disease.

However, the standard laws of the physical chemistry of crystallization can explain the occurrence of crystals in a static solution. But normal urine is not a static solution, it flows continuously and new solutes are added and subtracted from the solution. The point of greatest super-saturation is usually the renal papilla [159]. The lumen of the nephron at the level of collecting duct is 50 to 200 ìm. A newly formed crystal within nephron needs time from ninety to fifteen hundred minutes to grow to a diameter of 200 ìm at levels of conventional urinary super-saturation. Although, crystal aggregation can result in urinary microliths large enough to occlude collecting ducts, in many cases, this mechanism is not enough to explain the genesis of renal calculi. Thus, factors must exist that causes crystals to remain within the kidney. If a crystal mass is lodged in a renal papilla or tubul, it is no longer allowed to move through the system. Thus, if a crystal is retained in a kidney, growth can occur for long periods of time whenever urinary super-saturation or aggregation of new crystals occurs. It has been found that many kidney stones have a layered structure, which suggests intermittent growth during the periods of super-saturations. There are many theories of crystal growth and still new theories are being proposed. The present author deals with the growth inhibition of urinary type only calcium hydrogen phosphate dihydrate CHPD) crystals by weak organic acids, i.e., citric acid and tartaric acid, which are found in many fruits and natural food products. This study is carried out on the macro size and micro size CHPD crystals to further augment the inhibition theory in the *in vitro* conditions, which is discussed in detail in Chapter-VIII.

In general, the theories of urolithiasis are as follows; (1) Nucleation theory, (2) Crystal inhibition theory, (3) Epitaxy, heterogeneous nucleation theory,

(4) Mass precipitation theory (Intera-nephronic calculosis), (5) Fixed particle hypothesis, (6) Randall's theory, and (7) Carr's hypothesis.

Altogether, five common basis of etiology of urinary stones are mentioned as follows:

(1) Super-saturation / Crystallization theory, (2) The matrix nucleation theory, (3) Inhibitor absence theory, (4) Epitaxy, and (5) Combination of super-saturation and inhibitor absence theory.

2.3.3 Inhibitors and Promoters of Urinary Calculi:

Urine is having several substances that change or modify crystal formation [160-163]. These can further be divided into inhibitors, complexers and promoters. Urinary inhibitors attach to growth sites on crystals, retarding further growth and aggregation. Urinary inhibitors can be organic or inorganic.

In urine, inhibitors have been identified for the calcium phosphate and calcium oxalate crystal systems, but not the urate systems. Magnesium citrate, pyrophosphate and nephrocalcin make up the most of the inhibitors for the calcium phosphate crystal system [164].

Inhibitors of calcium oxalate crystal formation present in urine include citrate, pyrophosphate, glycosaminoglycans, RNA fragments and nephrocalcin, with much of the inhibition is exhibited from large molecular weight compounds [163, 165].

Two urinary glycoproteins, namely, nephrocalcin and Tamm-Horsfall glycoprotein are potent inhibitors of calcium oxalate monohydrate crystal aggregation [158]. Another important inhibitor of calcium oxalate crystal growth present in urine is uropontin [166]. These substances are listed in table (2.5).

Table (2.5)

Inhibitors of Crystallization

Ionic:	Low molecular weight, macromolecules.
Magnesium:	Tamm Horsfall, glycoprotein, citrate, glycosaminoglycans, phosphocitrate, Nephrocalcin pyrophosphate, Uropontin (Osteopontin), Tartrate Bikunin (Inter inhibitor of tripsin), Calgranulin, (Calprotectin), Urinary prothrombin fragment- 1.

.

Certain substances that form soluble complexes with the lattice ions of specific crystals, such as, calcium oxalate, decrease the free ion activity of that ion and effectively decrease the state of saturation for that ion system. Citrate is known to be the most potent complexor of calcium and gives its maximum effect at a pH of 6.5. In the calcium oxalate system magnesium forms soluble complexes with oxalate by complexation. This way, both citrate and magnesium act not only as inhibitors, but also as complexors [167-170].

A third type of substance act as a promoter of crystal formation. Sometimes, a substance may promote one stage of crystal formation such as growth and inhibit another stage such as aggregation. For example glycosaminoglaycans promote crystal nucleation but inhibit crystal aggregation and growth [171]. The effect of different additive solutions and fruit juices as an inhibitor or promoter in urinary crystal growth system will be discussed in detail section 8.3 of Chapter -VIII.

2.3.4 Calcium Phosphate Stone Formation:

The metabolism of calcium oxalate, brushite and struvite stone formation is discussed in detail by Menon et al [10]. Inasmuch as the present author deals with the

growth and inhibition of macro size and micro size CHPD crystals in this thesis, the discussion on metabolism of other stones except the phosphate stones is avoided.

Calcium phosphate stones occur only when the chemical pressure of respective ions for crystallization is quite high and hence, generally, seen in active stone disease [172]. Calcium phosphate stones mainly occur due to the renal tubular acidosis (RTA), hyperparathyroidism (HPT), hypercalcuria, hyperphosphaturia, hypocitraturia, urinary tract infection, urinary tract dysfunctions [173].

The RTA is a clinical syndrome that results from specific defects in renal tubular H^+ secretion and urinary acidification. If the kidneys lose some of their ability to lower urinary pH, the resulting higher pH increases the divalent and trivalent forms of phosphate, which raises calcium phosphate super-saturation [174].
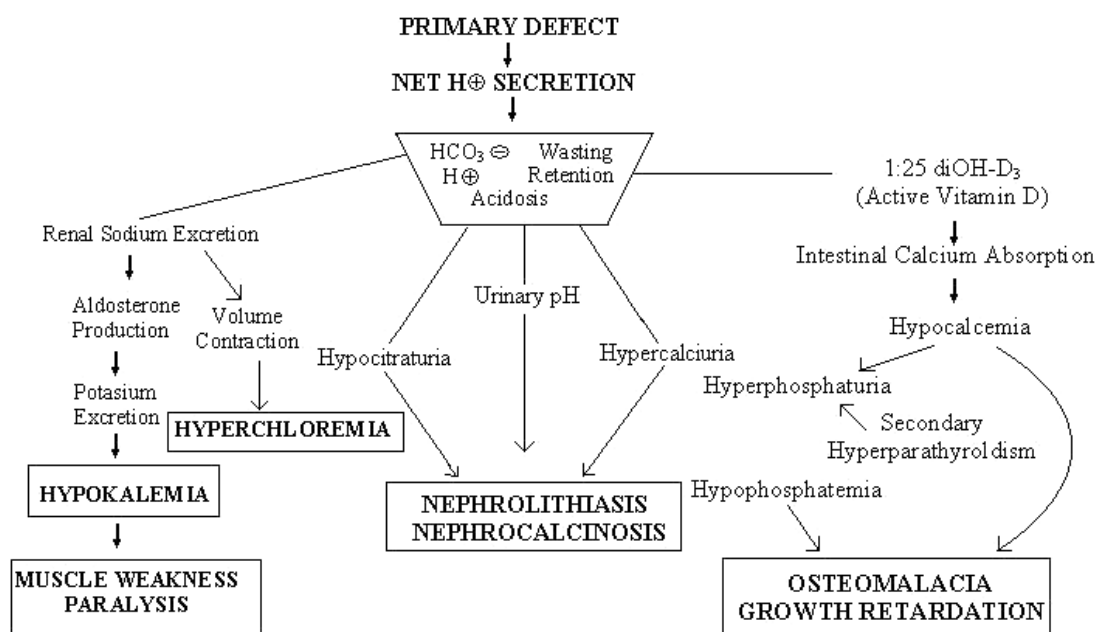
Figure (2.9): Pathophysiologic mechanisms for Type-I RTA (Distal) and metabolic abnormalities that produce the clinical syndromes seen in renal tubular acidosis.

Three major type of RTA are currently recognized; (1) Type-I RTA (Distal), (2) Type-II RTA (Proximal RTA) and (3) type-III RTA. Carunana and Buckalew [175] have reported that up to 70% of adults with distal RTA (Type-I) had urinary stones. Figure (2.9) shows the physiologic basis for the features seen in patients with distal RTA (Type-I).

Stone formation is the result of hypercalciuria, hypocitraturia and increased urinary pH. Hypercalciuria is the result of the effects of systemic acidosis on bone demineralization and secondary hyperparathyroidism as a result of decreased production of 1, 25-dihydroxyvitamin D_3. Hypocitraturia results from a primary defect in renal tubular citrate transport, again, that is the result of metabolic acidosis. Urinary citrate levels may be less than 50 mg per 24 hours in the presence of systemic acidosis [176]. Systemic acidosis increases trans-mitochondrial citrate transport and mitochondrial citrate metabolism [177]. Hypocitraturia is probably the most important metabolic factor for stone formation in patients with type- I RTA.

Table (2.6)

Causes of hypocitraturic calcium nephrolithiasis

Distal renal tubular acidosis

    Complete

    Incomplete

Chronic diarheal syndrome

Thiazide-induced hypocitraturia

Idiopathic

    Diet high in animal protein

    Strenuous physical exercise

    High sodium intake

    Active urinary Tract infection

    Intestinal mal-absorption of citrate

Hypocitraturia has been reported in 15% to 63% of patients with nephrolithiasis [148, 178]. In about 10% of patients, hypocitraturia exists as an isolated anomaly; in the rest it coexists with other metabolic abnormalities [178, 179]. Scott et al [180] have reported the role of citric acid in urolithiasis but much of the understanding about hypocitraturic calcium nephrolithiasis comes from the work of Pak and colleagues [148, 181 and 182]. Causes of hypocitraturic calcium nephrolithiasis are outlined in Table (2.6). Acidosis is probably the most important etiology factor in hypocitraturia.

The primary mechanism of action of citrate is as a complexing agent for calcium. Calcium citrate complexes are considerably more soluble than calcium oxalate or calcium phosphate. In addition, citrate inhibits the spontaneous nucleation, growth and aggregation of calcium oxalate as well as calcium phosphate crystals [183, 184] Tiselius and colleagues [185] demonstrated the physiologic concentrations of citrate inhibited calcium oxalate monohydrate sedimentation and aggregation.

The development of stones in the urinary tract is a complex, poorly understood multi-factorial process. A number of chemical and physical factors are known to play their roles. Several attempts have been made later on in the present millennium to study the crystallization of calcium oxalate and other urinary systems *in vitro* with help of thermodynamics and computer modeling. Thermodynamic modeling has been given by Königsberger and Königsberger [186] of various crystal depositions in human. The same authors have suggested through the computer simulation that a large consumption of pure water is not helpful for the treatment of calcium oxalate monohydrate (COM) crystals, because it does not significantly reduce the super-saturation of COM in urine. A relatively high intake of fluid containing complexing agent, such as magnesium, would be a better choice for reduction of super-saturation.

In another study, the effect of seed crystals of hydroxyapatite and brushite on the crystallization of calcium oxalate in undiluted human urine *in vitro* is reported by Grover et al [187] in terms of implications for urinary stone pathogenesis. *Prothrombin* is precursor of *thrombin* formed in liver. Effect of prothrombin and its activation fragments on calcium oxalate crystal growth and aggregation in undiluted human urine *in vitro* has been reported by Grover and Ryall [188] by keeping in view the relationship between protein structure and its inhibitory activity.

Moreover, the role of so-called nano-bacteria has been explored in the formation of urinary stones. Some nano-bacteria were found in kidney stones and have been claimed to induce calcification in urine that eventually lead to urolithiasis. [189]. A new method is proposed by Aoki and Yokoyama [190] of using a bacterium for dissolution of urinary stones.

As mentioned earlier the effect of as an inhibitor on urinary crystal growth will be discussed in section 8.3 of Chapter -VIII.

Several authors have written detailed reviews on the etiology, epidemiology, constitutions, theories, therapies, medical managements and metabolic factors of urinary stones. The predecessors of the present author [191, 192] have written detailed reviews on urolithiasis, therefore, it is avoided in greater details in the present thesis. Also they have dedicated their thesis on growth inhibition studies.

References:

[1]   A. A. Chernov; *Crystallization Physics and Biomacromolecular Systems,* ISSCG-12, August 1-7, 2004, Berlin

[2]   A. A. Chernov; *J. Struct.Biol.***142** (2003).

[3]   S. Veesler; *Growth of Biological Crystals,* ISSCG-12, August 1-7, 2004, Berlin.

[4]   L. Addadi and S. Weiner; *Nature N & V,* **411** (2001) 735.

[5]   M. Aizawa; *Bio-nanotechnology/ Nano-biotechnology Challenges for Intelligent Materials and S,ystems.* ICMAT-2005, July 3-8, 2005 , Singapore.

[6]   J. Y. Ying, *Nanostructured Processing of Advanced Biomaterials*, ICMAT-2005, July 3-8, 2005, Singapore.

[7]   C. Ray, C. Combes, C. Drouet, H. Sfihi and A. Barroug; *Physico- chemical Properties of Nano-crystalline Apatites*, ICMAT-2005, July 3-8, 2005, Singapore.

[8]   K. Vainio; *Abbottempo,* **4** (1970) 22.

[9]   S. J. Gupta; *J. Indian Rheumatol Assoc.,* **10,** (2002), 5-13.

[10]   M. Menon, B. G. Parulkar, and G. W. Drach; *Campbell's Urology*, W. B. Saunders, New York, 9th Edition, (1998), Vol.3, pp. 2662 – 2676.

[11]   T. M. G. Chu, S. J. Hollister, J. W. Halloran, S. E. Feinberg and D.G. Orton; *Ann.N.Y. Acad. Sci.* **961** (2002) 114.

[12]   J. Arendes, J. Christoffersen, M. R. Christoffersen, H. Eckert, B. O. Fowler, J. C. Heughebaert, G. H. Nancollas, J. P. Yesinowski and S. J. Zawacki; *J. Cryst. Growth,* **84** (1987) 515.

[13]   P. W. Brown, N. Hocker, S. Hoyle; *J. Am. Ceram. Soc.*, 74 (1991) 1848.

[14]   G. V. Gordon, T. Villanueva, H. R. Shumacher and V. J. Goel; *Rheumatology,* **11** (1984)861.

[15]   A. L. Boskey and P.G. Bullogh; *Scann. Electron Micros.,* **28** (1984) 511.

[16]   F. J. Schöen and R. J. Levy; *Cardiol. Clin.,* **2** (1984) 713,

[17]   M. Valente, U. Bortloti, G. Thiene; *Am. J. Pathol.,* **119** (1985) 12.

[18]   G. H. Nancollas; *J. Crystal Growth,* **42** (1977) 185.

[19]   J. G. Morales, J. J. Burgues, T. Boix, J. Fraileand R. R. Clemente; *Cryst. Res. and Technol.,* **36** (2000) 15.

[20]   M. Aizawa, T. Hanazawa, K. Itatani, F. S. Howell and A. Kishioka; *J. Mater. Sci., 34* (1999) 2865.

[21]   M. Aizawa, F. S. Howell, K. Itatani, Y. Yokogawa, K. Nishizawa, M. Toriyama and T. Kameyama; *J. Ceram. Soc. Jpn.,* **108** (2000) 249.

[22]   H. Tanaka, M. Chikazawa, K. Kandori and T. Ishikaw; *Phy. Chem. Phys.,* **2** (2000) 2467.

[23]   R. N. Panda, Fa-H. Ming, R. J. Chung and T. S. Chin; *Jpn. J. Appl. Phys.,* **40** (2001) 5030.

[24]   M. A. Verges, C. F. Ganzalez, M. M. Gallego, J. D. Solier, I. Cachadina and E. Matijevic; *J. Mater.Res.,* **15** (2000) 2526.

[25]   M. P. Mahabole, R.C. Aiyer, C.V. Ramakrishna, B. Sreedhar and R. S. Khainar; *Bull. Mater.Sci.,* **28** (2005)535.

[26]   http://www.geocities.com/SoHo/Gallery/6412/CCDarthropathies.htm

[27]   http://www.arc.org.uk/about_arth/booklets/6051/6051.htm

[28]   J. E. Z. Canceer, and J. L. Decker; *Am. J. Med.* **36** (1964)571.

[29]   C. T. Chou, A. Wasserstein., H. R. Schumacher and P. Frenandez;. *J. Rheumatol.* **12**(1985) 1149.

[30] P. B.Halverson, H. S. Cheung, D. J. McCarty, J. Garancis and N. Mandel; *Arthritis Rheum.* **24** (1981) 474.

[31] H. S. Cheung, P. B. Halverson, and D. J. McCarty; *Arthritis Rheum.*, **24** (1981) 1338.

[32] H. S. Cheung, P. B. Halverson and D. J. McCarty; *Proc. Soc. Exp. Biol. Med.* **173** (1983) 181.

[33] H. S. Cheung, M. T. Story and D. J McCarty; *Arthritis Rrheum.* **27** (1984) 668.

[34] D. J. McCarty, J. R. Lehr and P. B. Halverson; *Arthritis Rheum*, **26** (1983) 1220.

[35] D. J. Mc Carty and R. A. Gatter; Arthritis *Rheum.*, **9** (1966) 804.

[36] H. Paul, A. J. Reginato and H. R. Schumacher; *Arthritis Rheum,* **26** (1983)191.

[37] K. Yanagisawa, H. Toya, Qi Feng, N. Yamasaki; *Phosphorus Res. Bulletin,* **5,** (1995), 43.

[38] A. C. Tas; *Powder Diffract.*, **16** (2001) 102.

[39] A.C. Tas; F. Korkus8uz, M. Timucin, N. Akkas; *J. Mater. Sci., Mater. In Medicine,* **8** (1997) 91.

[40] N. Özgür Engin and A. Cüneyt Tas; *J. Am. Ceram. Soc.,* **83(7)** (2000)1581.

[41] A. Cüneyt Tas, *Biomaterials,* **21**, (2000) 1429.

[42] S. Bharati, M. K. Sinha and D. Basu; *Bull. Mater. Sci,* **28** (2005) 617.

[43] Jinghong Li, Yuanjian zhang, Lihen Zhou, Naicun Xue, and Di Li; *ICMRS-ICEM 2002*, China, 10-14 June 2002.

[44] S. Koutsopoulos and E. Dalas; *J. Coll. Interf. Sci.,* **231** (2000) 207.

[45] S. Koutsopoulos, E. Dalas and N. Klouras; *Langmuir, 16* (2000) 6745.

[46] S. Koutsopoulos and E. Dalas; *Langmuir, 16* (2000) 6739.

[47]   S. Koutsopoulos and E. Dalas; *J. Cryst. Growth,* **217** (2000) 410.

[48]   S. Koutsopoulos and E. Dalas; *J. Cryst. Growth,* **216** (2000) 443.

[49]   S. Koutsopoulos, E. Dalas, N. Tzavellas, N. Klouras and P. Amoratis; *J. Cryst. Growth,* **183** (1998) 251.

[50]   S. Koutsopoulos, E. Dalas, N. Tzavellas, N. Klouras and P. Amoratis; *J. Chem. Soc. Faraday Trans.,* **93** (1997) 4183.

[51]   S. Koutsopoulos,I. Demakopoulos, X. Argiriou, E. Dalas, N. Klouras and N. Spanos; *Langmuir,* **11**(1995) 1831

[52]   K. O. Weselrnan and C.A. Agudelo; *Bulletin on the Rheumatic Diseases,* **5(9)** (2001) 1.

[53]   W. S. C. Copeman; *'A Short History of the Gout',* Berkeley, University of California Press, (1964).

[54]   E. Neuwirth; *Arch. Intern. Med.,***72 (**1943) 377.

[55]   M. A. Schnitker; *Bull. Inst. Hist. Med.* **4** (1936) 89.

[56]   J. H. Talbott; *'Gout'* 3rd ed. Grune & Stratton, NewYOrk, (1967) 5.

[57]   G. P. Rodnan; *Arthritis Rheum.*, **4** (1961) 27.

[58]   G. P. Rodnan, and T. G. Benedek; *Arthritis Rheum,* **6** (1963) 789.

[59]   G. P. Rodnan and T. G. Benedek; *Arthritis Rheum.,* **6 (**1963) 317.

[60]   E. G. L. Bywaters; *Ann. Rheum . Dis.* **21** (1962) 325.

[61]   M. B. Strauss; *Familiar Medical Quotations.,* Little, Brown & Company, Boston (1968), 186.

[62]   Hippocrates; *'The Genuine works of Hippocrates',* Vols. I and II. Translated from the Greek with a Preliminary discourse and annotations by Francis Adams. New York, (1886).

[63]   F. H. Garrison; *'An introduction to the history of medicine: with Medical Chornology, suggestions for study and Bibliographic Data'*, 4th Ed. W.B. Saunders Co. (1929).

[64]   C. Galen; *Opera Omina,* Ed. by Kuhn. Leipzig (1821).

[65]   D. J. McCarty; *Arthritis Rheum.* **13** (1970) 414.

[66]   K. W. Scheele; *Opuscula,* **2** (1776) 73.

[67]   W. H. Wollaston; *Philos. Trans. R. Soc. Lond.*, **87** (1848) 386.

[68]   J. Want; *Med. Physiol. J. Lond.* **32** (1814), 312.

[69]   A. B. Garrod; *Trans. M-Chir. Soc. Edinb*, **31** (1848) 83.

[70]   M. Freudweiler; *Disch. Arch. Klin. Med.* **69** (1909) 155, (English translation: Experimental investigations into the origin of guty tophi. *Arthritis Rheum.,* **1** (1965) 270.

[71]   J. H. Talbott, C. Bhishop and B. M. Norcross; *Trans. Assoc. Am. Physicians,* **64** (1951) 372.

[72]   A. B. Gutman and T. F. Yu; *Trans. Assoc. Am. Physicians,* **64** (1951) 279.

[73]   R. W. Rundles, J. B. Wyngaarden, G. H. Hitchings; *Trans. Assoc. Am. Physicians,* **76** (1963) 126.

[74]   W. N. Kelley, E. M. Rosenbloom, J. F. Henderson; *Proc. Natl. Acad. Sci.* **57** (1967) 1735.

[75]   J. D. Wynfarden and W. N. Kelley; *Gout and Hyperuricemia',* Grune & Stratton, New York, 1976.

[76]   N. Dalbeth and D. O. Haskard; *Rheumatol.* **44** (2005) 1090.

[77]   J. Zalokar, J. Lelouch, and J. R. Claude; *Semin. Hop. Paris,* **57** (1981) 664.

[78]   K. Nishioka and K. Mikanagi; *Adv. Exp. Med. BIol.,* **122A** (1980) 155.

[79]   E. W. Campion, R. J. Glynn and L.O. deLabry; *Am. J. Med.,* **82** (1987) 421.

[80]   J. N. Loeb; *Arthritis Rheum,* **15** (1972) 189.

[81]   R. Grahame, J. T. Scott; *'Ann Rheum Dis.'* **29** (1970) 461.

[82]   J. G. Puig, A. D. Michan, M. L. Jimenez, C. Perez de Ayala, F. A. Mateos, C.F.Capitan et al.; *Arch Intern Med.,* **151** (1991) 726.

[83]   P. S. Hench; *J Lab Clin Med.* **220** (1936) 48.

[84]   A. B. Gutman; *Arthritis Rheum.*,**16** (1973) 431.

[85]   D. A. Nakayama, C. Barthelemy, G. Carrera, Jr R. W. Lightfoot, R. L. Wortmann; *Arthritis Rheum*, **27** (1984) 468.

[86]   www. Medscape.com

[87]   D. Shemin, and D. Rittenberg; *J. Biol. Chem.*, **167** (1947) 875,.

[88]   J. M. Buchanan, J. C. Somnne and A. M. Delluva; *J. Biol. Chem.,* **173** (1948) 81.

[89]   J. L. Karlson and H. A. Braker; *J. biol. Chem.,* **177** (1949) 597.

[90]   J. C. Sonne, J. M.Buchanan, and A. M. Delluva; *J. Biol. Chem.* **173** (1948) 81.

[91]   M. R. Hinrich and D. W. Wilson; *J. Biol. Chem.* **186** (1950) 447.

[92]   J. C. Sonne, I. Lin and J. M. Buchanan; *J. Biol. Chem.,* **220** (1956) 369.

[93]   B. Levenberg, S.C. Hartman and J. M. Buchanan; .*J. Biol. Chem.,* **220** (1956) 379.

[94]   D. A. Goldthwait, R.A. Peabody and G.R. Greenberg; *J. Biol. Chem.,* **221** (1956) 569.

[95]   J. H. Kippel and P.A. Dieppe; *"Rhemutalogy",* Mosby Publishers (1998).

[96]   J. G. Flakes, M.J. Erwin and J.M. Buchanan; *J. Biol. Chem.* **228** (1957) 201.

[97]   M. Hori and J. F. Henderson; *J. Biol. Chem.* **241** (1966) 3304.

[98]   L. N. Lukens and K. A. Herrington; *Biochem. Biophys. Acta,* **24** (1957) 432.

[99]   J. F. Henderson, L.W. Brox and W.N. Kelly; *J. Biol. Chem.,* **243** (1968) 2514.

[100] N. Friedkin and N. Kalckar, *'Nucleoside Phosphorylase',* in P.D. Boyer, H. Lardy and K. Myrback, (eds): The Enzymes, Vol. 5. Academic Press, New York (1961) 237.

[101] G. D. Kersley; *"A short History of Gout",* In *"Gout: A Clinical Comprehensive",* Eds: A.B. Gutman, W. J. Fessel, A.P. Hall et al, Medcom Inc. New York, (1971) 8.

[102] M. A. Snaith; *Rheumatology oxford,* **43** (2004) 1054.

[103] R. A Jacob, G. M. Spinozzi, V.A. Simon et al; *J. Natr.* **133** (2003) 1826.

[104] T. Unno, A. Sugimoto, T. Kakudo; *J. Ethnopharmacol.* **93** (2004) 391.

[105] P. L. Owen, T. Jhons; *J. Ethnopharmacol.* **64** (1999) 149.

[106] A. G. Fam; *"Hyperuricemia and Gout",* In R.E. Rackel, E.T. Bope Edits Conn's Current Therapy", W.B. Saunders, Philadelphia, (2005) 681.

[107] A. Bayraktar, S. Hudson, A. Watson, S. Fraser; *Pharmacer J.* **264** (2000) 57.

[108] R. L. Wortmann and W. N. Kelley, *"Textbook on rheumatology",* 6th Ed. W.B. Saunders, Philadelphia, USA (2001) 1339.

[109] D.W. Hawkins and D.W. Rahn; *'Gout and Hyperuricemia",* 3rd edition, Pharmacotheraphy: A Pathophysiologic Approach, Editor, Dipiro, Talbot, et al Appeiton and Lange, (1997) 1755.

[110] S. L. Wallace, J. Z. Singer; *Rheum. Di.s Clin. North. Am*., **14** (1988) 441.

[111] A. Cohen; *Am. J. Med. Sci.,* **192** (1936) 448.

[112] M. Medellin, A. Erckson, R. Enzenauer; *J. Clin. Rheumatol.,* **3** (1997) 24.

[113] N. Bellamy, J. R. Gilbert, P. M. Brooks, B. T. Emerson; J. Campbell, *J. Rheumatol.*, 15 (1988) 1841.

[114] A.G. Fam; *BJM,* **325** (2002) 980.

[115] S. Nalbant, L.X. Chen, M.S. Sieck G. Clayburne and H. R. Schumacher; *J. of Rheum.* **32** (2005) 1762.

[116] A. Raut, N. Pandita, M.J. Joshi and S. Mengi; '*Progress Report on: Preclinical Development of Herbal Formulation for Inflammatory Arthropathy',* Submitted to the Department of Biotechnology, Govt. of India, (2003-04)

[117] F. Mandl; *Arch Klin Chir,* **146** (1927) 149.

[118] D. J. McCarty and J.L. Hollander; Ann. *Intern. Med.* **54** (1961) 452.

[119]   D. J. McCarty, N. N. Kohn R. E. Hughes; *Ann Intern Med* **56** (1962) 738.

[120] D. J. McCarty; *Arthritis Rheum* , **19 (**1976) 275.

[121] A. Bjelle; *Scand. J. Rheumatol.* **8** (1979) 145.

[122] www. webrheum.bham.ac.uk/.../ general/Immunology.htm

[123] G. Fam Adel; *Curr Opin Rheumatol,* **12** (2000) 228.

[124] K. Rosenthal Anee; *'Crystal Arthopathies.* In; P.J. Madidison, D.A. Isenberg, P. Woo, and D.A. Glass, Eds.: Oxford textbook of Rheumatology 2nd Edn , Oxford University Press, (1998) 1567.

[125] M.J. Luzar and B. Altawil; *Arthr Rheum.* **41** (1998) 939.

[126] www. Orthop.washington.edu

[127] Y. Zhang and M.A. Brown; *Curr. Opin. In Rheumat.* **17** (2005) 330.

[128] E. Hamilton, M. Patrick and M. Doherty; *Br J Rheumatol,* **21** (1994) 912.

[129] A. O. Bjelle; *Ann Rheum Dis,* **31** (1972) 449.

[130] K. Ishikawa, I. Masuda, T. Ohira and M. Yokoyama; *J Bone Joint Surg,* **71A** (1989) 875.

[131] J. W. Rachow and L. M. Ryan; *Rheum Dis Clin North Am*., **14** (1988) 289.

[132]   A. Hughes, D. McGibbon, E. Woodward, J. Dixey and M. Doherty; *Hum Mol Gene,* **4** (1995) 1225.

[133]   G. D. Wright, M. Doherty;

http://www.arc.org.uk/about_arth/med_reports/series3/tr/6414/6414.htm.

[134]   M. Doherty and P. A. Dieppe; Arthritis *Rheum,* **24** (1981) 954.

[135]   M. Doherty, P. A. Dieppe and I. Watt; Br *J Rheumatol,* **32** (1993) 189.

[136]   T. Shinozaki and K.P. Pritzker; *J. Rheumatol.,* **22(10)** (1995) 1907.

[137]   Y. Xu, T. Cruz, P.T. Cheng and K.P. Pritzker; *J. Rheumatol.,* **18(1)** (1991) 66.

[138]   R. Cini, D. Chindamo, M. Catenaccio, S./ Lorenzini, E. Selvi, F. Neracci, M.P. Picchi, G. Berti and R. Maricolongo; *Ann. Rheumat. Dis.,* **60** (2001) 962.

[139]   Hong-Korng and Liote; *Curr.Rheum. Rep.,* **6** (2004) 221.

[140]   C. Wheeless; http://www.orthopaedicweblinks.com/Detailed/5896.html

[141]   http://www.merck.com/mrkshared/mmanual/section5/chapter49/49a.jsp

[142]   C. J. Gaskell, *Vet. Rec.,* **102** (1978) 546.

[143]   J. S. Elliot; *"Urinary Calculi Disease",* SCHA 4th Edition (1965).

[144]   A.B. Soni; *'Dessertation for the Degree of M.D.,* Gujarat Ayurveda University, Jamnagar (1999).

[145]   B. Finlayson; *Urol. Clin. North Am.,* **1** (1974) 181.

[146]   T. L. Fetter and P.D. Zimskind; *JAMA,* **186,** (1961) 21.

[147]   N. J. Blacklock; *"The patterns of Urolithiasis in the Royal Navy",* Eds. A. Hodgkinson and B.E. C. Wozdin, in *"Renal Stone Research Symposium"*, J. and A. Churchill Ltd., London (1969).

[148]   C. Y. C. Pak; *Miner. Electrol. Metab.,* **13** (1987) 257.

[149]   C.Y. C. Pak; *Renal Stone Disease,* Martinus Nijhoff Publishing, Boston (1987).

[150] S.P. Dretler, C.H. Coggins, M. A. McIves and S.O. Their; *J. Urol.,* **102** (1969) 665.

[151] R. Sierakowski, B. Finlayson and R. Landes; *Urol. Res.,* **7** (1978) 157.

[152]   A. Hodgkinson; *Br. J. Urol.* **8** (1976) 1.

[153] W.C. Thomas; Jr., *J. Urol.,* **113** (1975) 423.

[154] L. Marshal, M. D. Stoller, and M. Damien; Urinary Stone Disease.

[155] A. Randall; *New Engl. J. Med.*, **214** (1936) 234.

[156] D. J. Kok, S. E. Papapulos and O. L. Bijovet; *Kidney Int.*, **37** (1990) 51.

[157] Y. Nakagawa, M. Ahmed and S. L. Hall; *J. Clin. Invest.,* **79** (1987) 1782.

[158] J. Asplin, De. Gannellis, Y. Nakagawa and F. I. Coe; *Am. J. Physiol.* **260** (1991) 569.

[159] R. Hautmann, A. Lehmann and S. Kumar; *J. Urol.,* **123** (1980) 317.

[160] G. W. Drach and W. H. Boyce; *J. Urol.*, **107** (1972) 897.

[161] H. Fleisch; *Kidney Int.,* **13** (1978) 361.

[162] F. L. Coe, H. C. Margolis and L. H. Deutsch; *Miner. Electr. Metab.,* **3** (1980) 268.

[163] J. Garside; *Biological Mineralization and Demineralization,* Ed. Nancollas G. H., Springer - Verlag, New York, (1982).

[164] H . Ito and F. L. Coe; *Am. J. Physiol.*, **233** (1977) F455.

[165] S. R. Khan, P. N. Shevock and R. L.Hackett; *J. Urol.*, **139** (1988) 418.

[166] H. Shiraga, W. Min, and W. J. Van Dusen; *Proc. Natl. Acad. Sci. USA,* **89** (1992) 426.

[167] R. S. Malek and W. H. Boyce; *J. Urol.,* **109** (1973) 551.

[168] M. H. Malagodi and H. A. Moye; *Urol. Surv.,* **31** (1981) 81.

[169] J. L.Meyer and L. H. Smith; *Invest Urol.,* **13** (1975) 36.

[170]   C. Y. C. Pak; *J. Urol.,* **128** (1982) 1157.

[171]   R. S. Malek and W. H. Boyce; *J. Urol.,* **117** (1977) 336.

[172]   H. G. Tiselius and L. Larson; *Urol. Res.* **21** (1993) 175.

[173]   http://www.med.uni-jena.de/urologie/_en/research/urinarystone/info03.php].

[174]   F. L. Coe, J. H. Parks and Jr. Asplin; *N. engl. J. Med.* **327** (1992) 1141.

[175]   R. J. Caruana and V. M. Buckalew; *Medicine,* **67** (1988) 84.

[176]   L. H. Smith; *Renal Tubular Acidosis',* AUA office of Education, Boston (1986).

[177]   P. J. Oshter, A. B. Hansen, H. F. Rohl; *Br. J. Urol.,* **63** (1989) 581.

[178]   M. Menon and C. J. Mahle; *Prevalence of Hyperoxaluria in Iidopathic' Calcium Oxalate Urolithiasis: Relationship to other Metabolic Abnonotmalities* (Abstract 458) Presented at American Urological Association, Las Vegas, (1983)

[179]   C. Y. C. Pak, C. Fuller, K. Sakhaee et al; *J. Urol.,* **134** (1985) 11.

[180]   W. W. Scott, C. Huggins and B. C. Selman; *J. Urol.*, **50** (1943) 202.

[181]   C. Y. C. Pak, K. Sakhaee and C. Fuller; *Kidney. Int.,* **30** (1986) 422.

[182]   M. J. Nicar, K. Hill, C.Y. Pak; *J. Bone Miner Res.* **2** (1987) 215.

[183]   B. B. Parekh and M. J. Joshi; *Ind. J. Phys.*, **43** (2005) 675.

[184]   H. G. Tiselius, A.M. Fornander, M.A. Nilsson; *Urol. Res..,* **21 (**1993) 363.

[185]   H. G. Tiselius, C. Breg, A.M. Fornander, M.A. Nilsson; *Scann. Microsc.,* **7** (1993) 381.

[186]   E. Königsberger and L.C. Königsberger; *Pure. Appl. Chem.* 73 (2001) 785.

[187]   P. K. Grover, D. S. Kim and R. L. Ryall; *Mol Med.* **8(4)** (2002) 200.

[188]   P. K. Grover and R. L. Ryall; *Clin Sci (Lond)*, **102(4)** (2002) 425.

[189]   E. O. Kajander and E. Ciftcioglu; *Proc. Nat. Acad. Sci.***959** (1998) 8274.

[190]   N. S. Aoki and M. Yokoyama; *Aktuelle. Urol.,* **34** (2003) 253.

[191]   V. S. Joshi; *Ph.D. Thesis,* Saurashtra University Rajkot (2001).

[192]   K. C. Joseph; *Ph.D. Thesis,* Saurashtra University Rajkot (2005).

Chapter III

Crystal Growth and Methodologies

3.1 Introduction:

Ahh, finally I made it, critical size,

Surface energy no longer a barrier

Being outside the spinodal, Arrhenius lent me a hand

Against probability I've made it this far.

Collecting from around me I will expand

Starting for that lowest free energy

As long as I stay ahead of my curve, above average

I will survive. My brothers around me will savage

It is a grain eats grain crystal.

-Jennifer Mc Keehan (2002)

Systematic study of the growth and properties of crystals is covered under the subject *crystal growth*. The growth of crystals occurs either in nature or artificially in a laboratory. The Mother Nature grows a variety of crystals in the crust of Earth, which are the natural mineral crystals. However, the demand of the modern day science and technology has tempted scientists to synthesize and grow several new varieties of crystals. This has brought the field of crystal growth into the lime light. As a result the congeries of crystals is ever expanding day by day.

3.2   Basic Theories and Developments:

Crystal growth has been long cherished for the fascinating observations, where the atomic nature of matter clearly shows itself. It has been realized that the subject can be divided into two parts: (1) the study of the equilibrium between the crystal and surrounding medium and (2) the study of the kinetics of growth.

The Kossel model [1] is helpful to understand the basic theories of crystal growth. In figure (3.1a), a low index face of a perfect (001) face of crystal at the *absolute zero temperature*, at which no thermal vibrations of component molecules are available, is shown.
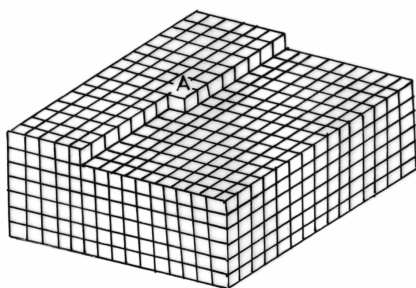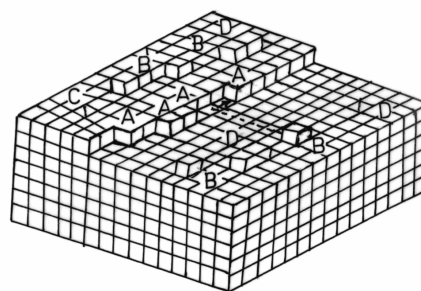
| Figure (3.1a) | Figure (3.1b) |

Figure (3.1): (a) Step on a perfect crystalline surface, (b) Step with kinks and vacancies

This represents the profile of a completely flat surface partially covered by another layer. The boundary line, where there is a difference of level equal to an inter-molecular spacing between the two sides of the line, is called a *step* on the crystal surface. If a crystal is in stable equilibrium with its vapor, which is neither super-saturated nor under-saturated, then a step in equilibrium in the crystal surface will exhibit a constant mean direction h, inclined at an angle $è$ to the principal direction given by the following expression,

$$tan\ è = n_+\ n_-$$

Where, n_+ and n_- are the numbers of kinks of opposite sign per atom spacing. The potential energy considerations suggest that at absolute zero temperature, a step will tend to remain as straight as possible.

As the temperature increases from absolute zero, the component molecules will start vibrating relative to one another. As the temperature increases the vibrations become progressively stronger. Now the scenario changes, some molecules will be able to overcome the energy that binds them to the crystal and will jump in the space surrounding it. In this manner, a certain vapor concentration, which is the average number of vapor molecules per unit volume, will occur in contact with the crystal surface. With comparison to the other molecules, the molecules positioned at the kink are more prone to depart from the crystal and vaporize. The molecules at the kinks are bound by three molecules. Moreover, the molecules on the straight portions of the step are bound by four molecules and those on the flat portions of the surface by five. The energy required for a molecule to leave the kink position such as A in figure (3.1b) is equal to the evaporation energy W. Here two different processes will occur simultaneously; in one process some molecules will be leaving the crystal and in the other one the molecules will be arriving at the crystal from the vapor. Equilibrium is reached when the rates of these two processes are equal. Now, the surface will look like as shown in figure (3.1b).

One can notice the changes in the surface easily by comparing the figures (3.1a) and (3.1b). The two main changes are noticeable; which are (1) the step has acquired a number of kinks such as A and (2) a small number of molecules have been adsorbed on the crystal surface and on the step, indicated as B in the figure (3.1b), and also a similar number of surface vacancies C, a small number of pairs of adsorbed molecules D or pairs of vacancies have been created.

The mean distance x_o between the kinks is estimated in terms of the inter-atomic distance, a, by

$$x_o = \frac{1}{2} [exp(\grave{u} / k T) + 2] \quad \frac{1}{2} a [exp (\grave{u} / k T)]$$

Now, introducing the nearest neighbor interaction as, $\ddot{O}$, which is related to the evaporation energy, W, by the expression as follows

$$\ddot{O} = 1/6 \ (W)$$

Therefore, the mean distance x_o can be obtained as

$$x_o = \frac{1}{2} exp [\ddot{O} / 2kT]$$

It was first realized by Volmer [2] in 1922 that the adsorbed molecules diffuse with considerable ease over the crystal surfaces. The process of growth of a crystal surfaces with steps is the result of mainly three processes; (1) a transport of molecules from the vapor to the adsorbed layer, (2) the diffusion of the adsorbed molecules towards the steps and (3) the diffusion of adsorbed molecules along the edge of the steps towards kinks. This process is shown in Figure (3.1b).

The proportion n_s of the surface sites covered by adsorbed molecules has been given by Burton, Cabrera and Frank [3] approximately as,

$$n_s = exp [-W_s / kT]$$

Where W_s is the energy of evaporation from the kinks on to the surface, that is, the energy required to transfer a molecule from a site A to site B in figure (3.1b), which was estimated to be about $\frac{1}{2} W$.

The mean displacement x_s of adsorbed molecules, which is the average distance a molecule would wander on the crystal surface between the time it hits the surface and the time it evaporates again is given by Burton, Cabrera and Frank [3] as

$$x_s = a \ exp \{ (W'_s - U_s)/ 2k T\}$$

where U_s is the activation energy for surface diffusion, that is, migration from one surface site to another, and this has been estimated to be of the order of *1/20 ;* W'$_s$ is the evaporation energy from the surface to the vapor and is given by, $W_s = 3\ Ö$, that is, half the total evaporation energy *W.* One can further neglect U_s and estimate that x_s

a exp (3 Ö / 2 kT), which is of the order of *4 x 10^{2}a* for the typical values of *Ö / kT*

4. This indicates that $x_s >> a$, therefore, the molecules diffuse considerable distance before evaporating. This leads to conclude that the direct arrival of molecules from vapor at any particular point on a crystal surface is, generally, small as compared with the rate of indirect arrival through the surface migration.

Nevertheless, the concept of *minimum total surface free energy* is also important in crystal growth. Gibbs [4] in 1878 developed a consistent phenomenological treatment (thermodynamic treatment) of the equilibrium problem, which is still essential as an introduction to the study of crystal growth. Gibbs made use of the analogy of *liquid drops,* and applied it to the conditions governing the growth of water droplets in a mist to the growth of a crystal. The free energy, which resides on the surface separating the two phases, retards the formation of the second phase in the first. The condition for the stability of an isolated drop of a liquid is that its surface free energy, and hence its area, minimum. Altogether, in a similar manner for a crystal in equilibrium with its surrounding at constant temperature and pressure, this condition implies that the Gibbs free energy is the minimum for a given volume. Considering the volume free energy per unit volume as constant through out the crystal, one gets the condition,

$$Ó\ ó_i\,F_i = minimum, \text{(Where } i = 1,2,....n)$$

Where, $ó_i$ is the surface free energy per unit area of the ith face of area F_i on a crystal bounded by *n* faces. Therefore, those faces will develop which leads to a minimum

total surface free energy for a given volume. In a drop of liquid the atoms or molecules are randomly arranged, in contrast to this in a crystal the structural units are arrange in a regular way in three dimensions as per the prevailing symmetries. Curie [5] in 1878 calculated the shapes and end form of crystals in equilibrium with solution or vapor, which was consistent with the condition that the free energy must be a minimum for a given volume. Later on, Wulff [6] extended this theory and showed that Gibbs equilibrium shape of crystal was related to the relative surface free energies of the faces in a very simple manner.

It was thought that on perfect crystal faces steps could be created by the thermodynamic fluctuations in much similar way as the kinks are formed on a step. However, in the earlier theoretical considerations the problem was to start the nucleation on the perfect crystal face. Gibbs [4] considered that before a new layer can grow, a two dimensional nucleus or *island* monolayer, probably of 100 molecular diameters, has to be formed and on the edges of which the growth can proceed. Once such type of layer is formed, it spreads quickly across the whole face and the process of growth is held until a new nucleus is formed. This has been described in Figure (3.2).
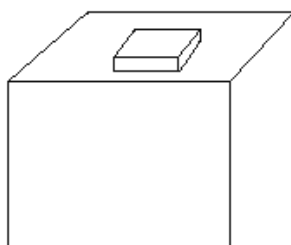

Figure 3.2: Surface with island monolayer

The problem of nucleating an island monolayer on a closed-packed crystal surface is analogous to the nucleation of a water droplet as mentioned earlier. For a given

degree of super-saturation, there a critical radius $\tilde{n}_c$ of the nucleus of circular nature such that a nucleus of radius greater than $\tilde{n}_c$ will grow and if less it will evaporate. This is due to the line energy of the step of island monolayer causes a local equilibrium vapor pressure, which is inversely proportional to its radius of curvature. In the case of circular nucleus of radius $\tilde{n}$, the free energy is,

$$F = -\eth \, \tilde{n}^2 \, ^o + 2\eth \, \acute{o}$$

Where ^{o} is the free energy gained per unit area when an adsorbed molecule becomes attached to the nucleus, and $\acute{o}$ is the free energy per unit length of the step at boundary of the nucleus. From this expression one finds interesting behavior, initially, as $\tilde{n}$ increases from zero, the F also increases until it reaches a maximum value of F_o for $\tilde{n}_c = \tilde{n}$; thereafter, it decreases with increasing $\tilde{n}$.

Burton, Cabrera and Frank [3] have re-examined the shape of the nucleus. Their arduous analysis shows that the nucleus is, *ipso-facto,* not circular but varying in the shape and hence the free energy per unit length of the edge changes with the crystallographic directions. In more general manner, $\tilde{n}_c$ can be regarded to be the radius of circumscribing circle to the critical nucleus. The rate of the formation of nuclei is given by,

$$Z = (S / s_o) \, exp \, (- F_o / k \, T)$$

Where, Z gives the rate of arrival of fresh molecules at single surface lattice site, S is the surface area of the crystal face under consideration and s_o is the area per molecule in the layer. Usually, Z cannot exceed $10^{13} \, sec^{-1}$ even in a dense environment, however, the pre-exponential factor is about 10^{22}. For the observable growth rate on the time scale of a laboratory experiments, for example, 10^{-3} layers per second or one micron per month, it follows that the logarithm of saturation ratio, *log á,* must be at least $(\ddot{O} / k \, T)^2/90,$ where $\ddot{O}$ is the binding energy of nearest neighbor,

with typical value of $\ddot{O} / k T$ requires a super-saturation of at least 25 to 50 percent. Therefore, the nucleation rate is very sensitive function of super-saturation. It is worth noting that above this critical super-saturation, the growth process is not limited by nucleation but below this critical super-saturation, the probability of nucleation would diminish to the negligible value.

The effect of presence of impurities on the nucleation rate has been reported by many researchers. Turnbull [7] proposed that the free energy of formation of a critical nucleus can by catalyzed by a suitable surface in contact with the nucleus. Nucleation catalysts or nucleates may be solid particles suspended in liquid, the surface of the container or a solid surface. This process of nucleation is known as *heterogeneous nucleation*. In heterogeneous nucleation, the reaction may be the direct exchange of monomers between the parent phase and embryo, that is, a cluster of molecules, or through the surface, which is normally known as *substrate.* The theories of heterogeneous nucleation are developed well by many authors and edited by Zettlemoyer [8]. Moreover, in highly polar molecules, the dipole-dipole interaction is expected to play a prominent role in modifying the surface free energy of micro-cluster at the critical stage. In order to determine the effect of dipole-dipole interaction on the surface free energy, a model was proposed by Abraham. [9] This has been discussed for various shapes of nucleation.

One of the major drawbacks of early nucleation theories is that once the kinked ledge receives sufficient ad-atoms to move it to the edge of the crystal, it can no longer work as a low energy nucleation site. Now, the generation of a new ledge requires an adsorption on a flat surface, for which the estimated super-saturation is of the order of 50%. But in 1931 Volmer and Schultze [10] found astonishing results, while studying the growth rate of individual iodine crystals at slightly supersaturated

vapor at 0^0 C. They found that the growth rate was proportional to the super-saturation down to 1%. Only below this degree of super-saturation did it fall below proportionality and that also not abruptly.

New experimental evidences made earlier theory apocryphal; an attempt was made by Frank [11] and Burton [12] to propose a new concept by considering dislocations. A screw dislocation emerging on the face of a crystal provides it with a step. This step, containing kinks, offers a mechanism for growth of crystals at low super-saturations. When the atoms are adsorbed on the crystal surfaces they diffuse to the step and finally to the kinks and thus the step advances. The step provided by the screw dislocation, terminates at the dislocation point, where it remains fixed. Hence, when growth takes place, the step can advance only by rotating around dislocation point. At particular super-saturation each point on a straight step will advance with the same speed, therefore, the section of the step near the dislocation will have higher angular velocity for the same linear velocity and consequently make a larger number of revolutions in a given time than the section farther away. Actually, for the portion of the step near the centre, having higher curvature, there will be higher equilibrium vapor pressure and therefore a lower local super-saturation, hence the rate of advance is bit slower. When steady state has been reached, the whole spiral will rotate uniformly about dislocation. This has been described in figure (3.3). Varma has given a detailed account of the various growth spirals and their significances [13].
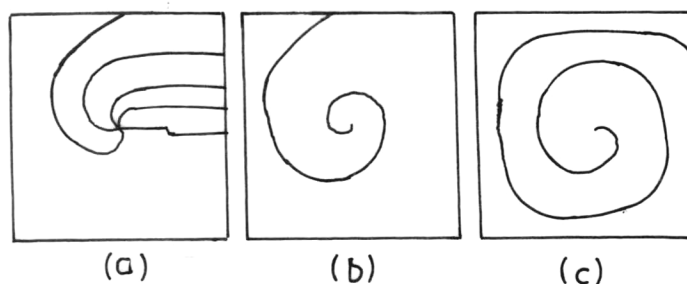

Figure (3.3): Growth spirals

A theory of crystal growth, incorporating the mechanism of step generation and transport into the step, was given by Burton, Cabrera and Frank (BCF) [3] in 1951, in their celebrated paper. This theory has gained importance because much of the content will apply to any theory of crystal growth. Varma has elaborated great significances of Kossel- Transki- Volmer theory and BCF theory in his well appreciated book [13]. This BCF theory was originally proposed for growth from the vapor phase but its applicability to solution growth has been strongly advocated by Bennema and Gilmer [14].

Numerous other theories and models have been developed not only for the vapor growth but solution growth and melt growth also [15, 16, and 17]. Many models are based on Monte Carlo simulations [18]. Derby [19] has recently given minute details of the present challenges of the crystal growth models. According to him the requirements are that one needs more realistically represent the many important interactions in crystal growth systems, models must be capable of describing detailed system geometry and design , three dimensional and transient continuum transport, phase change phenomenon, and, ultimately, atomistic events. Altogether, Neugebauer [20] high lighted the challenges in the accurate simulations on crystal growth. According to his views, one naturally gets interested in a problem on a meso-scopic scale , where the size of typical surface features such as quantum dots, surface roughness, terrace length is in the order of *10* to *1000* nm and the characteristic timescale to form such features is in the order of seconds, the mechanisms leading to these structures, such as ad-atoms, adsorption, diffusion, de-sorption, island nucleation, require an atomic scale resolution , that is, a resolution in the length scale of 10^{-1} nm and in the time scale of 10^{-13} s^{-1}.

3.3   Crystal Growth Techniques:

Crystal growth deals with the control of a phase change. Hence it may be defined by the three basic categories of crystal growth processes [15]:

Solid growth: $S \to S$ processes involving solid-solid phase transitions.

Melt growth: $L \to S$ processes involving liquid-solid phase transitions.

Vapor growth: $V \to S$ processes involving vapor-solid phase transitions.

The $S \to S$ processes are not commonly used except for certain metals where strain annealing is effective and certain cases where a crystal structure alters between the melting point and room temperature. These processes include annealing or sintering, strain annealing, deformation growth and polymorphic phase transitions.

The $L \to S$ processes are many and important. The normal freezing or directional freezing is a very important process for the crystals which melt congruently with out decomposing. When an ingot is gradually frozen from one end to the other, it is said to be frozen normally or directionally. This process comprises of many techniques, which are used world wide for industrial crystallizations, including growth of semiconductor crystals for electronic and computer chip making industries. Sometimes the liquid phase contains deliberately added foreign materials as in solution growth or flux growth or liquid phase epitaxy. The solution growth is also very popular for the growth of numerous crystals for industry.

The $V \to S$ processes include sublimation, which is strictly speaking a kind of $S \to V \to S$ process, and vapor phase reactions which are used in the epitaxial growth of semiconductors. Sometimes deliberately added gases are helpful as transporting agents for the growing materials.

Crystal Growth Methods

Solid Solid		Liquid Solid		Gas Solid	
Monocomponent (Solid Growth)	**Polycomponent (Solid Growth)**	**Monocomponent (Melt Growth)**	**Polycomponent (Solution Growth)**	**Monocomponent (Vapor Growth)**	**Polycomponent (Vapor Growth)**
1. Strain annealing	**1. Precipitating from solid solution**	**1. Conservative**	**1. Growth from solution** (evaporation, slow cooling and temperature differential)	**1. Sublimation-condensation**	**1. Growth by reversible reaction** (Temperature change, Concentration change)
		(a) Directional Stockbarger (Bridgman-Stockbarger)	(a) Aqueous Solvents		(a) Van Arkel (Hot wire process)
		(b) Cooled seed (Kyropolous)	(b) Organic Solvents		
		(c) Pulling (Czochralski)	(c) Molten-salts solvents		
			(d) Solvent under hydrothermal		
			(e) Other organic solvents		
2. Devtrification		**2. Non-Conservative**	**2. Growth by Reaction** (media as above temperature change concentration change)	**2. Sputtering**	**2. Growth by irreversible reaction**
		(a) Zoning (Horizontal, Vertical, Float zone, Growth on pedestal)	(a) Chemical Reaction		(a) Epitaxial Process
		(b) Verneuil (Flame fusion)	(b) Electrochemical reaction		

The development and refinement of methods of crystal growth to achieve useful products have relied heavily on empirical engineering and on trial and error methods. Crystal growth still remains, by and large, as an art along with a science [16]. A phalanx of crystal growers has developed various crystal growth techniques after their pain staking efforts of years together. The classification scheme for various growth techniques are summarized by Laudise, which is very important for the neophytes [21].

3.4   Solution Growth Techniques:

Crystal growth from solution is one of the most widely used techniques for the growth of crystals. This technique is practiced among the crystal growth community next to the melt growth technique. The main advantage of the solution growth is that the crystals are grown at temperatures well below their melting points. A detailed inherent knowledge is required for the melt growth techniques such as, melting point, melting behavior, stability in reduced pressure and atmosphere, however, which is not needed in the solution growth. Myriad technologically important crystals are grown by this technique. Solution growth techniques can broadly be subdivided as follows [22]

(1)   Low temperature solution growth

This technique is used for materials having very good solubility at room temperature in water or any other solvents. In the aqueous solution growth technique, water is used as a solvent; while in non-aqueous techniques other than water is used as a solvent. This method hinges on achieving super-saturation without inducing spontaneous nucleation, so that the growth can proceed on the seed material. Super-saturation can be achieved and maintained in a number of ways, depending upon the conditions of the experiment and desired results. Broadly speaking, in the solution

growth, the water can be evaporated (*slow evaporation technique*), the solution temperature can be decreased (*slow cooling technique*} or solution, saturated at a temperature higher than the growth temperature, can be continuously added into the growth vessel (temperature differential method). Many ionic salt crystals as well as organic material crystals have been grown for different applications. Recently, large size KDP (Potassium Dihydrogen Phosphate) single crystals have been grown for LASER applications. The dimensions of KDP crystals are 26 x 21 x 23 inches, and weighing 700 lbs [23].

(2)   High temperature solution growth

This technique is also known as flux growth. Molten salts are the only solvents for oxides or solid solutions of oxides, which are having very high melting points and/or decompose before melting. Oxides or fluorides are dissolved in a flux and the growth proceeds at relatively low temperatures, often as much as $1000^0 C$ below the melting point of the solute. The common fluxes are KF, PbO, PbF_2, and B_2O_3. Different ferrites and garnets can be grown by this technique.

(3)   Hydrothermal growth

This technique is essentially aqueous solution growth at high temperature and pressure, which is applicable for the materials having limited solubility under ordinary conditions. This technique is used to grow quartz and calcite crystals.

(4)   Metallic – Solution growth

This method is used to grow single crystals of metallic phases and inorganic compounds, which are readily obtained by solidification of saturated metallic solutions. Diamonds are commercially grown from transition-metal solutions under high pressure. Cubic SiC crystals are harvested from iron melts saturated with C and

Si. Nowadays, this technique is preferred for semi-conducting material crystals like GaAs for industry.

(4)   Gel growth

Crystals can be grown in the gel media. This is a one kind of modified version of solution growth technique. In which the growth occurs due to reaction between two solutions in a gel medium or achieving super-saturation by diffusion in gel medium.

The present author has employed the low temperature solution growth technique up to a certain extent and the gel growth technique up to a large extent to grow his biomaterials crystals; therefore, these techniques are dealt with in details. However, the gel growth technique has been discussed in some what more elaborately, hereby.

3.5   Gel Growth:

The growth of crystals from gel is the simplest technique under ambient conditions. This technique is well suited for the crystal growth of compounds, which are sparingly soluble and decompose at fairly low temperatures. Crystal growth by the gel technique has attracted the attention of numerous researchers, as this technique is comparatively simple and can be set up in a laboratory with simple glass-wares and without any need of sophisticated instruments and high temperature furnaces. By carefully selecting the gel density, pH of the reactants and concentration of the reactants, good quality single crystals can be grown at room temperatures.

In the gel growth, interestingly, the gel acts as a '*three dimensional crucible*' which supports the crystals; at the same time yields to its growth without exerting major forces upon it. This relative freedom from constraint is believed to be an important factor in the achievement of high structural perfection. Because of this, some times, the growth of crystals in gel is considered to be similar to the growth of

an embryo in womb. This technique also finds applications in growth of different bio-material crystals, which has been well explored in the present thesis. The gel growth technique is elaborately described by Henisch [24], Henisch and Hanoka [25] as well as Patel and Venkateswara Rao [26]. An attempt has been made by the present author to review the gel growth technique briefly.

3.5.1   Types of Gels:

Out of four states of matter- solid, liquid, gas and plasma, the three states of matter-solid, liquid and gas are more the familiar ones. Even there are many exotic materials, which are yet not fully understood. Material scientists are trying to understand their structures and properties to derive their useful applications.

One exotic state of matter is gels. They are neither solids nor liquids. A gel has been defined as "a two component system of a semi solid nature rich in liquid" [27]. According to the colloid chemistry definition, gels have a semi solid consistency, they are flexible but stable in form; deform systems produced by the interaction of a gel forming compound with a solvating medium. A characteristic property of gel is that they contain a conspicuously high percentage of solvent and little solid matter. The gel forming substances and solvating solvents stabilize each other in the gel structure and are functional parts of one another. Gels may lose their solvent content during dehydration, and may pick up some spontaneously while swelling. Although the loss or the uptake of solvents is generally reversible, the removal of the solvating molecules may cause reversible or irreversible changes in the gel structure.

Gels fall into two groups, on the basis of the structural changes caused by solvation. The structure of xero-gels collapses on the removal of the dispersive medium, whereas the solid structure-the so called matrix of the steric networks of

aero-gels remains unchanged even after the removal of the dispersive medium. An example of xero-gel is the dextran gel (sephadex), and of the aero-gel is the silica gel.

The cross-linked structure of gels is the result of the cross-linkage of polymer molecules with straight or branched chains. Depending on the type of bond, the gel structures are of two types.

(1)   In most natural biopolymers, like Polysaccharides (starch, agar, latex, pectin, collagen, gelatin, etc.) gel forming, apart from the substantial properties (molecular weight, chemical structure), is a spontaneous reversible process, which depends on the temperature and concentration of the colloid solution of the polymer. The solution of colloidal particles and macromolecules is known as sols. The sol-to-gel conversion is induced by loose-secondary chemical forces, hydrogen bonds, polarization interactions and the London-van der Waals dispersive forces. Such gel structures may be disrupted by slight physicochemical effects (i.e. warming up), which cause sol formation. When it is cooled down the bonds will recombine and the sol once more solidifies into a gel.

(2)   In this second type of gel, the gel formation is irreversible; the polymer chains are built up by primary covalent bonds. The colloidal- size macromolecules, which are characteristic of gels, are often produced by the polymerization of low molecular weight monomers (acrylamide, acrylic acid, styrene etc.). In other cases, as for instance in the production of sephadex gels, the cross-links come about by cross-linkage between high molecular weight polymer (dextran) chains. Gel structures fixed by primary chemical bonds show higher resistance to slight physicochemical affects and cannot be converted into sols by warming. The gel structure cannot be disrupted except by breakdown of the polymer molecules.

The structure of synthetic and semi-synthetic gel is generally depending on the chemical properties of the basic substances, the relative concentration of the reagents and the solubility conditions during gel formation. The functional reactivity of monomers and their spatial orientation has pronounced effect on cross-linking. The reactions inducing cross-linkages are random processes governed by the laws of statistical probability. These processes cause voids of dimensions and geometry, which are the characteristic of the type of gel used to form the polymer chains. These voids are known as the *pores of the gel*. Since the gel structure is not a rigid system but a mobile one, more-or-less, fixed network of polymer chains, the terms used in practice are average or effective pore size. The pore size is one of the most important parameters of the molecular phenomena (diffusion, permeability). Pore sizes may be influenced by the conditions of manufacture, and the solubility relationships of the initial substances and the end product.

From the aspect of pore size, Kum and Kunin [28] distinguished two principal types of gel structures, which are micro-reticular (micro-porous) and macro-reticular structures. The more uniform repetition of the cross-links in micro-reticular gels produces smaller pores and renders the gel suitable for the separation of smaller molecules. Micro-reticular gels are obtained if the solubility of the starting substances (monomers) and the end product do not differ greatly, and if the cross-links assume the desired gel structure only gradually, for instances, by increasing the number of cross-links between the polymer chains already fixed.

On the other hand, the structure of the macro-reticular gel is rather heterogeneous, the spatial distribution of the matrix being uneven. Their large pores render them suitable for the permeation and separation even of macromolecules. Most

macro-reticular gels are aero-gels; in spite of their high porosity, they are resistant to mechanical effects [29].

One of the most common gels is the silica gel; the synonyms are silica hydro-gel and water of silicate glass. This is prepared from sodium meta-silicate solution. The pores are separated by a solid film of about 2×10^{-5}cm thicknesses. The dimensions of pores depend on the concentration of gel material. The effective pore diameter of silica hydro-gel is of the order of 50-100 Å. In order to obtain a gel medium of desired pH, a requisite amount of aqueous sodium meta-silicate solution is normally added to the constantly agitated suitable acid of desired concentration. The acidity of the resulting solution determines the course and the rate of polymerization [26].

Agar is probably the oldest hydrophilic gel. Raw purified polysacchrides (agar-agar) extracted from algae are widely used in food industry and in laboratory (bacteriology, immunology and electrophoresis). While semi-synthetic gels are produced by small or large-scale purification, fractionation and chemical conversion of natural base material, namely, dextran. The well-known dextran derivative semi-synthetic gel is under trade name sephadex.

When the dispersion medium is water, it is called a hydro-gel. There is a distribution of pore sizes within each gel and one gel is distinguished from another by the nature of this distribution. In course of some early experiments on gels, Biltz [30] concluded that hydro-gels are characterized by two types of pores; the 'primary' pores are of nearly molecular dimensions and the other ones are much coarser 'secondary' pores which behave as normal capillaries.

Because of their different properties, gels have many applications in various fields. The DNA samples can be separated using gel electrophoresis. Polyacrylamide

gel electrophoresis technique was introduced by Raymond and Weintraub in 1959. The pore size of the gel may be varied to produce different molecular sieving effects for separating proteins of different sizes [31].

The recent advancements in the intelligent gels have brought numerous advantages. Poly-electrolytes are a special kind of macromolecules, in which many of the side groups can easily become charged by gaining or losing electrons. By developing branches and intermolecular connections (cross-linking) these macromolecules can form 3-dimensional networks. If water is filled it can swell up to form gels. Interconnections between water and the polymer network determine the swelling or shrinking. The intelligent gel, which expands upon application of electric field, has many applications. Insulin is encapsulated in such a gel and implanted into diabetic patients. The controlled release is achieved by applying an electric field external to the body; the needle pricks are thus spared. Some medications are destroyed by acidic environment; therefore, they can not be used in the acidic environment of stomach. A gel, which shrinks in acidic conditions and expands in alkaline condition, can be used to encapsulate the medication. When the medication is encapsulated in such a gel, it will be tightly protected as it passes through stomach; however, in relative alkaline conditions of the intestines, the gel will expand and release the medications.

The poly-electrolyte gels undergo phase transitions and can have sudden change in volume, ranging from 100 to 500 times to original size. These transitions are caused by small changes in temperatures, solvent composition, salinity, pH, ionic strength and electric field. For example, poly (N-isopropylacrylamide) can suddenly swell 100-fold when the temperature is changed as little as one degree from 31 ºC to 32ºC.

Certain gels have been developed, which can change both their size and shape and thereby converting chemical energy directly into mechanical work. They act, more-or-less, like biological systems consist mostly of soft and wet substances, for example, the sea-cucumber, which is consider as something like a water swollen gel with primitive organs. Researchers have developed new gels that swell or shrink in response to many stimuli- temperature, pH and electric fields- depending upon the chemical composition of the gel and solvent. This type of gels can form a base for *soft machine* similar to a muscle [32].

3.5.2 Structure of Silica Hydro-gel: -

Silica hydro-gel is the most favorite gel for the crystal growth experiments; hence the study of its gelling mechanism and gel structure carries considerable importance. When sodium meta-silicate goes into aqueous solution, mono-silicic acid is produced in accordance with the dynamic equilibrium,

$$Na_2SiO_3 + 3H_2O \rightarrow H_4SiO_4 + 2NaOH$$
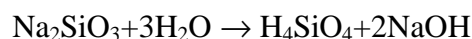
This mono-silicic acid can polymerize with the liberation of water,
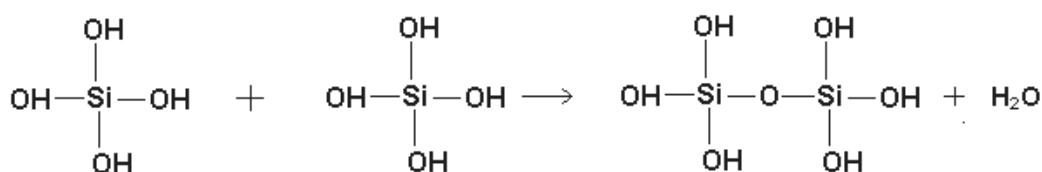
This can occur repeatedly and a three dimensional network of Si-O links is established as silica hydro-gel.
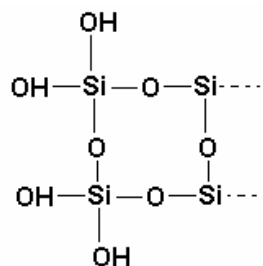
As the polymerization process continues, water accumulates on top of the gel surface. This phenomenon is known as "Syneresis". Much of the water has its origin in the above condensation process, and some may arise from purely mechanical factors connected with a small amount of gel shrinkage. The well-known stability of the silicon-oxygen bonds is responsible for the fact that the polymerization is largely irreversible. It is interesting to note that Kononenko et al, [33] studied the characteristics of light scattering in the initial stage of gel formation in silicic acid, which provides valuable information.

The time required for gelation is very sensitive to pH. As the gelation is a gradual process, there is no unique definition for gelation time. It is known that two types of ions are produced during the gelation; $H_3SiO_4^-$ and $H_2SiO_4^{-2}$, in relative amount which depends on the hydrogen ion concentration. The latter one, favored by high pH values, is in principle more reactive, but higher charge implies a greater degree of repulsions. The $H_3SiO_4^-$ is favored by moderately low pH values and found to be responsible for initial formation for long chain polymerization products [34]. Between these chains the cross-linkages are formed in due course, and these contribute to the sharp increase of viscosity that signals the onset of gelation. Because of their low mobility, very long chains will cross-link more slowly than short chains. At very low pH values, the tendency towards polymerization is diminished and chain formation is slowed. Gelation time is strongly dependent on temperature [27]. This has been described in detail by Henisch [24].

A weak acid is generally preferred to adjust the pH values, because pH of the set gel changes only slightly with time, and secondly, the mineral acids tend to spoil the growing crystals. It is noteworthy that in less acidic gel solutions the reaction between the acid and sodium meta-silicate occurs with liberation of hydroxyl ions and

thus pH of the solution rapidly increases with the process of polymerization, while in highly acidic gel there is no change in pH except due to very little difference in dissociation of acids of different complexities, as well as requirements of reaction mechanism. Hence pH has profound influence on the gel structure [35].

3.5.3 Gel Growth Methods: -

Crystal growth in gel has been mainly divided into the following five different methods

1. Reaction Method.

2. Chemical Reduction Method.

3. Complex Decomplexion Method.

4. Solubility Reduction Method.

5. Electrolytic Method.

3.5.3.1 Crystal Growth by Reaction: -

Crystals which are insoluble or slightly soluble in water and which decompose before reaching their melting points can be conveniently grown by this method. The basic requirements to grow single crystals by this method are,

(1) The reactants used must be soluble in the solvent (usually water) and the product crystal must be relatively less soluble.

(2) The gel must remain stable in the presence of the reacting solutions and must not react with these solutions or with the product formed.

(3) Some solubility of the product crystal is needed in order to grow crystals of any size [36].

Two aqueous solutions of soluble salts are suitably chosen and allowed to diffuse through the gel, so that there can be a slow and controlled segregation of ions and molecules resulting into the precipitation of an insoluble phase as the crystal. The

gel affords to limit the number of critical size nuclei and decreases the rate of crystal growth either by controlling the diffusion of reacting ions or by governing the reaction velocity on the surfaces of the growing crystals. Resulting chemical reaction can be expressed as:

$$AX + BY \rightarrow AY + BX$$
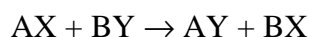
Where, A and B are the cations, X and Y are the anions.

This can be achieved by the test tube technique, in which one of the reactants is incorporated in the gel and the other reactant is diffused into it, or by the U-tube technique as shown in Fig. (3.4), or its modification in which the two reactants are allowed to react by diffusion into an essentially inactive gel.
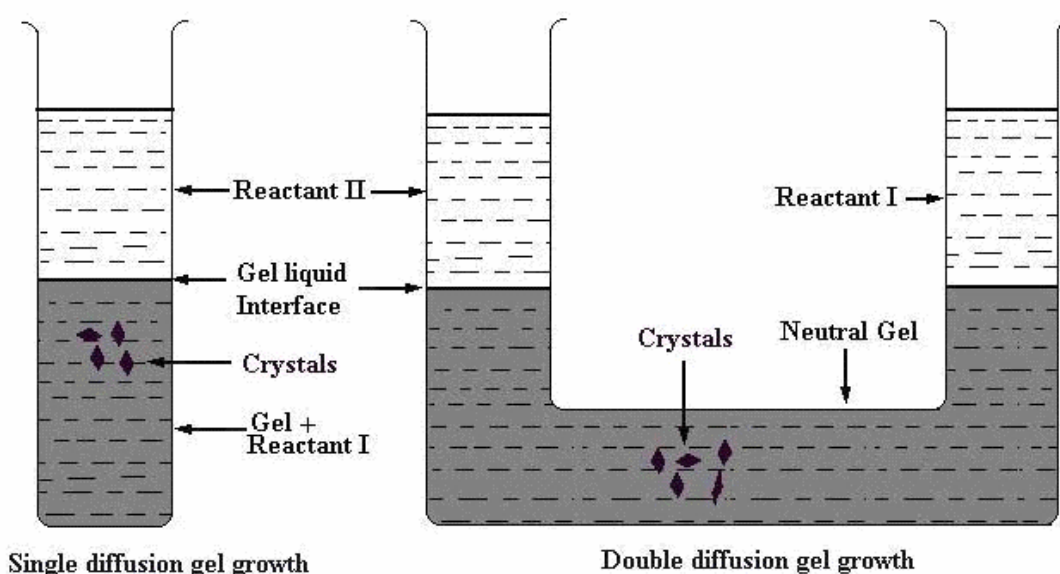
Figure (3.4): Crystal Growth by reaction method

There is a variety of crystallization apparatus employed to grow single crystals by this method. The disadvantages of these crystallization apparatus are the depletion of one the reactants which is inside the gel, the incorporation of reaction waste products by the growing crystals, supporting, handling and cleaning of the apparatus and gel preparation inside the horizontal tube open at both the ends [24].

3.5.3.2. Chemical Reduction Method: -

This method is suitable for growing only metal crystals from gel media. Hatschek and Simons [37] were the first to report the growth of gold crystals by adding 8 % oxalic acid solution over a set gel containing gold chloride solution. By this particular method crystals of Nickel ,Cobalt, Selenium, Lead and Copper have been obtained.

3.5.3.3. Complex Decomplexion Method: -

This method requires first forming a chemical complex of the material of the crystals to be grown with aqueous solutions of some suitable substance, called complexing agent, in which the former is homogeneously mixable and then providing externally a condition conducive to de-complexing or dissociation of the complex formed. A standard procedure adopted for decomplexion is to increase the dilution steadily, while complex solution is diffused through the gel. Crystal growth by this method was first attempted by O' Connor et al. [38] for the growth of cupric halide crystals.

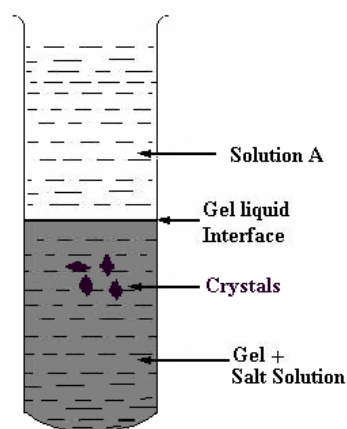### 3.5.3.4. Solubility Reduction Method:

Figure (3.5): Crystal Growth by solubility reduction method

This method is applicable to grow single crystals of highly water-soluble substances. The growth of ammonium dihydrogen phosphate (ADP) single crystals by this method has been first reported by Gloker and Soest [39].

In this method, the substance to be grown is dissolved in water and is incorporated with the gel forming solution. Then a solution, which reduces the solubility of the substance is added over the set gel to induce crystallization as in Fig. (3.5). For instance, potassium dihydrogen phosphate (KDP) crystals have been grown by adding ethyl alcohol over the gel containing a saturated solution of KDP [40]. Crystals are grown due to the reduction of solubility of KDP in the liquid phase by the diffusing alcohol.

3.5.3.5   Electrolytic Method: -

The electrolytic method can also be used for the growth of metallic crystals by selecting the gel medium for controlled growth. For this a very low d.c. electric current, usually of the order of 2-10 mA, is passed through a silica gel charged with suitable acid or electrolytic solution.
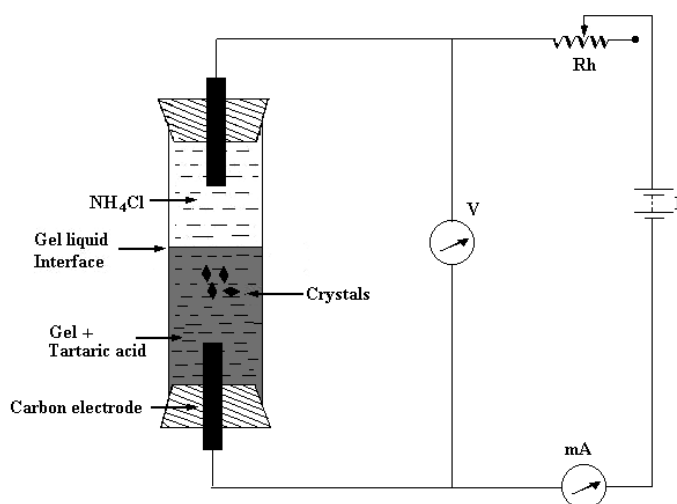

Figure (3.6): Crystal Growth by electrolytic Method

Details are given in Fig. (3.6). It has been found that the pH of the gel medium, the concentration of the supernatant solution, the current density and the material used as

electrode, have considerable influence on the habit of the crystals grown. Mohanan Pillai et al. [41] grew lead dendrites, while George and Vaidyan [42] grew copper dendrites and silver dendrites and single crystals [43] using the electrolytic technique.

3.6   Growth Mechanism:

Even though crystals can be grown by using a variety of gels, it is found that silica gels are the best to grow good quality single crystals. As gels are neither liquid nor solid in nature there are only a few methods available for quantitative investigations. From the SEM observations of dried silica gels, it has been found that the gel consists of sheet- like structures of varying degrees of surface roughness and porosity, forming interconnected cells. Generally, the cell walls are curved. It has been estimated from the SEM pictures that the cell walls in dense gels (0.4 M Na_2SiO_3) have pores from 0.1μ to 0.5μ and $0.1~\mu$ to 4μ in low density (0.2M Na_2SiO_3) gels. The cell walls are thicker in dense gels. During gelling the pH has a profound influence on the gel structure, changes from a distinctly box like network to a structure consisting of loosely bound platelets which appear to lack cross- linkages and the cellular nature becoming less distinct [44].

In the absence of convection, the only mechanism available for the supply of solute to the growing crystal is diffusion. One may envisage that the solute super-saturation f_∞ at large distances from the crystal remains unchanged during growth. However, at the crystal surface f would initially have the same value but would then adjust itself in the course of growth to the lower value f_0. Hence this is determined by the dynamics of the growth processes.

For different idealized geometries, Frank [45] has developed equations, which give a description of diffusion controlled growth rates. The growth rates calculated by Frank involve the "reduced radius" (*S*) which for spherical system is defined as *r /*

$(Dt)^{1/2}$, where 'r' is the radius of the crystal, 'D' is the diffusion constant and 't' is the time. The theory presents a simple relation,

$$\boldsymbol{f_{¥}} - \boldsymbol{f_0} = F\,(S)$$

By measuring 'S' and knowing the function 'F' the value of $\boldsymbol{f_0}$ at any time could be determined. As long as 'D' does not alter, a constant value of 'S' implies a constant value of $\boldsymbol{f_0}$. The constancy of 'S' can be checked by plotting r^2 versus t.

However, some limitations exist; one arising from the initial transient period during which steady–state concentration is established, and one arising from exhaustion of available solute. Both factors must be expected to give rise to nonlinearity. In general, there remains substantial uncertainty as to the effect of which the disruption of the gel structure has on the local value of 'D'. This also applies to the effect of pH changes, which occurs during growth. This has been described for various crystals grown in detail by Henisch [24].

Cipanov et al. [46] have developed a mathematical model of crystal growth process in gels. Calculations suggest that there is a locality in a gel that provides the best condition for nucleation and growth of crystals. They have compared the model with experimental results. Moreover, theoretical aspects of the crystal growth in gel medium have been proposed by Desai and Hanchinal [47].

In growth systems, which depend on the diffusion of the reactant through a gel incorporating the other reagent, it has been found that the growth rate is more near the gel solution interface where the concentration gradients are high and away from the interface, the gradients are relatively low. Dislocation density is also different corresponding to the different growth rates. This further suggests that the growth rate itself determines the number of defects grown into the crystal even in the absence of foreign impurities. Occasionally, crystals grown in gels are found to have dislocation

densities less than $10^3/cm^2$. The high degree of perfection of these crystals has been demonstrated by many authors [48, 49].

In general, crystals growing in gel either displace the gel as they grow [50] or incorporate [51]. In the case of gel displacing, cusp will be formed around the growing crystals, whereas in the other case, since the crystals incorporate the gel as they grow, final crystals turn turbid instead of being transparent. The cusps like cavities are the regions in which the gel has been split and separated from the growing faces.

3.7   Nucleation Control:

Even though gel helps in suppressing nucleation, crystals growing in a gel system compete with one another for the solute atoms. This competition limits their size and perfection. It is, therefore, desirable to suppress nucleation so that only a few crystals are formed. There are some methods which control nucleation :

1. Using suitable reactants

2. Using gels prepared with various acids

3. Changing the gel structure

4. Using intermediate neutral gel

5. Concentration programming

Several authors [24, 26, 52] have discussed these methods in great details hence the elaborate discussion is avoided.

3.8   Crystal Habit:

Crystals with various habits are important both commercially and also in studying their physical properties. In gel growth, crystals with various habits can be grown by changing concentration of feed solutions, crystallization temperature,

adding impurities and using various types of gels. Moreover, in some cases various habits in different regions of gel are also observed.

The habit modification can be obtained by changing concentration of the feed solution. McCauley and Gehrhardt [53] observed that during the growth of neodymium carbonate, a sodium carbonate incorporated gel enhanced the formation of dendrites and spherulites, while a neodymium chloride incorporated gel favored the growth of rhombic plates. Also, Bandhopadhyay and De [54] found that as the strength of feed solution was increased from 0.2 to 0.3 M, the calcium carbonate crystals were of rhombohedral habit and for 0.4 to 0.6 M concentrations the crystals were with the edges having wavy and ripple like features. On further increasing the strength of feed solution to 1M or more, a large number of nucleation centers with dendritic growth were observed.

The temperature of the growth has pronounced effect on habit of crystals. For example, in the case of strontium sulphate, all crystals grown at about 35ºC exhibited {011} and {102} as their habit faces, whereas the crystals grown at about 20ºC developed {022} habit faces in addition to {011} and {102} faces [51].

The habit modification can be observed for various gel structures. Mc Cauley and Roy [55] investigated the growth of calcite crystals and found that decrease in pH of the gel turned spherulites (pH 10.5) into feathery polycrystalline aggregates (pH 9 to 10.5) and, ultimately, into single crystals of rhombic habits (pH 7 to 9).

Alike to 'solution growth', it is possible to change the crystal habit by adding impurities in the gel growth also. Various habits of calcite were obtained by adding impurities of magnesium, strontium, nickel and barium in different proportions during the growth of these crystals [56]. A similar study was carried out by Rosmalen et al [57] on gypsum crystals.

However, the habit modification is observed by using various types of gels for crystal growth. A comparison of crystals of calcium sulphate dihydrate grown in two different gel media, sodium silicate gel and bentonite clay gel showed that the two media clearly affect the crystal habit and surface topography [58].

Interestingly, various crystal habits have been observed at different regions of gel. For lead molybdate growth, there were different regions inside the gel, where lead molybdate crystals of different habits were grown. Near lead nitrate solute, i.e. at the gel-liquid interface, polyhedral pyramidal crystals were formed. Altogether, octahedral bi-pyramidal crystals and platelets were observed in the central region and near the ammonium molybdate solution, respectively [59].Nucleation of crystals in gel is also influenced by light [25, 60]. Calcium tartrate crystals were observed to have grown more perfectly with irradiation of the gel than in darkness, but copper chloride crystals grown from gel had an adverse effect [61].

3.9   Spherulitic Crystals: -

Spherulites were first observed by Bunn and Alcock in a polymer system in 1945 [62], however, Price [63] studied in detail about the kinetics of spherulitic formation. In most of crystal growth, after attaining a stable size a typical primary nucleus grows into a crystallite having a discrete crystallographic orientation. This continues to develop as a single crystal until it impinges either upon external boundaries or upon other similar crystallites advancing from neighboring nuclei. In certain systems, primary nuclei are incapable of such a development and each one giving rise instead to a more complicated structure. It is with a radiating array of crystalline fibers, all having the same fiber axis. The fibers branching will be in such a way that the crystallographic orientation of a branch departs slightly, but appreciably from that of its parent fibers. It is a characteristic property of these particular systems

that the primary nuclei initiate the formation of polycrystalline aggregates, which are more-or-less radially symmetric. The growths of these aggregates, which are called spherulites, occur naturally in silicate minerals and found in igneous rock strata. Apart from this, artificial spherulites have been grown in organic and inorganic compounds. According to McCauley et al. [36] a spherulite is a crystalline spherical body, which is formed by the growth of radiating crystallites or a concentric banding, is a polycrystalline aggregate and not a single crystal. Many materials can form spherulites under suitable conditions; the main requirement is the high viscosity of the medium [64].

Impurities may play a crucial role in promoting a fibrous habit in spherulitic crystallization, which has been suggested by Bernauer [65].

Many authors have observed spherulitic crystal growth, for example, alkaline earth molybdates [66], rare earth tartrates [67], iron (II) tartrate [68] and zinc tartrate [69].

3.10   Liesegang Rings:

Chemical reactions leading to the formation of precipitates in gels are ideal in sense that the particles of precipitates remain where they are produced and the reagent reach each other only by diffusion. This study is very important, because chemical reactions in biological media, whether leaving or dead, and in many geological structures are of this type. The diffusion of a soluble substance from an aqueous solution into gel follows the ordinary Fick's diffusion law.

The main feature of chemical reactions is that the diffusion of one reagent into the other contained in the gel produces not only the ordinary chemical change, but also definite mechanical structure. This structure varies with conditions and can be controlled.

Hedges [70] has identified the following four types of structures produced by chemical reaction in gels.

1.   Precipitates of continuous structure, which consists of small particles uniformly distributed so that the whole mass appears homogeneous to the eye.

2.   Discrete structures consist of particles of relatively large size, separated by considerable spaces and may contain well-formed crystals having a length of a few millimeters.

3.   Cellular structures comprise of a network of honey–comb like cells of precipitates enclosing clear gel, frequently obtained with a large number of a precipitate.

4.   Periodic structures contain definite bends or rings of precipitants separated by clear spaces, which often contain the precipitate as discrete structures [71].

The first interesting study of a periodic structure was made by Liesegang in 1896 [72, 73]. He covered a glass plate with a layer of gelatin impregnated with potassium chromate and added a small drop of silver nitrate. As a result, silver chromate was precipitated in the form of a series of concentric rings; well develop with regularly varying spacing. These types of fascinating formations are called as *Liesegang rings*.

Several workers have observed that, in many cases, the space between the rings contains a considerable amount of precipitate. Often the rings contain a large number of small particles and the intervening spaces contain a small number of large particles. Hatschek [74] had reported very interesting case of a cadmium sulphide precipitates in silicic acid gel, where the precipitates consisted of alternate pink and yellow bands with the difference in the size of particles. Dhar and Chatterji [75] had

recognized that a layer of precipitates was followed by a clear zone in some structures and by a zone of differently dispersed precipitates in others.

Generally, the distance between successive bands of Liesegang rings increases as the diffusion proceeds further. Schleussner [76] had found the spacing to confirm with the geometric series and this conclusion had been confirmed by several other investigators [77, 78]. However, a different nature was observed by Davis [79], when mercurous nitrate was allowed to diffuse into Agar gel containing sodium formate, the distance between successive bands was found to decrease.

Generally, two types of Liesegang rings have been reported in literature [80]; they are *direct type* and *revert type*. In the direct type, the spacing between successive rings increases with increase in the order of the ring from the gel boundary. Gnanam et al. [81] have reported the direct type Liesegang rings of calcite. In contrast to this, the revert type Liesegang rings exhibit the spacing between successive rings decreasing as the order of ring increases from the gel boundary.

Many parameters influence the formation of Liesegang rings which are listed as follows [71]:

(1)   Concentration

(2)   Light

(3)   Temperature

(4)   Reaction medium

(5)   Presence of impurities

(6)   Electric field

(7)   Gravity

(8)   Tension

(9)   Age of the gel

Many authors have attempted to give explanations of the formation of Liesegang rings by different models, theories and computer simulations. Henisch and Gracia-Ruiz [82] suggested a numerical method to obtain the formation of Liesegang rings on the basis of Fick's diffusion equation for reagents in gel as a function of time. In other study, Henisch and Gracia-Ruiz [83] extended the condition under which two diffusing reagents could form precipitates either continuous or periodic in a gel media. Moreover, several other theories and models have been suggested by different workers. A microscopic approach to the formation of Liesegang patterns, based on a cellular automate model has been proposed by Chopard et al. [84]. While in another model, Chernavskii et al. [85] take into account of the effects of super-saturation, competition between nucleation centers and droplet growth kinetics as well as redistribution of matter between particles of precipitants. Also, many researchers have presented diffusion based models and theories. A turning type reaction-diffusion model is explored by Brechet and Kirkaldy [86], which can be applicable to Liesegang bands, rings and spirals evolving by precipitation in the environments of an equilibrium solubility product reaction. Diffusion coefficient of barium ions from Liesegang rings formation have been estimated by Dharmaprakash and Mohan Rao [87] using the simple mathematical model based on Kirov model [88]. Moreover, Varghese et al. [89] estimated diffusion coefficient in multi-component systems forming Liesegang ring. Apart from this, some computer simulation experiments also have been carried out. Bueki et al. [90] studied regular Liesegang structure by means of computer simulation. Also, the same authors [91] studied two dimensional chemical patterns formation in gels by experiments as well as computer simulations.

Many natural phenomena exhibit the Liesegang ring type of structures, for example, the periodicity in the structure of urinary calculi [92]; the concentric rings of

beet roots [93]; the periodic structures found in geological objects like agates and malachite [71] and the periodical layering in bones [94]. It is interesting to note that the solid state reaction in Ag-Ti-Si system produces periodic layer formation, which resembles the Liesegang ring phenomenon [95]. Gerard et al. [96, 97] studied conditions for formation and development of the Liesegang rings produced by sodium chloride aerosols. Moreover, Liesegang ring type periodic precipitation reaction has been investigated in anodic oxide films, on titanium and zirconium and grown in the presence of sodium tungstate, by X-ray, photoelectron spectroscopy and Rutherford back scattering spectrometry [98]. Also, Liesegang ring type periodic microstructures have been observed on single crystal surfaces of oxide superconductors $Ba_{0.6}K_{0.4}BiO_3$ [99].

3.11   Crystals Grown by Gel Method: -

Numerous workers have grown various crystals by the gel growth technique. It is a tedious and laborious task to cover the entire list of crystals; nevertheless, some important biomaterials crystals, grown for special interest and applications, are reported hereby.

Quite significant work has been reported on different kinds of urinary crystals such as, calcium oxalate monohydrate (COM) [100-103], calcium hydrogen phosphate dihydrate (CHPD) [101,104-106]], ammonium magnesium phosphate (AMP) [107,108], uric acid crystals [109], hydroxyapatite crystals [110].

Interestingly, the growths of various bio-molecule crystals have been carried out by different researchers in view to understand their formations in body. The worth noting examples are, the gel growth of cholesterol crystal [111]; growth of fibrous crystals of cholesterol in silica gel [112]; growth of steroid crystals of cholesteryl acetate [113]; single crystal growth of testosterone monohydrate ($C_{19}H_{28}O_2H_2O$) in

silica gel [114]; growth of plant steroid Beta sitosterol in silica gel [115]; and growth of egg white lysozyme (protein) in agarose gel using hanging drop technique [116]. Spherulites and polycrystalline aggregates of calcite produced by the bacteria activity of Escherichia Coli within the gel medium were also reported [117]. Natarajan et al. [118] have grown single crystals of amino acids, such as α-glycine, in silica gel using reduction in solubility method.

Understanding of organo-crystalline interactions is very vital in study of the formation of bio-mineralized structures inducing bones and teeth. Crystal faces of same form but on opposite sides of mirror of symmetry in monoclinic gypsum were shown for 28 cases to exhibit unequal affinity for chiral organic molecules [119]. Rinaudo et al. [120] grew gypsum ($CaSO_4.2H_2O$) crystals and characterized them with X-ray topography, whereas, Raju [121] reported tracking of dislocations in gel grown gypsum crystals. Statoliths of coronate medusa, *Periphylla periplylla* consist of crystals of calcium sulphate [122]. Recently, gel grown crystals are characterized by XRD, thermal and FTIR studies [123].

In the present author's laboratory, his predecessors [52,103,124] have made detailed survey of various crystals grown by the gel techniques, therefore, a detailed survey has been avoided here and the concentration is focused on the bio-materials crystals growth only. Chapters- VI, VII, VIII and IX deal with the growth of various bio-materials crystals the author has grown.

3.12   Crystal Growth Observation Techniques:

It is always of great interest for a curious mind to know how the crystal growth process occurs and to observe it at every instance of time. Holographic interferometry has proved to be a very powerful optical technique to study the micro-topography of crystal faces and crystal growth from solution. Double exposure, depth

contouring and real time have been described to check crystal morphology by Bedarida [125]. However, the real time interferometry was revealed to be a very useful tool to study crystal growth from solution and form a transparent gel. Later on, Lafaucheux et al. [126] applied the holographic interferometry to study mass transfer induced by nucleation and growth in gel media. Real time observations were made on growth of insoluble ($CaHPO_4$ $2H2O$) and soluble (KDP) materials.

3.13 Advantages and Limitation of Gel Growth: -

Gel method has many advantages and it is preferred to grow certain crystals, which are otherwise very difficult to grow by other techniques. This method is quite popular to grow crystals which are sparingly soluble in water or decompose on heating. Because for these crystals the application of techniques like solution growth and melt growth is not feasible.

The gel framework, which is chemically inert and harmless, acts like a three dimensional crucible wherein the crystal nuclei are delicately held in the position of their formation and growth, thereby preventing the damage, if any, due to impact with either the bottom or the walls of the container. Also, the crystals can be observed practically in all stages of their growth. All crystal nuclei are spatially separated and hence the effects of precipitations are eliminated. The gel medium considerably prevents convection currents and turbulence.

Thermodynamic consideration reveals that as the growth proceeds at ambient temperature, the grown crystals would contain relatively less concentration of equilibrium defects.

Growth of crystals with different morphologies is commonly found in bio-mineralization. In the gel growth technique, by changing the growth conditions, crystals with different morphologies and sizes can be obtained.

Inasmuch as this method is extremely simple and inexpensive, good quality crystals can be grown even in small laboratories, which do not possess sophisticated equipments, however, it requires delicate art of growing crystals.

This gives the gel growth the cutting edge over other techniques for *in vitro* studies of growth of different bio-materials crystals, because the bio-crystallization or bio-mineralization usually occurs in the slow and steady media. This technique can mimic the bio-environment for the growth. It is worth noting, hereby, that this advantage of the gel growth is well explored by the present author in this thesis.

With lots of advantages, notwithstanding, the gel method posses several limitations also. Crystal size is generally small and the growth period is large, therefore, large crystals cannot be grown by this method. In case of using silica gel, the gel inclusion occurs during growth in some crystals. Also, there is a chance of lattice contamination by impurities from the gel itself.

3.14   Modified Gel Growth Technique for the Micro-crystal Growth:

The growth of micro-crystals is playing important role in various systems, including the human body. Gout is an inflammatory arthritis caused by the deposition of micro-crystals of mono-sodium urate (MSU) in a joint [127]. Calcium oxalate micro-crystals in urine are important to study the conditions for urinary stones [128, 129]. Also, many other micro-crystals have been studied for various purposes. The concentration dependence of free electron mobility in InSb micro-crystals, obtained from chemical transport reactions, studied for different doping combinations [130]. A closed packed arrays of micro-crystals, within the domain or through out the framboidal pyrite was reported [131]. The growth rate enhancement of Potash Alum crystals by micro-crystals was reported as well [132].

However, many authors have attempted to grow micro-crystals by various techniques. By using the micro-batch technique Chayen [133] has grown micro-crystals of glucose isomerase under paraffin oil in a 1.3 micro-liter drop. In another study, using a microscopic set up; Oosterhof et al. [134] have reported the growth of sodium nitrate micro-crystals from mixture of water and iso-propoxyethanol. Moreover, Holmback and Rasmuson [135] have grown Benzoic acid micro-crystals in a semi-batch operation by feeding water or water-ethanol mixture into agitated, saturated, ethanol water solutions. The growth of crystals from the gels is well-explored technique and Henisch [24] has described it elaborately in his book. Notwithstanding, the growth of micro-crystals by gel technique is not well reported, except one report by Ivan van As [137].

In the present thesis, the *in situ* growth observations of micro-crystals of calcium hydrogen phosphate dihydrate (CHPD) or brushite and its growth inhibition study is reported in Chapter-VIII.

In the usual experimental technique for micro-crystal growth, glass slides with cover slips and Petri dishes are used as the growth apparatus. The glass slides are arranged in the Petri dish in form of a plus sign, where the lower slide is used just for the support and the upper slide is used for the micro-crystal growth. To grow the micro-crystals in a silica gel medium, a sodium meta-silicate solution of desired specific gravity is mixed with weak acid so that appropriate pH could be set for the mixture. Thereafter, with help of suitable glass dropper a small drop of this mixture is put at the middle of glass slide. The cover slip is put on this drop of mixture in such a way that it floats on the mixture and covers almost the area of a cover slip size, without spillage beyond the cover slip. To assure that the gelling process occurs properly without drying the solution, the slides are put in a Petri dish in such a way

that water poured in the Petri dish does not touch the cover slip, but remains slightly below the upper surface of the slide. These experimental arrangements are described in figure (3.7). After setting the gel, water is sucked from the Petri dish with the help of suitable dropper. Thereafter, other solution of appropriate salt is added with dropper carefully so that it should cover the slide up to the cover slip.
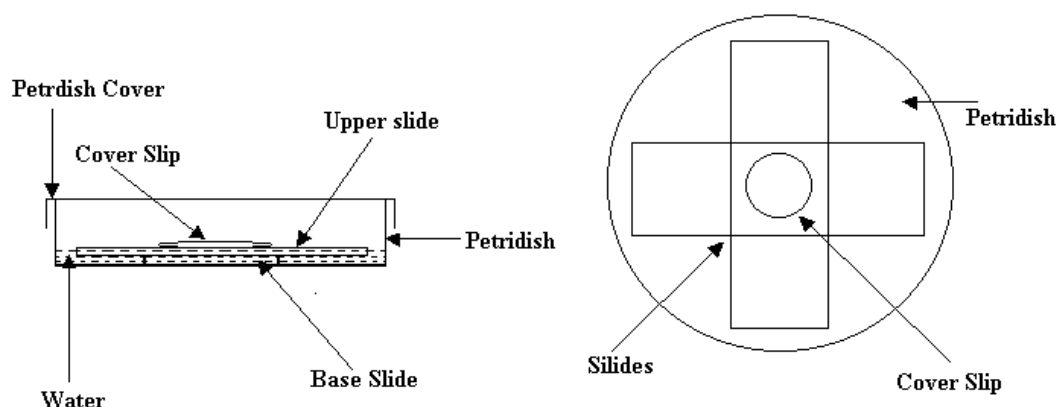

Figure (3.7): Set up for modified gel growth technique

The poured solution diffuses through the gel and a reaction takes place between the weak acid impregnated in the gel and the salt solution poured afterwards and, subsequently, nucleation and growth of micro-crystals occurs within 24 hours. Usually, the cover slip is having diameter 18 mm and total area 254.34 mm^2. If the drop put on the slide to form the gel is of the order of 10 micro-liter, then the thickness of the gel can be estimated to be of the order of 0.039 mm. The slides can be observed regularly by using normal optical microscope and can be photographed either by a normal camera or a CCD camera attached with microscope.

This is an inexpensive technique, which requires a good quality optical microscope with measurement facilities; otherwise, comparatively costly techniques are employed to observe the growth of micro-crystals such as, AFM [138], on-line x-

ray diffraction [139], ultrasonic spectroscopy [140], etc. This technique can also be used for screening samples in biological media, observing changes in morphology as well as growth inhibition and promotion studies. This technique gives results quite rapidly within a day or two, requires very less amount of chemicals and, of course, economical also. Therefore, it is preferred over the other conventional techniques.

3.15   Solution Growth:

The growth of crystals is a result of addition of new atoms, molecules or more complex aggregates. The addition of a new particle of the same substance is not necessarily the same thing as crystal growth. For example, adsorption on a atomically smooth surface is not sufficient to be regarded as growth, because it may stop once a certain concentration of ad-atoms is achieved; this happens when the chemical potential of the adsorbed atoms or molecules becomes equal to that of the identical atoms or molecules in vapor or solution, as the case may be [141].

The solution growth usually occurs in a layer wise manner. The crystallizing substance is delivered to the step by either bulk or surface diffusion. However, their relative role is not well established.

Recently, many authors have discussed different crystal growth topics covering mainly the solution growth, which are thermodynamics versus kinetics[142], the terrace-step-kink approach and the capillary wave approach to the fluctuation properties[143] and a comprehensive treatise on crystal growth from solutions[144].

All methods of growing crystals from solutions are based on the dependence of the solubility of a substance on the thermodynamic parameters of the process, temperature, pressure, and solvent concentration. In the majority of the cases the temperature dependence of the solubility is employed.

The state of super-saturation is very essential for crystallization to occur. One of the convenient ways in which the degree of super-saturation can be expressed is by the means of the following expression,

$$S = c / c^*$$

Where, c is the concentration of the solution and c^* is the equilibrium saturation concentration at the same temperature. Hence different three states of saturations are denoted by the values of S; namely, a saturated solution indicates $S = 1$, under-saturated solution denotes $S < 1$, and supersaturated solution indicates $S > 1$. Other common expressions of super-saturation are the concentration driving force, $\ddot{A} c$, and relative super-saturation, ó, defined by [145]

$$\ddot{A} c = c - c^* \quad \text{and} \quad ó = \ddot{A} c / c^* = S - 1$$

For any solution growth experiments it is required to study the temperature-concentration (T-C) diagram. This has been discussed by Chernov [141] in detail hence elaborative discussion is avoided here.

3.16 Choice of Solvents and Additives:

It is important to select proper solvent for the solution growth so that one can yield prismatic growth habits of crystals. A good solvent ideally displays the following characteristics:

(a) Moderate reversible solubility

(b) A reasonable positive temperature coefficient of solubility

(c) A small vapor pressure

(d) Non-corrosiveness

(e) Non-toxicity

(f) Low price in a pure state

(g) Non-flammability

Solvents possessing all these characteristics, altogether, do not exist. However, solvent in practical use include water-both light (H_2O) and heavy (D_2O),

ethyl alcohol, acetone, carbon tetrachloride, hexane, xylene and many others. Water is used in about 90% of cases, and heavy water, alcohol and acetone each contributes about 1%.

Usually, a solvent is used in which the solute is soluble to the extent of 10 to 60 %. If the solvent is volatile, precautions must be taken to prevent volatilization which promotes spurious nucleation due to temperature and concentration changes.

The experiments of Bunn and Emmett [146] show that electrostatic forces between crystal and solution are involved in crystal growth, and therefore the polarity of the solvent must be considered. Kohman [147] has observed that crystals of non-polar organic compounds grow from non- polar organic solvents at rates comparable to the solidification of melts, suggesting that the main difference between two processes is the interaction of solute and solvent molecule. Many additives that influence crystal growth morphology [148] and the crystal growth rates [149] are studied. Many times a change in the growing crystalline habit is desirable. A habit of growing crystal can be altered by changing the temperature of growth, changing the pH of solution, adding a habit modifying agent and changing the solvent.

Moreover, to have a regular and even growth, the level of super-saturation has to be maintained equally around the surface of the growing crystal. An uneven growth leads to localized stresses at the surface generating imperfection in the bulk crystal. The concentration gradients that exist in the growth vessel at different faces of crystal cause fluctuations in super-saturation, which seriously affects the growth rate of individual faces. The gradient at the bottom of the growth vessel exceeds the meta-stable zone width, resulting into spurious nucleation. However, the degree of formation of concentration gradients around the crystal depends on the efficiency of

agitation of the solution. For these reasons, the agitation of saturated solution in either direction at an optimized speed of stirrer motor is advisable.

3.17   Selection of Seeds:

Gilman [16] compared the artificial growth of crystals with *agriculture.* Alike in agriculture, good crystal growth needs good quality *seeds,* uninterrupted supply of *nutrients*   and allowing the fittest to grow. Getting a proper quality of seed crystals is a prime factor in crystal growth. The classical method is by evaporating or slow cooling saturated solution. But it is frequently more practical to use a piece from a natural or a previously grown crystal, or to produce oriented over growth on a seed of similar material. Any fragment of the desired crystal can serve as a seed. A piece bounded by the natural faces is not always the most preferable one. The most efficient seed is a plate whose faces are normal to the most rapid growth direction [150].

3.18   Solution Growth Methods:

A variety of crystals are grown by the solution growth techniques for industrial applications. The size of the crystallizer vessels varies depending upon the requirements, whether it is for the research or industry. A large number of ionic salt crystals, organic crystals and semi-organic crystals are grown by these methods. Various authors [15, 16,141,151-153] have given elaborative discussions on various solution growth techniques and hence a brief review is presented here.

Usually, *slow cooling* method is employed to achieve the required degree of super-saturation. The simplest illustration of the method is crystallization in a closed vessel, which is depicted in Figure (3.8).
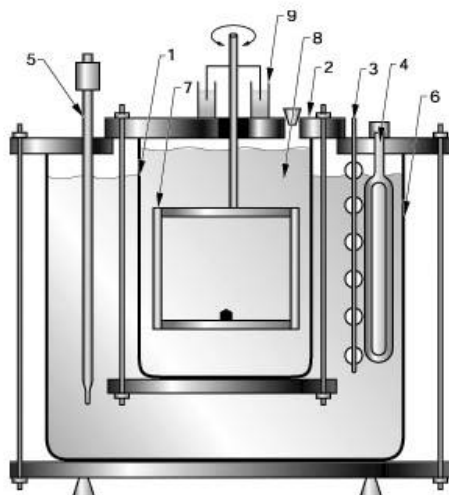
Figure (3.8): Schematic diagram of a crystallizer used for rapid crystal growth: (1) growth tank; (2) air-sealed lead; (3) stirrer; (4) heater; (5) thermo-controller; (6) water bath; (7) platform with the seed; (8) growth solution; (9) water cup seal.

A solution saturated at an above room temperature is poured into a crystallizer, which is then hermetically sealed. Prior to this, the solution is heated to a temperature slightly above the saturation point in order to avoid spontaneous crystallization at the moment it is filled into the crystallizer. A seeding crystal is suspended in the solution, and the crystallizer is placed in a water thermostat whose temperature is reduced according to a pre-assigned plan. Super-saturation is maintained by slow cooling and the rates required can be as low as 0.1 ^{0}C to 1 ^{0}C per day. This has made big demands of appropriate temperature controllers and also made easier to achieve solution temperature near the room temperature. The solution is agitated either by mechanical stirrer or the rotating seed holder. The fluid flow thus provided breaks up the boundary layer of rejected solvent and leads to more perfect and faster growth. This method often produces sufficiently large crystals. A very large size, in terms of several kilograms of weight, KDP crystals have been grown for LASER applications by this method [23]

Temperature difference methods are based on the formation of two regions with different temperatures in the crystallizer. In one of them, the substance which is always in excess in the form of the solid phase is dissolved and in the other, crystal growth takes place. In this case two vessels connected by tubes are usually employed. The substance is dissolved in the vessel with the higher temperature, and the crystal is grown in the other. The exchange between the vessel is achieved both by natural convection of the solution and by stirring with a mechanical agitator. Due to natural convection, the solution from the dissolution chamber moves along the upper tube into the growth chamber, and along the water tube in the reverse direction. The large size crystals of various compounds can be grown successfully by this method. Figure (3.9) shows the schematic diagram of this method.
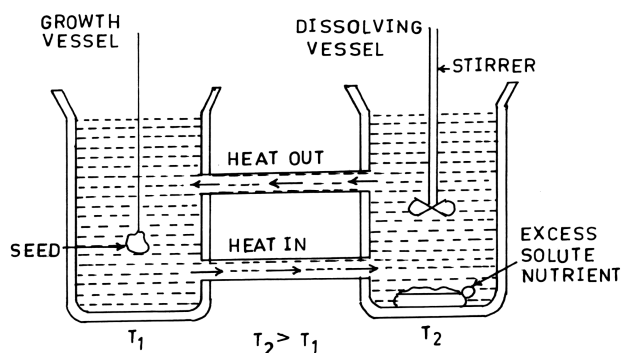

Figure (3.9) Temperature difference method

The super-saturation is achieved, in another method, by evaporating the solvent, as it evaporates the solute concentration increases to above equilibrium value. This is known as the *slow evaporation* method. The process is carried out at a constant temperature under strictly isothermal conditions. Preferential evaporation of the solvent occurs "spontaneously" if contact is provided between the solution and the atmosphere, for non-toxic solvents. The rate of evaporation can readily be controlled

by changing the solution temperature or controlling the passage using a screw-capped jar. The details of this technique are given by Chernov [141].

3.19   Advantages of Growth from Solution:

There are several advantages of crystal growth from solution. This technique makes it possible to grow crystals that are unstable at their melting points or that exist in several crystal forms depending on the temperature and provides control over temperature of growth [154]

Many times an advantage in control of viscosity in solution growth methods which permits crystals that tends to form glasses when cooled from their melts to be grown. Low viscosity solvents such as water greatly accelerate diversification of silica glass [155].

Generally, the rates of growth from melts are very large than those from solution. Crystals grown from solution usually have well defined faces as compared with those grown from melts.

Solution growth methods are comparatively inexpensive. In addition, the growth from solution can be visually inspected; in fact it has been extensively used for studying the growth parameters, including convection and transport, by means of photography. However, the solution growth techniques are comparatively slower, requires high purity solvents and a good deal of designing and parameter settings for good quality crystal growth [156].

References:

[1]   W. Kossel; *Nachr. Ges. Wiss.,* Göttingen, (1927) 135.

[2]   M. Volmer; *Z. Phys. Chem.* **102** (1922) 267.

[3]   W. K. Burton, N. Cabrera and F. C. Frank*; Phil*. Trans. **A243** (1951) 299.

[4]   J. W. Gibbs, *Collected Works*, Longman & Green, London (1928).

[5]   P. Curie; *Bull. Soc. Franc. Miner*., **8** (1885) 145.

[6]   G. Wulff; *Z. Kristallogr*., **34** (1901) 449.

[7]   D. Turnbull; *J. Chem. Phys*., **20** (1952) 411

[8]   A.C. Zettlemoyer; *Nucleation* , Decker, New York (1969).

[9]   A.A. Abraham*; Homogeneous Nucleation Theory*, Academic Press, New York, (1974).

[10]   M. Volmer and W. Shultze; *Z. Phys.Chem.,* **A156** (1931)1

[11]   F. C. Frank; *Advances in Physics*, *Phil. Mag. Supply*, **1** (1952) 91.

[12]   W. K. Burton; *Penguin Sci. News*, **21** (1951) 286.

[13]   A. R. Varma; *Crystal Growth and Dislocations*, Butterworths , London,(1953).

[14]   P. Bennema and G. H. Gilmer; *Kinetics of crystal growth*, in "Crystal *Growth: An Introduction"* Ed. P. Hartman, North Holland, Amsterdam (1973).

[15]   B. R. Pamplin; "*Crystal Growth*", Peragamon Press, Oxford, (1975).

[16]   J. J. Gilman; "*The Art and Science of Growing Crystals*", John Wiley, NewYork, (1964).

[17]   P. Ramasamy and P. Santhana Raghvan; "*Fundamentals of Crystal Growth*", KRU Publications (2001).

[18]   W. Miller and J. Neugebauer; *Modeling of Crystal Growth*, ISSCG-12, Aug 1-7, Berlin, (2004)

[19] J. J. Derby; Modeling *of Crystal Growth Processes*, ISSCG-12, Aug 1-7, Berlin, (2004).

[20] J. Neugebauer; *Multi-scale Growth Simulations*, Abstract, ICCG-14, Grenoble, France, (2004).

[21] R. A. Laudise; *"Crystal Growth*,' *"Techniques of crystal growth"*, Proc. Int. Conf. on Crystal Growth, Boston, Peragamon Press, Oxford. (1966).

[22] W. Bradsley; D. T. J. Hurle and J. B. Mullin, *"Crystal Growth: A Tutorial Approach",* North- Holland, Series in Crystal Growth, vol. -2, Amsterdam, (1979).

[23] N. Zaitseva; Lawrence Livermore National Laboratory, U.S.A.

[24] H. K. Henisch; *"Crystal Growth in Gels"* Dover Publication, New York, (1993).

[25] H. K. Henisch, J. Dennis and H. I. Hanoka; *Chem. Solids.*, **26** (1965) 493.

[26] A. R. Patel and A. V. Rao; *Bull. Mater. Sci.*, **4** (1982) 527.

[27] A. E. Alexander and P. Johnson; *Colloid Science,* Vol.2; Clarendon Press, Oxford (1949).

[28] K. A. Kum and R. Kunin; *J. Polymer Sci.*, **132** (1964) 587.

[29] T. Kremmer and L. Bross; *"Gel Chromatography Theory, Methodology, Applications"*, John Willey & Sons, New York, (1979).

[30] M. Z. Biltz; *Phys. Chem.,* **126** (1927) 356.

[31] N. Pernodet, B. Tinland, J. Sturm and G. Weill; *Biopolymers*, **50** (1999) 45.

[32] Y. Osada and S. B. Ross-Murphy; *Scientific American,* **1268** (1993) 42.

[33] V. G. Kononenko, S. I. Kontovovich and E. D. Shechukin; *Colloid J.*, USSR. **39** (1977) 497.

[34] C. J. Plank; *J. Colloid Science*, **2** (1947) 413.

[35] A. R. Patel and A. V. Rao; *J. Cryst. Growth.,* **43** (1978) 351.

[36] A. F. Armington and J. J. O'Connor; *AFCRL* (USA) (1967) 3251.

[37] E. Hatschek and Simon; *Kolloid Z.,* **10** (1912) 265.

[38] J. J. O'Connor, M. A. Dipietro, A. F. Armington and B. Rubin; *Nature,* **212** (1968) 68.

[39] D. A. Glocker and I. F. Soest; *J. Chem. Phys.,* **51** (1969) 3143.

[40] B. Brezina and J. Havrankova; *Mater. Res. Bull.,* **87** (1971) 537.

[41] K. Mohanan Pillai, M. A. Ittyachen and V. K. Vaidyan; *Natl. Acad. Sci. Lett.,* **3** (1980) 37.

[42] M. T. George and V. K. Vaidyan; *Crystal Res. Technol.,* **15** (1980) 653.

[43] M. T. George and V. K. Vaidyan; *J. Crystal Growth,* **53** (1981) 300.

[44] E. S. Halberstadt, H. K. Henisch, H. J. Nickl and E. W. White; *J. Colloid Interface Sci.,* **29** (1969) 469.

[45] F. C. Frank; *Proc. Roy. Soc.,* **201A** (1950) 586.

[46] A. V. Cipanov, L. L. Goshka, S. I. Kolosov and V. P. Ruzov; *Cryst. Res. Technol.,* **25** (1990) 119.

[47] C. C. Desai and A. N. Hanchinal; *Cryst. Res. Technol.,* **22** (1987) 1117.

[48] A. R. Patel and A. V. Rao; *J. Cryst. Growth,* **47** (1979) 213.

[49] J. J. O'Connor and A. F. Armington; *Mater. Res. Bull.,* **6** (1971) 765.

[50] A. R. Patel and A. V. Rao; *J. Cryst. Growth,* **38** (1977) 288.

[51] A. R. Patel and H. L. Bhatt; *J. Cryst. Growth,* **18** (1973) 288.

[52] S. Joseph, *Ph.D. Thesis,* Saurashtra University, Rajkot, (1987).

[53] J. W. McCauley and H. M. Gehrhardt; Report AMMRC TR-70-13 (AD-710236), (1970) 25.

[54] T. Bandyopadhyay and Ashok De; *Indian J. Earth Sci.,* **4** (1977) 95.

[55]   J. W. McCauley and R. Roy; *Am. Miner.,* **59** (1974) 947.

[56]   A. R. Patel and S. K. Arora; *J. Cryst. Growth*, **18** (1973) 199.

[57]   G. N. V. Rosmalen, W. G. J. Marchee and P. Bennema; *J. Cryst. Growth.,* **35** (1976) 169.

[58]   R. D. Cody and H. R. Shanks; *J. Cryst. Growth,* **23** (1974) 275.

[59]   K. S. Pillai and M. A. Ittyachen; *J. Cryst. Growth*, **39** (1977) 287.

[60]   J. Dennis; *Ph. D. Thesis*, Pennsylvania State Univ., (1968).

[61]   A. F. Armington, M. A. Dipietro and J. O'Connor, Air Force Cambridge Research Laboratories [Reference 67-0445, "Physical Science Research" Paper No. 334, July 1967].

[62]   C. W. Bunn and T. C. Alcock; *Trans Faraday Soc*., **41** (1945) 317.

[63]   F. P. Price; *J. Am. Chem. Soc*., **74** (1952) 311.

[64]   J. W. Mc Cauley and H. M. Gehrhardt; Tech. Report Number AMMRC TR-70-13, Army Material and Mechanics Research Center, Watertown Mass, June (1970).

[65]   F. Bernauer; "*Gedrillte Kristalle*", Borntrager, Berlin, (1929).

[66]   K. V. Kurian and M. A. Ittyachen; *Indian J. Pure. Appl. Phys*., **19** (1981) 154.

[67]   K. K. Raina; *Ph. D. Thesis*, University of Jammu, Jammu (1985).

[68]   S. Joseph, H. S. Joshi and M. J. Joshi; *Cryst. Res. Technol.*, **32** (1997) 339.

[69]   R. M. Dabhi and M. J. Joshi; *Indian. J. of Phys*., **76A** (2002) 211.

[70]   E. S. Hedges; "*Colloids",* Arnold & Co, (1931).

[71]   E. S. Hedges; "*Liesegang Rings and Other Periodic Structures",* Chapman & Hall, W.C. (1932).

[72]   R. E. Liesegang; *Naturwiss. Wochenschr.,* **11** (1896) 353.

[73]   R. E. Liesegang; *Phot. Archiv.,* (1896) 221.

[74]   E. Hatschek; *J. Soc. Chem. Ind*., **30** (1911) 256.

[75]   N.R. Dhar and A.C. Chatterji; *Kolloid Z.*, **31** (1922) 15.

[76]   C.A. Schleussner; *Kolloid Z.*, **31** (1922) 347.

[77]   K. Jableczynski and S. Kobryner; *Bull. of Soc. Chem*., **39** (1926) 383.

[78]   R. J., Doyle and H. Ryan; *Proc. Roy. Irish Acad*, **38B** (1929) 435.

[79]   H. S. Davis; *J. Amer. Chem. Soc.,* **39** (1917) 1312.

[80]   K. H. Stern; *"Bibliography of Liesegang Rings",* National Bureau of Standards, Washington, (1967).

[81]   F. D. Gnanam, S. Krishnan, P. Ramasamy and G. S. Laddha; *J. of Colloid Interface Sci.,* **73** (1980) 193.

[82]   H. K. Henisch and J. M. Grasia-Ruiz; *J. Cryst. Growth,* **75** (1986) 195.

[83]   H. K. Henisch and J. M. Grasia-Ruiz; *J. Cryst. Growth,***75** (1986) 203.

[84]   B. Chopard, P. Luthi, and M. Droz; *J. Statistical Phys.,* **76** (1994) 661.

[85]   D. S. Chernavskii, A. A. Polezhaev and S.C. Muller; *Physica D.,* **54** (1991) 160.

[86]   Y. Brechet and J. S. Kirkaldy; *J. chem. Phys.,* **90** (1989) 1499.

[87]   S. N. DharmaPrakash and P. Mohan Rao; *J. Mater. Sci. Lett.,* **8** (1989) 141.

[88]   G. K. Kirov; *J. Cryst. Growth,* **15** (1972) 102.

[89]   G. Verghese, M.A. Ittyachen, and C. Joseph; *J. Mater. Sci.,* **28** (1993) 6357.

[90]   A. Bueki, E. Karpati-Smidroczki and M. Zrinyi; *J. Chem. Phys.,* **103** (1995) 10387.

[91]   A. Bueki, E. Karpati-Smidroczki and M. Zrinyi; *Physica-A.,* **220** (1995) 357.

[92]   H. van Schady; *Kolloid-Z,* **4** (1909) 175.

[93]   S. S. Bhatnagar, J. L. Sahegal; *Kolloid-Z,* **39 (**1926) 264.

[94]   R.E. Liesegang; *Kolloid-Z,* **10** (1912) 225.

[95]   M. R. Rajinders, J. A. Van Beek, A. A. Kodentsov and J. J. van Loof; *Zeitschriff fur netalkunde,* **87** (1996) 732.

[96]   R. Gerard, A. Viallard and R. Serpolay; *Atmospheric Res.,* **22** (1989) 335.

[97]   R. Gerard, A. Viallard and R. Serpolay; *Atmospheric Res.,* **22** (1989) 351.

[98]   N. Magnussen. L. Quinones, D. L. Cocke, E. A. Schweikert, B. K. Patnaik L. C. V. Barros and G. B. Baptista; *Thin Solid Films,* **167** (1988) 245.

[99]   X. G. Zheng, M. Taria, M. Suzuki and C. N. Xu; *Appl. Phys. Lett.,* **72** (1998) 1155.

[100]   M. Deepa, K. RajendraBabu and V.K. Vaidyan; *J. Mater. Sci.*, **14** (1995) 1321.

[101]   N. Srinivasan and S. Natarajan; *Indian J. Phys.,* **70B** (1996) 563.

[102]   V. S. Joshi, B. B. Parekh, M. J. Joshi and A. B. Vaidya; *J. Cryst. Growth,* **275** (2005) 1-2.

[103]   V. S. Joshi; *Ph.D. Thesis,* Saurashtra University, Rajkot (2001).

[104]   V. S. Joshi and M. J. Joshi; Cryst. *Res. and Technol.* **38** (2003) 817.

[105]   V. S. Joshi, B. B. Parekh, M. J. Joshi and A. D. B. Vaidya, *Urol. Res.,* **33**, (2005), 80.

[106]   K. C. Joseph, B. B. Parekh and M. J. Joshi; *Curr. Sci.,* **85** (2005) 1232.

[107]   T. Irusan, D. Arivuoli and P. Ramasamy; *Cryst. Res. Technol.,* **25** (1990)   K-104.

[108]   K. C. Joseph, *Ph. D. Thesis,* Saurashtra University, Rajkot (2005).

[109]   S. N. Kalkura, V. K. Vaidyan, M. Kanakavel and P. Ramasamy; *J. Cryst. Growth,* **132** (1993) 405.

[110] M. Ashok, N. Meenakshi Sundaram, S. Narayana Kalkura; *Mater.Lett.*,**57** (2003) 2066.

[111] S. N. Kalkura and S. Devanarayanan; *J. Mater. Sci., Lett.*, **5** (1986) 741.

[112] S. N. Kalkura and S. Devanarayanan; *J. Cryst. Growth.*, **83** (1987) 446.

[113] S. Devanarayanan and S. N. Kalkura; *J. Mater. Sci., Lett.*, **10** (1991) 497.

[114] S. N. Kalkura and S. Devanarayanan; *J. Cryst. Growth.*, **94** (1989) 810.

[115] S. N. Kalkura and S. Devanarayanan; *J. Mater. Sci.*, **8** (1988) 481.

[116] K. Provost and M. C. Robert; *J. Cryst. Growth*, **110** (1991) 258.

[117] V. I. Katkova and V. I. Rakin; *J. Cryst. Growth*, **142** (1994) 271.

[118] S. Natarajan, H. A. Devacloss and K. Alwan; *Cryst. Res. Tech.*, **23** (1988) 1343.

[119] R. M. Cody and R. D. Cody; *J. Cryst. Growth*, **113** (1991) 508.

[120] C. Rinaudo, M.C. Robert and F. Lefaucheux; *J. Cryst. Growth*, **71** (1985) 803.

[121] K. S. Raju; *J. Mater.Sci.*, **20** (1985) 756.

[122] H. Tiemann, I. Sotje, G. Jarms, C. Paulmann, M. Epple, and B. Hasse; *J. Chem. Soc., Dalton Trans.,* **7,** (2002), 1266.

[123] E. Ramchandran and S. Natarajan; *Indian J. Phys.,* **79(1)** (2005) 77-80.

[124] R. Dabhi, *Ph.D. Thesis; Saurashtra University*, Rajkot (2002).

[125] F. Bedarida; *Prog. Cryst. Growth and Charact.,* **5** (1982) 221.

[126] F. Lefaucheux, M. C. Robert, Y. Bernard and S. Gits; *Cryst.Res. Technol.*, **19,** (1984) 1541.

[127] C. A. Agudelo, C. M. Wise, *Crystal Deposition Disease* in *Treatment of the Rheumatic Disease,* 2nd ed. Eds. M. Weisman, et. al., W.B. Saunders, New York, (2001).

[128] P. K. Grower, R. L. Moritz, R. J. Simpson and R. L. Ryall; *European J. Biochem.,* **253** (1998) 637.

[129] A. M. Cody and R. D. Cody; *J. Cryst. Growth,* **151** (1995) 369.

[130] I. Bolshakova, P. Koptsev, I. Melnyk, T. Moskovets, S. Krukovsky and D. Zayachuk; *Cryst. Res. Technol.,* **36** (2001) 989.

[131] I. Bulta, D. Rickard and S. Grimes, *J. of Conf. Abstracts,* **5** (2000) 276.

[132] M. Matsuoka, T. Kamada and H. Takiyama; *J. Cryst. Growth,* **158** (1996) 322.

[133] N. E. Chayen; *J. Cryst. Growth,* **198/199** (1999) 649.

[134] H. Ooosterhof, R. M. Geertman, G.J. Witkmp and G.M. van Rosmalen; *J. Cryst. Growth,* **198/199** (1999) 754.

[135] X. Holmbäck and Å. C. Rasmuson; *J. of Cryst. Growth,* **198/199** (1999) 780.

[136] H. K. Henisch; *Crystal Growth in Gels,* Dover Publication, New York, (1993).

[137] Ivan van as http://www.sas.org/E-Bulletin/2002-03-15/features2/body.html.

[138] A. McPherson, Yu, G. Kuznetsov, A.J. Malkin and M. Plomp; *6th Int. workshop on the Crystal Growth of Organic Materials,* University of Strathclyde, Glasgow. (U.K.), 18th-21st Aug. 2003.

[139] M. Taylor, R. Bytheway, P.Millican, S. Menzer, J. Wall and G. Fraser; *6th Int. workshop on the Crystal Growth of Organic Materials,* University of Strathclyde, Glasgow. (U.K.), 18th-21st Aug. 2003.

[140] M. Li, P. Mougin, K.J. Roberts and D. Wilkinson, *6th Int. workshop on the Crystal Growth of Organic Materials.,* University of Strathclyde, Glasgow. (U.K.), 18th-21st Aug. 2003.

[141] A. A. Chernov; *"Modern Crystallography"*, Vol. III: Crystal Growth", Springer Verlag, Berlin, (1984).

[142] K. Nishioka; *"Advances in the Understanding of Crystal Growth Mechanisms"*, Eds. T. Nishinaga, K.Nishioka, J. Harda, and A.Sasaki, Book News, Portland, (1999).

[143] T. Yamamoto, N. Akutsu, and Y. Akutsu; *"Advances in the Understanding of Crystal Growth Mechanisms",* Eds. T. Nishinaga, K. Nishioka, J. Harda, and A. Sasaki, Book News, Portland, (1999).

[144] T. Ogawa; *" Advances in the Understanding of Crystal Growth Mechanisms"*, Eds. T. Nishinaga, K. Nishioka, J. Harda, & A. Sasaki, Book News, Portland, (1999).

[145] J. W. Mullin; *Bulk Crystallization* in *"Crystal Growth"*, Ed. B. Pamplin, Pergamon Press, Oxford (1975).

[146] C. W. Bunn and H. Emmett; *Discussion Faraday Soc.,* **5** (1949) 119.

[147] G. T. Kohman; *"Precipitation of Crystals from Solution",* in the*" Arts and Science of Crystal Growth",* Ed. J.J. Gillman, John Wiley, New York, (1963).

[148] A. C. Walker; *J. Franklin Inst.,* **250** (1950) 481.

[149] G. W. Sears; *J. Chem. Phys.,* **27** (1957) 1308.

[150] P. H. Egli and L. R. Johnson.; *Ionic Salts in "Arts and Science of Crystal Growth"* Ed. J. J. Gilman., John willey, NewYork, (1964).

[151] J. C. Brice; *The Growth of Crystals from Liquids*, Wiley, New York, (1972).

[152] J. C. Brice; *Crystal Growth Processes*, John Wiley, New York, (1986).

[153] H. E. Buckley; *"Crystal Growth",* John Wiley, New York, (1951).

[154] M. Tanenbaum; *"Methods of Experimental Physics",* Vol.-6, Academic Press, New York, (1961).

[155] A.C. Walker; *J.Franklin, Inst.* **250** (1950) 481.

[156] H. C. Gatos; *On the Selection of Methods for Crystal Growth. The Methods in Crystal Growth: A Tutorial Approach,* Eds. W. Bradsley, D. T. J. Hurle and J. B. Mullin, North Holland Series in Crystal Growth, no.2, North Holland, Amsterdam,(1979), 1.

Chapter IV

Experimental Techniques

4.1   Introduction:

Nowadays, scientists and engineers have an impressive array of powerful and elegant tools for acquiring quantitative and qualitative informations about the composition and structure of matter. There are variety of crystals grown having numerous applications in science and technology. It is always important to characterize these crystals with various angles of interests by different instruments [1]. The present chapter gives a brief review of experimental techniques, which are used by the present author to characterize the crystal grown.

4.2   Crystal Growth:

The crystals for the present investigations have been grown by the gel technique using single diffusion column, the wet chemical techniques and the solution growth. These particular techniques were discussed elaborately in the following chapters.

4.3   Thermo-gravimetric Analysis (TGA):

According to widely accepted definition of *thermal analysis,* it is a group of techniques in which physical properties of a substance and/or its reaction products are measured as a function of temperature whilst the substance is subjected to a controlled temperature program [1]. Nearly over a dozen thermal methods can be identified, which differ in the properties measured and temperature programs [2-4]. These methods find widespread use for both quality control and research applications of

various substances, such as, polymers, pharmaceuticals, crystals, clays, minerals, metals and alloys. Various thermal techniques are categorized in figure (4.1).
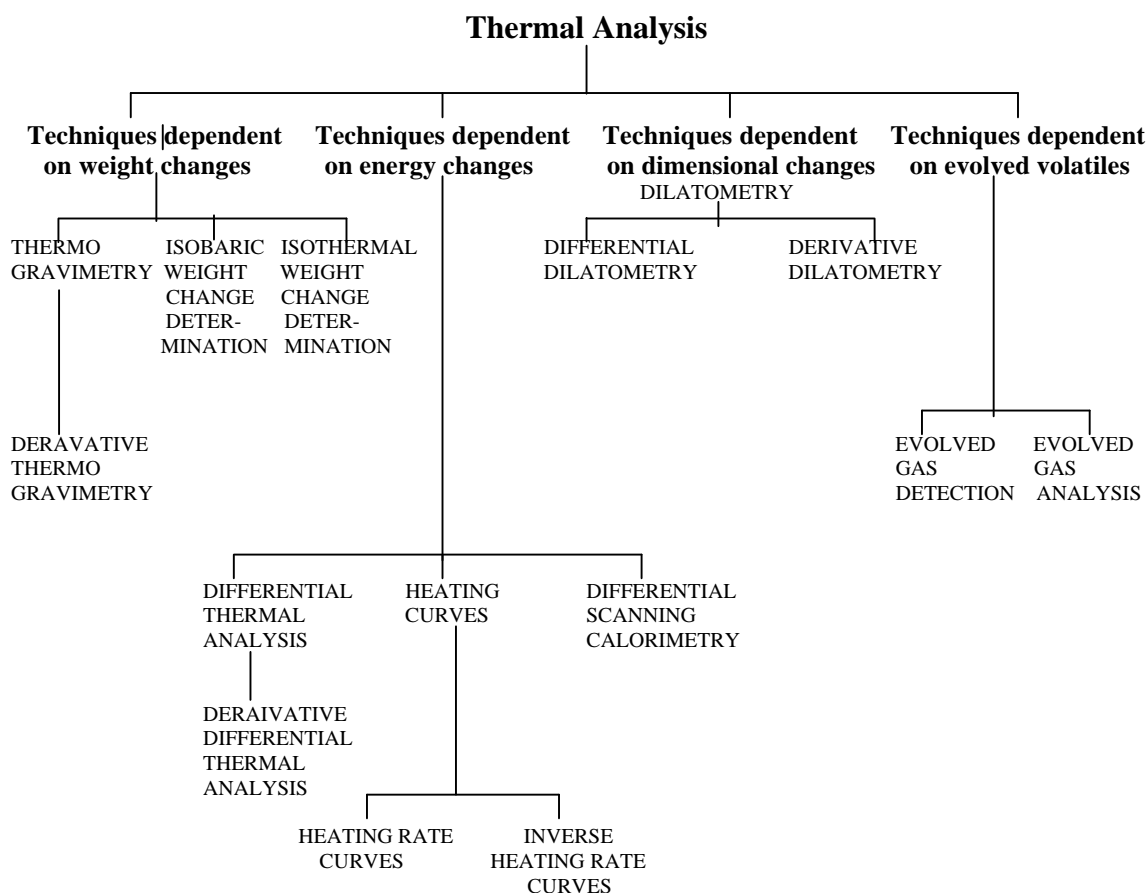
Thermal Analysis

```
Techniques dependent     Techniques dependent    Techniques dependent      Techniques dependent
  on weight changes        on energy changes     on dimensional changes     on evolved volatiles
                                                      DILATOMETRY

THERMO      ISOBARIC  ISOTHERMAL         DIFFERENTIAL      DERIVATIVE
GRAVIMETRY  WEIGHT    WEIGHT             DILATOMETRY       DILATOMETRY
            CHANGE    CHANGE
            DETER-    DETER-
            MINATION  MINATION

DERAVATIVE                                                              EVOLVED     EVOLVED
THERMO                                                                  GAS         GAS
GRAVIMETRY                                                              DETECTION   ANALYSIS


                 DIFFERENTIAL    HEATING      DIFFERENTIAL
                 THERMAL         CURVES       SCANNING
                 ANALYSIS                     CALORIMETRY

                 DERAIVATIVE
                 DIFFERENTIAL
                 THERMAL
                 ANALYSIS

                        HEATING RATE      INVERSE
                        CURVES            HEATING RATE
                                          CURVES
```

Figure (4.1): Various thermal techniques

The TGA involves change in weight with respect to temperature. The acquired data obtained as a plot of mass or loss of mass in percentage as a function of temperature is considered as a *thermal spectrum,* or a *thermogram,* or a *thermal decomposition curve.* These thermo-grams characterize a system in terms of temperature dependence of its thermodynamic properties and physical-chemical kinetics.

The TGA involves measurement of a change in weight of a system as the temperature is increased at pre-determined rate. Changes in weight are a result of the rupture and/or formation of various physical and chemical bonds at elevated temperatures that lead to the evaluation of volatile products or the formation of

heavier reaction products. From such curves data is obtained concerning the thermodynamics and kinetics of the various chemical reactions, reaction mechanism and the intermediate and final reaction products. Usually the temperature range is from ambient to 1200 °C with inert or reactive atmospheres. The derivative in TG is often used to pinpoint completion of weight- loss steps or to increase resolution of overlapping weight-loss occurrences.

Modern commercial variety of instruments for TGA usually consists of; (1) a sensitive analytical balance, (2) a furnace, (3) a pure gas system (for providing an inert or sometimes reactive gas atmosphere), and (4) a microcomputer or microprocessor for instrumental control and data acquisition and display. A block diagram of TGA is as shown in figure (4.2).
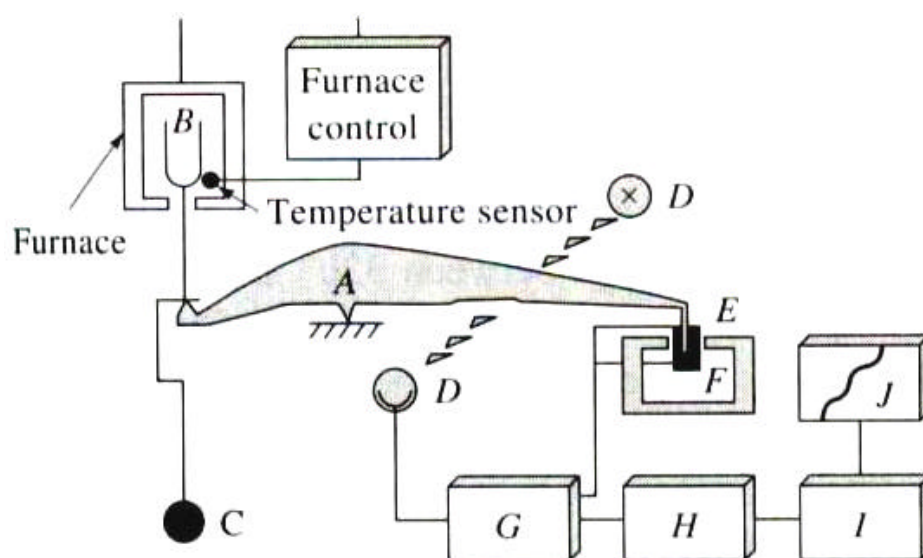
Figure (4.2): Components of a thermal balance: A, beam: B, sample cup and holder; C, counterweight; D, lamp and photodiodes; E, coil; F, magnet; G, control amplifier; H, tare calculator; I, amplifier; J recorder. (Courtsey of metter Instrument Corp. Hightston, NL)

There are mainly two types of thermo-gravimetry available, one is a *dynamic thermo-gravimetry* and the other is a *static or endothermic thermo-gravimetry*. In the dynamic thermo-gravimerty, the sample is subjected at continuous and linearly

increasing temperature. Whereas, in the static or endothermic thermo-gravimetry, the sample is maintained at constant temperature for a certain period of time during which any change in weight is recorded. The basic requirements for the analysis are a precision balance and a recorder. At present the availability of automatic recording thermo-balances in market are, usually, ranging from 1 mg to 100 g. In general a furnace should have a linear rise of temperature with time and should be capable to work in inert, oxidizing or reducing atmosphere from ambient to 1500°C. Often the heating and cooling rate of the furnace can be selected from slightly higher than zero to as high as 200° C/min. Because of the continuous record of weight and temperature no features of thermo-grams are overlooked. The shape of thermo-gravimetric curve of a particular compound is influenced by the rate of heating of the sample and the atmosphere surrounding it [2, 5, 6].

The TGA for the present samples was carried out from the room temperature to 800 °C at a heating rate of 15 °C/ min in an atmosphere of air using α-Al_2O_3 as standard reference. The analysis was done in the temperature range from room temperature to 950 °C and the heating rates from ± 2 to ± 100 °C/ min. Powdered samples were used for this study.

The analyses were carried out at Regional Sophisticated Instrumentation Center (RSIC), Chennai (IIT, Madras), and Sophisticated Instrumentation Center for Applied Research and Testing (SICART), Vallabh Vidyanagar, Gujarat.

4.4 Infrared (IR) Spectroscopy and FTIR spectroscopy:

Infrared spectroscopy is one of the most powerful analytical techniques, which indicates the possibility of chemical identifications [7]. Till the early 1980s, instruments for the mid-infrared region were mostly of dispersive type based on diffraction gratings. Due to the advent of Fourier transform technology, the scenario is

completely changed. Photometers based on interference filters also find applications in measuring the composition of gases and atmospheric contaminants. Before the appearance of these new instruments, the mid- infrared frequency region of spectra were largely used for qualitative organic analysis and structural determination based on absorption spectra. Nowadays, in contrast the mid-infrared spectroscopy is used in addition for quantitative analysis for complex samples by both absorption and emission spectrometry. In addition to this the mid- infrared spectral regions find applications in microscopic studies of surfaces, analysis of solids by attenuated total reflectance and diffuse reflectance, photo-acoustic instruments and others [1].

The infrared region of the electromagnetic spectrum extends from the red end of the visible spectrum out to the microwave region. Infrared spectral region can be divided into three regions; near infrared, mid-infrared and far infrared.

Table (4.1)

Different Infrared Spectral Regions and its Applications

Spectral regions	Wave numbers (cm^{-1})	Type of Measurement	Type Analysis	Type sample
Near-infrared	12,800 to 4000	Diffuse reflectance	Quantitative	Solid or liquid materials
		Absorption	Quantitative	Gaseous mixtures
Mid-infrared	4000 to 200	Absorption	Qualitative	Pure solid, liquid liquid or gaseous compounds. (mainly organic)
			Quantitative	Complex Gaseous Liquid or solid mixtures
		Reflectance	Qualitative	Pure solid or liquid compounds
		Emission	Quantitative	Atmospheric samples
Far-infrared	200 to 10	Adsorption	Qualitative	Pure inorganic or metal organic species

Table (1) gives the details of different infrared spectral regions. Molecular vibrations are falling into basic categories of *stretching* and *bending.* A stretching vibration involves a continuous change in the inter-atomic distance along the axis of bond between two atoms. However, the bending vibrations are characterized by a change in the angle between two bonds, which are of four types, *scissoring, rocking, wagging* and *twisting,* Figure (4.3)*.*
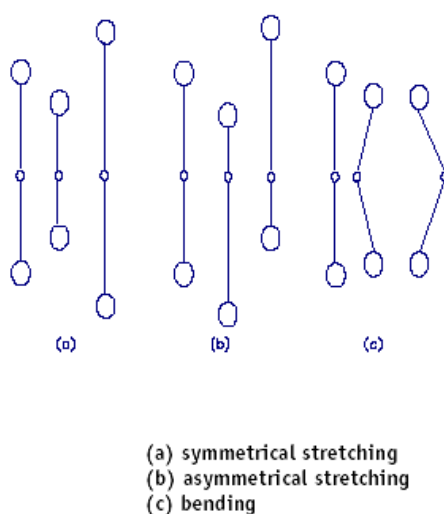

(a) symmetrical stretching
(b) asymmetrical stretching
(c) bending

Figure (4.3): Stretching and bending

Because of the interaction with infrared radiation, portions of the incident radiation are absorbed at particular wavelengths. The multiplicity of vibrations occurring simultaneously produces a highly complex absorption spectrum, which is a unique characteristic of the overall configuration of the atoms as well. Details of assignments of different frequencies with different vibrations of bonds, such as H-O, N-H, C = O, C-C, C-H and many others were given in detail by many authors [1, 7-9]. Many times it is given in the chart and tabular form to facilitate the user to identify the specific bond vibrations from the frequency in wave numbers.

There are mainly three types of instruments available, which are (1) dispersive grating type, (2) multiplex type and (3) non-dispersive type. Variety of infrared sources are developed depending upon requirements, which include the

Nernst glow-bar, incandescent wire sources, mercury arc, tungsten filament lamp, etc. Good transducers such as, thermal transducers, pyro-electric transducers and photo-conducting transducers are also equally important in the detection and measurement of infrared radiation. For different regions, different type of radiation sources, optical systems and detectors are needed. The standard infrared spectrometer is a filter-grating or prism- grating instrument covering range from 4000 to 650 cm^{-1} (2.5 to 15.4 μm). However the grating instruments offer high resolution that permits separation of closely spaced absorption bands, accurate measurements of band position and intensities, and high scanning speeds for a given resolution and noise level. Modern spectrometers generally have attachments that permit speed suppression, scale expansion, repetitive scanning and automatic control of slit, period and gain. These are very often under the control of a microprocessor. Accessories such as beam condensers, reflectance units, polarizers and microcells can usually be added to extend versatility or accuracy [10].

4.5 Fourier Transform Infrared Spectroscopy:

Multiplex type of instruments employs the mathematical tool of *Fourier Transform* [11]. The apparatus of Fourier Transform Infrared (FTIR) spectrometer is derived from *Michaelson interferometer,* which is shown in figure (4.4). The main components of the FT-IR spectrometers are (1) drive mechanism, (2) beam splitters, and (3) sources and transducers. In Figure (4.5) a parallel beam of radiation is directed from the source to the interferometer, consisting of a beam splitter (B) and two mirrors (M_1 and M_2). It is well known that for monochromatic radiation the interference patterns are obtained.
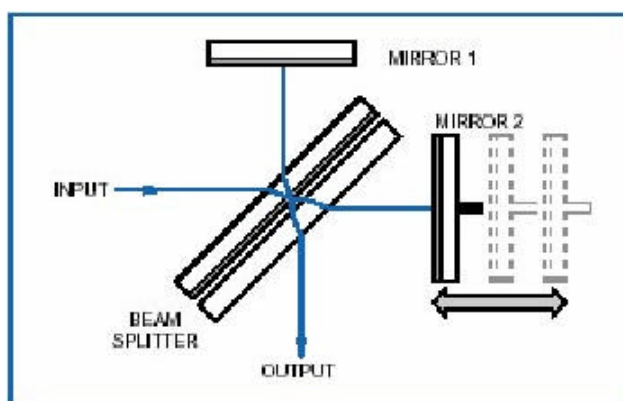
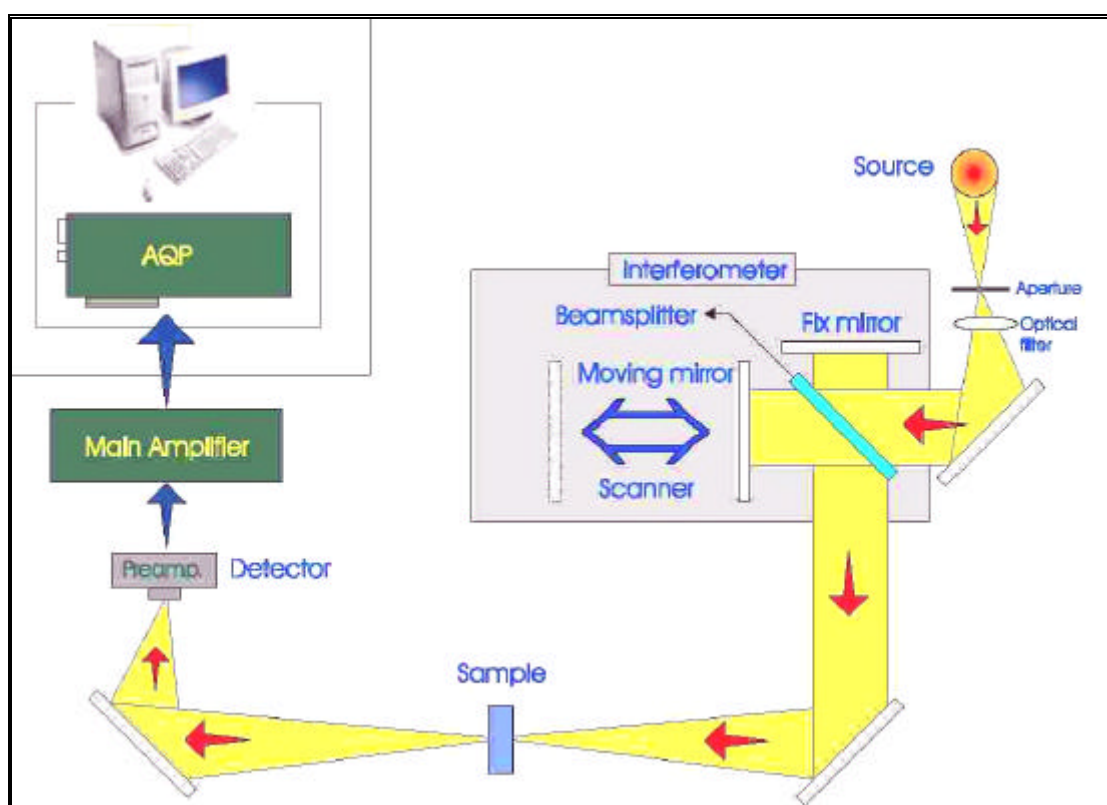**Figure (4.4): Schematic diagram of Michaelson interferometer**

Figure (4.5): The principle of FT-IR

The constructive or destructive interference is produced depending on the relative path lengths B to M_1 and B to M_2. When mirror M_2 moves smoothly towards or away from B, a detector sees radiation of changing intensity. If *white* radiation is used, the interference patterns are obtained which can be transferred back to the original frequency distribution. This can be achieved by a mathematical process known as *Fourier transform*, nowadays, this process is carried out by a computer or

microprocessor of the spectrometer. Under these conditions, the detector response fluctuates at a rate, which depends upon the rate of movement of mirror and the wavelength of radiation. In general, any combination of frequencies with corresponding amplitudes will produce an interferogram containing all the spectral information of the original radiation. The interferogram is the Fourier transform of the spectrum and the task of the computer is to apply the *inverse Fourier transform.*

Interferometric or Fourier transform spectroscopy makes use of all the frequencies from the source simultaneously, rather than sequentially as in scanning instrument. This was first proposed by Fellgett and hence also called as *Fellgett advantage FTS*. The Fellgett advantage is an improvement in signal to noise ratio of $(M)^{1/2}$, where M is the number of resolution elements desired in the particular spectrum. It is worth noting that the resolving power of Fourier transform instrument is constant over the entire spectrum, whereas it varies with frequency in the conventional technique [12]. Fourier transform spectroscopy is providing simultaneous and almost instantaneous recording of whole spectrum in the magnetic resonance, microwave and infrared regions. *Fourier Transform (FT) Spectroscopy* is equally applicable to both emission and absorption spectroscopy.

The FT-IR set up has, as noted earlier, design based on *Michaelson interferometer,* which is having mainly three important components:

(1)   A *drive mechanism* is important for satisfactory interferograms, which needs that the speed of the moving mirror be constant and its position be known exactly at any instant. The planarity of the mirror must remain constant during the entire sweep of 10 cm or more.

(2)   Beam splitters are constructed of transparent materials with refractive indices such that approximately 50% of the radiation is transmitted and 50% is

reflected. A thin film of germanium or silicon coated on cesium iodide or bromide, sodium chloride, or potassium bromide is employed for mid infrared region.

(3)   The sources of FTIR are usually the same as IR ones. Inasmuch as the slow response times the thermal transducers are not generally preferred in FT-IR, the Triglycine sulphate transducers are widely preferred in the mid frequency range.

The FTIR instrument has many advantages. It has better signal to noise ratio than good quality dispersive type instrument. Another important advantage is that its optics provides a much larger energy throughput (one or two orders of magnitude) than the dispersive type, where it is limited by the necessity of having the narrow slit widths. The prime advantage of FT-IR is that the interferometer is free from the problem of stray radiation because each infrared frequency is chopped at a different frequency.

There are many applications of FT-IR spectroscopy, which are spectroscopic investigations of gaseous mixtures having complex spectra resulting from superposition of vibrational and rotational bands as found in atmosphere; study of samples with high absorbances; study of the substances with weak absorption bands; collecting data from very small samples; investigations requiring fast scanning such as kinetic studies or detection of chromatographic effluents and infrared emission studies.

There are different versions, modifications and attachments are available with FT-IR. *Diffuse reflectance infrared Fourier transform spectroscopy* (DRIFTS) uses an effective way of obtaining infrared spectra directly on powdered samples with a minimum sample preparation [13,14]. The advantage is that it permits conventional

infrared spectral data to be obtained on the samples that are not altered much from their original state. Apart from this, the *photo-acoustic infrared spectroscopy* is another popular technique. This technique was introduced in 1970s, which provides a mean for obtaining ultraviolet, visible and infrared absorption spectra of solids, semisolids, or turbid liquids. This is based on the effect first investigated by Alexander Graham Bell in 1880. When a gas in a closed cell is irradiated with a chopped beam of radiation of a wavelength that is absorbed by a gas, the absorbed radiation causes periodic heating of the gas which, consequently, gives in regular pressure fluctuations in the chamber. This method has been used for detecting the components of mixtures separated by *thin- layer* and *high-performance liquid chromatography*. Most manufacturers offer photo-acoustic cell along with FT-IR as the accessories.

The FT-IR spectra for the present study were taken at Regional Sophisticated Instrumentation Center (R.S.I.C), Chennai and Chemistry Department, Saurashtra university, Rajkot , using NICOLET MAGMA IR 550 Series II FTIR Spectrometer, and Simadzu 8400 FTIR Spectrometer, respectively. The spectra of powder samples in KBr medium were recorded in the range from 400 cm^{-1} to 4000cm^{-1}.

4.6   X-ray Diffraction by Powder Method:

The powder X-ray diffraction (XRD) was devised independently in 1916 by Peter Joseph William Debye, a Nobel Laureate, and P. Scherrer in Germany and in 1917 by A. W. Hull in United States [15 -17]. The powder XRD is a non-destructive technique widely used for the characterization of a variety of crystalline materials. This method has been conventionally used for phase identification, quantitative analysis and the determination of structure imperfections. However, in recent years

the applications have been extended to new areas, such as the determination of crystal structures and the extraction of three-dimensional micro-structural properties.

Generally, the method is applied to data collected under ambient conditions, but *in situ* diffraction as a function of an external constraint, such as temperature, pressure, stress, electric field, atmosphere, etc, is important for the interpretation of solid state transformations and materials behaviors. Various types of micro and nano crystalline materials can be characterized by powder- XRD, including organic and inorganic materials, drugs, minerals, zeolites, catalysts, metals and ceramics. In the pharmaceutical industries the powder-XRD is popular for identification of drug molecule and its polymorphs. The physical states of the materials can be loose powders, thin films, poly-crystalline and bulk materials. By properly using this technique one can yield a great deal of structural information about the material under investigation. For most applications, the amount of information which is possible to extract depends on the nature of the sample microstructure (crystallinity, structure imperfections, crystallite size and texture) the complexity of the crystal structure (number of atoms in the asymmetric unit cell and unit cell volume), the quality of the experimental data (instrument performances and counting statistics) [18].

Basically, this method involves the diffraction of monochromatic X-ray by a powdered specimen. Usually 'monochromatic' means the strong characteristic K component of the filtered radiation from an X-ray tube operated above the K excitation potential of the target material. The "Powder" can mean either an actual, physical powder held together with suitable binder or any specimen in polycrystalline form. Since single crystals are not always available, this method is more suitable for structural determination of various substances. The powder method is also known as the *Debye-Scherrer method.*
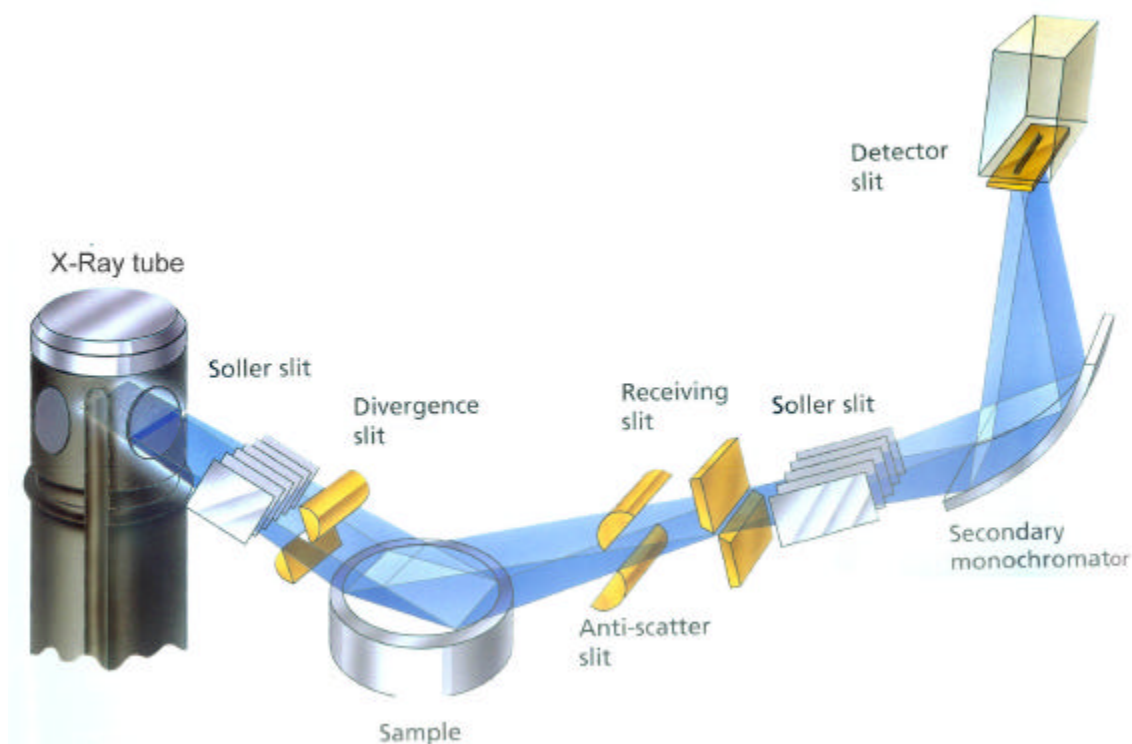
Figure (4.6 a): The Principle of Powder X-ray Diffraction

The fundamental law, which governs the x-ray diffraction phenomenon, is the Bragg's Law and the equation is as follows ;

$$S \quad n\lambda \quad 2d \sin q \qquad \text{or} \qquad d = \frac{n\lambda}{2\sin q} \qquad \text{----------------(4.1)}$$
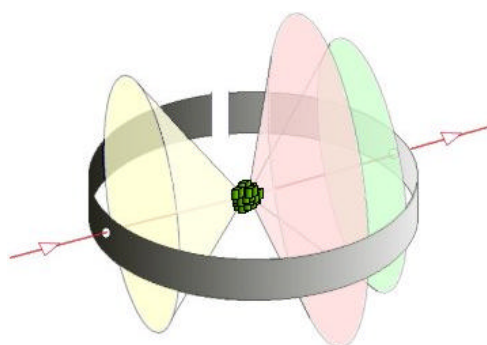

Figure (4.6 b): Powder Sample Diffract X-ray Beam in Cones

When X-ray is incident on the crystalline powdered sample it gets diffracted according to the above mentioned equation in form of cones, which is exhibited in Figure (4.6 b).

There are many applications of the powder method. Fundamentally this method provides a way of investigating, within limits, the crystallography of the crystal in the powder form. The powder method can be used as a tool to identify crystals, since the powder XRD patterns produced by a crystalline substance is a characteristic of that particular substance. One of the most important uses of the powder method is in the identification of an unknown material. If a set of standard diagrams of known substances, or tabular representations of them, available, then it is possible to identify a pure substance with the aid of a set of rules for finding an unknown diagram. The ASTM data cards as well as JCPDS data files are available for large number of substances for identifications and comparison. Statistical study of the relative orientations of the individual crystals of an aggregate is one of the important secondary uses of the powder method [19]. Identification of phases can be done by powder technique without solving crystal structure or assigning indices to the reflections. Apart from these, cold work, recovery and re-crystallization are readily recognized by their effect on the powder patterns.

Diffraction Line	Parameter of Applications
Peak position	Unit-cell parameter refinement
	Pattern indexing
	Space group determination ($2\grave{e}^0$/absent reflections)
	Anisotropic thermal expansion
	Macrostress: $\sin^2\phi$ method
	Phase identification (d/I)
Intensity	Phase abundance
	Reaction kinetics
	Crystal structure analysis (whole pattern)
	Rietveld refinement (whole pattern)
	Search/match, phase identification
	Preferred orientation, texture analysis
Width/breadth and shape	Instrumental resolution function
	Microstructure: line profile analysis
	Microstructure (crystallite size, size distribution, lattice distortion, structure mistakes, dislocations, composition gradient), crystallite growth kinetics
	Three-dimensional microstructure (whole pattern)
Non-ambient and	*in situ* diffraction under external dynamic diffraction constraints reaction kinetics

There are three types of powder methods, differentiated by the relative position of the specimen and the film.

1. Debye-Scherrer Method:

The film is placed on the surface of a cylinder and specimen on the axis of the cylinder.

2. Focusing Method:

The film, specimen, and X-ray source are all placed on the surface of a cylinder.

3. Pinhole Method:

The film is flat, perpendicular to the incident X-ray beam, and located at any convenient distance from the specimen.

For the purpose of simultaneous and quick measurement of the positions and intensities of diffraction lines the diffracto-meters are advantageous; on the other hand, the diffraction cameras are preferred when a very small amount of specimen is available, if an entire diffraction ring is required to be recorded in order to do the rapid estimation of grain size and preferred orientation and in case of large immovable specimen.

The powder photographic methods are well described by Klug and Alexander [20] as well as Azaroff and Buerger [19].

The simplest and most inexpensive way of practicing the powder method is to record the X-ray diffraction on photographic film, using a powder camera. A more elaborate way is to detect the diffracted radiation by means as a quantum counter, like Geiger counter. The use of counter diffracto-meter, and recorder equipment is justified chiefly when one wants to examine many different samples rapidly. Such

methods also have a real advantage whenever accurately measured intensities are necessary.

In the present work crystals were analyzed by PW 1710 BASED diffracto-meter with Cu-K$_{\acute{a}}$ radiation by using PC-APD Diffraction software. The crystal structures were determined by a computer software Powder-X.

Moreover, the single crystal x-ray diffraction method has its own advantages, but it is very expensive. The single crystal x-ray diffracto-meters use small single crystalline samples instead of powder samples. The data are analyzed with the help of various computer soft-wares and the molecular packing in the unit cell, the molecular structure, the bond lengths, the bond angles, unit cell parameters, etc. are available. The single crystal XRD the cynosure of many disciplines, such as physics, chemistry, bio-chemistry, biology, pharmacy, etc. In the modern times the identification of new substances with their molecular structures, their active bond sites, their crystal structures, etc. are very important for the drug designing. Various viruses, including HIV virus, have been crystallized and studied with the single crystal XRD.

The single crystal XRD was carried out on organic molecular crystal 4-(2-hydroxy-phenylamino)-pent-3-en-2-one Organic Crystal Crystallography Laboratory of University of Jammu, Jammu, using M$_{o}$ K$_{\acute{a}}$ radiation. The crystallographic data, bond angle and bond length ORTEP diagram and packing of molecules in unit cells were obtained by suitable soft-wares, which are discussed in detail in section 9.3 Chapter-IX.

4.7   Dielectric Studies:

Materials, which are electric insulators or in which an electric field can be sustained with a minimum dissipation power are known as dielectric materials. In the general sense, dielectric includes all materials except condensed states of metals.

A dielectric is characterized by its dielectric constant, $\hat{I}$ (some times denoted by $\hat{e}$), which relates the electric flux density to the electric field by the following relation

$$D = \hat{I} \ e \qquad\qquad \text{--------------------(4.2)}$$

In the MKS system $\hat{I}$ is the product of $\hat{I}_0$ (permittivity of free space) and $\hat{I}_r$ (relative dielectric constant). In the earlier experiments Faraday found that by inserting a dielectric material between the condenser plates, the capacitance could be increase by a factor of $\hat{I}_r$. The reason is the appearance of charges on the surface of the dielectric necessitating the arrival of fresh charges from the battery in order to keep the voltage constant. This is described in a schematic diagram of figure (4.7).
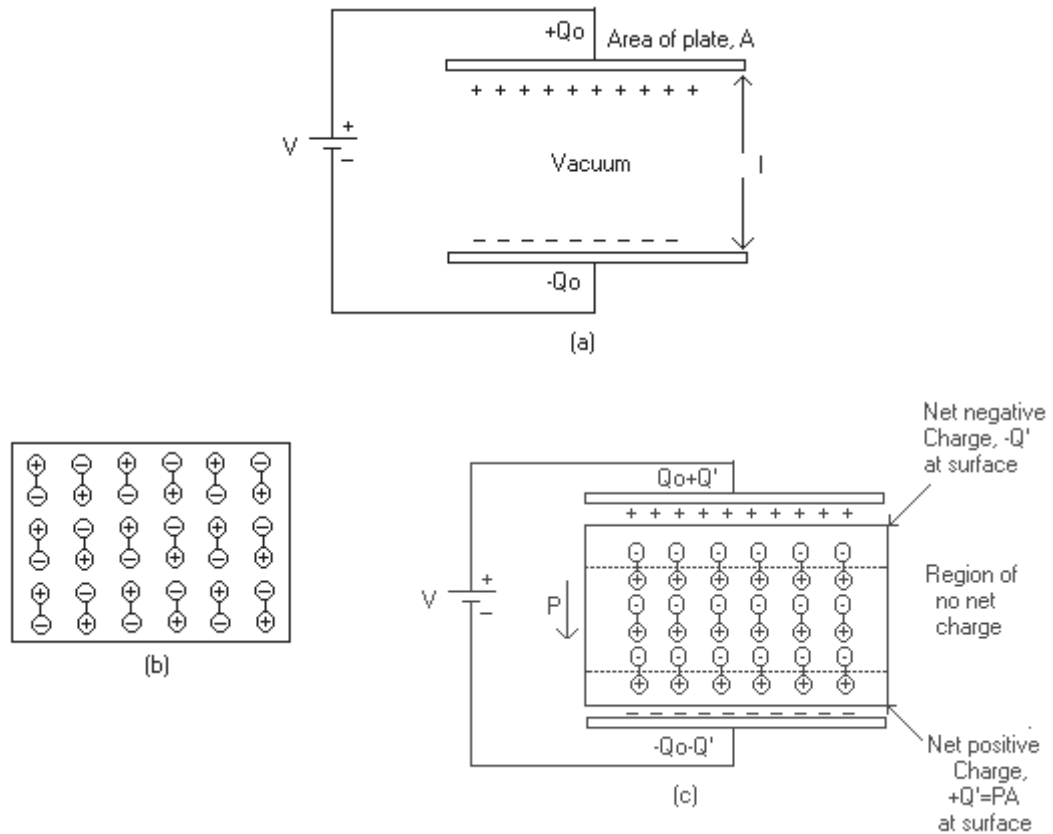
Figure (4.7): Schematic representations of (a) the charge stored on capacitor plates for a vacuum. (b) the dipole arrangement in an unpolarized dielectric, and (c) the increased charge storing capacity resulting from the polarization of a dielectric material.

In vacuum the surface charge density on the condenser plate is represented as

$$Q = \hat{I}_0 \, V/d \qquad \text{-------------------- (4.3)}$$

Where, d, is the distance between the plates. In the presence of dielectric, the surface charge density increase to

$$Q' = \hat{I}_0 \hat{I}_r \, V/d \qquad \text{-------------- ------- (4.4)}$$

Denoting the increase in surface charge density by P and defining the *dielectric susceptibility* by

$$c = \hat{I}_r - 1 \qquad \text{------------------ (4.5)}$$

From equation (4.3) and (4.4) the following relationship can be obtained

$$P = D - \hat{I}_0 å \quad \text{and} \quad P = \hat{I}_0 c å \qquad \text{------------------ (4.6)}$$

Usually, the dielectric constant for a given material is defined as the ratio of electric capacitance of a dielectric field capacitor to a vacuum capacitor of identical dimensions. This can be represented by the following relationship,

$$\hat{I} = C/C_0 \qquad \text{------------------- (4.7)}$$

Where, C is the capacitance of the dielectric field capacitor and C_0 is the capacitance of vacuum capacitor. The dielectric constant $\hat{I}$ is also known as the *specific inductive capacity* or as the *relative permittivity*. For a given charge distribution, the dielectric constant expresses the ratio of electric field strength in vacuum to that in a dielectric, the latter field being reduced by the polarization of the dielectric medium.

Considering a microscopic approach, an atom has a positively charged nucleus surrounded by an electron cloud. In the absence of an electric field, the statistical centers of positive and negative charges coincide. When an electric field is applied a shift is expected in the charge centers, particularly of the electrons. If this separation is d and the total charge is q then the molecule has an induced dipole moment,

$$m = q \, d \qquad \text{--------------------- (4.8)}$$

If the center of electron charge moves by an amount, *d*, then the total volume occupied by this electrons is *A**d**, where *A* is the area. This is actually true for class of molecules also. Denoting the number of molecules per unit volume by N_m and taking account of the fact that each molecule has a charge *q*, the total charge appearing in the volume *A**d** is then A**d**N_m *q* or simply $N_m q$**d** per unit area, in other words, the surface charge density.

It is interesting to note that this polarized surface charge density *P* is exactly equal to the amount of dipole moment per unit volume, which is from equation (4.8) is also $N_m q$**d**. The first relationship between microscopic and macroscopic quantities are obtained as follows

$$P = N_m \boldsymbol{m} \qquad\qquad \text{-------------------- (4.9)}$$

For low electric fields, one may assume that the dipole-moment is proportional to the local electric field *å'*,

$$\boldsymbol{m} = \boldsymbol{a}\,å' \qquad\qquad \text{------------------(4.10)}$$

Where, **a** is the constant known as *polarizability*. Notice that the presence of dipoles increases the local field, which will thus always be larger than the applied electric field. This has been schematically shown in figure (4.8).
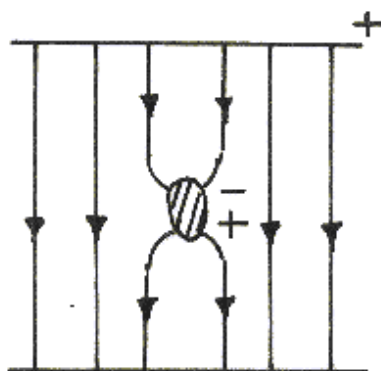
Figure (4.8): Formation of Dipole in Electric Field

There are several types of polarizations, such as, ionic polarization, interstitial polarization, electronic polarizability of atoms, lattice polarization and molecular polarizability. The main three types of polarizations are explained as follows.

(i) *Electronic: -*

All materials consist of ions surrounded by electron clouds. As electrons are very light they have a rapid response to field changes; they may even follow the field at optical frequencies.

(ii) *Molecular: -*

Bonds between atoms are stretched by applied electric fields when the lattice ions are charged. This is easily visualized with an alkali halide crystal figure (4.9)
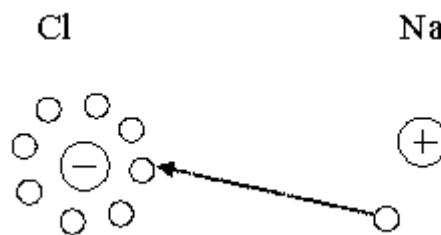
Figure (4.9): Stretching of Alkalihallide bonds when ion is charged

Where small deformations of the ionic bond will occur when a field is applied, increasing the dipole moment of the lattice.

(ii) *Orientational***: –**

This occurs in liquids or gases when whole molecules having a permanent or induced dipole moment move into line with the applied field.

Physically, one may consider the dipole-moments as trying to line up but, jostled by their thermal motion, not all of them are successful. Since the energy of dipole is an electric field *å* is given by

$$E = -\boldsymbol{m}å \cos \boldsymbol{q} \qquad\qquad \text{----------------------- (4.11)}$$

The number of dipoles in a solid angle *d* is

$$A \exp (ià \cos \boldsymbol{q} / kT) 2\boldsymbol{p} \sin\boldsymbol{q}\text{-} \qquad\qquad \text{----------------------- (4.12)}$$

Where, *A* is a constant. Hence the average dipole moment is given as

$< m >$ = net number of the assembly / total number of dipoles

Integrating in the interval of *0* to *p*, one yields

$< m >/m = L(a) = cotha - 1/a'$, where $a = må / kT$ ----------------------(4.13)

And *L(a)* is called the *Langevin function*.

If *a* is small, which is true under quite wide conditions, equation (4.13) may be approximated by,

$< m > = m^2å / kT$ ------------------ (4.14)

i.e.,the polarizability is inversely proportional to the absolute temperature.

The electric response of a normal dielectric can be explained by its *dielectric* or *breakdown strength, conductivity* or *dielectric loss,* and *dielectric constant.* The behavior of nonlinear dielectric depends also on the amplitude and time variation of the electric field.

Dielectric strength is defined as the maximum electric field, which can be applied to a dielectric without causing *breakdown,* the abrupt irreversible drop in resistively at high fields often accompanied by destruction of the material. Dielectric strength of most insulating materials is in the range from 10^4 to 10^7 V/in. at room temperature and low frequencies and it decreases at higher temperatures.

Dielectric loss is the power dissipation in a dielectric because of conduction process. This power loss results from thermal dissipation of the electrical energy expended by the field. It is caused by molecular collisions. It can be described by any of the following related parameters; the conductivity, *ó*, the factor $\hat{I}$ ", the power factor *cosq* and the *loss tangent* or *dissipation factor, tand* ;of these, only *ó* is applicable to direct current problems. The conductivity *ó* is the current density *I* per unit field strength *E* in phase with the applied voltage. The loss factor $\hat{I}$ ", which is the

imaginary part of the permittivity, is related to the conductivity by $\sigma = \omega \varepsilon''/\gamma$, where

ω equals 2π times the frequency. The power factor, $\cos\theta$, is the ratio of conduction or

loss current in phase with the applied voltage to the total current in any circuit, and θ

is the phase angle between current and voltage. The dissipation factor, $\tan\delta$, is the

ratio of loss current to reactive or charging current, where $\delta = 90° - \theta$. This is

expressed in terms of permittivity as in equation (4.15),

where, $|\varepsilon^*| = \sqrt{\varepsilon'^2 + \varepsilon''^2}$, $\varepsilon^* = \varepsilon' - i\varepsilon''$, $\cos\theta = \varepsilon'/|\varepsilon^*|$ --------(4.15)

and $\tan\delta = \varepsilon''/\varepsilon'$. For low loss materials, $\cos\theta$ and $\tan\delta$ are nearly equal.

The power dissipated per unit volume is $P = \sigma|E|^2 = |J|\cos\theta$. This power

loss increases at high temperatures and, in many substances, at high frequencies and

also it increases for a given field strength. This effect is commercially employed in

dielectric heating equipment for industrial and therapeutic purposes.

Distinction is often made for semiconductors and dielectrics. A non-polar

material is having no permanent dipoles, for example, silicon, germanium and carbon

(diamond). The III-V compounds such as GaAs, InSb and GaP share their valance

electrons in such a manner that the ions forming the lattice tend to be positive (group-

V) or negative (group-III). Hence, the lattice is a mass of permanent dipoles whose

moment can be changed by applied field. There are compounds, such as hydrocarbons

(C_6H_6 and paraffins), having permanent dipole arrangements but surprisingly zero net

dipole moment. There are molecules like water and many transformer oils that have

permanent dipole moments and the total dipole moment is determined by their

orientational polarizability.

Depending upon the frequency range under investigation the experimental

method of measuring dielectric constant varies. For frequencies below 10^9Hz the

permittivity or impedance of a dielectric sample, inserted in a parallel plate capacitor,

can be measured by suitable circuits. A *Schering bridge* arrangement is used up to 10^7 Hz and resonance circuit in the range of 10^4 to 10^9Hz. In the case of frequencies above 10^8Hz, the dielectric constant may be determined by measuring the interaction of electromagnetic waves with the medium. From 10^8 to 10^{11}Hz the material is generally inserted in *wave-guides* or *co-axial lines* and the standing wave patterns are measured. However, at still higher frequencies, *optical techniques* involving reflections and transmission measurements are employed.

The applicability of dielectric materials not only requires the knowledge of their electric properties, but also their general physical and chemical properties, such as, mechanical strength, elasticity, resistance to heat and cold, thermal conductivity, hygroscopicity, stability, crystalline structure and other parameters.

There are many applications of dielectric materials. Because the dielectric constant is related to the chemical structure, it can be used for both qualitative and quantitative analysis. If the dielectric constants for all constituents except one constituent, in a multi-component system, are similar and there is little interaction between them in solution, then the unique component can often be determined. Interestingly, in the analysis for toluene in the presence of complex mixtures of aliphatic hydrocarbons in petroleum refining as well as determining moisture in cereal grains and other solids uses this type of dielectric measurement techniques. When the nominally electric insulating material is placed in a varying electrostatic field, the heating effect of a material due to its own electric (dielectric) losses is known as dielectric heating. The material to be heated is placed between two metallic electrodes and high frequency signals of 2 to 90 MHz are applied by high frequency oscillator. The resultant heat is generated within the material and in the homogeneous materials it is through out uniform.

Solid dielectrics are employed for the vast majority of commercial applications. Important solid dielectrics include many ceramics and glasses; plastics and rubber; minerals such as quartz, mica, magnesia, and asbestos; and paper and fibrous products. The mechanical and thermal properties as well as the electrical response are important in the choice of dielectric for a particular product. For high mechanical strength and temperature resistance, ceramic and mineral insulators are preferred, while plastic and rubber are employed where flexibility is desired. Low-loss, non-polar dielectric, such as polyethylene or polystyrene, is necessary for many ultra high frequency applications.

The material requirements for dielectric devices are usually determined by the specific electrical characteristics desired for the operating frequencies selected. Semiconductors, such as silicon and germanium, and piezo-electric or ferroelectric ceramics, including heavy metal titanates, zirconates, and niobates, have found considerable application.

Many authors discussed various dielectric properties, dielectric applications and dielectric theories in details [21-31]. Classical theory of dielectric constant was also been given by Kachhava and Saxena [32].

Figure (4.10): LCR meter

In the present investigation, a precision LCR meter Agilent 42848 capable of measuring different impedance parameters at test frequencies from 20Hz to 1MHz has been used. The measurements were made at the ferrites laboratory of the Physics Department, Saurashtra University. Figure (4.10) shows the photograph of the set up.

The powdered samples were palletized by using a die of 1cm diameter by apply 2 tone pressure. The pallets were placed in a suitably design spring-loaded holder. Figure (4.11) describes the design of the sample holder.

Figure (4.11): The sample holder

The frequency of the applied signal was varied from 500Hz to 1MHz and the values of capacitance were measured at different frequency at room temperature. The dielectric constant $(\hat{e})$ is measured by employing the following expressions,

$$C = \mathring{a}A / t = \quad \mathring{a}_0 \ \hat{e} \ A / t, \qquad \hat{e} = Ct / \mathring{a}_0 A \qquad \text{------------------} (4.16)$$

Where, C = Capacitance, $\in$ = Relative permittivity, $\hat{e}$ = Dielectric constant, A = Area of sample, and $\in_0$ = Permittivity of free space.

The dissipation factor (*D*) is measured along with the capacitance at different temperatures and frequencies. The dielectric loss *tand* is calculated by using the following relation

$$tan\boldsymbol{d}= D \qquad\qquad --------(4.17)$$

Where, *D*= dissipation factor.

4.8   Photoconductivity and NLO Properties Measurements:

The generation of charge carrier density under illumination of a sample increases the electrical conductivity, which is known as the phenomenon of *photoconductivity*. This occurs when the energy of incident photon $h\acute{\imath}$ is higher than the energy band gap E_g. When $h\acute{\imath} > E_g$, an electron absorbs a photon of incident beam and jumps from the valance band to the conduction band. Thus, the new electron hole pairs created by the incident radiation increases the conductivity.
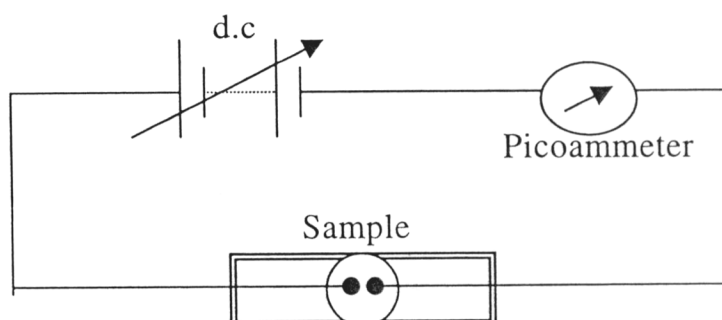
Figure (4.12): Schematic diagram of the photoconductivity study

Figure (4.12) shows the schematic diagram for the photoconductivity study. The electrical contacts were made on the polished surface of the sample by silver paint at a suitable spacing *d* between the two conducting wires. The d.c. input was increased from 0 to 300 volts in steps of 20 volts and current readings were noted down by Keithley 485 Pico- ammeter. For the photocurrent measurements, the sample was illuminated with halogen lamp of 100W by focusing a spot of light on the sample with the help of a convex lens. The experiment was performed at Physics Department

of Loyala College, Chennai, on organic crystals. This will be discussed in detail in section 9.3 of Chapter-IX.

The powder technique is the most convenient and simple technique for measurement of second orders non-linear optical (NLO) properties of materials. The experimental set up employed is shown schematically in figure (4.13).
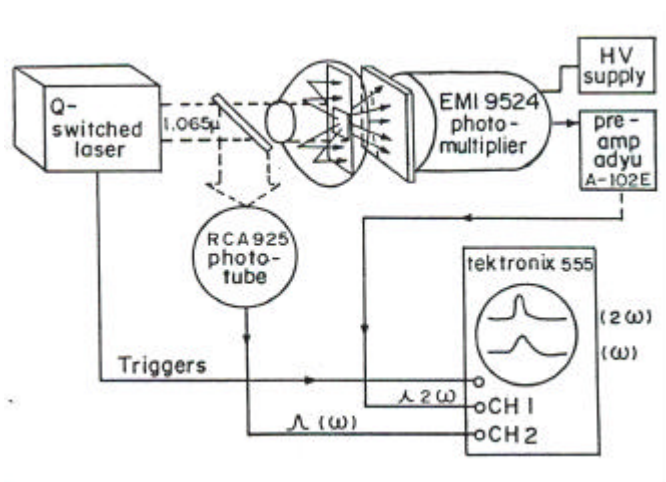

Figure (4.13): Krutz powder experimental set-up

It consists of Q- switched Laser and the sample is illuminated using UV-visible cut filter. The second harmonic generation is detected by photomultiplier tube and displayed on an oscilloscope. To increase the efficiency of a second harmonic collection at the detector, many times, a parabolic reflector is placed directly in front of the sample with a small access hole for laser beam.

For qualitative analysis, a thin layer of un-graded powder was placed on a microscope slide and held with a transparent tape. The experimental details are discussed elsewhere by several authors [33, 34].

4.9   Herbal Extract Preparation:

Growth inhibition study of three main crystals responsible for arthropathy, that is, MSUM, CPPD, and HA, has been carried out by using various herbal extracts. The details of selected plants for herbal extracts are as follows in Table (4.2).

Table (4.2)

Details of Herbal extracts and its applications

Sr. No.	Sanskrit Name	Latin Name	Part used	Plant chemicals	uses
1	Purnarnava	Boerhaavia diffusa Linn	Whole Plant, Root	Boerhavic acid, borhavine, punarnavine, sitosterols, alanine etc…	Anti inflammatory, and anti arthritis etc…
2	Pashanabheda	Routla Aquatica Lour.	Whole Plant, Root	Rhabdiol, Allant	Cough, cardiac disorder, fever, ulcers, bladder stone.
3	Gokshuru	Tribulus terrestris Linn	Whole Plant, Fruit	Syeroidal saponins gitonin, hecogenin, neotigogenin etc...	Antiinflammatory, diuretic, Arthritis.
4	Guggul	Commiphora wightii Engl.	Gum resin	Gugglesterone-E, Gugglesterone-Z, Gugg;esterpne I-IV,	Antiinflammatory, rheumatoid arthritis, heart diseases.
5	Salai Guggul	Boswellia serrta Roxb.	Gum resin	á- Thujene, P-cymene, â-pipine, linalool, essential oils, galactaronic acid	Arthritis, nervous & skin disorders, anti fungal, anti inflammatory etc..
6	Gorakshanganja/ Kapur Madhura	Aerva lanata Juss ex. Schult	Whole Plant, Root	á-amyrin, Campesterol, â-sitosterol, â-sitosteryl.	Calculus affection, Coughs, diuretic, anthelmentic, demulcent, etc..

Figure (4.14) shows the photographs of the plants used in the extract preparations.

The phyto-chemical study and the tanardization of different extracts were done by

Bhavan's SPARC, Mumbai [35].

Extraction:

Preparation techniques of different herbal extracts are broadly described as follows.

Hot alcoholic and hydroalcoholic extraction:

50 or 100 g of plant material packed in a thimble

↓

Placed in a soxhlet

↓

Hot extraction carried out with 3 to 4 times the volumes of solvent

For alcoholic extractions, a temperature of 65 ^{0}C is maintained through out the extraction process, while for hydroalcoholic extracts, the temperature used is 70 ^{0}C. The extractions are carried out for one-and-a-half hours each day for three successive days.
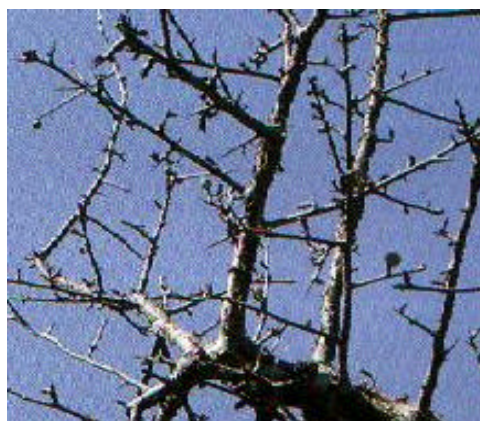

B. diffusa

R. aquatica root

T. terrestris

C. wightii

B. serrata

A. lanata

Figure (4.14): Photographs of the plants used in extract preparation

Hot aqueous extracts:

50 g of plant material placed in a beaker

↓

400 ml of Distilled water added to the plant material (1:8 ratio)

↓

Heated in a boiling water bath until the kwath reduces to half of the original volume

All extracts are dried in a rotary vacuum evaporator to a syrupy consistency and then in a steam bath to thick, pasty consistency. All the extracts are stored in glass vials kept in airtight plastic boxes at -20 ^{0}C. The extractive values and pH values for different plants are given in Table (4.3) [35]. .

Table (4.3)

Extractive value and pH values of different plant extracts

Plant name	Extractive value (%)			pH Values		
	Hot aqueous	Hot ethanolic	Hot hydroet-hanolic	Hot aqueous	Hot ethanolic	Hot hydroeth-anolic
Boerhaavia diffusa Linn (root)	10.58	5.45	6.49	6.0	6.5	6.5
Routla Aquatica Lour. (root)	8.97	10.09	12.27	4.0	6.0	6.5
Tribulus terrestris Linn (fruit)	13.36	9.77	7.44	3.5	5.0	6.5
Commiphora wightii Engl. (gum resin)	9.36	31.59	25.75	3.5	3.5	6.0
Boswellia serrta Roxb. (gum resin)	8.52	46.62	41.35	4.5	6.5	7.0
Aerva lanata Juss ex. Schult (whole plant)	8.9	3.95	21.44	6.5	5.5	6.5

The extract of *Boerhaavia diffusa* is brown colored and pasty in nature with positive results of sugar test, phenol test, tannin test and saponin test. However, the same type of nature of *Rotula aquatica* extracts was observed. Extracts of *Tribulus terrestris* are brown in color and syrupy in the consistency for ethanolic extracts and

the pasty consistency for hydroethanolic and aqueous extracts. Hydroethanolic and ethanolic extracts of *Commiphora wightii* are light brown in color and are gum like in consistency, but oily consistency with yellow color is found for cold hexane extracts. The hot aqueous extract of *Boswellia serrata* is brown in color and pasty in the consistency. A thorough investigation of these herbal extracts has been carried out by Bhavan's SPARC at Mumbai.

References:

[1]   D. A. Skoog, F. J. Holler and T. A. Nieman; *'Principles of Instrumental Analysis',* Saundrs College Publishing, Philadelphia, (1998).

[2]   W. W. Wendlandt; *'Thermal Analysis',* Wiley, New York, (1985).

[3]   M. E. Brown; *' Introduction to Thermal Analysis: Techniques and Applications',* Chapman and Hall, New York, (1988).

[4]   P. J. Haines; *'Thermal Methods of Analysis',* Blackie, London, (1995).

[5]   L. Erdey; *'Gravimetric Analysis'*, Pergamon Press Ltd., (1963).

[6]   S. M. Khopkar; *Basic Concept of Analytical Chemistry'*, Wiley Eastern., New Delhi (1984).

[7]   N. B. Colthup, L. H. Daly and S. E. Wiberiey; "*Introduction to Infrared and Raman Spectroscopy*", Academic Press, London (1975).

[8]   G. Socrates; *'Infrared Characteristic Group Frequencies',* John Wiley, Chichester (1980).

[9]   M. J. D. Lon; *Anal. Chem.*, **97A,** (1969), 41.

[10]   E. G. Brame (Jr.) and J. G. Grasselli; "*Infrared and Raman Spectroscopy*", Vol. 1, Parts A, B, and C, in Practical Spectroscopy Series, Marcell Decker, New York (1977).

[11]   B. C. Smith; '*Fourier Transform Infrared Spectroscopy',* CRC Press, Boca Raton, (1996).

[12]   B. K. Sharma; *'Spectroscopy'* Goel Publ., Meerut, (1997).

[13]   M. P. Fuller and P. R. Griffiths; *Ana. Chem,* **50** (1978) 1906.

[14]   M. P. Fuller and P.R, Griffiths; *Appl. Spectrosc.*, **34** (1980) 533.

[15]   P. Debye and P. Scherrer; *Physik. Z.*, **27** (1917) 277.

[16]   A. W. Hull; *Phys. Rev. (2),* **9** (1917) 84.

[17]   A. W. Hull; *Phys. Rev. (2)*, **10** (1917) 84.

[18]   D. Louër and E. J. Mittemeijer, *"Powder Diffraction in Material Science",*

[19]   L. V. Azaroff and M. J. Buerger; *"The Power Method in X-ray Crystallography"*, Mc Graw-Hill, New York, (1958).

[20]   H. P. Klug and L. E. Alexander; *"X-ray Diffraction Procedures"* 2nd ed., Wiley, New York, (1974).

[21]   L. Solymar and D. Walsh; '*Lectures on the Electrical Properties of Materials'*, Oxford University Press, New York (1984).

[22]   B. Tareev; '*Physics of Dielectric Materials'*, Mir Publishers, Moscow (1975).

[23]   R. D. Waldron; '*Encly. Sci. & Technol'*., Vol.4, Mc.Graw Hill (19-). p.128.

[24]   N. E. Hill, W. E. Vaughan, A. H. Price and M. Darives; '*Dielectric Properties and Molecular Behavior'*, Van Nostrand Reinhold , Landon (1969).

[25]   H. Frohlic; '*Theory of Dielectrics'*, Clarendon Press, Oxford, (1949).

[26]   Y. Ishibashi; '*In Incommensurate Phase in Dielectrics'*, Vol.2, Ed. C. Blinc and A.P.Lavanyak, Elsevier Sci., (1986).

[27]   J. C. Anderson; '*Dielectrics'*, Chapman and Hall, London, (1963).

[28]   J. Beynon; '*Conduction of Electricity in Gases'*, Harrap, London,(1972).

[29]   J. B. Birks et al. (Ed.); '*Progress in Dielectrics*,' Vol. I-V, Heywood, London (1959-1963).

[30]   P. J. Harrop; '*Dielectrics',* Butterworth,London, (1972).

[31]   T. C. Jain; '*Properties of Electrical Engineering Materials'*, Harper and Row, New York, (1967).

[32]   C. M. Kachhava and S. C. Saxena; *Indian J. Phys*., **41** (1967) 440.

[33]   S. K. Krutz and T. T. Perry; *J. Appl. Phys.,* **39** (1968) 3798.,

[34] B. L. Davydov, L. D. Derkacheva, V. V. Dunina, M. E. Zhabotinskil, V. K. Zolin, L. G. Kreneva and M. A. Samokhina; *JEPT Lett.* **12** (1970) 16.

[35] A. Raut, N. Pandita, M.J. Joshi and S. Mengi; '*Progress Report on: Preclinical Development of Herbal Formulation for Inflammatory Arthropathy',* Submitted to the Department of Biotechnology, Govt. of India, (2003-04)

Chapter V

Growth and Characterization of

Hydroxyapatite Crystals

5.1   Introduction:

There are various applications of bio-materials and bio-ceramics, but most important objective of the science of the bio-materials is to develop a new material for bone substitution. The chemical compositions of various calcium phosphates are roughly equivalent to that of the inorganic matrix of the human bone and they are found to be the most suitable as implant materials [1]. The major phase found in bone is Hydroxyapatite (HA, $Ca_{10}(PO_4)_6(OH)_2$) and the other commonly known phases are octacalcium phosphate, tricalcium phosphate, dicalcium phosphate dihydrate and dicalcium phosphate [2]. The HA is not only bio-compatible but also bioactive material, it directly bonds to the bone and favours the implant fixation due to its various interesting properties like, osteoconductivity, nontoxicity, non-inflammatory behavior, and non-immunogenicity [3, 4]. Therefore, the coatings of HA are often applied to metallic implants (most commonly titanium/titanium alloys and stainless steels) to alter the surface properties. In this manner, the body feels the foreign material as the HA-type material only and readily accepts it [5]. Apatites are not only biologically important materials, but they have also great importance in the industry as catalysts, in environmental remediation and in ceramic membranes [6].

Hydroxyapatite is a very useful compound but it is not always true; because HA is also responsible for the ailments called the arthritis, particularly, calcific

periarthritis, acute/ chronic inflammatory arthritis, destructive arthropathy and soft tissue calcinosis. The HA associated arthritis is explained as; the tiny crystals of HA form in or around joints can cause inflammation of joints and also the tissues around the joints, such as tendons and ligaments. They have been described particularly as a cause of *rotator cuff* inflammation of the shoulder. The inflammation caused by HA crystals has been referred to as the *hydroxyapatite crystal disease* [7].

Hydroxyapatite is the most stable calcium phosphate salt under physiological conditions, therefore, various researchers have used HA to study the hard tissue calcification, such as bone and teeth, and in many undesirable cases of pathological mineralization of articular cartilage [8, 9], cardiac valves [10-12] and kidney stones [13]. Many researchers have studied the HA crystals with different aspects. Cuneyt Tas et al. [14, 15] have reported the synthesis process as well as the sintering behavior of HA, composites of HA and tri calcium phosphate at high temperatures. While Vilacampa et al. [16] have reported the synthesis of HA-Si composite material. Koutsopoulos et al [17, 18] have studied the crystallization of HA in the presence of various amino acids and also studied their inhibition effect. Prabakaran et al [19] have reported the development of calcium phosphate based apatite from hen's eggshell. Recently, Vandiver et al. [20] have reported the detection of nano-scale variation in the surface charge of synthetic HA by chemically and spatially specific high-resolution force spectroscopy.

5.2   Physical and Chemical Properties of HA:

Hydroxyapatite is a naturally occurring mineral and the predominant mineral component of vertebrate bone and tooth enamel. It is the most stable and most bio-compatible calcium phosphate [21]. At temperatures higher than 900 ^{0}C, partial decomposition of HA may take place resulting in oxyapatite (OXA). Hydroxyapatite,

partially dehydrated HA, or OXA decompose above 1300 ^{0}C into á-tricalcium phosphate (á- TCP) and tetracalcium phosphate (TetCP).

Many researchers have studied various properties of apatites due to their vast applications. Recently, Rey et al. [22] have studied the physico-chemical properties of nano-crystalline apatites; while Mericier et al. [23] have studied the crystal chemistry of various apatites from the geometrical aspects. The following Table (5.1) represents the physical and chemical properties [24].

Table (5.1)

Physical and chemical properties of HA

General Hydroxyapatite Information	
Chemical Formula:	$Ca_5(PO_4)_3(OH)$
Composition:	Molecular Weight = 502.31 gm
	Calcium 39.89 % Ca 55.82 % CaO
	Phosphorus 18.50 % P 42.39 % P_2O_5
	Hydrogen 0.20 % H 1.79 % H_2O
	Oxygen 41.41 % O
	100.00 % 100.00 % = total oxide
Empirical Formula:	$Ca_5(PO_4)_3(OH)$
IMA Status:	Valid Species (Pre-IMA) 1856
Locality:	Holly Springs, Cherokee County, Georgia, USA.
Name Origin:	Named as the hydroxyl end-member and from the Greek apatao - "I am misleading."
Synonym:	Apatite
	Deltaite-mixture with crandellite
	Hydroxy Apatite
	ICSD 203027
	PDF 9-432
Hydroxyapatite Crystallography	
Axial Ratios:	a:c = 1:0.72998
Cell Dimensions: (in Å)	a = 9.418, c = 6.875, Z = 2; V = 528.11 Den(Calc)= 3.16
Crystal System:	Hexagonal - Dipyramidal H-M Symbol (6/m) Space Group: P 6_3/m or monoclinic
X Ray Diffraction:	By Intensity(I/I_o): 2.814(1), 2.72(0.6), 2.778(0.6),
Physical Properties of Hydroxyapatite	
Cleavage:	Indistinct
Color:	Colorless, White, Gray, Yellow, Yellowish green.
Density:	3.08
Diaphaniety:	Transparent to Opaque

Habit:	Massive - Granular - Common texture observed in granite and other igneous rock.
Hardness:	5 - Apatite
Luster:	Vitreous - Dull
Streak:	white

Optical Properties of Hydroxyapatite	
Gladstone-Dale:	CI meas= -0.046 (Good) - where the CI = (1-KPDmeas/KC) CI calc= -0.02 (Excellent) - where the CI = (1-KPDcalc/KC) KPDcalc= 0.2049,KPDmeas= 0.2102,KC= 0.2009
Optical Data:	Uniaxial (-), e=1.644, w=1.651, bire=0.0070.

Calculated Properties of Hydroxyapatite	
Electron Density:	$ñ_{electron}$=3.15 gm/cc note: $ñ_{Hydroxylapatite}$ =3.16 gm/cc.
Fermion Index	Fermion Index = 0.00073 Boson Index = 0.99927
Photoelectric:	$PE_{Hydroxylapatite}$ = 5.78 barns/electron U=$PE_{Hydroxylapatite}$ x $ñ_{electron}$= 18.19 barns/cc.
Radioactivity:	GRapi = 0 (Gamma Ray American Petroleum Institute Units) Hydroxylapatite is Not Radioactive

Hydroxyapatite Classification	
Dana Class:	41.8.1.3 (41) Anhydrous Phosphates, etc. Containing Hydroxyl or Halogen
	(41.8)where (A)5 (XO4)3 Zq
	(41.8.1)Dana Group
Strunz Class:	VII/B.39-30 VII - Phosphates, Arsenates and Vanadates
	VII/B - Waterfree phosphates with unfamiliar anions F, Cl, O, OH. cations of medium and big size: Mg, Cu, Zn, and Ca, Na, K, Ba, Pb
	VII/B.39 - Apatite - Pyromorphite group

Other Hydroxyapatite Information	
References:	NAME(Dana8) PHYS. PROP.(Dana8) OPTIC PROP.(Enc. of Minerals,2nd ed.,1990)

5.3   Growth of HA Crystal:

Generally, HA crystals are grown by hydrothermal methods at elevated temperatures and pressures [25]. The synthesis of HA nano-wires through wet chemical process has been reported [26]; where as Kamiya et al. [27] have reported the growth of fibrous HA. Precipitation of HA and calcium deficient HA from

aqueous solution was also reported [28, 29]. The crystal growth of HA at ambient conditions of temperature and pressure, generally, yielded nano-crystals. There is only one report [3] on the growth of platy HA single crystals by gel growth technique at physiological temperature.

(a) Gel preparation:

In the present case, AR grade sodium meta-silicate powder was used for preparation of the gel medium. To remove the impurities, 250g sodium meta-silicate was dissolved in one liter of water in a beaker. On stirring it thoroughly, a dense milky solution of sodium meta-silicate was formed. It was left for a couple of days, so that heavy insoluble impurities could accumulate at the bottom of a beaker. This was decanted into another beaker and filtered twice with Whatman (cat No 1001 125) filter paper of 12.5 cm diameter. Then the solution was centrifuged on MSE high-speed centrifuge unit for about half an hour at 10000 revolutions per minute. Practically the solution got rid off all suspended impurities and as a result, transparent, slightly golden colored solution of sodium meta-silicate was obtained. This could be preserved as a stock solution for quite a long period. By adding double distilled water of appropriate volume, one can make solution of desired specific gravity. In the present study, the specific gravity was selected as 1.06. This solution was acidified by 1 N, ortho-phosphoric acid in such a manner that appropriate pH was obtained. The pH values between 6.0 to 6.5 were selected. This solution was transferred to different test tubes for setting the gel.

(b) Hydroxyapatite Crystal growth:

Glass test-tubes of 25 mm diameter and 150 mm length were used as crystal growth apparatus. The above mentioned mixture was poured in equal volumes in different test tubes and allowed to set into the gel form. Within 48 hours good quality

gel was set. After setting the gel, 1 M calcium chloride solution was poured gently on to the set gel. Good quality, very small crystals were found in the form of Liesegang rings, which is shown in the following figure (5.1).

Figure (5.1): HA crystals growth in the form of Liesegang rings

The particle size measurement has also been carried out using the Model Master Sizer 2000, at CSMCRI, Bhavnagar, the results are given in Table (5.2)

Table (5.2)

Particle size measurement data of HA crystals

Sample code	D(0.1) micron	D(0.5) micron	D(0.9) micron
HA (Aqueous)	47.25	82.68	107.54

From the table (5.2), it can be interpreted that 10% of the particles were less than 47.25 micron, 50% of particles were less than 82.68 micron and 90% particles were less than 107.54 micron.

5.4   Characterization of HA Crystals:

5.4.1   FT-IR Spectroscopic Studies: -

Infrared spectroscopy is a very powerful analytical tool for examining both inorganic and organic materials [30-32]. It is an easy way to identify the presence of

certain functional groups in a molecule. Also, one can use the unique collection of absorption bands to confirm the identity of a pure compound or to detect the presence of specific impurities. Infrared spectroscopy reveals information about molecular vibrations that cause a change in the dipole moment of molecules. It offers a fingerprint of the chemical bonds present within materials. When radiation passes through a sample (solid, liquid or gas), certain frequencies of the radiation are absorbed by the molecules of the substance leading to the molecular vibrations. The frequencies of absorbed radiation are unique for each molecule which provides the characteristics of a substance.

FT-IR spectroscopy is the further advancement of IR spectroscopy by using the mathematical concept of *Fourier Transform* through proper electronic circuit and computer interfacing. From the earliest days of infrared spectroscopy it was observed that functional groups of atoms could be associated with definite characteristic absorption bands, i.e., the absorption of infrared radiation over certain frequency intervals. The infrared spectrum of any given substance is interpreted by the use of the known group frequencies and thus it will be easy to characterize the substance as one containing a given type of group or groups. Although group frequencies occur within narrow limits, interference or perturbation may cause a shift of the characteristic bands due to (a) the electro negativity of neighboring groups or atoms, (b) the spatial geometry of the molecule, or (c) the mechanical mixing of vibrational modes.

Functional groups sometimes have more than one characteristic absorption band associated with them. On the other hand, two or more functional groups may absorb in the same region and hence, in general, can only be distinguished from each other by means of other characteristic infrared bands, which occur in non-overlapping regions.

Absorption bands may be considered as having two origins, these being the fundamental vibrations of (a) functional groups, e.g. C=O, C=C, C N, -CH$_2$-, -CH$_3$-, and (b) skeletal groups, i.e. the molecular backbone or skeleton of the molecule e.g., C-C-C-C. Absorption bands may also be aroused from stretching vibrations, i.e., vibrations involving bond-length changes, or deformation vibration, i.e., vibrations involving bond-angle changes, of the group. Each of these, in some cases, may be considered as arising from symmetric or asymmetric vibrations.

For a given functional group, the vibration bands due to stretching occur at higher frequencies than those due to deformation. This is because more energy is required to stretch the group than to deform it due to the bonding force directly opposing the change.

Many workers have studied the IR spectra of different phosphates and biomaterial compounds. FT-IR spectra of calcium hydrogen phosphate dihydrate (CHPD) and calcium oxalate type urinary crystals have been reported by Joshi [33]. Cuneyt Tas [34] has studied the FT-IR spectrum of synthesized Ca-HA powders from synthetic body fluid at a physiological temperature of 37 ^{0}C. Whereas, Koutsopoulos et al. [35] have reported the crystallization of HA on sodium cholate and confirmed the presences of HA through the FT-IR and other techniques. Moreover, Kontonasaki et al. [36] have studied the *in vitro* formation of hydroxycarbonate apatite on the bio-glass and through the FT-IR and SEM they confirmed the development of hydroxy carbonate apatite layer on the commercially available bio-glass.

The FT-IR spectrum of HA crystals is shown in figure (5.2), which was recorded on a Shimadzu 8400 instrument in KBr disc, in the range of 400 cm^{-1} to 4000 cm^{-1}. From figure (5.2) one notices that the absorptions occurring at 3344.3 cm^{-1} and 1596.9 cm^{-1} are due to the O - H stretching and O-H plane-bending

vibration, respectively. The PO_4^{-3} bands were recorded at 467 cm^{-1} (u_2), 562.2 cm^{-1}, 602.7 cm^{-1} (u_4), 961.4 cm^{-1} (u_1) and 1029 cm^{-1}(u_3). The absorptions between 400 cm^{-1} to 520 cm^{-1} are due to the presence of oxygen-calcium bond. From the figure (5.2) one can confirm that the crystal is completely free from C=O bond inclusion. Table (5.1) represents the assignments of different absorptions bands in Fourier Transform Infrared (FT-IR) spectrum for HA crystals.
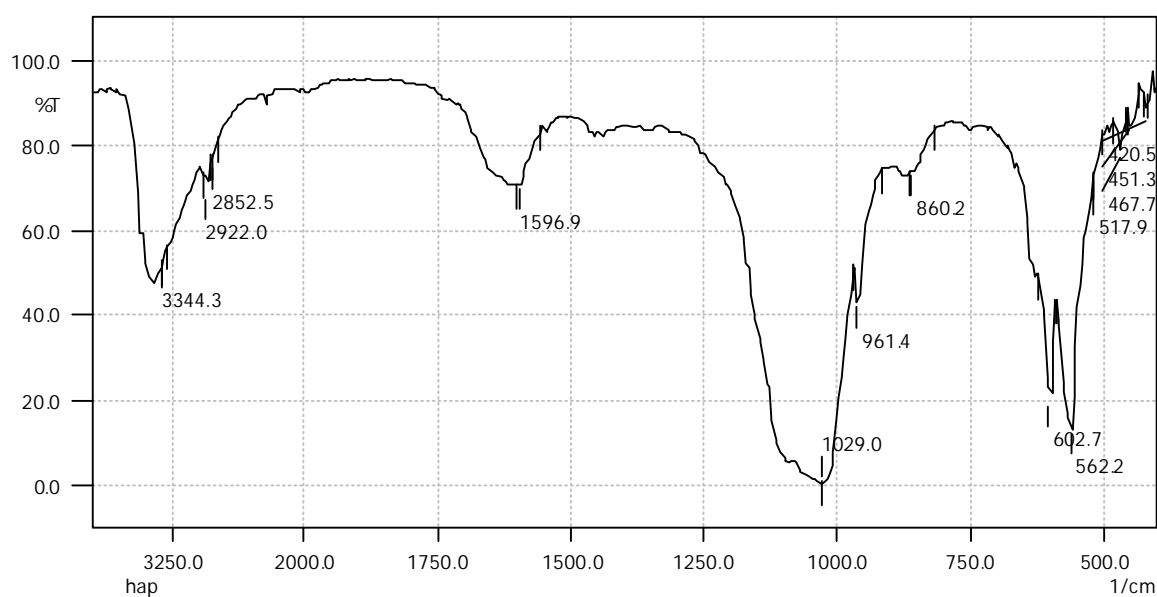
Figure (5.2): FT-IR spectrum of HA crystals

Table (5.3)

Assignments of different absorption bands in the FT-IR spectra of HA crystals

Hydroxyapatite $Ca_{10}(PO_4)_6(OH)_2$	
Assignments	**Observed frequencies (cm^{-1})**
O–P–O bending	467.7
	562.2
	602.7
P-O Symmetric stretching bonds	860.2
	961.4
P-O Asymmetric stretching	1029.0
O-H in plane bending	1596.9
O-H Stretching	3344.3

Considering a molecular model where the nuclei are represented by point masses and the inter atomic bonds are represented by mass-less springs, which follows Hooke's law. If masses are expressed in unified atomic mass unit and the force constant is expressed in mdynes /Å, then

$$\bar{u} = 1303 \sqrt{\frac{F}{(1/M_1 + 1/M_2)}} \qquad \text{------ (5.1)}$$

Where, 1303 is equal to $(N_A \times 10^5)^{\frac{1}{2}} / 2pC$, N_A is Avogadro's number, 6.0225×10^{23} mol^{-1} [37]. A complex molecule consists of a number of atoms with different bonds. Each bond between two atoms, which can oscillate about some equilibrium bond length or for a bond angle between two bonds, can oscillate about some equilibrium bond angle. Two such oscillators, which are arranged so that they exert forces on each other, when they oscillate, are known as coupled oscillators. By taking account of this simple model, the force constant has been calculated for O-H vibrations. Which is found to be 6.200 mdynes/Å.

From the FT-IR spectra, the presence of O-H bond and symmetric and asymmetric stretching of PO_4^{-3} bonds are confirmed.

5.4.2 Powder X-ray Diffraction:

Powder X-ray Diffraction(XRD) is perhaps the most widely used x-ray diffraction technique for characterizing inorganic and organic crystalline materials. As the name suggests, the sample is usually in a powder form, consisting of fine grains of single crystalline material to be studied. The technique is also used widely for studying particles in liquid suspensions or polycrystalline solids (bulk or thin film materials) [38]. The term 'powder' really means that the crystalline domains are randomly oriented in the sample. Therefore, when the 2-D diffraction pattern is recorded, it shows concentric rings of scattering peaks corresponding to the various d

spacings in the crystal lattice. The positions and the intensities of the peaks are used for identifying the underlying structure (or phase) of the material. The method has been traditionally used for phase identification, quantitative analysis and the determination of structure imperfections. In recent years, applications have been extended to new areas, such as the determination of crystal structures and the extraction of three-dimensional micro-structural properties [39]. Further details are already given in the section 4.6 of Chapter-IV.

The apatite prototype, $(A_5(BO_4)_3X)$, $Ca_5(PO_4)_3F$ structure was first determined by Naray-Szabo [40] in 1930 and was confirmed to adopt $P6_3/m$ symmetry. An extensive apatite compilation was prepared by Wyckoff [41], who noted that the lack of thorough structure determinations let many unanswered questions about the distribution of metals and oxygen anions. Subsequently, numerous studies of biological, mineralogical and synthetic apatites and apatite related substances greatly expanded the range of known chemistries. McConnell [42] summarized the work up to the 1970's and highlighted the limitations associated with failing to consider the underlying chemical principles that govern apatite crystallography and the need for precise chemical analyses to properly account for apatite properties. Elliot [43] updated and expanded the work of McConnell by covering a wider range of apatites, reviewing iso- and altervalent substitutions, and detailing the identification of compounds of lower symmetry. Since then there has been a substantial increase in the number of apatites for which excellent crystallographic data exist. Recently, White and Zhili [6] have summarized the current knowledge of apatite structures, particularly, with respect to the literature that has appeared since the publication of Elliot's [43] work and have reported the complementary work of Niragu and Moore [44] and Brown and Constabtz [45] on phosphate compounds.

The apatites are represented, generally, as $A_5(BO_4)_3X$, where, A represents divalent cations (Ca^{2+}, Pb^{2+}, Ba^{2+} etc…), BO_4 represents trivalent anions (PO_4^{-3}, VO_4^{-3}, SiO_4^{-3}, etc.) and X represents the an anion mono-valent (F^-, Cl^-, OH^-, Br^- ,etc.). In general, drawings are projected along [001] direction and give prominence to the BO_4 tetrahedra, either in ball and stick or tetrahedral display, as shown in figure (5.3a) [46]; on the other hand, Sudarsanan and Young [47] have represented the projection in such a way that it highlights the symmetry and the regular polyhydra both together for apatite crystals, which is exhibited in figure (5.3b). In the following figures (5.3a & b), the projection of a fluroapatite ,$Ca_5(PO_4)_3F$, is represented, where F can be replaced by mono-valent anion, such as OH^-, Cl^-, and Br^-.
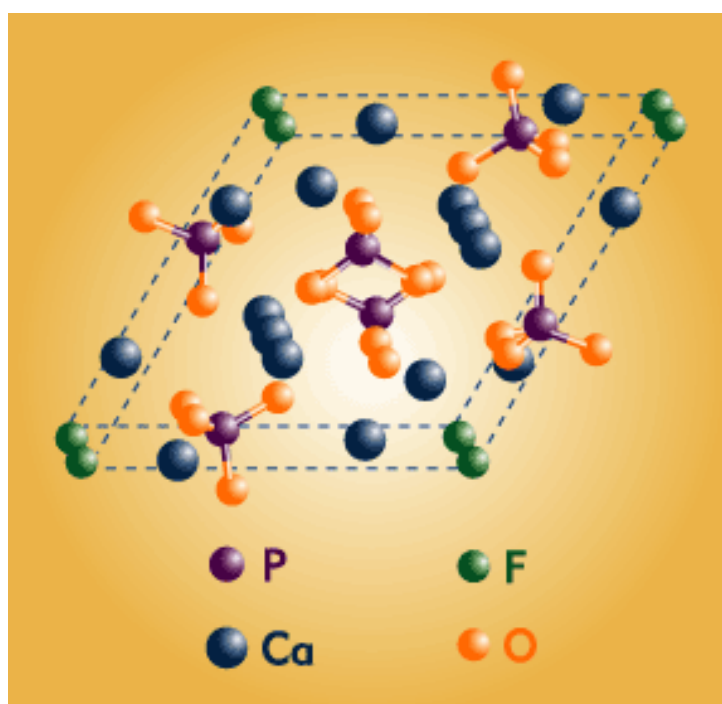
Figure (5.3a): The [001] projection of the fluorapatite $Ca_5(PO_4)_3F$ [46]
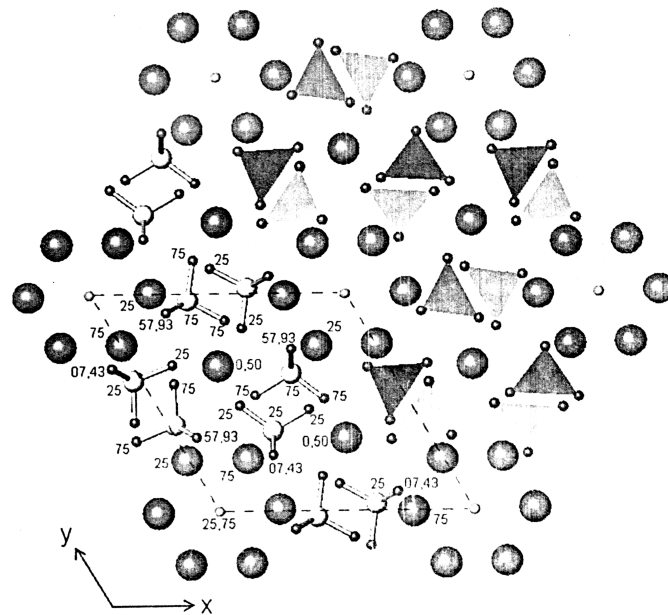
Figure (5.3b): The [001] projection of the fluorapatite Ca₅(PO₄)₃F with the

crystal symmetry

The following figure (5.4) represents the morphology of the HA crystal with the

Miller indices of different faces [48].
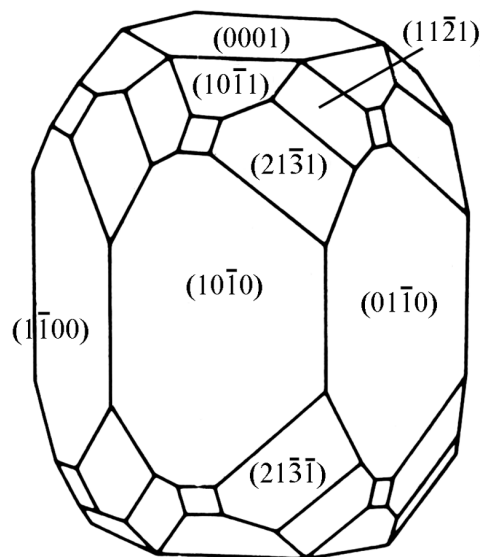
Figure (5.4): Morphology of the hydroxyapatite crystal [48]

Various researchers have carried out X-ray characterization of different apatite

crystals; for instance, Sudarsanan and Young [47], and Kim et al. [49] and Elloit et al.

[50] have characterized the fluroapatite, chloroapatite and bromoapatite crystals,

respectively. Hydroxyapatite is the main inorganic constituent of natural bone and a rare naturally occurring mineral [43]. Crystallographic study of HA crystals has also been reported by various researchers [49, 51, 52]. Kim et al. [49] have determined the crystal structures of $M_{10}(PO_4)_6X_2$ type crystals, where M = Ca or Pb and X = OH$^-$, F$^-$, Cl$^-$ or Br$^-$, by Rietveld refinement of powder synchrotron, X -ray and neutron diffraction data. Moreover, Calderin et al. [53] have studied the electronic and crystallographic structures of oxyapatite, hydroxyapatite, fluorapatite, and chlorapatite. Recently, Ashok et al. [3] have reported the growth and characterization of HA crystals at physiological temperature.

Calcium apatites have the general chemical formula $Ca_5(PO_4)_3X$, where X is an electronegative element or group such as a halogen or an OH group. The structure of the apatites can be viewed as consisting of unconnected PO_4^{-3} tetrahedra with Ca^{+2} in the space between and a column of X$^-$ ions along the c axis to balance the charge. The type and location of these anions distinguish various calcium apatites. Two kinds of structures have been found experimentally depending on the stoichiometry, temperature, and pressure [40]. These are the hexagonal and the monoclinic structures, where the monoclinic unit cell is obtained from the hexagonal one by doubling the b lattice parameter with an alternating arrangement of the anion chain.

Various researchers [49, 51] have reported the hexagonal crystal structure with following unit cell parameters,

$a = b = 9.4302$ Å, $c = 6.8911$ Å

$á = â = ã = 90^0$

It is also reported [43, 52, 54-55] that HA has a monoclinic structure with four formula units per unit cell and a phase transition to a hexagonal structure around 370 °C. The lattice parameters are as follows.

$a = 9.241\ (1)\ ,\quad b = 18.843\ (2)\quad , c = 6.881\ (1)$

$á = â = 90^0, ã = 120.0\ (1)^0$

Calderín et al. [53] have studied the possibility of having hexagonal as well as monoclinic structures in the case of hydroxyapatite, chloroapatite (CAP), fluroapatite and oxyapatie using *density functional theory* (DFT) [56] with the *local-density approximation* (DFT-LDA), which provides a theoretical frame work for calculation. From the calculation, it has been reported that hexagonal system is possible in all the studied apatites, even in the case of HA and CAP, while the monoclinic structure is possible only in HA and CAP and has almost the same total energy per molecule as the hexagonal system. By X-rays study, Van Rees et al. [57] have shown that stoichiometric HA exhibits a monoclinic-hexagonal transition at 211.5 ^{0}C. In the hexagonal HA structure, OH $^-$ ions are in statistical disorder in channels parallel to the c-axis while in the monoclinic HA these ions are pointing in the same direction in one column and in the opposite orientation in the neighboring columns.

In the present study, an attempt is made to find out the cell parameters of HA crystals and compare the same with the reported values. Using Powder-X computer software the *h, k,* and *l* parameters as well as *d* and *2è* values are generated in such a way that these values match with the powder X-ray diffraction pattern. The present investigation suggests that the cell parameters are closely matching with the values reported by Elliot et al. [52], within the limits of estimated standard deviation.

The estimated values of cell parameters are as follows.

$a = 9.432 \qquad b = 18.843 \qquad c = 6.923$

$á = â = 90.01^0, ã = 119.05^0$

Figure (5.5) is the X-ray diffraction pattern and Table (5.4) represents the powder X-ray diffraction results of HA crystals.
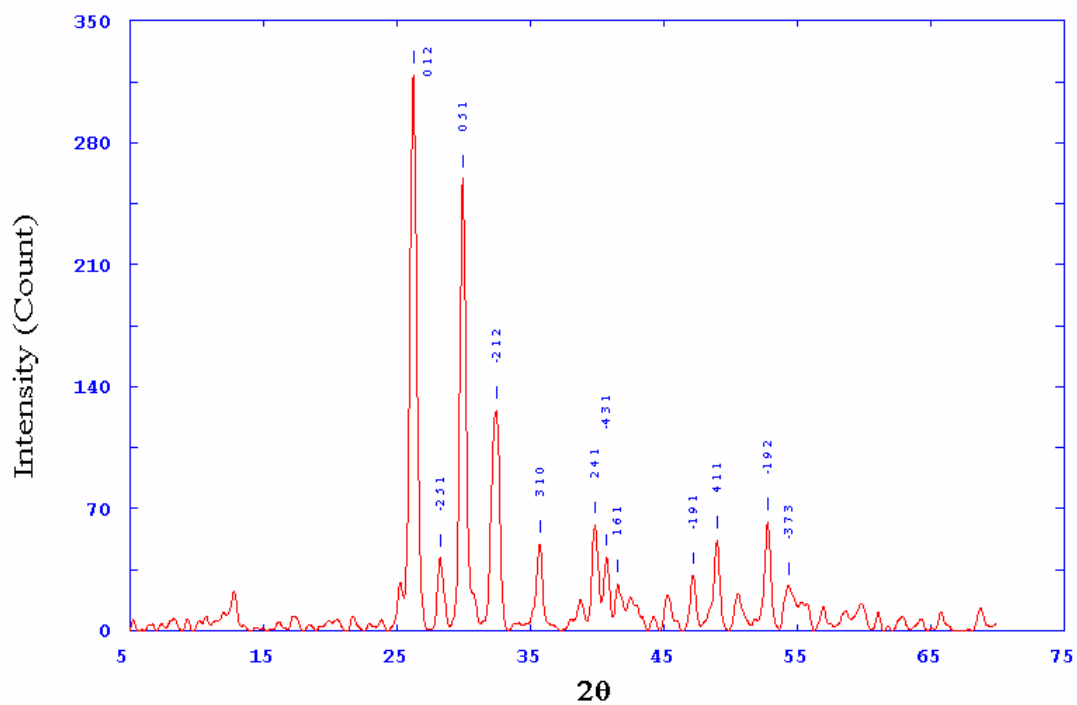
Figure (5.5): Powder X-ray diffractogram of HA crystals

Table (5.4)

X-ray diffraction results for HAP crystals

2è Degree	Relative Intensity (%)	d ( )	(h k l)
26.248	318.80	3.39505	(012)
28.255	41.55	3.15830	(-251)
29.948	259.43	2.98351	(051)
32.458	126.32	2.75829	(-212)
35.717	49.43	2.51380	(310)
39.853	60.47	2.26190	(241)
40.735	41.77	2.21492	(-431)
41.569	26.72	2.17242	(161)
47.206	31.40	1.92531	(-191)
49.006	51.83	1.85872	(411)
52.799	62.48	1.73380	(-192)
54.357	25.53	1.68773	(-373)

The above result suggests that the structure is monoclinic type. However, an attempt is made to analyze the crystal structure of HA by considering the hexagonal structure [49, 51]. The values of cell parameters indicate the large number of deviation in standard errors and the sigma can not be minimized appreciably low. This further suggests that the crystal structure is monoclinic, in the present case, and the value is much more nearer to the value suggested by Elliot et al [52].

The figure (5.6) shows the unit cell and molecular packing of the HA crystals [58].
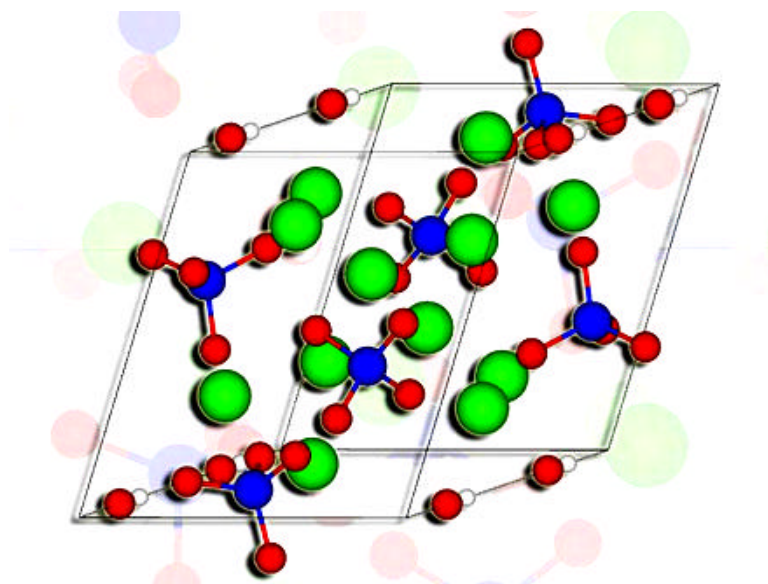
Figure (5.6): The unit cell diagram of HA crystals [58]

5.4.3 Dielectric Studies of HA Crystals:

There are many theories of dielectrics; however, an attempt has been made hereby to briefly review these theories.

(i) *Macroscopic Theory***:** -

The dielectric constant ê in equation (5.2) is a dimensionless parameter relating the following quantities,

$$\hat{e} = \hat{I}/\hat{I}_0 = D/\hat{I}_0 E = 1 + (g P /\hat{I}_0 E) = 1 + gc \qquad \text{---------(5.2)}$$

Where, D is the displacement, P is the polarization, E is the electric field, χ is the electric susceptibility , $\boldsymbol{g}$ is a geometrical factor ($\hat{\boldsymbol{I}}_0$ =1 and $\boldsymbol{g} = 4\,\pi$ in CGS electro-statistic units; $\hat{\boldsymbol{I}}_0 = 8.854 \times 10^{-12}$ farad/m and $\boldsymbol{c}$ =1 in rationalized MKS units), $\hat{\boldsymbol{I}}$ and $\hat{\boldsymbol{I}}_0$ are the permittivities of dielectric and vacuum, respectively. The quantities ê and $\boldsymbol{c}$ are *scalar* or *tensor* quantities depending on whether it is isotropic or anisotropic dielectrics, respectively.

For electric fields varying sinusoidally with time, the *phase* of the displacement may be regarded with respect to the field. In that condition, the equation (5.2) is having the *complex number* notations. Thus, ê * = ê'- i ê", where ê' and ê" designate the components of the permittivity ratio in phase with E and retarded ¼ cycle, respectively. The term dielectric constant is usually restricted to the real part, ê', while ê $*$ is designated as the complex relative permittivity.

(ii)   Microscopic Theory: -

The dielectric constant of a material depends on its polarization in an applied field or, microscopically, on the relative displacement of the electrons and nuclei composing the molecules of the dielectric, in the field direction. These displacements are associated with changes in rotational and vibrational motions of the electrons and nuclei upon application of an electric field. This leads to a frequency dependence and temperature dependence resulting from the inertial characteristics of the motions and the initial state of excitation of the system. The dielectric constant also depends on field strength, since for sufficiently high fields the polarization will no longer be proportional to the field because a saturation or breakdown phenomenon occurs. In these cases, the nonlinear portions of the polarization lead to harmonic frequency generation and interaction between two or more electromagnetic waves.

(a)   ***Theory of Static Polarization: -***

A molecule in an electric field develops an average dipole moment $(m)_{av} = a\,E$, where a is the polarizability. For a polar molecule, a may be expressed as $a = a_0 + a_p$, where a_p is the polarizability arising from the partial orientation of the permanent dipole moment m_p, and a_0 is the polarizability due to all other processes. Then $(m)_{av} = a_0\,E + (m_p\,cos q\,)_{av}$, where $(m_p\,cos q\,)_{av}$ is the average value of the component of m_p in the field direction, q being angle between m_p and E.

The potential energy U of the permanent dipole is given by $U = -|\,m_p\,|\,|\,E\,|\,cos q$. For a system in thermodynamic equilibrium, the probabilities of the possible states is given by the Boltzmann distribution. It can be shown that $(m_p\,cos q\,)_{av} = cot\,h\,x = m_p\,L(x)$, (here, the Langevin function is $L(x) = cot\,h\,x - (1/x)$ and $x = |\,m_p\,|\,|\,E\,|\,/\,kT$, where k is the Boltzmann constant, and T is the absolute temperature). For $x << 1$, $L(x) \cong x/3$; in this approximation the microscopic parameters have been multiplied by N, the number of molecules per unit volume, to give the polarization.

$$P = N\,(m)_{av} = N\,(a_0 + |\,m_p\,|^2\,/\,3kT\,)\,E \qquad \text{-------(5.3)}$$

Equation (5.3) is the *Langevin - Debye* formula, from which the permanent dipole moments of polar molecules may be obtained from the temperature variation of measured values of polarization.

(b)   ***Local Field: -***

For gases at low densities, the molecular interactions can usually be neglected; but for matter at higher densities, the interaction becomes important and is usually treated by introducing the concept of local field E_l, the average electric field strength at molecular site. The E_l is conveniently divided into two parts, E_s and E_r, where E_s is the field due to polarization by molecules inside a small sphere centered at the

molecular site, and E_r is the field due to external charges and polarization by molecules outside the sphere; the sphere is taken sufficiently large that the medium outside may be considered continuous. The E_r is obtained by subtracting the field E_p at the center of a uniformly polarized isolated sphere from the macroscopic field E in the dielectric. Thus, a sphere of uniform polarization, P, has a surface charge density $S = |P| \cos\mathbf{q}$, where, $\mathbf{q}$ is the angle between P and the normal to the surface. The field at the center contributed by a unit area of the surface is equal to $\mathbf{g}s /4\,\mathbf{p}\,\hat{\mathbf{I}}_0 R^2$, where R is the radius of the sphere, and where its component in the direction of P is z $\mathbf{g}s\,\cos\mathbf{q}$ $/4\mathbf{p}\hat{\mathbf{I}}_0 R^2$. By integrating over surface gives the net field $E_P = \mathbf{g}P/3\,\hat{\mathbf{I}}_0$. Finally, E_r is expressed as follows

$$E_r = E - E_p = E\,(\hat{e}' + 2)\,/3 = E\,(1 + \mathbf{g}c/3) \qquad \text{------- (5.4)}$$

By assuming that $E_S = 0$, one obtains the Lorentz local field $E_l = E_r$, Which leads to the expressions as follows for P, c and $\hat{e}'$

$$P = N\,(\mathbf{m})_{av} = NaE\,(\,1 - \mathbf{g}Na/3\hat{\mathbf{I}}_0\,) \qquad \text{--------(5.5)}$$

$$\mathbf{c} = P\,/\,\hat{\mathbf{I}}_0\,E = (\,N\,\mathbf{a}\,/\hat{\mathbf{I}}_0\,)\,(1 - \mathbf{g}N\,\mathbf{a}\,/\,3\hat{\mathbf{I}}_0) \qquad \text{--------(5.6)}$$

$$\hat{e}' = 1 + \mathbf{g}\,\mathbf{c} = 1 + \mathbf{g}Na\,/\,(\hat{\mathbf{I}}_0\,-\,\mathbf{g}Na\,/3) \qquad \text{-------(5.7)}$$

The last equation may be solved for $\mathbf{a}$, giving

$$\mathbf{g}N\mathbf{a}\,/\,3\,\hat{\mathbf{I}}_0 = (\hat{e}'-1)\,/\,(\hat{e}'+2) \qquad \text{------- (5.8)}$$

This is a form of the *Clausius – Mosotti* equation. This formula gives fairly good agreement with experiments up to moderate densities for non-polar molecules, but fails to account for the behaviour of strongly polar molecules.

In the Lorentz field approximation, the susceptibility becomes infinite if $\mathbf{g}N\,\mathbf{a}$ $= 3\,\hat{\mathbf{I}}_0$. Since $\mathbf{a}$ for polar molecules is given by $\mathbf{a} = \mathbf{a}_0 + |\mathbf{m}|^2/3kT$, there exists a critical temperature below which $\mathbf{a} > 3\,\hat{\mathbf{I}}_0\,/\,\mathbf{g}N$ and the material should under go

spontaneous polarization. This *polarization catastrophe* is not confirmed by experiment except for a class of crystals known as *ferroelectrics*.

(c)   Onsager Theory: -

The polarization catastrophe is avoided in a dielectric theory of polar molecules due to L. Onsager. In his treatment, the local field is calculated for an actual spherical cavity of molecular size in the dielectric using Laplace's equation, which gives $E_l = 3 ê'_{E/} (2 ê'+1)$. A polar molecule with dipole moment m_p is inserted in the cavity induces an additional reaction field as given by the following equation,

$$E_R = g m_p 2 (ê'-1) / \hat{I}_0 V3(2 ê'+1) \qquad \text{--------(5.9)}$$

Where, *V* is the volume of the cavity. This reaction field is parallel to m_p and thus exerts no aligning torque on the molecule. For this theory, the polarization is given by,

$$P = NaE_l = N \, a3 \, ê'E/2 \, ê'+1 \qquad \text{------- (5.10)}$$

Since, $g P = (ê'-1) \hat{I}_0 E.$

The equation may be written as,

$$ê' = ¼ [1 + 3Z + 3 (1+2Z/3 + Z^2)^{½}] \qquad \text{-------(5.11)}$$

Where $Z = g N a / \hat{I}_0$. The agreement with theory is satisfactory for most polar liquids, but it is inadequate for systems with hydrogen bonds.

A detailed discussion of these theories is presented elsewhere [59-60]. The electrical conduction of crystal dielectrics has been discussed by Tareev [60] on the basis of crystalline defects. Apart from this, the same author has discussed ionic and mol-ionic electrical conduction of dielectrics in detail.

(d) Debye Theory: -

There is one powerful generalization due to Debye of how materials with orientational polarizability behave in the region where the dielectric polarization is

relaxing, i.e. the period of the a.c. wave is comparable to the alignment time of the molecule. When the applied frequency is much greater than the reciprocal of the alignment time, the relative dielectric constant is $\hat{I}_\infty$ (representing atomic and electronic polarization). For much lower frequencies it becomes $\hat{I}_s$, the static relative dielectric constant. One needs to find an expression of the form

$$\hat{I}\,(w) = \hat{I}_\infty + f\,(w) \qquad \text{------ (5.12)}$$

Which, for w 0 reduces to

$$f\,(0)\;=\;\hat{I}_s - \hat{I}_\infty \qquad \text{--------(5.13)}$$

Now, suppose that a steady field is applied to align the molecules and then switched off.

The polarization and hence the internal field will diminish. One can notice that it decays exponentially with a time constant, $\hat{o}$, the characteristic relaxation time of the dipole moment of the molecule is,

$$P(t) = P_0\,exp(\,-t/\hat{o}\,) \qquad \text{---------(5.14)}$$

It is well known that time variation and frequency spectrum is related by the Fourier transform. In this particular case it happens to be true that the relationship is,

$$f(w) = k_0\;{}^\infty P(t)\,e^{\,iwt}\,dt$$

$$= k\,P_0/\,(-iw + 1/\hat{o}) \qquad \text{--------- (5.15)}$$

Where k is a constant ensuring that $f(w)$ has the right dimension. Using the condition (5.13) for the limit when $w = 0$. One obtains

$$kP_0\,\hat{o} = \hat{I}_s - \hat{I}_\infty \qquad \text{--------(5.16)}$$

Hence equation (5.12) becomes

$$\hat{I}\,(w) = \hat{I}_\infty + [\hat{I}_s - \hat{I}_\infty/(-iw\hat{o} + 1')] \qquad \text{-------- (5.17)}$$

This, after the separation of the real and imaginary parts, reduces to

$$\hat{I}' = \hat{I}_\infty + [\hat{I}_s - \hat{I}_\infty/\,1 + w^2\,\hat{o}^2] \qquad \text{-------- (5.18)}$$

$$\hat{I}\text{''} = w\hat{o}\,(\hat{I}_s - \hat{I}_\infty)\,/\,1 + w^2\,\hat{o}^2 \qquad\qquad \text{--------(5.19)}$$

These equations agree well with experimental results. Their general shape is shown in Figure (5.7).
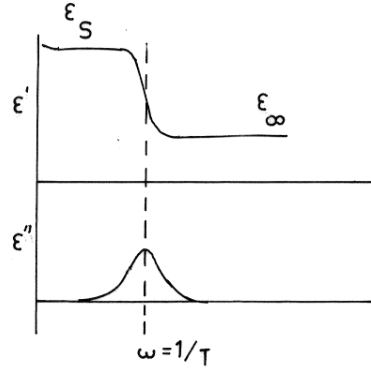
Figure (5.7): The Plots for å' and å'' versus ù

Notice, particularly, that $\hat{I}\text{''}$ has a peak at $w\hat{o} = 1$, where the slope of the $\hat{I}\text{'}$ curve is maximum.

(iii)   Dependence of Permittivity on Various Factors: -

The permittivity $\hat{I}$ depends on the external factors such as frequency of applied voltage to the dielectric material, temperature, pressure, humidity etc [60]. This has been summarized hereby briefly.

The permittivity of non-polar dielectrics does not depend on frequency, when it is changed within very broad range. On the other hand, in the case of polar dielectrics when the frequency of alternating voltage increase the value of $\hat{I}$ remains invariable, initially, but beginning with certain frequency f_0 the polarization fails to settle itself completely during one half cycles and $\hat{I}$ begins to drop at very high frequencies. The value of f_0 can approximately be obtained if *relaxation time* ($\hat{o}$) is equated to half period *$1/2f_0$* of voltage when

$$f_0 = kT\,/\,8\mathbf{ph}r^3 \qquad\qquad \text{---------(5.20)}$$

Where, h is the dynamic viscosity, r is the radius of the molecule, T is the absolute temperature and k is the Boltzmann constant. In the case of water, $\hat{o}$ is estimated to be of the order of 10^{-11} sec, hence the value of f_0 should be of order of 10^{11}Hz or 100 GHz. A phenomenon of *migrational polarization* is observed in inhomogeneous trielectrics, particularly in dielectrics with water inclusions. The phenomenon of the so called *resonance- polarization* may cause maxima in $\hat{I}$ at very high frequencies.

Temperature is not expected to affect the process of electronic polarization in non-polar dielectrics. A relative sharp change in $\hat{I}$ of non-polar dielectric is observed for temperature variation when crystalline material goes into transition to liquid. The nature of dependence of permittivity on temperature may be different in solid ionic linear dielectrics. In most cases an ionic mechanism of polarization increases $\hat{I}$, when temperature grows. Generally, the molecules cannot orient themselves in polar dielectrics in the low temperature region. When the temperature is raised the orientation of dipoles is facilitated, and this increases permittivity. As temperature grows the chaotic thermal oscillations of molecules are intensified and the degree of orderliness of their orientation diminishes. This causes the curve of $\hat{I}$ versus temperature to pass through the maximum and drop. Also, in case of chemically individual polar material a jump like change in $\hat{I}$ is observed at the melting point.

In the dielectrics, which obey the Clausius- Mosotti law, the magnitude of permittivity increases as pressure rises due to increase in the density of the substance.

Moreover, in hygroscopic dielectrics with $\hat{I}$ smaller than that of water, the permittivity is expected to increase with moistening.

A strong dependence of permittivity on the applied voltage to dielectrics is typical in ferroelectrics. As regards in linear dielectrics the $\hat{I}$ can be assumed to be

practically independent of voltage, however, a saturation effect can be expected in the polar liquid and gases.

(iv)   ***Dependence of tan*** d ***on Various Factors: -***

The values of *tan* d are not strictly constant and depend on various external factors [60], which are briefly mentioned as follows,

The variation of *tan* d with frequency is often considered. The problem is usually analyzed in following interval

$lim_{w \, 0} \; tan d = ¥$

$lim_{w \; ¥} \, tan d \; = 0$

Tareev [60] has remarked that the physical meaning of these limits, both $w = 0$ and $w = ¥$, gives finite values of *P* and he has explained the physical significances. Dielectric losses in polar dielectric and also the losses only due to electric conduction in various cases were considered.

The dependence of *tan* d on temperature, generally, suggests that *tan* d appreciably increases when temperature rises. Therefore, with an increased *tan* d , as in the case of decreasing r (conductivity), the insulation will operate under more strain at high temperatures. The dielectric losses caused by the dipole mechanism reach their maximum at a certain definite temperature T_k. At very low temperatures, the *tan* d of various dielectrics is extremely small.

The value of *tan* d noticeably increases in hygroscopic dielectrics when humidity grows.

Moreover, the variation of *tan* d with voltage gives valuable information regarding the quality of insulation material. When the insulation is studied the

importance is given, apart from the absolute value of *tand*, to the nature of change in *tand* depending on the applied value.

Many researcher have studied the dielectric properties of various biomaterials [61], ceramics [62-66], single crystalline materials [67], glasses [68-70], acrylic acid doped ethyl cellulose films [71], poly (N- Methyl Pyrrole) thin films [72], copper ferrite- barium titanate composites [73], $MgFe_2O_4$ from iron ore rejects [74], ferrites [75], rubber ferrites composites [76], fly ash [77], etc.

Dielectric properties of bone are extensively studied since the discovery of bone piezoelectricity by Fukada and Yasuda [78]. The bone is made up of organic materials, mainly collagen, and inorganic materials, mainly HA, and other phosphates [79]. Because of complex composition and structure of bone, its dielectric properties are anisotropic [80]. Moreover, like most biological tissues, bone dielectric properties depend on moisture content and fluid conductivity [81]. Recently, Bonincontro et al [82] have studied the dielectric behavior of organic bio-materials such as, Lysozyme and Ferricytochrome-c, which are generally used as model proteins. Prieto Valdes et al. [83] have used different conditions, like sintering at 1150 ^{0}C in air or under H_2O vapor flow, quenched in water at room temperature after sintering, or slow cooling inside the furnace, for preparation of HA-ceramics and reported that, depending on the specific combinations of these preparation conditions, resulting HA-ceramics shows the significant differences in the phase composition and dielectric properties, which are ranging from capacitive to a semiconducting response. Hitmi et al. [84] have studied dielectric properties of different synthetic apatites and led to the conclusion that the high temperature dielectric loss peak comes from dipolar reorientations of ions inside apatite channels.

In the present investigation, the values of dielectric constant were calculated

from the measured values of capacitance at room temperature within frequency range from 500 Hz to 1 MHz, by applying formulae of equation (4.15) and (4.16) of Chapter- IV. The variation of dielectric constant with frequency is displayed in figure (5.8). From this plot one can observe that as the frequency increases the dielectric constant initially decreases very rapidly and then slowly as the frequency increases.
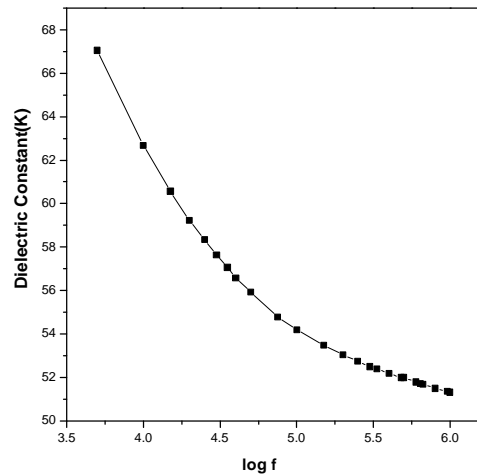

Figure (5.8): Plot of dielectric constant versus *log f*

This type of variation suggests that the higher space charge polarizability at lower frequency region. This type of behaviour is due to the electronic exchange of the number of ions in the crystal gives local displacement of electrons in the direction of applied field, which gives the polarization. As the frequency increases, a point is reached where the space charge cannot sustain and comply with the external field. Therefore, the polarization decreases and exhibits the reduction in the values of dielectric constant as the frequency increases. This behaviour is similar to those of observed by Lopez et al. [85] and Dabhi et al. [86] for zinc tartrate and Arora et al. [87] for strontium tartrate.

Figure (5.9) represents the plot of *tan ä* versus *log f* at room temperature. The nature of the plot is similar to that of the variation of dielectric constant with frequency. Figure (5.10) represents the plots of a.c. resistivity and a.c. conductivity

versus *log f*. The a.c. resistivity ($\tilde{n}_{ac}$) and a.c. conductivity ($\acute{o}_{ac}$) were calculated from the following formula,

$$r_{ac} = \frac{2pfcdt}{A} \qquad \text{----------- (5.21a)} \qquad s_{ac} = \frac{1}{r_{ac}} \qquad \text{-----------(5.21b)}$$
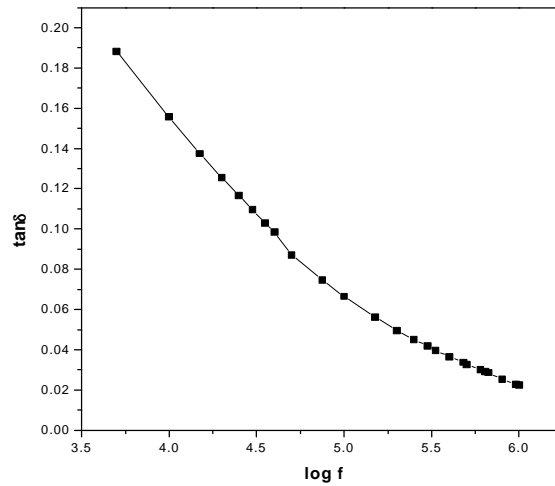
Figure (5.9): Plot of *tan ä* versus *log f*
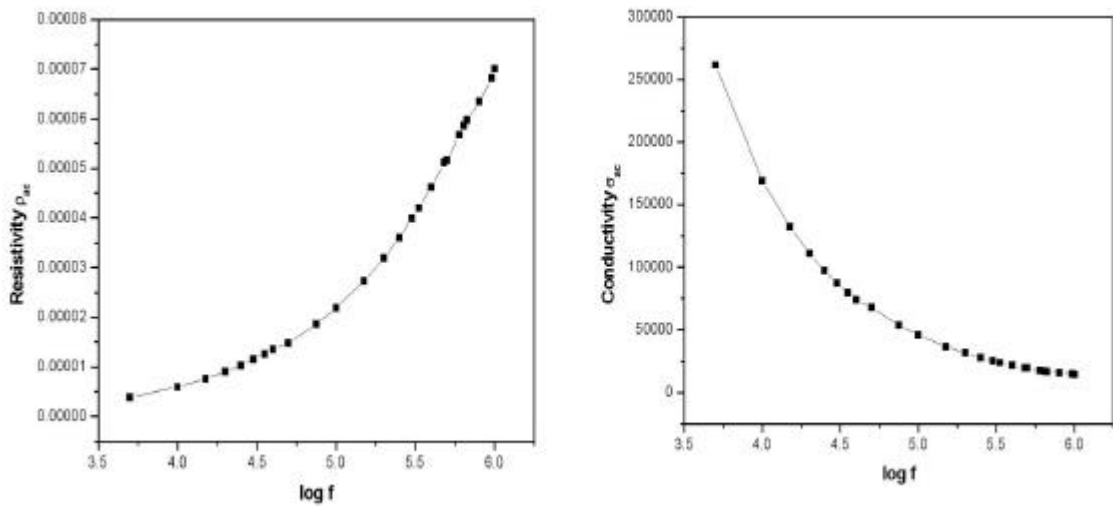
Figure (5.10a & b): The plot of ac resistivity ($\tilde{n}_{ac}$) and ac conductivity ($\acute{o}_{ac}$)

versus *log f*

From these figures, one can easily notice that as the frequency increases the a.c. conductivity decreases and, obviously, the a.c. resistivity increases.

5.5 *In vitro* Inhibition Study of the HA Crystals for Different Herbal Extracts:

Acute, sub-acute, and chronic musculoskeletal symptoms, such as bursitis and tendonitis, are well known to occur in response to calcium apatite deposition at joints other than the shoulder [88, 89]. Therefore, many researchers have studied the growth and inhibition of HA crystals by various techniques. Hunter et al. [90] have studied the effect of different concentration of chondroition sulphate on the growth of HA, crystals, formed in type-I collagen gel. From this study they have concluded that a high concentration of chondroition sulphate inhibits the formation of HA *in vitro*; while, recently, Jiang and Liu [91] have studied the effect of chondroition sulphate on the nucleation of HA. Titanocene dihalides and gold (I) compexes, such as Auranofin, are clinically well approved therapeutic drugs against arthritis [92, 93]. Koutsopoulos et al. [94-97] have studied the inhibition of HA crystals by different therapeutic drugs, namely, zirconocenes, hafnocene dichlorides, vanadocene dichlorides and ferricenium salt, and reported that the vanadocene dichlorides inhibited maximum 54 to 94 %, followed by hafnocene dichlorides (46 to 86 %), zirconocenes (42 to 95%) and ferricenium salt (12 to 60%). This inhibitory effect may be explained by the absorption and subsequent blocking of the active growth sites. Koutsopoulos et al [18, 19, 98, 99] have also studied the effect of various amino acids with hydrophobic side groups (alanine, phenlyanine, proline and methionine), polar side groups (serine, tyrosine and 4-hydroxyproline), and non-polar sides groups (glycine, cystine and glutamine) on the growth of HA crystals. Recently, Pampena et al. [100] have reported the inhibition of HA formation by osteopontin phosphopeptides (OPN). The OPN is an acidic glycoprotein involved in a variety of pathological and physiological processes; such as cell migration, adhesion and signaling [101].Normally, OPN is not

expressed in blood vessels but found in atherosclerotic plaques [102, 103], which has proposed that OPN is expressed by soft tissue to protect against dystrophic calcification [104]. However, there is no major work reported on the inhibition study of HA crystal through the herbal extracts.

In the present investigation, single diffusion gel growth technique was used to study the growth and inhibition of HA crystal. The gel frame-work acts like a three dimensional crucible in which the crystal nuclei are delicately held in the position of their formation and nutrients are supplied for the growth. This technique can be utilized as a simplified screening model to study the growth and inhibition of bio-material crystals *in vitro*. The growth of HA crystals is mentioned in the section 5.3. Hydroxyapatite crystals are obtained in the form of Liesegang rings, which are due to the periodic precipitation and diffusion in gel. The inhibition study was carried out by considering certain parameters, for instance, the diffusion length in gel, the numbers of rings obtained, and the distance between the two rings. The following herbal extracts were used in the present growth inhibition study of HA. The 1 % extract solutions were prepared by adding 10 mg concentrated extracts into 10 ml of water. The more details regarding the extract preparations are given in the Chapter-IV.

(1)   *Boswellia serrata gum* resin

(2)   *Tribulus terrestris* fruit

(3)   *Rotula aquatica* root

(4)   *Boerhaavia diffusa* root

(5)   *Commiphora wightii*

Figure (5.11) is the photograph showing the comparative growth of HA crystals, in the form of Liesegang rings, for different herbal extract solutions. From the experiment it was observed that the pure $CaCl_2$ gave thick, sharp rings with deep

diffusion in the gel in comparison to others.

Pure CaCl$_2$ B. serreta   T. terrestris,   R. aquatica   B. diffusia   C. wightti
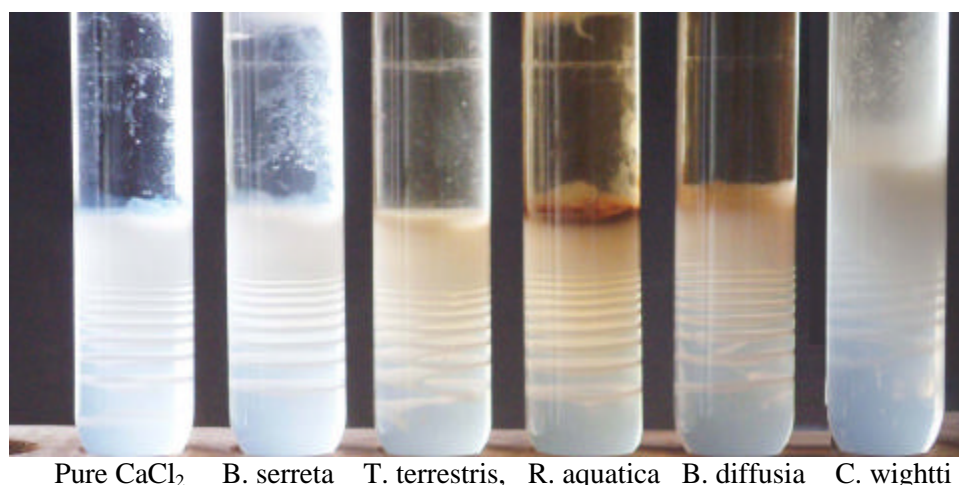
Figure (5.11): Comparison of growth of HA crystals in the form of Liesegang

rings in different herbal extract solution.

In the case of *B. serrata*, thick, sharp rings, comparatively less in number and less in diffusion length in the gel were noticed. While, *T. terrestris* gave spiral rings, which were interconnected with each other, and the diffusion length in the gel was the same as those of pure CaCl$_2$. For *R. aquatica,* the rings were sharp and very thin but the number of rings was more and the diffusion length was comparatively less. However, for *B. diffusa*, the number of rings was the same but the last few rings were not completely formed and the diffusion length was also the same. The same types of results were observed in the case of *C. wightti*. The following Table (5.5) gives the number of rings as well as the diffusion length in gel.

Table (5.5)

Comparative growth inhibition study of HA in the presence of different herbal extracts

No.	Herbal Extracts	Number of Liesegang Ring	Diffusion length (in cm)
1	Pure CaCl$_2$	16	3.8
2.	*T. terrestris*	Spiral ring	3.75
2	*B. serrata*	12	2.8
3	*R. aquatica*	10	2.75
4	*B. diffusa*	12**	2.75
5	*C.wightti*	12**	2.75

** Last few rings are not completely formed

In the present study, the diffusion length is defined as the distance of last Liesegang ring from the gel-liquid interface. When the diffusion length is small, it indicates less diffusion of the supernatant solution in to the gel and insufficient amount reactants to form crystals in the form of further ring. If the number of rings is less, it also indicates less periodic precipitation and the less amount of growth.

The average thickness of Liesegang rings was 0.09 to 0.1 cm in pure $CaCl_2$ solution and extracts; except for *R. aquatica*, it was of the order of 0.079cm. It is concluded that the precipitation of HA crystals is less in the case of *R. aquatica*. The diffusion length and the thickness of Liesegang rings were measured by using traveling microscope of least count 0.001 cm.

Figures (5.12 a, & b) exhibit the histograms of the number of Liesegang rings and the diffusion length, respectively, in the presences of various herbal extracts and pure $CaCl_2$ solution.
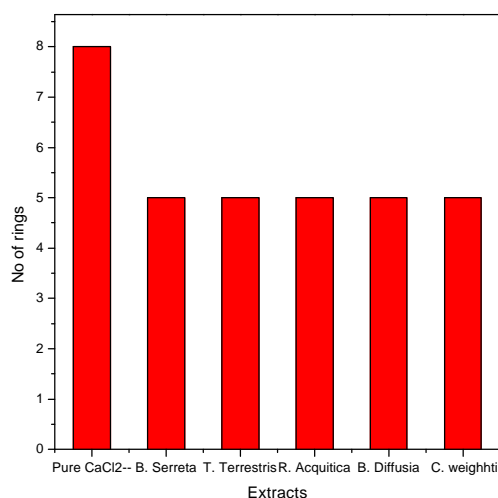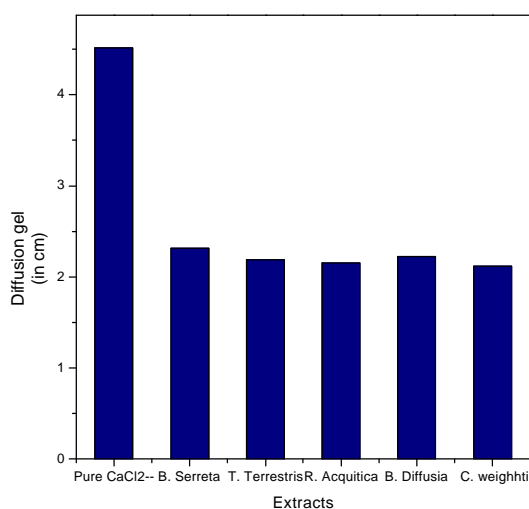
| Figure (5.12a) | Figure (5.12b) |

Figure (5.12 a and b): Histograms of numberof rings diffusin distance in gel for different extracts

Figures (5.12 a &b) clearly indicates the reduction in the number of Liesegang rings in the present of different herbal extracts as well the reduction in the diffusion length in the presence of herbal extracts. Figure (5.13) shows a set of plots

drawn for the spacing between consecutive two rings versus the number of rings. From these plots it can be clearly seen that *R. aquatica* gives maximum spacing between the initial two rings and then it increases exponentially, which indicates that it delayed the periodic precipitations in the gel. On the other hand, all other extracts do not exhibit significant change in the ring spacing which indicates that they do not bring significant change in the rate of periodic precipitations. However, the extracts of *B. diffusa* did not bring large change in the periodic precipitation but brought better changes in the diffusion length. Similar results were observed for *B. serrata.* One can easily notice this from the table (5.5)
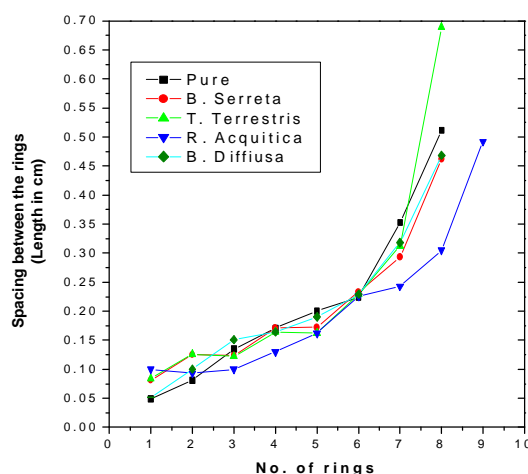
Figure (5.13): The plots of spacing betweens two consecutive rings versus   the number of rings

Table (5.6)

Single factor ANOVA analysis results for growth inhibition study of HA crystals in the presence of different extracts

ANOVA						
Source of Variation	*SS*	*df*	*MS*	*F*	*P-value*	*F crit*
Between Groups	173.1330088	5	34.626602	27.264159	5.86584E-13	2.4085125
Within Groups	60.961972	48	1.2700411			
Total	234.0949808	53				

Table (5.6) shows the results of ANOVA single factor statistical analysis, which shows that the behaviors are highly significant (p< 0.0001). Aqueous extracts of *R. aquatica* and *B. diffusa* are giving good results in terms of less periodic precipitation rate and less diffusion length, respectively.

Also, the ethanolic as well as the hydroethanolic extracts of the same plants were used, to study the inhibition effect on HA crystals. When ethanolic extracts were used the number of rings was reduced. All extracts had the same number of five rings and the first band thickness was 2.223 cm. Diffusion length in the gel was 4 cm for *B. serrata, R. aquatica* and *C. wightt;,* whereas, in the case of *B. diffusa* and *T. terrestris* it was 3.5 cm. For hydroethanolic extracts, the thick bands were obtained for all extracts and it was not possible to measure the spacing and other parameters. The width of band was in average 4.3 cm for all extracts.

Particle size measurement study has also been carried out for all the three types of extracts, i.e., aqueous, ethanolic and hydroethanolic extracts. It was observed that the minimum particle size was found in the case of aqueous extracts, which was followed by ethanolic and hydroethanolic extracts. The following table (5.7) gives results of the particle size measurements.

Table (5.7)

Particle size measurement of HA crystals in the presences of aqueous, ethanolic and hydroethanolic extracts

Sample code	d (0.1) micron	d (0.5) micron	D (0.9) micron
BCP (Aqueous)	47.25	82.68	107.54
BCP (ethanolic)	43.64	77.01	132.08
BCP (Hydroethanolic)	46.18	79.47	135.46

From the above results one can find that the aqueous extracts gave good inhibition in comparison to ethanolic and hydroethanolic extracts. Figure (5.14) shows the comparative inhibition study in the case of already grown crystals.
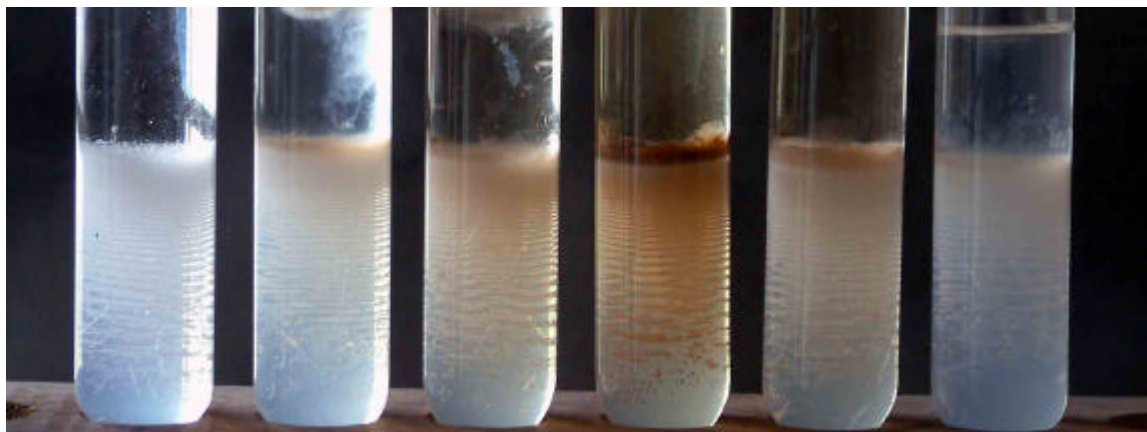
Pure CaCl$_2$ B. serreta   T. terrestris   R. aquatica   B. diffusia   C. wightii

Figure (5.14): Comparative inhibition study in the case of already grown crystals

From Figure (5.14) one can easily notice that the extracts did not show any significant inhibition on the already grown HA crystals. Here, it is to be noted that the extract solutions were poured after achieving the complete formation of Liesegang rings i.e., HA crystals, and the growth inhibition was studied in terms of changes produced in Liesegang rings.

5.6   Calculation of Diffusion Coefficient for Calcium Ions for HA Crystals Growth:

The spontaneous equalization of concentration of molecules, ions or colloidal particles in a system as results of their chaotic motion is called diffusion. Several authors [105, 106] have reviewed the role of diffusion in crystal growth. Among the diffusion controlled reaction systems, one of the most interesting cases occurs when an electrolyte (outer electrolyte) diffuses and reacts with another electrolyte (inner electrolyte) that contained in a gel. The chemical reactions between the two diffusing electrolytes lead to an insoluble product that precipitates rhythmically in bands or

rings perpendicular to the direction of diffusion, this mechanism is called *Liesegang phenomenon* [107]. Liesegang phenomenon is widely studied because it offers a model to explain a great variety of formations in nature, ranging from agate rocks and gold veins to the growth of bacterial rings in agar and gallstones [108].

Using the theory of one dimensional Liesegang phenomenon, Shinohara [109] has estimated the diffusion coefficient of the diffusing ions. Dharmaprakash and Mohan Rao [110] reported the diffusion coefficient of barium ions from Liesegang ring formation of barium oxalate.

Liesegang pattern on macroscopic scale is visible to the naked eye. The role of the gel matrix is to prevent sedimentation of the precipitate or convection of solutions. In general, these Liesegang structures appear to follow three laws, (1) the time law, (2) the space law and (3) the width law.

The position X_n (measured from the gel surface) of the nth band is related to the time t_n of its formation [111] by,

$$X^2_n \sim t_n \qquad \text{------------ (5.22)}$$

This relation is often called the time law.

The second law governs the Liesegang phenomenon is the spacing law given by Jablczynski [112] as,

$$X_{n+1} / X_n = (1 + p) \qquad \text{--------- (5.23)}$$

The quantity *(1 + p)* is referred to as the spacing coefficient.

The third law is the 'width law'; generally, it is observed that the width W_n of the band increases with their position according to the relation [113, 114],

$$W_n \sim X^j_n \qquad \text{--------- (5.24)}$$

where, the width exponent ö depends on C_{A0} and C_{B0}, the initial concentrations of the outer and inner electrolyte *A* and *B,* respectively.

Recently, George and Varghese [108, 113 and 114] have proposed the new scenario; they treated the formation of the periodic ring system as a moving boundary problem. They assumed that the boundary, which separates *A* and *B* ions was the gel solution interfaces. When the first precipitation zone (ring) is formed; *A*-type ions occupy up to this region and its concentration reaches the reservoir concentration C_{A0}. This implies that the boundary of *A*-type ions has been shifted to the region of the precipitation front. This assumption holds good as the reservoir concentration C_{A0} of the *A*-type ions is sufficiently large compared with the initial concentration C_{B0} of the *B*-type ions. This will repeat in time and the boundary region moves from one ring to the other. For a one dimensional system the concentration levels of *A* species at the boundary are:

$$C_A(x,\ t) = C_{A0}\,; \quad at\ t \le t_n\ and\ x_0 \le x\,, \le x_n \qquad \text{---------- (5.25)}$$

Where, *n* denotes the number of the ring. The initial value x_0 corresponds to the position of the gel solution interface and $x_1,\ x_2$, etc, are the positions of the first, second, etc., rings, respectively.

When a new ring is established at $x_n(t)$, the concentration profile of *A*-type ions in the gel medium is assumed to be ,

$$C_A(x,t) = \exp\left\{-\boldsymbol{b}\,\frac{x - x_n(t)}{\boldsymbol{x}_{n+1}}\right\}; \qquad x_n \le x \le x_{n+1} \qquad \text{---------- (5.26)}$$

Where $\hat{a}$ is regarded as a constant for a system, called the *concentration profile index,* which can easily be calculated and $\boldsymbol{x}_{n+1}$ is the separation between the nth and $(n+1)^{th}$ rings.

For an infinitesimal boundary layer advancing into the positive *x*-direction, the equilibrium condition for the amount of diffusants exchanged per unit area per unit time is;

$$vC_A(x^+,t) + D_A \frac{\partial}{\partial x} C_A(x^+,t) = D_A \frac{\partial}{\partial x} C_A left(x^-,t)$$ --------- (5.27)

Where, D_A is the diffusion coefficient of the diffusant A.

From the above equations (5.25) and (5.26), George and Varghese [108, 113 and 114] have derived the simple equation for the diffusion coefficient, which is shown as follows,

$$D_A = \frac{x_n^2}{2t_n}$$ --------- (5.28)

In the present investigation, sodium meta-silicate gel of 1.06 specific gravity and 1 M concentration of outer electrolyte, i.e., calcium chloride, were selected. The formation time of different Liesegang rings and their positions were precisely noted down for pure $CaCl_2$ and $CaCl_2$ plus herbal extract solutions. Traveling microscope of 0.01 cm least count was used. The diffusion coefficient was calculated by using relation (5.28) and the values are summarized in Table (5.8)

Table (5.8)

Values of diffusion coefficient in the presence of various extracts

Extracts	Diffusion coefficient (m^2s^{-1})
Pure $CaCl_2$	1.61×10^{-14}
B. serrata	2.91×10^{-14}
R. aquatica	4.66×10^{-15}
B. diffusa	4.72×10^{-14}

From the table one can conclude that in the case of pure $CaCl_2$ the value of diffusion coefficient is maximum and it decreases for different herbal extracts in decreasing order from *B. serrata, B. diffusa* to *R. aquatica*. It is easy to conclude that the herbal

extracts reduced the value of diffusion coefficient and hence show inhibition of formation of crystalline product of HA.

5.7   Conclusion:

(1)   The growth of Hydroxyapatite (HA) crystals was carried out by using the single diffusion gel growth technique in normal test tubes. HA crystals were grown in the form of Liesegang rings. The crystals were very small and the size of the crystals was in micron level. 90% of the crystals were less than 107.54 microns.

(2)   The FT-IR spectrum confirms the presence of the O-P-O bending, P-O symmetric and asymmetric stretching, O-H bending and stretching and oxygen-calcium bonds. It also confirms that the HA crystals were   completely free from C=O inclusion.

(3)   The powder XRD analysis results suggested that the values of cell parameters were matching closely with the values reported by Elliot et al [50]. The cell parameters of HA crystals were estimated as follows.

a =9.432   b=18.843   C =6.923

á = â =90.010, ã = 119.050

Hexagonal crystal structure is widely reported but, in the present study, the monoclinic crystal structure of the gel grown HA was found. Perhaps it is because of the HA crystal growth was carried   out at comparatively low temperatures. The monoclinic unit cell of HA crystals is achieved from the hexagonal one by doubling the *b* lattice parameter with an alternating arrangement of the anion chain. It is also reported in the literature that the phase transition occurs in the monoclinic system around 370 ^{0}C and it converts in to the hexagonal system.

(4)   For the HA crystals, the values of dielectric constant decrease with frequency. Initially, the dielectric constant decreases rapidly with increasing frequency and then decreases very slowly. In general, the variation of dielectric constant with frequency suggests the presence of higher space charge polarizability of the material in the low frequency region. This nature may be explained on the basis of the mechanism of polarization similar to that of conduction process. The electronic exchange of the number of ions in the crystal gives local displacement of electrons in the direction of applied field, which gives the polarization. As the frequency increases, a point is reached where the space charge cannot sustain and comply with the external field. Therefore, the polarization decreases and exhibits the reduction in the values of dielectric constant as the frequency increases.

(5)   The effect of five different herbal extracts on the growth of HA crystals were studied. The HA crystals were formed in the form of Liesegang rings, therefore, the inhibition study was carried out by measuring the diffusion length in gel, the number of rings and the spacing between the rings. Aqueous extracts of *R. aquatica* and *B. diffusa* were giving good results in terms of less periodic precipitation and less diffusion length, respectively. But *B. serrata* and *C.wightti* did not show significant inhibition. While, in the case of *T. terrestris* the diffusion length was maximum among all extracts and it gave the interconnected spiral rings.

(6)   Ethanolic and hydroethanolic extracts did not give good inhibition in comparison to the aqueous extracts. The particle size was found to be the maximum in the case of hydroethanolic extracts followed by ethanolic and aqueous ones. The herbal extracts did not show any significant inhibition or

the dissolution of the already grown HA crystals.

(7)   The value of diffusion coefficient was maximum for pure $CaCl_2$ solution and for herbal extract solutions it was found to be comparatively less. It was also found to be the minimum for *R. aquatica* extracts, which is in accordance with the conclusion (5). The lower values of diffusion coefficient for herbal extracts suggest lower diffusion of ionic species for the formation of crystalline products of HA. This suggests inhibition in terms of lower diffusion constant values for herbal extracts.

References:

[1] J. C. Merry, I. R. Gibson, S. M. Best and W. Bonfield; *J. Mater. Sci: Mater. Med,* **9** (1998) 779.

[2] L. C. Clapham, R. J. C. McLeam, J. C. Nickel and J. Downey; *J. Cryst. Growth*, **104** (1990) 475.

[3] M. Ashok, N. Meenakshi Sundaram and S. Narayana Kalkura; *Materials Letters,* **57** (2003) 2066.

[4] R. Z. LeGeros, '*Calcium Phosphates in Oral Biology and Medicine',* Karger: Basel, Switzerland, 1991.

[5] http://www.azom.com/details.asp?ArticleID=107#_Key_Properties

[6] T. J. White and Dong Zhili; *Acta Cryst.,* **B59** (2003) 1.

[7] http://www.medicinenet.com/hydroxyapatite/article.htm

[8] A. L. Boskey and P.G. Bullogh; *Scann. Electron Micros.,* **28** (1984) 511.

[9] G. V. Gordon, T. Villanueva, H. R. Shumacher and V. J. Gohel, R*heumatology,* **11** (1984) 861.

[10] F. J. Schöen and R. J. Levy; *Cardiol. Clin,* **2** (1984) 713.

[11] M. Valente, U. Bortloti, and G. Thiene, *Am. J. Pathol.,* **119** (1985) 12.

[12] S. Koutsopoulos, A. Kontogeorgou, J. Petroheilos and E. Dalas; *J. Mater. Med.,* **9** (1998) 421.

[13] G. H. Nancollas; *J. Cryst. Growth,* **42** (1984) 185.

[14] A. C. Tas, F. Korkusuz, M. Timucin and N. Akkas; *J. Mater. Sci: Mater. Med,* 8 (1997) 91.

[15] N. Kivrak and A. C. Tas; *J. of Am. Ceram. Soc.,* **81** (1998) 2245.

[16] A. I. Villacampa and J. M. Garcia-Ruiz; *J. Cryst. Growth,* 211 (2000) 111.

[17]   S. Koutsopoulos and E. Dalas; *Langmuir,* **17(4)** (2001) 1074.

[18]   S. Koutsopoulos and E. Dalas; *J. Coll. Interf. Sci.*, **231** (2000) 207.

[19]   K. Prabakaran, A. Balamurgan and S. Rajeswari; *Bull. Mater. Sci.,* **28** (2005) 115.

[20]   J. Vandiver, D. Dean, N. Patel, W. Bonfield and C. Ortiz; *Biomaterials,* **26(3)** (2005) 271.

[21]   M. Bohner; *Calcium Orthophosphate in Medicine: From Ceramics to Calcium Phosphate Cements,* **31(4)** (2000) 37.

[22]   C. Rey, C. Combes, C. Drouet, H. Sfihi, and A. Barroug; *3rd International Conference on Materials for Advanced Technologies (ICMAT-2005),* Singapore, (A-3-KN-3), 3-8 July (2005), 4.

[23]   P. H. J. Mericier, Yuon Le Page, P. S. Whitfield, L. D. Mitchell, I. J. Davidson and T. Y. White; *3rd International Conference on Materials for Advanced Technologies (ICMAT-2005),* Singapore, (Q-6-OR22), 3-8 July (2005), 170.

[24]   http://www.webmineral.com/data/Hydroxylapatite.shtml.

[25]   K. Yanagisawa, H. Toya, Qi Feng and N. Yamasaki; *Phosphorus Res. Bulletin,* **5** (1995) 43.

[26]   J. Li, Y. Zhang, L. Zhou, N. Xue and Di Li; *'Advance Nanomaterials and Nanodevices', IUMRS-ICEM,* Xian, China, (2002).

[27]   K. Kamiya, T. Yobo, K. Tanaka and Y. Fujiyama; *J. Mater. Sci.,* **24** (1989) 827.

[28]   J. Arendes, J. Chirstoffersen, M. R. Chirstoffersen, H. Eckert, B. D. Flower, J. C. Heughebaert, G. H. Nancollas, J. P. Yensinowski, and S. J. Zawacki; *J. Cryst. Growth,* **84** (1987) 515.

[29]   P. W. Brown, N. Hocker and S. Hoyle; *J. Am. Ceram. Soc.,* **74** (1991) 1848.

[30]   G. Socrates; '*Infrared Characteristics Group Frequencies'*, John Wiley, Chichester, (1980).

[31]   R. R. Griffiths; '*Chemical Infrared Fourier Transform Spectroscopy'*, Academic Press, New York, (1972).

[32]   K. Nakamoto; '*Infrared and Raman Spectra of Inorganic and Coordination Compounds'*, John Wiley 5th Ed. (1997).

[33]   V. S. Joshi; *Ph. D. Thesis*, Saurashtra University, Rajkot (2001).

[34]   A. Cuneyt Tas; *Biomaterials,* **21** (2000) 1429.

[35]   S. Koutsopoulos and E. Dalas; *J. Cryst. Growth,* **22** (2001) 279.

[36]   E. Kontonasaki T. Zorba, L. Papadopoulou, E. Pavlidou, X. Chatzistavrou, K. Paraskevopoulos, and P. Koidis; *Cryst. Res. Technol.,* **37** (2002) 1165.

[37]   N. B. Colthup, L. H. Daly and S. E. Wiberly; '*Introduction to Infrared and Raman Spectroscopy'*, 2nd Ed., Academic, New York, (1975).

[38]   http://www.mrl.ucsb.edu/mrl/centralfacilities/xray/xray-basics/#x2

[39]   http://www.mf.mpg.de/de/abteilungen/mittemeijer/english/commentary/ Powder% 20Diffraction%20in%20Mat.Sci.pdf

[40]   S. Naray-Szabo; *Z. Kristallogr. Kristallgeom. Kristalphys. Kristallchem,* **75** (1930) 387.

[41]   R. W. G. Wyckoff; *Crystal Structures*; **Vol.3** John Wiley and Sons. (1965) pp-228.

[42]   D. McConnell; '*Apatites, Its Crystal Chemistry, Mineralogy, Utilization   and Geologic and Biologic Occurrences'*. Springer-Verlag, Wein (1973).

[43] J. C. Elliot; '*Structure and Chemistry of the Apatites and Other Calcium Orthophosphates',* Elsevier, Amsterdam, (1994).

[44] O. Niragu and P. B. Moore, Editors; '*Phosphate Minerals',*Springer-Verlag, Berlin, (1984).

[45] P. W. Brown and B. Constabtz, Editors; '*Hydroxyaptite and Related Materials',* CRC Press, Boca Raton, (1994).

[46] http://www.cea.fr/fr/Publications/clefs46/clefs46_52.html

[47] K. Sudarsanan and R. A. Young; *Acta Cryst.* **B28** (1972) 3668.

[48] www.chemistry.upatras.gr/ studs/sotk/hap.htm

[49] J. Y. Kim, R.R. Fenton, B. A. Hunter and B. J. Kennedy; *Aust. J. Chem.,* **50** (2000) 679.

[50] J. C. Elliot, E. Dykes and P. E. Mackie; *Acta Cryst.* **B37** (1981) 435.

[51] J. M. Hughes, M. Cameron and K. D. Crowley; *Am. Mineral.,* **74,** (1989) 870.

[52] J. C. Elliot, P. E. Mackie, and R. A. Young; *Science,* **180** (1973) 1055.

[53] L. Calderín and M. J. Sctott, and A. Rubio; *Phys. Rev. B*, **67** (2003) 134106.

[54] H. Morgan, R. M. Wilson, J. C. Elliot, S. E. P. Dowker, and P. Anderson; *Biomaterials,* **21** (2000) 617.

[55] T. Ikoma, A. Yamazaki, S. Nakamura, and M. Akao; *J. Solid State Chem.*, **144** (1999) 272.

[56] W. Kohn and L. J. Sham; *Phys. Rev.* **140** (1965) A1133.

[57] H. B. Van Rees, M. Mengeot, and E. Koistiner; *Mat. Res. Bull.,* **8** (1973), 1307.

[58] cas.umkc.edu/physics/ ching/project3.htm

[59] H. Frohlich, '*Theory of Dielectrics'*, Clarendon Press, Oxford, (1949).

[60]   B. Tareev; '*Physics of Dielectric Materials'*, Mir Publishers, Moscow, (1975).

[61]   A. Bonincontro, S. Cinelli, Y G. Onori and A. Stravato; *Biophys. J.,* **86** (2004) 1118.

[62]   P. S. Ram Shastry, G. S. Kumar, T. Bhimasankaran and G. Prasad; *Bull. Mater. Sci.*, **22** (1999) 59.

[63]   J. Koshy, J. Kurian, R. Jose, A. M. John, P. K. Sajita, J. James, S.P. Pai and R. Pinto; *Bull. Mater. Sci*., **22** (1999) 243.

[64]   H. Sharma, Kiran Kumari and S. N. Giri; *Bull. Mater. Sci*., **22** (1999) 757.

[65]   R. N. P. Choudhary, S. R. Shannigrahi and A. K. Singh; *Bull. Mater. Sci*., **22** (1999) 975.

[66]   N. K. Singh and R. N. P. Choudhary; *Bull. Mater. Sci*., **23** (2000) 239.

[67]   L. Sirdeshmukh, K. Krishna Kumar, S. Bal Laxman, A. Ram Krishna and G. Sathain; *Bull. Mater. Sci*., **21** (1998) 219.

[68]   A. V. Ravi Kumar, B. Appa Rao and N. Veeraiah; *Bull. Mater. Sci*., **21** (1998) 341.

[69]   M. Krishna Murthy, K. S. N. Murthy and N. Veeraiah; *Bull. Mater. Sci*., **23** (2000) 285.

[70]   D. K. Durga and N. Veeraiah; *Bull. Mater. Sci*., **24** (2001) 421.

[71]   P. K. Khare and S. K. Jain; *Bull. Mater. Sci*., **23** (2000) 17.

[72]   A. K. Narula, Ramadhar Singh and Subhas Chandra; *Bull. Mater. Sci*., **23** (2000) 227.

[73]   R. P. Mahajan, K. K. Patankar, M. B. Kothale and S. A. Patil; *Bull. Mater. Sci*., **23** (2000) 273.

[74]   K. S. Rane, V. M. S. Verenkar and P. Y. Sawant; *Bull. Mater. Sci.*, **24** (2001) 323.

[75]   D. Ravinder and K. Vijay Kumar; *Bull. Mater. Sci.*, **24** (2001) 505.

[76]   M. R. Anantharaman, K. A. Malini, S. Sindhu, E. M. Mohammed, S. K. Date, S. D. Kulkarni, P. A. Joy and Philip Kurian; *Bull. Mater. Sci.*, **24** (2001) 623.

[77]   S. C. Raghavendra, R. L. Raibagkar and A. B. Kulkarni; *Bull. Mater. Sci.*, **25** (2002) 37.

[78]   E. Fukada and I. Yasuda; *J. Phys. Soc. Jap.,* **12** (1957) 1158.

[79]   J. Green; *Miner. Electrolyte Metab.,* **20,** (1994) 7.

[80]   C. Rey; *Biomaterials,* **1 I** (1990) 13.

[81]   F. J. G. Sanchez and G. De Mercato; *Med. Prog. Techno.*, **21** (1996) 165.

[82]   A. Bonincontro, S. Cinelli, G. Onori, and A. Stravato; *Biophys. J.*, **86** (2004) 1118.

[83]   J. J. Prieto Valdes, A. Victorero Rodriguez, and J. Guevara Carrio; *J. Mater. Res.,* **10-9** (1995) 2174.

[84]   N. Hitmi, C. Lacabanne and R.A. Young; *J. Phys. Chem Solids,* **45** (1984) 701.

[85]   T. Lopez, J Stockel, J Peraza, M E Torres and A C Yanes, *Cryst. Res. Technol.*; **30** (1995) 677.

[86]   R. M. Dabhi, B. B. Parekh and M.J. Joshi; *Indian J. Phys.,* **79(5)** (2005) 503.

[87]   S. K Arora, V. Patel, B. Amin and A. Kothari; *Bull. Mater. Sci.,* **27** (2004) 141.

[88]   R. J. R. McKendry, H. K. Unthoff and K. Sarkar; *J. Rheumatol,* **9** (1982) 75.

[89]   H. K. Unthoff, K. Sarkar and J. A. Maynard; *Clin. Orthop. Rel.Res.,***118** (1976) 164.

[90]   G. K. Hunter, B. L. Allen, M. D. Grynpas and P. T. Chen, *Biochem. J.,***228** (1985) 463.

[91]   H. Jiang and X.Y. Lia, *3rd International Conference on Materials for Advanced Technologies (ICMAT-2005),* Singapore (S-6-PO27), 3-8 July (2005) 186.

[92]   T. M. Simon, D. H. Kunishima, G. J. Vibret, and A. Lobert; *Cancer Res.,* **41** (1981) 94.

[93]   D. P. Fairlie, M.W. Whitehouse and J. A. Broomhead; *Chem. Biol. Interact,* **61** (1987) 277.

[94]   S. Koutsopoulos, J. Demakopoulos, X. Argiriou, E. Dalas, N. Klouras and N. Spanos; *Langmuir,* **11** (1995) 1831.

[95]   S. Koutsopoulos, E. Dalas, N. Tzavellas and N. Klouras; *J. Chem. Soc., Faraday Trans.,* 93(23) (1997) 4183.

[96]   S. Koutsopoulos, E. Dalas, N. Tzavellas N. Klouras and P. Amoratis; *J. Cryst. Growth,* **183** (1998) 251.

[97]   S. Koutsopoulos, E. Pierri, E. Dalas, N. Tzavellas and N. Klouras; *J. Cryst. Growth,* **218** (2000) 353.

[98]   S. Koutsopoulos and E. dalas; *Langmuir,* **16** (2000) 6739.

[99]   S. Koutsopoulos and E. Dalas; *J. Cryst. Growth,* **216** (2000) 443.

[100] D. A. Pampena, K. A. Robertson, O. Litvinova, G. Lajoie and H. A. Goldberg; *Biochem J.,* **378** (2004) 1083.

[101] M. Chellaiah and K. Hruska; *Mol. Biol. Cell,* **7** (1996) 743.

[102] L. A. Fitzpatrick, A. Severson, W. D. Edwards and R. T. Lngram; *J. Clin Invest.* **94** (1994) 1597.

[103] C. M. Giachelli, N. Bae, M. Almeida, D. T. Danhardt, C. E. Alpers and S. M. Schwartz; *J. Clin. Invest,* **92** (1993) 1686.

[104] T. Wada, M. D. McKee, S. Steitz and C. M. Giachelli; *Circ. Res.,* **84** (1999) 166.

[105] F. A. Kroger; '*Chemistry of Imperfect Crystals'*, Inter Science, New York, (1964) 31.

[106] J. B. Schrofder and R.C. Finares; *'Progress in Ceramic Science',* Pergamon, London, (1966) 195.

[107] R. E. Liesegang; *Naturwiss Wochschr,* **11** (1986) 353.

[108] J. George and G. Varghese; *Colloid Polym. Sci.* **280** (2002) 1131.

[109] S. Shinohara; *J. Phys. Soc. Jpn.* **29** (1978) 1073.

[110] S. M. Dharmaprakash and P. Mohan Rao; *J. Mater. Sci. Lett., 8* (1989) 141.

[111] H. W. Morce and G. W. Pierce; *J. Phys. Chem.* **45** (1903) 589.

[112] K. Jablczynski; *Bull. Chem. Soc., France*, **33** (1923) 1592.

[113] J. George and G. Varghese; *Chem. Phys. Letters,* **362** (2002) 8.

[114] J. George, S. Nair and G. Varghese; *J. Mater. Sci.* **39** (2004) 311.

Chapter VI

Growth and Characterization of

Monosodium Urate Monohydrate Crystals

6.1   Introduction:

Gout is the term given to a group of metabolic conditions, in which the signs and symptoms results from the deposition of crystals of monosodium urate monohydrate (MSUM) in various connective tissues and joints [1, 2]. The deposition of these crystals, result from the raised levels of uric acid in blood (hyperuricemia) and various body fluids. Hyperuricemia is not essential requirement of diagnosis of gout, but the risk of gout and its presence increases with the degree and duration of hyperuricemia. The risk factor of gout is also associated with the uric acid and urate compound nephropathy [3]. Nephropathy of uric acid and urate substances is associated with the formation of monosodium urate (MSU), ammonium urate and uric acid in urinary tract system. The MSU is rarely observed in renal calculi in spite of human urine often being supersaturated with monosodium urate [4-7]. Only exceptionally pure monosodium urate calculi have been described and these were of vesical origin [8]. Monosodium urate could also act as an effective promoter of calcium oxalate crystallization through heterogeneous nucleation processes, according to *in vitro* experiments [9-12].

A very few attempts have been made to grow the uric acid or urate crystals. Irusan et al. [13] have reported the growth of ammonium urate crystals using the gel growth technique, whereas Kalkura et al. [14] have reported the growth of uric acid

crystals in the tetramethoxy silane and silica gel media. Ramachandran and Natarajan [15] have grown pure uric acid crystals using the silica hydro-gel. Some researchers have also studied the effect of uric acid and urate substances on the growth of urinary type calcium phosphate and calcium oxalate crystal formations [16, 17]. Grases et al. [18] have studied the structure of urate renal calculi after precipitation of ammonium and sodium urate from the synthetic urine; on the other hand, Grover et al. [19] have studied the *in vitro* growth of calcium oxalate crystals in the presence of pre-incubated seed crystals of uric acid and MSU with undiluted human urine.

From this description of accumulated knowledge about the role of monosodium urate monohydrate (MSUM) crystals in gout or gouty arthritis as well as urolithiasis, it is evident that till today there is no sufficient information available to clarify all aspects related to crystallization behavior under physiological conditions and its different characteristics. It is, therefore, important to grow and characterize MSUM crystals and study the inhibitive effect of various herbal extracts on its growth. The growth and inhibition study provides very useful information regarding the potent herbal extracts or herbal formulations, which can inhibit the growth of crystals *in vitro* and may be useful in prevention or cure of this crystal induce ailments.

6.2   Physical and Chemical Properties of MSUM:

Monosodium urate (MSU, $NaHC_5H_2N_4O_3$) is a white powder and soluble in water to the extent up to 120 mg per dl [20]; for the sake of comparison a much more limited solubility of uric acid in water is reported [21], which is only 6.5 mg per dl. The solubility product of MSU is 4.9×10^{-5}. Based on this value, aqueous solutions having the sodium content of 0.13M, nearly equivalent to that in serum, were saturated with urate at 6.4 mg per dl at 37 ^{0}C by Peters and Van Siyke [21]. Allen et

al. [22] and Loeb [23] have found that urate solubility in solutions of 140 mEq per liter sodium content is temperature dependent, with a two fold drop in solubility between 37 and 25 ^{0}C. Moreover, Wilcox et al. [7] have carefully reinvestigated the solubility of uric acid and monosodium urate and have found that both are dependent on pH. Uric acid is more soluble with increasing pH, whereas the MSU is less soluble. The solubility of MSU is dependent on sodium concentration and ionic strength as well. No stoichio-metric relationship between urate and sodium (or potassium) exists. Binding of mono-velant cations is a complex function of crystal shape, ion concentration, time, pH, and ion competition [24]. The solubility of urate in plasma is somewhat greater than the saturation value in aqueous solutions of 0.13 M sodium. Actual determination of solubility of monosodium urate in human plasma (or serum) indicates that the saturation occurs at concentrations about 7 mg per dl. [25-26].

Monosodium urate mainly forms due to the reaction between the Na^{+} ion and the urate ion of uric acid. The MSU crystals are highly negative birefringent, if those are observed through a polarized light microscope under a red filter they appear yellow in the plane of their long axis [27]. This is displayed in figure (6.1).
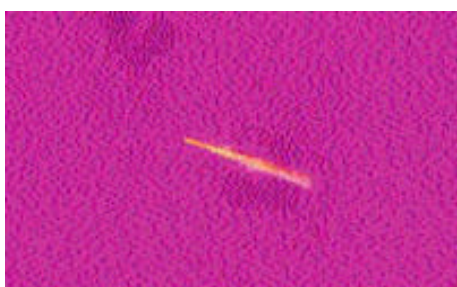
Figure (6.1): View of MSUM crystal in red filter using polarized light

In the present chapter, the growth of MSUM crystals is described by both the gel growth and the wet chemical precipitation techniques. The crystals have been characterized by different techniques and the growth inhibition study has been conducted by using different herbal extracts to identify the potent inhibitors.

6.3   Growth of MSUM Crystals:

The MSUM crystals were grown by employing two different techniques, which are as follows:

(1)   Single diffusion gel growth technique.

(2)   Wet chemical process

Single Diffusion Gel Growth Technique:

(a)   Gel preparation:

As already mentioned in the section 5.3 of Chapter-V, the stock solution of sodium meta-silicate was prepared. By adding double distilled water of appropriate volume into the stock solution, the solution of the desired specific gravity was prepared. In the present study, the specific gravity of sodium meta-silicate solution was selected as 1.05 and equal volume of 0.2 M, NaOH solution was added to prepare a mixture. This mixture was acidified by 2 N, acetic acid in such a manner that the appropriate pH was obtained. This mixture was used to set the gel. In the present study, the pH values were selected within 4.5 to 5.0.

(b)   MSUM crystal growth:

Glass test-tubes of 25mm diameter and 150mm length were used as crystal growth apparatus. The above mentioned mixture was poured in equal volumes in different test tubes and allowed to set into the gel form. Within 48 hours, good quality gels were set. After setting the gel, the 0.07 M uric acid solution was poured gently on that. Good quality needle shaped crystals were grown, which are shown in figure (6.2). However, the growth of MSUM crystals is not widely reported. Calvert et al. [28] have attempted to grow MSUM crystals. They measured the growth rates of MSUM crystals grown from the aqueous solution at 37 ^{0}C using microscopic method.

Figure (6.2): Crystal growth of MSUM crystal

Wet Chemical Process:

The MSUM crystals were also grown by the wet chemical precipitation technique. In this process, an aqueous solution 0.2 M, NaOH was stirred well and heated up to 70 ^{0}C. After achieving the required temperature, uric acid was added and made suspension of uric acid into the NaOH solution. Initially, the uric acid would dissolve into the solution because uric acid is a weak acid and NaOH solution is highly basic, but after adding sufficient quantity the solution would become suspended uric acid solution. The solution was stirred at constant temperature for four hours. Fine particles of MSUM crystals were found at the bottom. The coagulated form of particles looked like amorphous porous material, but from the powder XRD the well crystalline nature was confirmed. The probable reaction for the formation of MSUM is as follows.

$$NaOH + C_5H_4N_4O_3 \quad NaHC_5H_2N_4O_3 \cdot H_2O$$

From the thermo-gravimetric analysis (TGA), it was confirmed that the crystals were monohydrate. The particle size determination was also carried out, using Master Sizer 2000, at CSMCRI, Bhavnagar, for the precipitants of MSUM crystals obtained through the wet chemical method. The following table (6.1) gives the particle size measurements.

Table (6.1)

Particle size measurement data of MSUM crystals

Sample code	d (0.1) micron	d (0.5) micron	D (0.9) micron
MSUM	0.81	5.17	41.01
With ultra sonication			
MSUM	Sample dissolves in water		

From the Table (6.1), it can be interpreted that 10% of the particles were less than 0.81 micron, 50% of the particles were less than 5.17 micron and 90% particles were less than 41.01 micron.

6.4   Characterization of MSUM:

6.4.1   Thermo-gravimetry:

Thermo-gravimetric analysis (TGA) is a very useful technique to assess the thermal stability of various substances; many workers have demonstrated its usefulness [29-32].

In TGA, the weight of a sample in a controlled atmosphere is recorded continuously as a function of temperature or time, as the temperature of the sample is increased (usually linearly with time). A plot of mass or mass percent as a function of temperature is called a thermogram, or a thermal decomposition curve, or a pyrolysis curve. Often a pyrolysis occurs through many-stepped mechanisms, where the temperature ranges for each step overlap, resulting in irregular weight-temperature curve that may be difficult to analyze. Also, in many cases the trace follows a characteristics path common to a wide range of decomposition processes, which includes many polymer pyrolysis. The sample weight drops slowly as pyrolysis begins, then drops precipitously over a narrow range of temperature and finally turn back to zero slope as the reactants are used up.

Most of the uric acid and urate substances are decomposed without melting above 250 ^{0}C with the evolution of hydrogen cyanide. Only a few references are

available on the thermal study of urate substances. Recently, the Schnitzler et al. [33] have reported the thermo-analytical study of purine derivatives such as aminophylline, theophylline, caffeine and uric acid. Several investigators have used TGA and DTA for the study of drug substances, excipients and drug substances in the dosage forms. Wendlandt and Collins [34] used TGA and DTA as aids in the characterization and identification of commercial non-prescription analgesics.
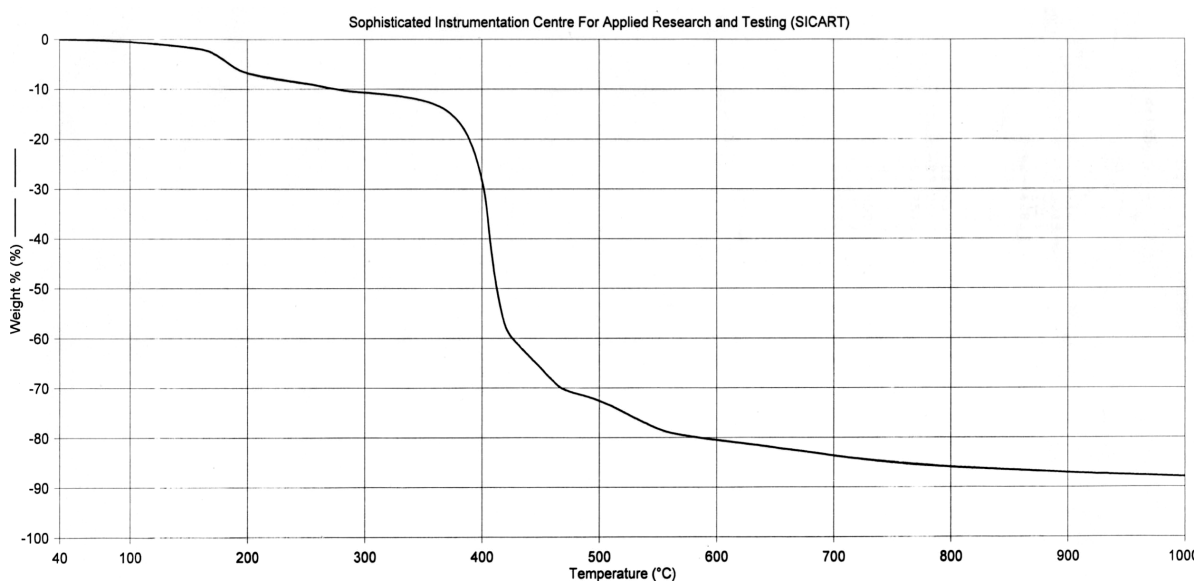
Figure (6.3): Thermogram of the MSUM crystals

Figure (6.3) shows the thermogram of MSUM, which indicates that the compound is stable up to 170 ^{0}C and then starts losing crystalline water and becomes anhydrous at 240 ^{0}C. Above this temperature up to 480 ^{0}C, the mass loss occurs through a rapid decomposition process and followed by a slow process between 480 ^{0}C to 750 ^{0}C with the loss of nearly 75 to 85 % of its original mass. The results are compiled in table (6.2). One water molecule was found to be associated with the crystals.

6.4.2 Kinetic Study of Dehydration: -

The use of thermo-gravimetric data to evaluate the kinetic parameters of solid-state reactions involving weight loss has been investigated by many workers [35-38].

If the pyrolysis occurs through a many-stepped mechanism, usually, the shape of the curve can be determined by the kinetic parameters of pyrolysis, such as order of reaction, frequency factor and energy of activation. Kotru et al. [39] reported the kinetics of solid-state decomposition of neodymium tartrate. They also calculated various kinetic parameters and suggested that the decomposition process took place according to cylindrical kinetic model. Recently, the kinetics of dehydration of gypsum [40], lithium sulphate monohydrate single crystals [41] as well as the kinetic and thermodynamic parameters of decomposition of chromate in different gas atmosphere [42] has been evaluated.

Usually, the kinetic parameters can be evaluated from the TG curves by applying several equations [35-38], which are proposed by different authors on the basis of different assumptions to the kinetics of the reaction and the Arrhenius law. These equations are as follows:

(1) The Coats and Redfern Relation

(2) The Horowitz and Metzger Relation

(3) The Freeman and Carroll Relation

However, in the present investigation, the Coats and Redfern relation is discussed in detail because it facilitates not only to evaluate the activation energy and order of reaction but also the frequency factor. Thus, it helps evaluate the thermodynamic parameters further.

6.4.2.1 Coats and Redfern (C-R) Relation: -

Coats and Redfern [35] derived the following equation to determine the values of activation energy and order of reaction.

$$\log_{10}\left(\frac{1-(1-a)^{1-n}}{T^2(1-n)}\right) = \left\{\log_{10}\left(\frac{AR}{aE}\right)\left(\frac{1-2RT}{E}\right)\right\} - \left\{\frac{E}{2.3RT}\right\} \qquad \text{-------- (6.1)}$$

Where,

á = Fraction of the original substance decomposed at time t

$á = (W_0-W)/ (W_0-W_f)$

W_0 = Initial weight

W = Weight at time t

W_f = Final weight

n = Order of reaction

A = Frequency factor

E = Activation energy of the reaction

R = Gas constant

a = Heating rate in deg. min^{-1}

Table (6.2)

The decomposition process of MSUM crystals and TG results.

Temperature (^{0}C)	Substance	Theoretical weight (%) (Calculated)	Practical weight (%) (from graph)
Room Temperature	$NaHC_5H_2N_4O_3 \cdot 0.98\,H_2O$	100	100
240 ^{0}C	$NaHC_5H_2N_4O_3$	91.5	91.49
750 ^{0}C	Na_2O	14.916	15.1

To determine the value of activation energy and order of reaction, a plot of $-log_{10} [\{1-(1-á)^{1-n}\}/\{T^2(1-n)\}]$ versus $1/T$ is drawn for different values of n and the best linear plot gives the correct value of n. The activation energy can be calculated from the slope of the plot. The frequency factor can be calculated for a particular temperature using relation (6.1).

The equation (6.1) is not valid for value $n = 1$, therefore, it is modified as follows

$$-\log_{10}\left[\frac{-\log(1-a)^{1-n}}{T^2}\right] = \left\{\log_{10}\left(\frac{AR}{aE}\right)\left(\frac{1-2RT}{E}\right)\right\} - \left\{\frac{E}{2.3RT}\right\} \qquad \text{------- (6.2)}$$

The Coats-Redfern relation was solved for various values of n. The statistical

regression analysis was applied to different values of *n* and the highest values of co-relation co-efficient indicated the best linear fit curve. This was found for n=1/4.

Figure (6.4) is a plot of Coats-Redfern equation for MSUM crystals for *n=1/4,* which is a best linear fit straight line.
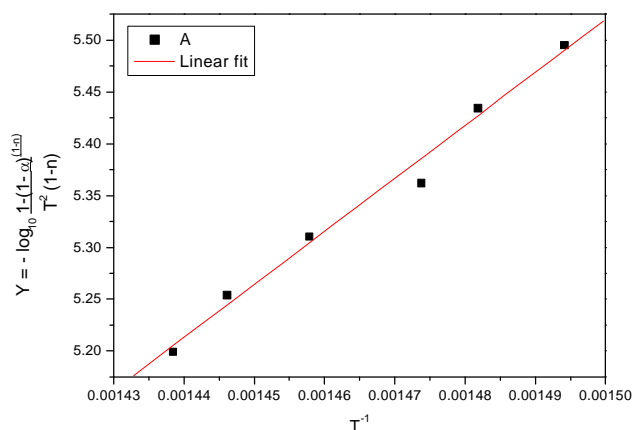
Figure (6.4): Plot of Coats and Redfern relation for MSUM crystals

Where, $X = (1/T)$ and $Y = -log_{10} [\{1-(1-á)^{1-n}\}/\{T^2(1-n)\}]$

The values of activation energy, frequency factor and the order of reaction are found to be 120.324 kJMol^{-1}, 1.0065 X 10^{20} and 1/4, respectively. Table (6.3) gives the values of different kinetic parameters obtained from the Coats and Redfern relation.

Table (6.3)

The values of different kinetic parameters obtained from the Coats and Redfern relation.

Samples	Kinetic Parameters
Monosodium urate monohydrate	Order of reaction (n) = ¼
	Activation energy (E) = 120.324 kJMol^{-1}
	Frequency factor (A) = 1.0065 X 10^{20}

6.4. 3   Thermodynamic Parameters:

The thermodynamic parameters have been evaluated from the dehydration stage of thermogram of MSUM crystals. The standard relations for estimation of these parameters are as follows [43].

The standard enthalpy of activation $Ä^{\#}H°$ was calculated by using the following relation,

$$Ä^{\#}H° = E\text{-}2RT \qquad\qquad \text{------ (6.3)}$$

The standard entropy of activation $Ä^{\#}S°$ could be calculated by using the following formula,

$$Ä^{\#}S° = 2.303 \times R \times log_{10}[Ah/kT_m] \qquad\qquad \text{------- (6.4)}$$

Where,

k = Boltzmann constant

h = Plank's constant

T_m = Temperature

R = Gas constant

A = Frequency factor

Here, the frequency factor is obtained from equation (6.1). Also, the standard Gibbs energy of activation $Ä^{\#}G°$ is possible to estimate from the following equation

$$Ä^{\#}G° = Ä^{\#}H°\text{-} T Ä^{\#}S° \qquad\qquad \text{------- (6.5)}$$

The standard change in the internal energy in passing from the initial to the activated state can be represented as

$$E = RT + Ä^{\#}U° \qquad\qquad \text{------- (6.6)}$$

Enthalpy is a state function whose absolute value cannot be known. ÄH can be ascertained, either by direct method or indirectly. An increase in the enthalpy of a system, for which ÄH is positive, is referred to as an endothermic process.

Conversely, loss of heat from a system, for which $\ddot{A}H$ has a negative value, is referred to as an exothermic process.

Entropy is a thermodynamic property of a system. It is a state function and it is defined in terms of entropy change rather than its absolute value. A spontaneous process has a natural tendency to occur, without the need for input work into the system. In contrast to this, the non-spontaneous process does not have a natural tendency to occur.

However, $\ddot{A}G$ is negative for a spontaneous process. An exothermic reaction ($\ddot{A}H > 0$) with positive ($\ddot{A}S > 0$) is always spontaneous. A reaction for which $\ddot{A}H < 0$ and $\ddot{A}S < 0$ is spontaneous only at low temperatures, whilst a reaction for which $\ddot{A}H > 0$ and $\ddot{A}S > 0$ is spontaneous only at high temperatures. The temperature at which the reaction becomes spontaneous in each case is given by $T = \ddot{A}H/ \ddot{A}S$.

The standard reaction free energy, $\ddot{A}G^0$, is the change in the Gibbs free energy, which accompanies the conversion of reactants in their standard states into products in their standard states. It can be calculated from the enthalpy and entropy changes for a reaction using $\ddot{A}G^0 = \ddot{A}H^0 - T\ddot{A}S^0$ or from tabulated value for the standard free energy of formation $\ddot{A}G^0$.

Substances with negative values of $\ddot{A}G^0_f$ (standard free energy of formation) are termed thermodynamically stable. Substances which have positive values of $\ddot{A}G^0_f$ are termed thermodynamically unstable.

For spontaneous process, $\ddot{A}S$ is positive and $\ddot{A}G$ is negative. The relationship $\ddot{A}G = \ddot{A}H - T\ddot{A}S$ allows predictions of the conditions under which a reaction is spontaneous. Temperature has a major effect on spontaneity of reactions. For the reactions where $\ddot{A}H < 0$ and $\ddot{A}S < 0$, $|T \ddot{A}S|$ will be less than $|\ddot{A}H|$ provided that T is small, and such a reaction will be spontaneous at lower temperatures. Conversely,

when ÄH >0 and ÄS>0, |T ÄS| will be greater than | ÄH| provided that T is large, and such a reaction will become spontaneous at higher temperatures. In both cases, the temperature at which the reaction becomes spontaneous (when ÄG = 0) is simply given by T = ÄH/ ÄS [44]. The prediction for the processes is given in table (6.4).

Table (6.4)

The conditions for the prediction of processes

ÄH	ÄS	Spontaneous or not	Spontaneity favored by
-ive	+ive	Under all conditions	All conditions
-ive	-ive	If | TÄS| < | ÄH|	Low temperature
+ive	+ive	If | TÄS| > | ÄH|	High temperature
+ive	-ive	Never	No condition

The thermodynamic parameters for dehydration of gel grown iron (II) tartrate have been estimated by Joseph et al [45]. Altogether, the thermodynamic parameters have been estimated for the reactivity at dislocation etch-pits on anthracene single crystal cleavages by Vaishnav et al. [46]. Recently, Dabhi and Joshi [47, 48] have reported the thermodynamic parameters for dehydration of various gel grown metal-tartrate crystals. Apart from this, thermodynamic properties and kinetics of the physical aging of amorphous bio-materials like, glucose and fructose and their mixtures [49] and kinetic and thermodynamic parameters of decomposition of chromates [42] have recently been reported.

Table (6.5)

The values of different thermodynamic parameters of MSUM crystals

Monosodium urate monohydrate crystalline sample	Standard Entropy $Ä^{\#} S°$ = 131.182 JkMol^{-1}
	Standard Enthalpy $Ä^{\#} H°$ = 113.956 kJ Mol $^{-1}$
	Standard Gibbs free energy $Ä^{\#} G°$=24.94 kJ Mol $^{-1}$
	Standard change in internal energy $Ä^{\#} U°$ = 117.140 kJ Mol $^{-1}$

Table (6.5) summarizes the values of different thermodynamic parameters, i.e., standard entropy, standard enthalpy, standard Gibbs free energy and standard change in internal energy, obtained for dehydration of MSUM crystalline sample. This suggests that the process is spontaneous at high temperatures.

6.4.4   FT-IR Spectroscopic Studies: -

Infrared (IR) spectroscopy is an excellent tool for both qualitative and quantitative analysis [50-52]. FT-IR spectroscopy is the further advancement of IR spectroscopy by using the mathematical concept of Fourier Transform through proper electronic circuit and computer interfacing.

Monosodium urate is a sodium salt of uric acid, which is a minor end product of nitrogen metabolism in human body and it is very stable. Uric acid is an organic compound of carbon, nitrogen, oxygen and hydrogen, with the chemical formula $C_5H_4N_4O_3$, and its sodium salt is having chemical formula $NaC_5H_3N_4O_3$. The molecular structure of MSUM is as follows.
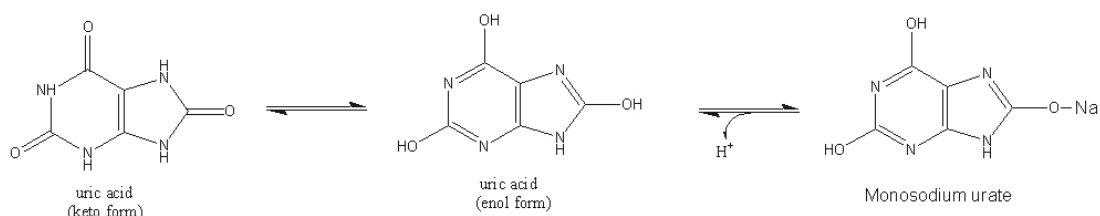
Figure (6.5) Chemical structure of MSU

Many researchers have paid their attention to the IR spectroscopic study of uric acid and urate compounds. Ramachandran and Natrajan [15] reported the gel growth of uric acid and its FT-IR study. Schnitzler et al. [33] have reported the FT-IR studies of various bio-materials like aminophylline, theophylline, caffeine and uric acid. Moreover, Joshi and Joshi [53] as well as Joshi [54] have reported the FT-IR

spectroscopic studies of the calcium hydrogen phosphate dihydrate (CHPD) and calcium oxalate type urinary crystals.

The characteristic FT-IR spectrum of MSUM is shown in figure (6.6), which was recorded on a Shimadzu 8400 instrument in KBr disc, in the range from 400 cm^{-1} to 4000 cm^{-1}.
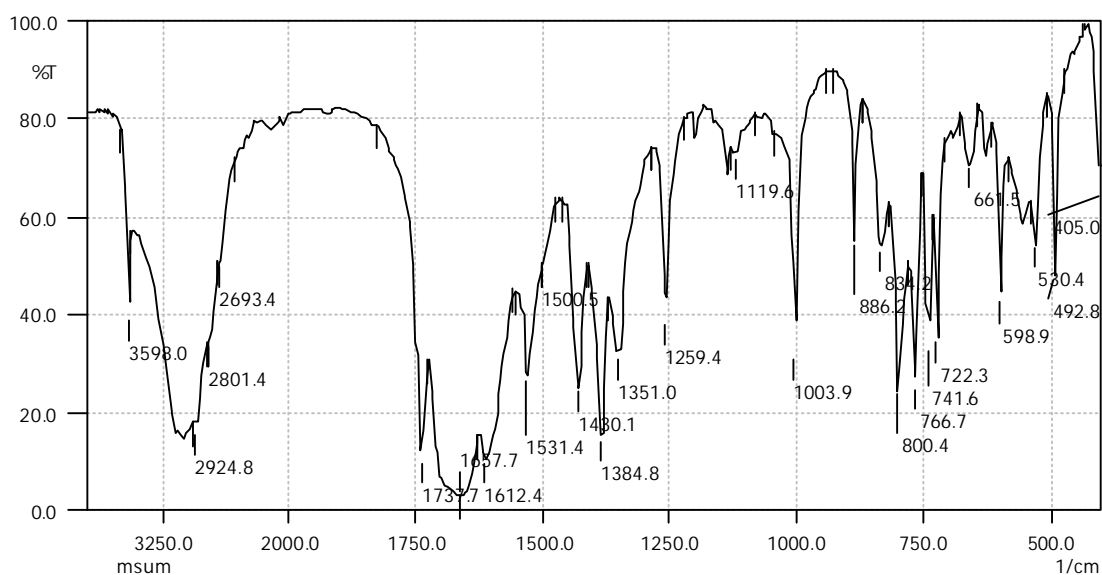
Figure (6.6): FT-IR spectrum of the MSUM crystals

Table (6.6)

Assignments of observed absorptions in FT-IR spectrum

Monosodium Urate Monohydrate NaHC$_5$H$_2$N$_4$O$_3$	
Assignments	Observed Vibrational frequencies (Cm^{-1})
C= O	1737.7
C = C	1531.4
	1500.5
C - N	1259.4
	1351.0
	1384.8
N –H Stretching	2924.8
N-H Rocking	722.3
	741.6
	766.7
	800.4
	886.0
	842.0
O-H Stretching	3598.0
Oxygen –Metallic bond	400-600

From this spectrum one can notice that the absorptions between 400 cm^{-1} to 600 cm^{-1} show the presences of oxygen-metal bond. A broad dip of absorption at 1737.7 cm^{-1} indicates the presence of more than one C=O bond, while the absorptions at 1531.4 cm^{-1} and 1500 cm^{-1} are due to C = C in enol or keto forms, and the absorptions at 1259 cm^{-1}, 1351 cm^{-1} and 1385 cm^{-1} are due to the C-N bond. The absorption at 2924.8 cm^{-1} is related to N-H stretching, while the absorptions between 722.3 cm^{-1} to 850 cm^{-1} are related to N-H rocking. The presence of water of hydration is primarily confirmed with the presence of a sharp dip at 3598 cm^{-1}, which is regarded due to O-H stretching. Table (6.6) represents the assignments of different absorption bands observed in FT-IR spectrum.

From the FT-IR spectrum one can confirm the presence of keton group (C=O), carbon-nitrogen bond (C-N), N-H stretching and rocking as well as the presence of water of hydration in the sample.

6.4.5 Powder X-ray Diffraction:

In gout the tissue deposits are composed of MSUM, where as the urinary stones largely gets uric acid [55, 56]. The MSUM crystals are needle or bar-shaped in a monoclinic or triclinic system, while the uric acid crystallizes in an orthorhombic system by forming rhombic plates. When MSUM is rapidly crystallized from pure solutions, the crystals are very fine and appear amorphous. Howell et al. [55] have reported the powder X-ray diffraction (XRD) patterns and *d* values for uric acid, MSUM and disodium urate dihydrate (DSUD), but unit cell parameters were not estimated. Powder XRD study of the tophaceous deposits in gout, identified that MSUM was the prime accuse of gouty tophi. By using similar method the author also concluded that the urinary stone from gouty person was having uric acid. Crystals formed in urine incorporate pigments and exist in a variety of crystalline forms.
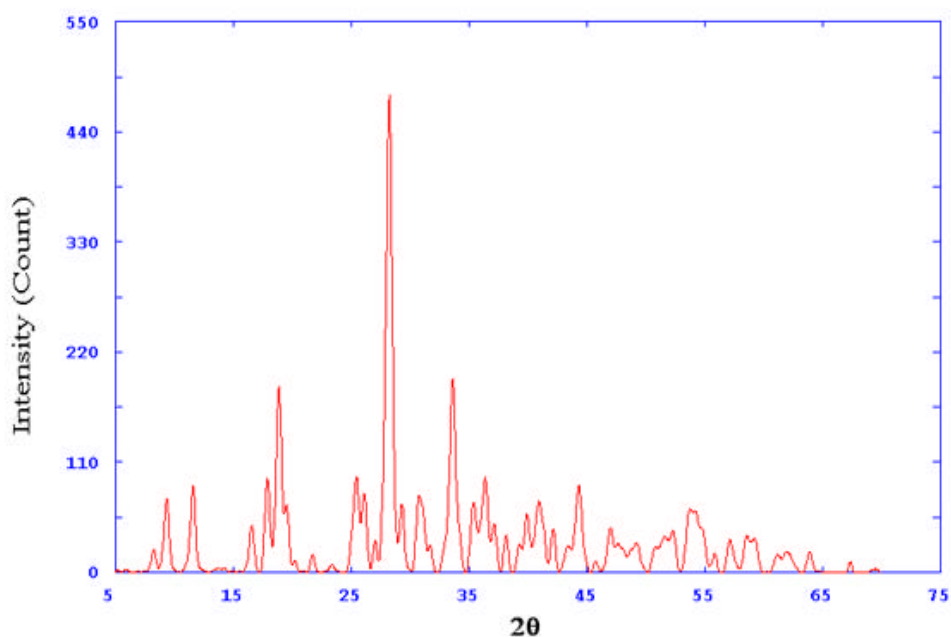
Figure (6.7): Powder X-ray diffractogram of the MSUM crystals

Table (6.7)

Powder XRD data of MSUM crystals.

2θ	d ( )	Height	FWHM
9.370	9.43082	73.4	0.5034
11.600	7.62221	86.0	0.4947
17.913	4.94785	93.5	0.5017
18.889	4.69429	185.2	0.5381
25.466	3.49486	95.9	1.2240
26.121	3.40877	78.8	1.3220
28.246	3.15688	476.9	0.5930
29.316	3.04410	67.7	0.4938
30.789	2.90170	75.7	0.8045
33.632	2.66260	193.3	0.5999
35.404	2.53332	69.4	1.6593
36.390	2.46695	94.9	0.7224
39.933	2.25581	57.8	0.6052
40.948	2.20223	70.8	0.8910
44.334	2.04158	86.2	0.6576
53.773	1.70337	63.2	1.6051

Identification and significance of these urate crystals in synovial fluids has been studied by various researchers [57, 58]. Crystallographic data of uric acid, uric acid dihydrate is available [59], but to the best of the present author's knowledge, no crystallographic data is available for MSUM crystals. From the earlier reported work it is mentioned that MSUM crystals occur, in form of tophi in gout, having monoclinic or triclinic system but no unit cell parameter values are available. It is very difficult to get single crystal XRD data of MSUM crystals because the crystals get degraded upon removal from the test tube on exposure of the atmosphere. The figure (6.7) gives the powder X-ray diffractogram of MSUM crystals and Table (6.7) gives the *2è* and *d* values.

6.4.6   Dielectric Studies of MSUM crystals:

Materials, which are electrical insulators or in which an electric field can be sustained with minimum dissipation of power, are known as dielectric materials. In the general sense, dielectric includes all materials except the condensed state of metals.

The value of dielectric constant was calculated by using the following formula,

$$C = åA / t = \quad å_0 \ ê A / t, \qquad ê = Ct / å_0 A$$

Where, *C* = Capacitance*, å* = Relative permittivity, *A* = Area of sample, and *å* $_0$ = Permittivity of free space and *ê* = Dielectric constant.

There is no major work reported on the dielectric study of the uric acid and its salts. Cyril et al. [60] have studied the dipole moment of various purine compounds like, 6-chloropurine, purine-6-thiol, hypoxanthine, theobromine, theophylline, caffeine, and uric acid, and discussed their dipole moment behaviors. In the present

investigation, the variation of capacitance with frequency, ranging between 500 Hz to 1 MHz, was studied at room temperature.

The following figure (6.8) shows the variation in dielectric constant with frequencies. It is observed from the figure that the dielectric constant continuously decreases with increasing frequency and reaches a constant value nearly at 10^6 Hz. A rapid decrease in dielectric constant is observed in the in the low frequency region of 100 Hz-1000 Hz.
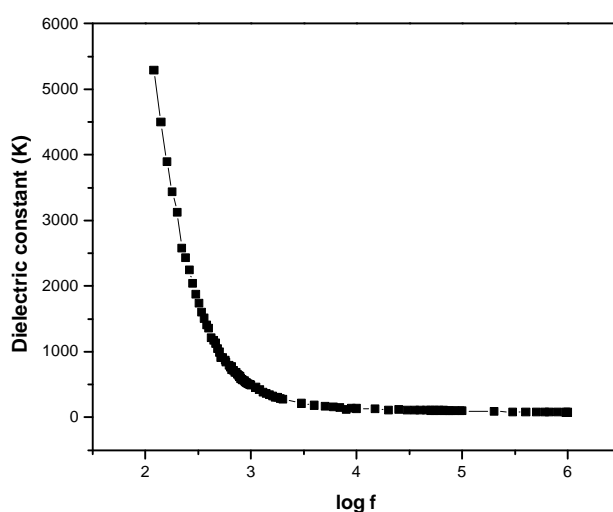
Figure (6.8): A plot of dielectric constant versus frequency

This may be attributed to the tendency of induced dipoles in molecules to orient themselves in the direction of the applied field in the low frequency rage. Nevertheless, in the high frequency range the induced dipoles are hardly able to orient themselves in the direction of the applied field and as a result the value of dielectric constant decreases [61]. It shows a relaxation type nature. This type of behavior was reported for PVA-H_3PO_4 electrolyte complexes by Gupta and Singh [62]. Dabhi et al. [63] have also reported similar behavior for zinc tartrate crystal. The figure (6.9) shows a plot of *tan ä* versus *log f* for MSUM crystals at room temperature. The frequency region 500 Hz to 1MHz is used in this study. The value of *tan ä* increases

initially and gets a maximum value at 824.696 Hz frequency and then starts slowly decreasing.
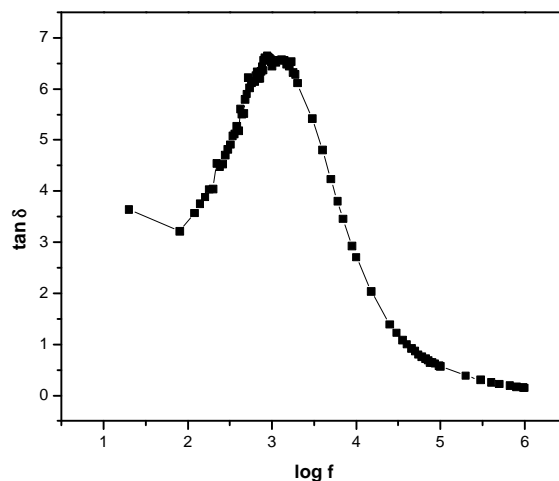
Figure (6.9): A plot of *tan ä* versus *log f* for MSUM

The variation in the a.c. resistivity ($ñ_{ac}$) and a.c. conductivity ($ó_{ac}$) with the frequency is shown by the following two curves of figures (6.10, a & b). One can notice from the plot that the resistivity increases with the increase in frequency and the conductivity decreases with the increase in frequency.
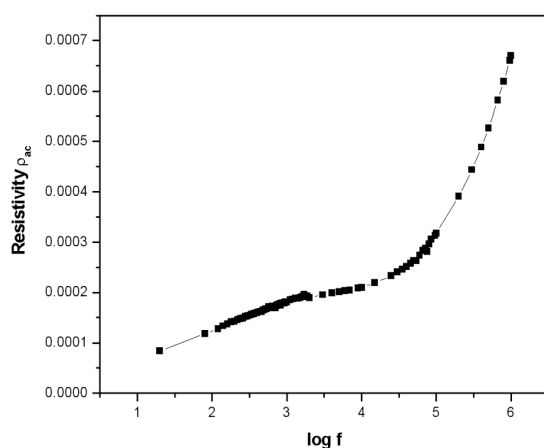
Figure (6.10a)
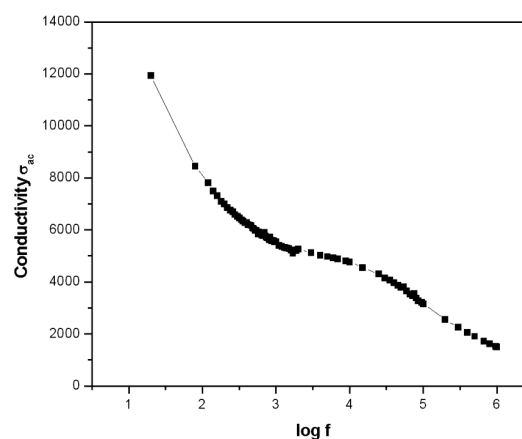
Figure (6.10b)

Figure (6.10): Plots of a.c. resistivity and a.c. conductivity versus frequency for MSUM.

6.5   *In vitro* Inhibition Study of the MSUM crystals for Different Herbal Extracts:

Many workers [54, 64, and 65] have reported the growth and inhibition study of various bio-material crystals, particularly, responsible for ailments related to urinary stones. Natarajan et al [66] have studied various inhibitors and promoters, based on hosts of fruit juices, extracts from vegetables and cereals and natural substances such as mint, lemon, tomato, grape, pineapple, reddish, barely, horse-gram, etc. Recently, Joseph et al. [67] have carried out the growth and inhibition study on CHPD crystals by using tartaric acid and tamarind. Altogether, Joshi et al. [68, 69] reported the effect of herbal extracts of *Bergenia ligulata* and *Tribulus terrestris* on the growth of calcium oxalate as well as CHPD type urinary crystals. However, no work is reported on the *in vitro* growth and inhibition study of MSUM crystals, except for one reference on the growth of MSUM crystals by Calvert et al. [28] as per the knowledge of the present author.

In this study, the single diffusion gel growth technique was used. As mentioned earlier, the gel growth technique serves as a very good model to verify the growth and inhibition of various bio-material crystals *in vitro,* the details are given in the Chapter-III. The growth of MSUM crystals has been discussed in the previous section 6.3.

After pouring the supernatant solution of uric acid, the MSUM crystals were grown within 7 days. Once the complete growth of MSUM crystals was achieved, 10 ml solutions of the following herbal extracts were poured into the supernatant solution and the effect on the crystals was observed. The solutions of herbal extracts were prepared by mixing 10 mg concentrated extracts into 10 ml water. The details of the herbal extracts are given in Chapter-IV.

1. *Boswellia Serrata* gum resin

2. *Aerva Lanata*

3. *Rotula aquatica* root

4. *Boerhaavia diffusa* root

The following figure (6.11) shows the test tubes having the mixture of uric acid and solution of herbal extracts, which were used for inhibition study.

In the case of pure uric acid the average length of grown crystals was 0.675 cm. But for the *B. serrata,* containing supernatant solution, no considerable change was observed. The same effect was observed in the case of *B. diffusa.*
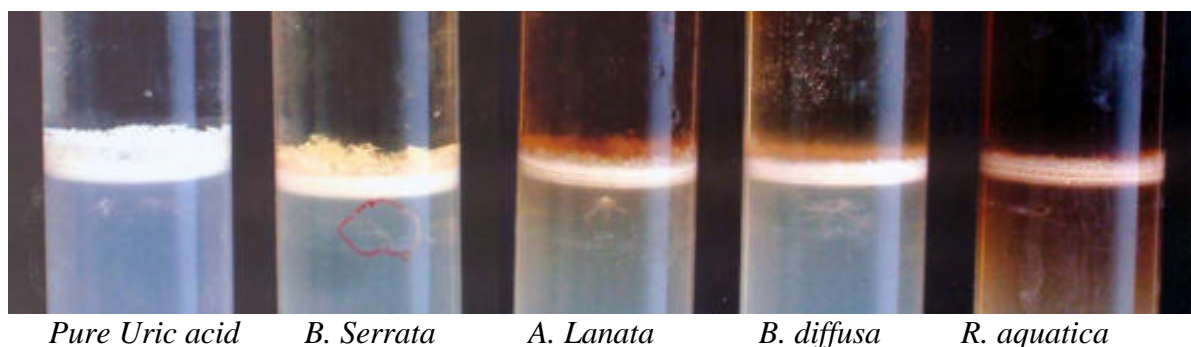

| *Pure Uric acid* | *B. Serrata* | *A. Lanata* | *B. diffusa* | *R. aquatica* |

Figure (6.11): Comparative study of growth inhibiton study of MSUM crystals

Table (6.8)

Result of inhibition study of MSUM crystals in terms of observed crystal length after seven days of pouring the herbal extract solutions.

No.	Solutions	Initial Length of Crystals	Final length of crystals	Remarks
1	Pure Uric acid	0.675	0.675	No change
2	*B. serrata* + uric acid	0.664	0.653	Minute change
3	*R. aquatica* + uric acid	0.880	0.812	After 15 days crystals completely dissolved
4	*B. diffusa* + uric acid	0.600	0.586	Minute Change
5	*A. lanata* + uric acid	0.865	0.768	Remarkable change

However, the encouraging results were obtained when *R. aquatica* and *A. lanata* were used; some remarkable changes were observed in the crystal length. The observed results are summarized in Table (6.8). From the Table, one can easily conclude that *R. aquatica* and *A. lanata* give comparatively good inhibition than the others. Ethanolic herbal extract solutions almost gave the same results. As uric acid is completely insoluble in ethanol, it was observed that by adding ethanolic extract the re-precipitation occurred in the supernatant solution. In another study the *R. aquatica* aqueous extract (80mg/ml) were found to be effective in dissolving MSUM crystals within 24 hours [70]. But aqueous extract of *B. diffusa* (80mg/ml) was found mildly active. These results were found to be encouraging for the *in vivo* studies and the formulation of the drug. This study may be helpful to design the therapies for the prevention and cure of gout.

6.6   Conclusion:

(1)   The growth of MSUM crystals was carried out by using single diffusion gel growth technique in normal test tubes. Very thin, transparent, needle type crystals were observed near the gel-liquid interface. A few needle type crystals were grown due to very less solubility of uric acid. When crystals were observed under polarized light microscope through a red filter they appeared yellow. That indicates that the crystals were negatively birefringent.

(2)   The MSUM crystals were thermally unstable and TGA suggested that the dehydration started with the liberation of water molecule at 170 ^{0}C. At 240 ^{0}C the water molecules were completely removed. Subsequently, when the temperature was further increased the mass loss occurred very sharply between 370 ^{0}C to 480 ^{0}C with the release of gases like hydrogen cynide, carbon dioxide and carbon monoxide. This was followed by a slow

process between 480 ^{0}C to 750 ^{0}C temperature with loss of nearly 75 to 80 % of original mass. Finally, it was converted into Na_2O, which remained stable up to the end of the analysis. One water molecule was associated with the compound.

(3)   The kinetic parameters of dehydration process were obtained by applying the Coats and Redfern relation, to the dehydration stage in the thermogram. The order of reaction and the activation energy was found to be ¼ and 120.324 kJmol^{-1} respectively.

(4)   The thermodynamic parameters were evaluated for the dehydration process. The values of standard Gibbs free energy, standard enthalpy and standard entropy were found to be 24.94 kJ Mol $^{-1}$, 13.956 kJ Mol $^{-1}$ and 131.182 JkMol^{-1}, respectively. The reaction was found to be spontaneous in the nature.

(5)   The FT-IR spectrum of MSUM crystals confirmed the presence of a water molecule and metal-oxygen bond, O-H stretching, N-H rocking and stretching, C = C bond, C= O carbonyl group (keton group), and C – N bond.

(6)   The MSUM crystal belongs to monoclinic or triclinic system but unit cell parameters are not reported yet. It is very difficult to grow MSUM single crystals due to very less solubility of uric acid in any solvent. The crystals prepared by wet chemical method were very tiny micro meter level; therefore, it was difficult to take single crystal XRD. The powder XRD data were obtained in terms of *2è* and *d* values.

(7)   The variation of dielectric constant with frequency (*log f*) indicated that as the frequency increased, initially, the dielectric constant decreased rapidly and became almost constant, suggesting a tendency of induced dipoles in molecules to orient along the applied field in the low frequency region and

diminishing this tendency at high frequency region. The plot of *tan ä* versus *log f* suggested that the maximum loss was observed at 824.6 Hz frequency and then it decreased. This might be due to water of hydration or dual loss mechanism, it requires further study. Due to the combine effect of frequency (*f)*, capacitance (*c*) and dissipation factor (*D*), as the frequency increased the a.c. resistivity increased and, naturally, the a.c. conductivity decreased for MSUM crystals.

(8)   The effects of four herbal medicinal plant extracts on the growth of MSUM crystals were reported. When pure uric acid was used as supernatant solution, the crystal length was found to be the maximum. In the case of 1% aqueous extract solutions of *B. serrata,* and *B.diffusa* the inhibition was not significant, but in the case of 1% aqueous extract solutions of *R. aquatica* and *A. lanata,* good amount of inhibition was shown. Till today there is no major remedy is available to dissolve the   MSUM crystal in synovial fluid, which is responsible for gout. This study may help the prevention or cure of gout.

References:

[1]   B. T. Emmerson; *J. of Med.,* **334** (1996) 445.

[2]   S. J. Gupta; *J. Ind. Rheumatol. Assoc.,* **10** (2002) 5.

[3]   K. Rosenthal Anne; *"Crystal Arthropathies",* In: Textbook of Rheumatology, 2nd Edn., Ed. P.J. Maddison, D.A. Isenberg, P. Woo, and D.A. Glass, Oxford University Press, (1998) p-1560.

[4]   H. Iwata, S. Nishio, M.Yokoyama, M. Matsumoto and M. Takeuchi; *J. Urol.*, **142** (1989) 1095.

[5]   C.Y.C. Pak, O. Waters, L. Arnold, K. Holt, C. Cox and D. Barilla; *J. Clin Invest,* **59** (1977) 426.

[6]   T. Shimizu, H. Matsushige, M. Nishikawa, M. Yashiwagi and T. Terauchi; *Uric Acid Res.*, **11** (1987) 7.

[7]   W. R Wilcox., A. Khalaf, A. Weinberger, I. Kippen and J.R. Klinenburg; *Med. Biol. Eng.,* **10** (1972) 522.

[8]   L. Cifuentes, *"Composicion y Estructura de los Calculus Renales. Salvat",* Barcelona, (1984) p-87.

[9]   F. L. Coe, R. L. Lawton andR. B. Goldstein; *J. Urol.*, **149** (1975) 926.

[10]   P. K.Grover, R. L. Ryall and V. R. Marshall; *Kidney Int.,* **41** (1992) 149.

[11]   C.Y. C. Pak and L.H. Arnold; *Bio Med.,* **149** (1975) 930.

[12]   C.Y. C. Pak and L.H. Arnold; *Proc., Soc. Exp. Bio. Med.,* **149,** (1975), 930.

[13]   T. Irusan, D. Arivuoli and P. Ramasamy; *J. Mater. Sci. Lett.,* **12** (1993) 405.

[14]   S. N. Kalkura, V. K. Vaidyan, M. Kanakavel and P. Ramasamy; *J. Cryst. Growth,* **132** (1993) 617.

[15]   E. Ramachandran and S. Natarajan, *"IXth National Seminar on Crystal Growth",* Chennai, February, (2003).

[16]   S. Koutopolous and E. Dalas; *J. of Mater. Sci. Lett.,* **17** (1998) 485.

[17]   R. M. Koka, E. Huang and J. C. Lieska; *Am. J. Physiol Renal Physiol,* **278(6)** (2000) F-989.

[18]   F. Grases, A.I. Villacampa and Costa-Bauza; *Urol. Res.,* **27** (1999) 141.

[19]   P. K. Grover and R. L. Ryall; *Mol. Med.,* **8(9),** (2002), 525.

[20]   Kirk Othmer, *"Encyclopedia of Chemical Technology",* 2nd Ed., Vol.21, Interscience, Division of John Willey & Sons Inc., (1970) p- 107.

[21]   J. P. Peters and K. K. Van Siyke,: *Quantitative Clinical Chemistry*, Vol.1 2nd Ed., Williams & Wilkins Company, Baltimore, 1946, p-937.

[22]   D. J. Allen, G. Milosovich, and A. M. Mattocks; *Arthritis Rheum.,* **8** (1965.) 1123.

[23]   J. N. Loeb, *Arthritis Rheum.*, **15** (1972) 189.

[24]   R. A. McNabb and F. M. A McNabb; *Comp. Biochem. Physiol.,* **67A** (1980) 27.

[25]   J. E. Seegmiller, *Arthritis Rheum.*, **8** (1965) 714.

[26]   J. R. Kilnenberg, S. E. Goldiner and J. E. Seegmiller; *Am. Intern. Med.,* **62**, (1965) 639.

 [27]   http://www.aafp.org/afp/990401ap/1799.html

[28]   P. D. Calvert, R. W. Fiddis and N. Vlachos; *Collids and Surf. ,* **14** (1985) 97.

[29]   D. A. Anderson and E. S. Freeman; *J. Polymer Sci*., **54** (1961) 253.

[30]   H. C. Anderson; *S. P. E. Trans*., **1** (1962) 202.

[31]   H. D. Anderson; *Nature*, **191** (1961) 1088.

[32]   C. D. Doyle; *Anal. Chem*., **33** (1961) 77.

[33] E. Schnitzler, M. Kobelnik, G. F. C. Sotelo, G. Bannach and M. Ionashiro; *Ecl. Quim, Sao Paulo,* **29(1)** (2004) 71.

[34] W. W. Wendlandt and L. W. Collins; *Anal. Chim. Acta,* **71** (1974) 411.

[35] A. W. Coats and J. P. Redfern; *Nature*, **201** (1964) 68.

[36] H. H. Horowitz and G. Metzger; *Anal. Chem.*, **35** (1963) 1464.

[37] E. S. Freeman and B. Carroll; *J. Phys. Chem.*, **62** (1958) 394.

[38] D. W. Van Krevelan, C. Van Hardeen and F. J. Huntlens; *Fuel*, **30** (1951) 253.

[39] P. N. Kotru, K. K. Raina and M. L.Koul; *Indian J. Pure and Appl. Phys.*, **25** (1987) 220.

[40] D. Fatu; *J. of Thermal Analysis and Calorimetry*, **65(1)** (2001) 205.

[41] A. N. Modestov, P. V. Poplankhin and N. Z. Lyakhov; *J. of Thermal Analysis and Calorimetry*, **65(1)** (2001) 103.

[42] S. A. Halawy, N. E. Fouad, M. A. Mohamed and M. I. Zaki; *J. of Thermal Analysis and Calorimetry*, **65(1)** (2001) 153.

[43] K. Laidler; *Chemical Kinetics*, 3rd Ed., Harper and Row Publications, New York, (1987).

[44] A. G. Whittaker, A. R. Mount and M. R. Hill;*"Physical Chemistry",* Viva, New Delhi (2001).

[45] S. Joseph and M. J. Joshi; *Indian J. Phys.*, **71A** (1997) 183.

[46] R. M. Vaishnav, L. K. Maniar, M. J. Joshi and R. M. Dabhi; *Indian J. Phys.*,**74(A)** (2000) 581.

[47] R. M. Dabhi and M. J. Joshi; *Indian J. Phys.,* **76A** (2003) 481.

[48] R. M. Dabhi and M. J. Joshi; *Indian J. Phys.*, **76A** (2002) 211.

[49] R. Wungtanagorn and S. J. Schmidt; *J. of Thermal Analysis and Calorimetry*, **65(1)** (2001) 3.

[50] G. Socrates; *Infrared Characteristics Group Frequencies*, John Wiley, Chichester, (1980).

[51] R. R. Griffiths; *Chemical Infrared Fourier Transform Spectroscopy*, Academic Press, New York, (1972).

[52] K. Nakamoto; *Infrared and Raman Spectra of Inorganic and Coordination Compounds*, John Wiley 3rd Ed

[53] V. S. Joshi and M. J. Joshi; *Cryst. Res. Technol.*, **38** (2003) 817.

[54] V. S. Joshi; *Ph.D. Thesis,* Saurashtra University, Rajkot, (2001).

[55] E. L. Prien and E. L. Prien; *Am. J. Med.*, **45** (1968) 654.

[56] R. R. Howell, E. D. Eanes and J. E. Seegmiller; *Arthrirtis Rheum.,* **6** (1963) 97.

[57] D. J. McCarty Jr., and J. L. Hollander; *Ann. Intern. Med.,* **54** (1961) 452.

[58] N. J. Zwaifler and T. J. Pekin; *Arch. Intern. Med.*, **111** (1963) 99.

[59] R. Shirley; *Science,* **152** (1966) 1512.

[60] P. Cyril , B. Christian, A. Jean-Jacques, B. Mihaela-MacNAIR and D. Marwan; *Czechoslovak Chem.l Comm.,* **67(8)** (2004) 1109.

[61] E. M. Reicha, M. El-Hi ti, A. Z. El-Sonabati and M. A. Diab; *J. Phys. D: Appl. Phys.,* **24** (1991) 369.

[62] P. N. Gupta and K. P. Singh, *"Dielectric Relaxation Characteristics of Solid State Polymer Electrolyte Complexes*,' in 'Solid State Ionics: New Developments" Eds. B.V.R. Chowdhari et al., World Science, Singapore, (1996) p-393.

[63]   R. M. Dabhi, B. B. Parekh and M. J. Joshi, *Indian J. Phys.* **79(5)** (2005) 503.

[64]   Gilda, T. Asaithambi and C. Mahadeven; *"IXth National Seminar on Crystal Growth",* Chennai, February, (2003).

[65]   J. L. Mayer and W. C. Thomas (Jr.); *J. Urol.,* **128** (1982) 1372.

[66]   S. Natarajan, E. Ramchandran and D. B. Suja; *Cryst. Res. Technol.,* **32** (1997) 553.

[67]   K. C. Joseph, B. B. Parekh and M. J. Joshi; *Current Science,* **85** (2005) 1232.

[68]   V. S. Joshi, B. B. Parekh, M. J. Joshi and A. B. Vaidya*; J. Cryst. Growth,* **275(1-2)** (2005) e-1403.

[69]   V. S. Joshi, B. B. Parekh and M. J. Joshi and A. D. B. Vaidya; *Urol. Res.*, **33** (2005) 80.

[70]   A. Raut, N. Pandita, M.J. Joshi and S. Mengi, "*Progress report:Preclinical Development of Herbal Formulation for Inflammatory Arthropathy",* Submitted to: Department of Biotechnology, Govt. of India, New Delhi (2002-03).

Chapter VII

Growth and Characterization of

Calcium Pyrophosphate Tetrahydrate Crystals

7.1   Introduction:

Formation of calcium pyrophosphate dihydrate (CPPD) crystals in soft tissues such as cartilage, meniscus and synovial tissue leads to CPPD deposition diseases. The appearance of these crystals in the synovial fluid can give rise to an acute arthritic attack with pain and inflammation of the joints, a condition called *pseudo-gout* [1-6]. The CPPD crystals are appeared to be formed extra-cellularly in the cartilage matrix. Also, CPPD crystals are found close to hypertrophied chondrocytes, which indicates abnormal metabolism. The main driving factor for the formation of CPPD crystals is believed to be an excess production of pyrophosphates, due to some disorder in the pyrophosphate metabolism of the aged chondrocytes, like hyperparathyroidism, hemochromatosis, hypothyroidism, hypomagnesemia, and hypophosphatsia [7-9]. During an acute attack of pseudo-gout, CPPD crystals are released (shedded) from cartilage in the diseased joints and enter the synovial fluid and cause severe pain and inflammation [10-11]. *In vivo* study has suggested that the most commonly found crystals in the synovial fluid are either triclinic CPPD (t-CPPD) or monoclinic CPPD (m-CPPD) [12-15].

Brown et al. [16] have reported, altogether, the preparation of twenty five different types of calcium pyrophosphate compounds, among them eight containing calcium ammonium pyrophosphates, ten containing calcium potassium

pyrophosphates and two pairs of dimorphic hydrated calcium pyrophosphates. The formation of crystals was confirmed by X-ray diffraction and polarized light microscopy. Many of these compounds are used in fertilizers prepared from condensed phosphates or their hydrolyzed products. Mirtchi et al. [17] have tested various additives, namely, calcium pyrophosphate (CPP), calcium sulphate dihydrate (CSD) and calcium sulphate hemihydrate (CSH), for setting as retarders of the beta-tricalcium phosphate-monocalcium phosphate monohydrate (beta-TCP-MCPM) cements. From this study they reported that the best result was obtained when CSD and CPP were added together with the cement. Also, CPP finds uses as a polishing agent in dentifrices [18].

Many researchers have carried out the growth and dissolution study of calcium pyrophosphate (CPP) crystals. Christoffersen et al. [19] have reported the growth of monoclinic calcium pyrophosphate tetrahydrate (m-CPPT) crystals by precipitation method, using 0.9 M $CaCl_2$ and 0.45 M $Na_4P_2O_7$. They have also reported that the auto-inhibition of m-CPPT is found at pH 7. Christoffersen et al. [20] have previously reported the dissolution kinetics of t-CPPD crystals. Also, Lin et al. [21] have studied the bio-degradation behavior of CPPD with addition of $Na_4P_2O_7$ $10H_2O$ and characterized it with SEM, atomic absorption analysis and ion coupled plasma analysis. Recently, Srinivasan et al. [22] have reported the role of CPPD in the cervical myelopathy (disease of spinal cord of neck).

The growth of CPP crystals has been carried out, in the present study, using the single diffusion gel growth technique and the crystals were characterized by different techniques. As the CPP crystals are associated with pseudo-gout, the growth inhibition study of CPP crystals is carried out in the presence of various herbal extracts.

7.2 Physical and Chemical Properties of CPP:

Table (7.1)

Physical and chemical properties of CPP [23]

General Information of CPP	
Chemical Formula:	$Ca_2P_2O_7$
Composition:	Molecular Weight = 254.12gm
	Calcium 31.54 % Ca
	Phosphorus 24.08 % P
	Oxygen 44.08 % O
	100.00 %
Empirical Formula:	$Ca_2P_2O_7$
Synonym:	Calcium diphosphate
CPP Crystallography	
Crystal System:	Mooclinc or Triclinic
Cell Dimensions:	Monoclinic: a=12.287 Å, b=7.511 Å, c=10.775 Å $á$= 90, $â$= 112.54 $ã$= 90 [24] Triclinic: a=7.335 Å, b=8.269 Å, c=6.667 Å $á$= 102.88, $â$= 72.74 $ã$= 94.92 [20]
Physical Properties of CPP	
Cleavage:	Indistinct
Color:	White
Density:	3.09
Melting Point:	1353 ^{0}C
Solubility:	Practically insoluble in water and soluble in dilute HCl or HNO_3

Generally, CPP crystals are weak positive birefringent [25]. If those crystals are observed through a high-power compensated polarized microscope,

<div align="center">
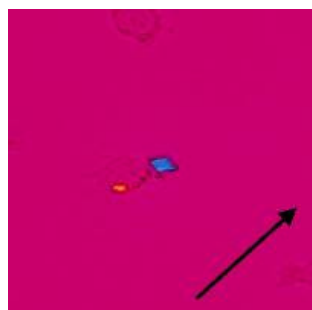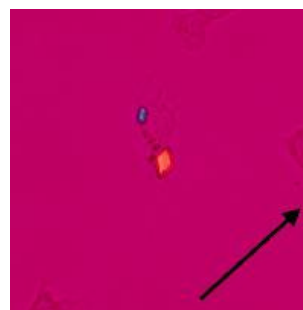
Figure (7.1a)   **Figure (7.1b)**

Figure (7.1 a & b): Photographs of CPP crystals under high-power compensated polarized microscope

</div>

the crystals appear blue when placed parallel to the compensator; on the other hand, the crystals placed perpendicular to the compensator appear yellow, which is displayed in figure (7.1a). If crystals are rotated by 90^0, this brings into a color change in both crystals, figure (7.1b). The black arrow indicates the direction of the compensator.

7.3 Growth of CPP Crystals:

The CPP crystals exhibits three polymorphic modifications, each one is meta-stable at room temperature; they are formed progressively upon heating calcium hydrogen phosphate dihydrate (CHPD) as shown hereby, [26].
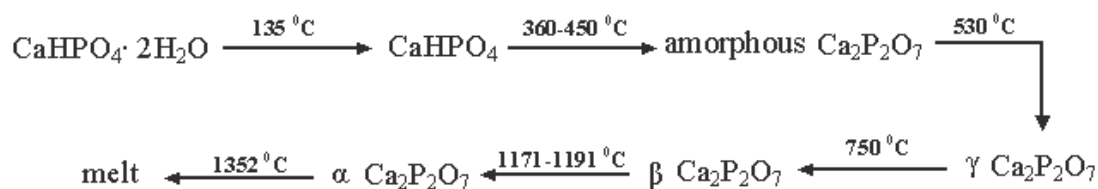
The growth of CPPT crystals is reported by many researchers [16, 27]. Christoffersen et al. [20] have reported the growth of CPPD crystals using precipitation method; Whereas, O'Brien et al [28] reported the formation of spherical granule type calcium pyrophosphate crystals. However, the gel growth of CPP crystals is yet not reported to the best of the present author's knowledge.

Two different techniques were employed to grow CPPT crystals:

(1)   Single diffusion gel growth technique.

(2)   Wet chemical process

7.3.1 Single Diffusion Gel Growth Technique:

(a)   Gel preparation:

As mentioned earlier in the section 5.3 of chapter-V, the stock solution of sodium meta-slicate was prepared and by adding double distilled water of appropriate volume it was possible to make a solution of desired specific gravity. In present gel

growth study, the specific gravity was selected as 1.05. Equal volumes of sodium meta-silicate and 0.25 M, $Na_4P_2O_7 \cdot 10\ H_2O$ solutions were added to prepare a mixture. This mixture was acidified by 2 N, Acetic acid in such a manner that appropriate pH was obtained. In the present study, the pH values between 4.5 to 5.0 were used. This mixture was poured in different test tubes to set in to the gel.

(b)   CPPT crystal growth:

Glass test-tubes of 25mm diameter and 150mm length were used as crystal growth apparatus. The above mentioned mixture was poured in equal volumes in different test tubes and allowed to set into the gel form. Within 48 hours, good quality gel was set and 0.25 M calcium nitrate tetrahydrate solution was poured gently on to the set gel.
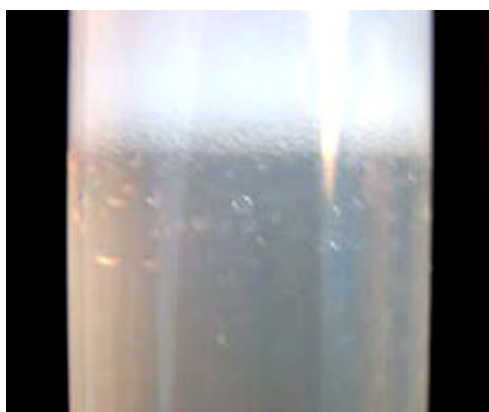
Figure (7.2): CPPT crystal growth

Good quality, transparent, spherical granules type crystals were grown, which are shown in figure (7.2).

7.3.2   Wet Chemical Process:

The CPPT crystals were also grown through the wet chemical precipitation technique. For this process, aqueous solution of 0.25 M, $Na_4P_2O_7$ was stirred well and heated up to 50 ^{0}C. After achieving the required temperature, calcium nitrate solution was added slowly in the drop-wise manner. This solution was stirred at constant

temperature for four hours. Fine crystalline particles of CPPT were found at the bottom of beaker. The coagulated form of particles looked like amorphous porous material, but from the powder XRD the crystalline nature was confirmed. The probable reaction for the formation of CPP is as follows:

$$Na_4P_2O_7 + 2\ Ca(NO_3)_2 \quad Ca_2P_2O_7 + 4\ Na(NO_3)$$
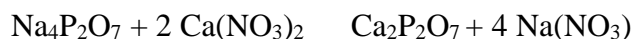
From the thermogravimetric analysis (TGA), it was confirmed that the crystals were in tetrahydrate form. The particle size determination was also carried out for the CPPT crystals obtained through the wet chemical method. The following table (7.1) gives the particle size measurements. The particle size was determined by using Master Sizer 2000, at CSMCRI, Bhavnagar.

Table (7.2)

Particle size measurement data of CPPT crystals

Sample code	d (0.1) micron	d (0.5) micron	D (0.9) micron
CPPT	4.15	22.52	90.80

From the table (7.1), it can be interpreted that 10% of the particles were less than 4.15 micron, 50% of particles were less than 22.52 micron and 90% particles were less than 90.80 micron.

7.4   Characterization of CPPT:

7.4.1   Thermogravimetry:

Thermogravimetric analysis (TGA) of various phosphate and pyrophosphate compounds was reported by various researchers [29-31]. Ashok et al. [32] have reported the growth of BCP (hydroxyapatite) crystals at physiological temperature and characterized the crystals using the TGA. From the study, they reported that the hydroxyapatite crystals were stable up to 1200 ^{0}C. Generally, inorganic phosphates and pyrophosphate compounds have high thermal stability. Losilla et al. [33] have

reported the synthesis procedure, structural and the thermal behaviors of the germanium pyrophosphates. Weil [34] studied the thermal behavior of mercury pyrophosphate dihydrate crystals. Mercury pyrophosphate crystals become anhydrous, upon heating above 160°C, with the liberation of both water molecules simultaneously. Thus formed anhydrous $Hg_2P_2O_7$ remains stable up to 660°C and beyond this temperature it decomposes completely. Recently, Jackson and Wright [35] have developed the new synthesis route of calcium pyrophosphate and also studied the thermal behavior.

Figure (7.3) shows the thermogram of CPPT crystals. From the thermogram it can be observed that the sample losses all four water molecules slowly around 110 ^{0}C and becomes anhydrous. A small change at 280 ^{0}C indicates some phase transitions. Anhydrous sample remains stable up to 900 ^{0}C, which is regarded as the high thermal stability of CPP. The observed weight loss earlier than 100 ^{0}C, suggests that one of the water molecules may be attached by the hydrogen bond. Table (7.3) indicates the dehydration process of CPPT crystals along with the theoretically calculated and experimentally obtained percentage weight.
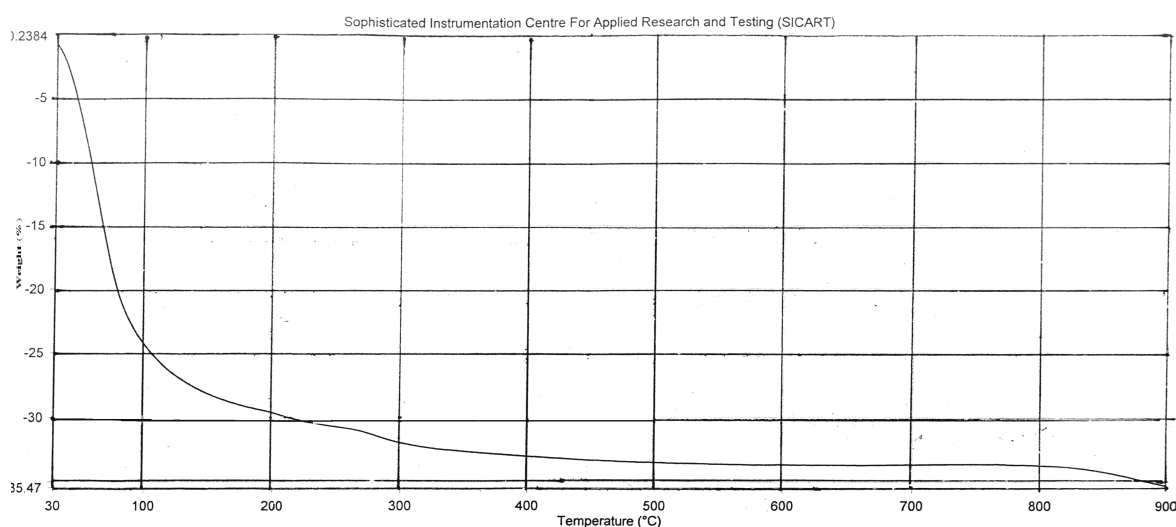
Figure (7.3): Thermogram of CPPT crystals

It can be seen from table (7.3) that both the results were matching well. However, in the present case, four water molecules are found to be present in the crystals.

Table (7.3)

The dehydration process of CPPT crystals and TG results

Temperature (^0C)	Substance	Theoretical weight (%) (Calculated)	Practical weight (%) (from graph)
Room Temperature	$Ca_2P_2O_7 \cdot 4H_2O$	100	100
110 ^0C	$Ca_2P_2O_7$	75.86 %	76.2 %

7.4.2 Kinetic Study of Dehydration:

The Coats and Redfern relation [36] is used for the calculation of various kinetic parameters of the dehydration process for the CPPT crystals. The Coats and Redfern relation is elaborately discussed in the section 6.4.2 of Chapter-VI. Figure (7.4) represents the best linear fitted plot of the Coats and Redfern relation for *n=5/2,* where *n* represents the order of reaction.
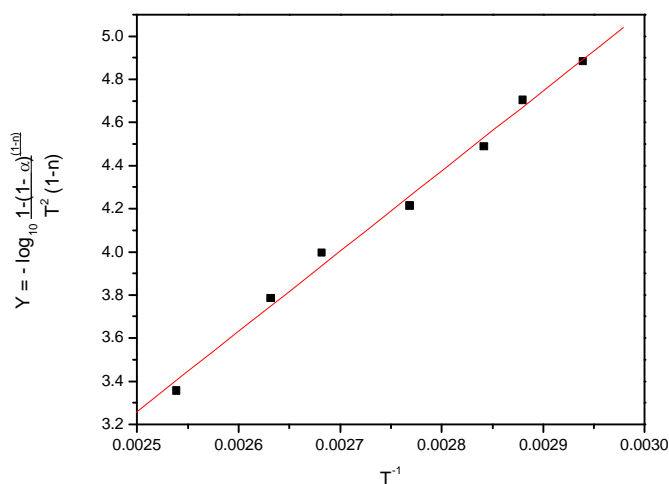
Figure (7.4): Plot of Coats and Redfern relation for CPPT crystals

The values of frequency factor and activation energy are estimated from equation (6.1) of section (6.4.2) of Chapter-VI, which are found to be 2.729 X 10^{19} and 71.214 kJMol^{-1}, respectively, for CPPT crystals.

Table (7.4)

The values of different kinetic parameters obtained from the Coats and Redfern relation for CPPT crystals

Samples	Kinetic Parameters
Calcium pyrophosphate tetrahydrate	Order of reaction (n) = 5/2
	Activation energy (E) = 71.214 kJMol^{-1}
	Frequency factor (A) = 2.729 X 10^{19}

7.4. 3 Thermodynamic Parameters: -

Various thermodynamic parameters have been evaluated from the dehydration stage of thermogram of CPPT crystals by using formulae given in the section 6.4.3 of Chapter -VI. The value of standard entropy ($Ä^{\#}S°$) was calculated using the value of frequency factor obtained from the Coats and Redfern relation. The value of standard enthalpy of activation ($Ä^{\#}H°$), standard change in internal energy ($Ä^{\#}U°$) and standard change in Gibbs free energy ($Ä^{\#}G°$) were estimated for CPPT crystals, which are listed in Table (7.5)

Table (7.5)

The values of different thermodynamic parameters for dehydration of CPPT crystals

Calcium pyrophosphate tetrahydrate crystals	Entropy $Ä^{\#}S° =$ 125.32 J mol^{-1}
	Enthalpy $Ä^{\#}H° = $ - 65.013 kJ Mol $^{-1}$
	Gibbs free energy $Ä^{\#}G°=$ -111.619 kJ Mol $^{-1}$
	Standard change in internal energy $Ä^{\#}U°$ = 68.113 kJ Mol $^{-1}$

The value of $Ä^{\#}G°$ is negative for spontaneous process. The negative value of $Ä^{\#}H°$ and the positive value of $Ä^{\#}S°$ suggest spontaneous type nature under all conditions.

7.4.4 FT-IR Spectroscopic Studies: -

Various researchers have reported the infrared spectroscopic studies of different bio-materials including different phosphates and pyrophosphate compounds [29, 32, 37-39]. Victoria and Gnanam [40] have reported the synthesis and characterization of biphasic calcium phosphate; consisting of hydroxyapatite (HA) and tricalcium phosphate. From the FT-IR study, they reported that above 800 ^{0}C the OH^{-1} bond deficient HA was reduced drastically. Derfus et al. [41] have studied the *in vitro* generation of both CPPD and HA crystals by human osteoarthritic cartilage matrix vesicles (OCMV) and confirmed the results using FT-IR spectroscopy. Several studies have been reported on different pyrophosphate compounds; which includes the study of the FT-IR spectrum of the cadmium calcium pyrophosphate [39]; the synthesis and structure determination of germanium pyrophosphate [33]; and recently, the hydrothermal growth of potassium iron (III) pyrophosphate crystals and its FT-IR spectral study [42].

Figure (7.5) describes the chemical structure of CPP molecule. It can be observed that the P-O bonds and Ca-O bonds are present in the molecule.
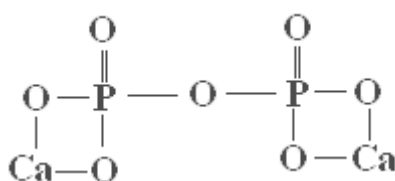
Figure (7.5): Chemical structure of CPP molecule

Figure (7.6) shows the FT-IR spectrum of the CPPT crystals, which was recorded, using KBr medium, on Shimadzu 8400 instrument in the range of 400 cm^{-1} to 4000 cm^{-1}.

Figure (7.6) indicates that the absorptions at 3558.4 cm^{-1} and 3153.4 cm^{-1} are due to the O-H stretching vibrations.
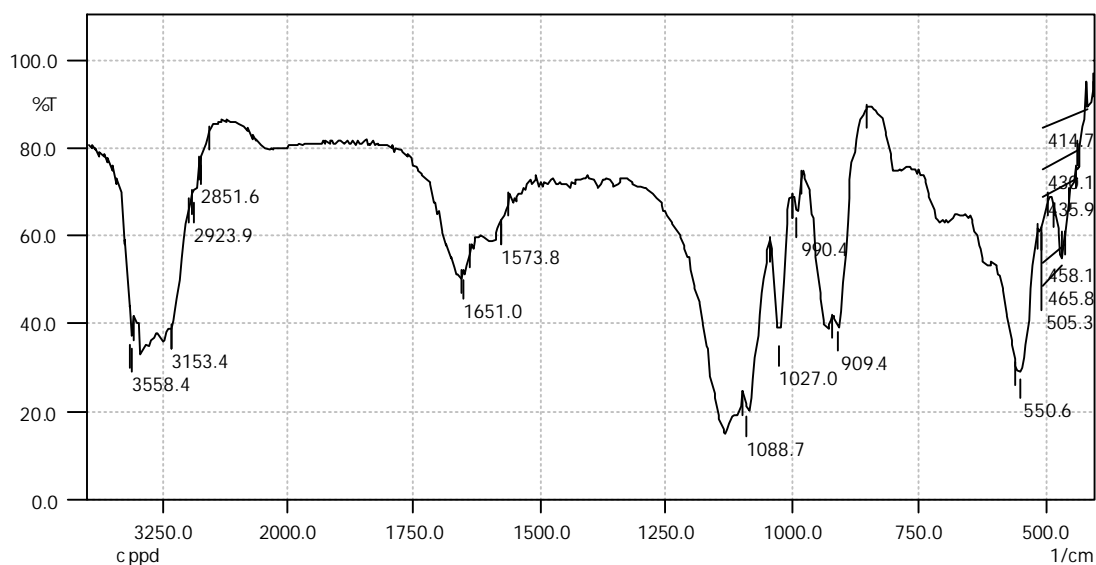
Figure (7.6): FTIR spectrum of CPPT crystals

The O-H plane-bending vibration is indicated by absorption at 1651.0 cm^{-1}. The O-P-O bending is recorded at 550.6 cm^{-1} and 505.3 cm^{-1}. The P-O symmetric stretching vibrations correspond the absorptions occurring at 909.4 cm^{-1} and 990.4 cm^{-1}, whereas the asymmetric stretching vibrations give rise to absorptions at 1027.0 cm^{-1} and 1088.7 cm^{-1}. The absorptions between 400 cm^{-1} to 520 cm^{-1} are due to the presences of oxygen-calcium bonds. Table (7.6) represents the assignments of different absorption bands in FT-IR spectrum of CPPT crystals**.**

Table (7.6)

Assignments of different absorption bands in the FT-IR spectrum of CPPT crystals

Calcium Pyrophosphate Tetrahydrate (Ca$_2$P$_2$O$_7\cdot$ 4H$_2$O)	
Assignments	**Observed frequencies (cm^{-1})**
O–P–O bending	550.6 505.3
P-O Symmetric stretching bonds	909.4 990.4
P-O Asymmetric stretching bonds	1027.0 1088.7
O-H in plane bending	1651.0
O-H Stretching	3558.4 3153.4
Metal-Oxygen bonds	400 to 520

The presence of O–P–O bending, P-O symmetric and asymmetric stretching, O-H bonds and metal-oxygen bonds are confirmed from the FT-IR spectrum of CPPT crystals.

7.4.5 Powder X-ray Diffraction:

Many researchers have paid their attention to the X-ray diffraction study of the various pyrophosphates for structural evaluations. Weil [34] reported crystal growth of mercury (II) pyrophosphate dihydrate crystals. Using four-circle diffractometer they determined the crystal structure of mercury (II) pyrophosphate dihydrate and confirmed that it is isotypic with that of $Ca_2P_2O_7$ $(H_2O)_2$. Moreover, Losilla et al. [33] have reported crystal growth and structure determination of germanium pyrophosphate.

The CPPD crystals exist in at least two polymorphs, one is triclinic (denoted t-CPPD) [27] and the other is monoclinic (denoted m-CPPD), [16, 43]. Both forms have been observed *in vivo* by Pritzker et al [44]. The existence of a third hexagonal polymorph prepared *in vitro* was also suggested by Mandel et al [43]. Besides t-CPPD and m-CPPD, a tetrahydrate $Ca_2P_2O_7 \cdot 4H_2O$ (denoted as CPPT) is also common in precipitates formed *in vitro* around neutral and acidic pH. The tetrahydrate is also polymorphic; with one monoclinic form of a known structure [45], and another orthorhombic form. The microscopic investigations of crystal morphology [16] and the indexing of powder patterns have been reported for the orthorhombic form [43]. Baliæ-Žuniæ et al. [24] have determined the structure of CPPT and reported that the CPPT crystal is having monoclinic system with *P2₁ / C* space group. The unit cell parameters are as follows.

a =12.287 Å, b= 7.511 Å,   c = 10.677 Å and   â = 112.57 (1)⁰
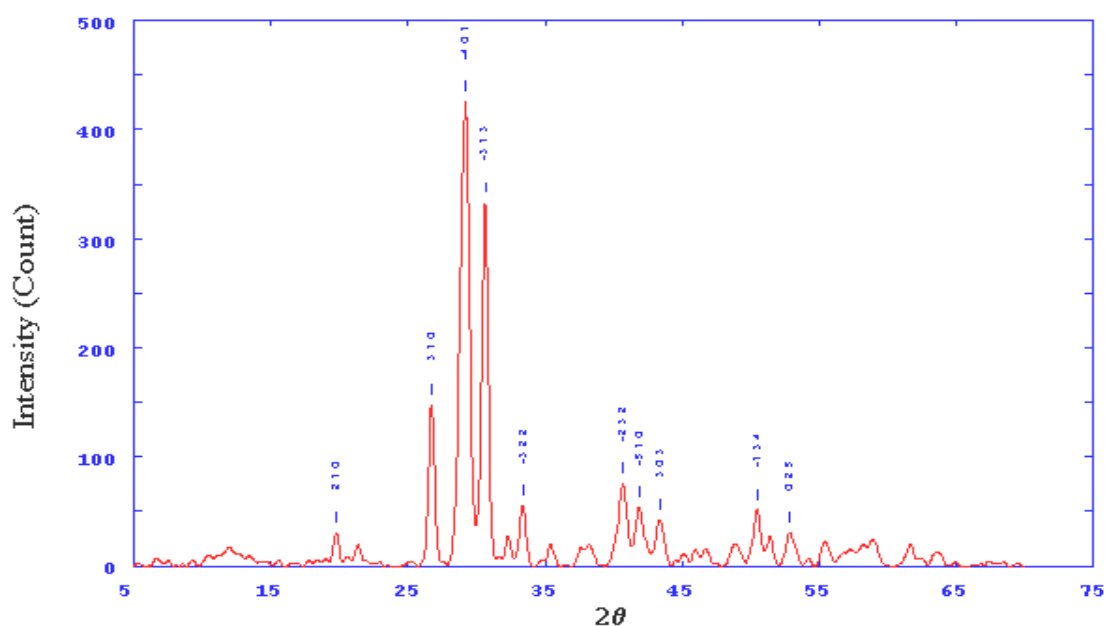
Figure (7.7): Powder X-ray diffractogram of CPPT crystals

The grown crystals were crushed into a fine powder form in a conventional manner for the powder XRD study. The powder XRD data were analyzed using Powder-X [46] computer software. The *h, k,* and *l* parameters as well as *d* and *2è* values are generated by the software in such a way that these values match with the X-ray powder diffraction pattern. Figure (7.7) shows the Powder X-ray diffractogram of the CPPT crystals and Table (7.7) gives Powder XRD results. The estimated values of cell parameters of CPPT are as follows.

a $=12.287\,\text{Å},$ *b*$= 7.511\,\text{Å},$ *c* $= 10.675\,\text{Å}$ and $\hat{a} = 113.57^0$

The present investigation suggests that the cell parameters are very closely matching with the values reported by Baliæ-Žuniæ et al. [24], within the limits of estimated standard deviation.

Table (7.7)

X-ray diffraction results for CPPT crystals

2è Degree	Relative Intensity (%)	d ( )	(h k l)
19.768	30.88	4.49093	(2 1 0)
26.721	148.29	3.33611	(3 1 0)
29.212	425.66	3.05707	(-4 0 1)
30.632	332.85	2.91849	(-3 1 3)
33.372	55.36	2.68481	(-3 2 2)
40.666	75.54	2.21855	(-2 3 2)
41.861	53.98	2.15794	(-5 1 0)
43.359	42.41	2.08680	(3 0 3)
50.465	51.69	1.80837	(-1 3 4)
52.851	30.63	1.73220	(0 2 5)

Makovicky and Balic-Zunic [24] have carried out the detailed crystal structure study of the â form of the CPPT crystal; their important results are complied in Table (7.8).

Generally, the pyrophosphate anion has characteristics similar to the other two known calcium pyrophosphate hydrate structures [27, 45]. The $P–O_B$ (B denotes bridging) distances are significantly longer than the $P–O_T$ (T denotes terminal) and the $P–O_B–P$ angle of 134^0 is relatively small. O atoms are situated at the vertices of the almost ideal tetrahedra surrounding the P atoms. The polyhedral volume distortions are under 1% when compared to an ideal tetrahedron [47]. Compared with the other two structures the main distinction is a smaller volume of the one tetrahedron (P1), most probably caused by a relatively short P1–O7 bond. O7, which is a terminal atom, is not bound to any Ca; while in the other two structures only the bridging O atoms do not bind to any Ca. The Ca atoms are seven-coordinated, as in the other two known calcium pyrophosphate hydrate structures. The two coordination modes in t-CPPD were already described as these two distinct types [27]. The following figure (7.8) gives the details of atomic coordination with the appropriate labeling.

Table (7.8)

Experimental details [24]

Crystal data	
Chemical formula	$Ca_2P_2O_7 \cdot 4H_2O$
Chemical formula weight	326.16
Cell setting	Monoclinic
Space group	P21/c
a (Å)	12.287 (6)
b (Å)	7.511 (3)
c (Å)	10.775 (5)
â (º)	112.542 (14)
V (Å^3)	918.4 (7)
Z	4
Dx (Mg m^{-3})	2.359
Radiation type	Mo Ká
Wavelength (Å)	0.71073
No. of reflections for cell parameters	173
ì (mm^{-1})	1.639
Temperature (K)	298 (2)
Crystal form	{100},{001},{011}
Crystal size (mm)	0.243 X 0.055 X 0.009
Crystal colour	Colourless
Data collection	
Absorption correction	Gaussian face-indexed
T$_{min}$	0.89064
T$_{max}$	0.98700
No. of measured reflections	2928
No. of independent reflections	959
No. of observed reflections	432
Criterion for observed reflections	I > 2ó(I)
è max(º)	20.80
Refinement	
Refinement on	F^2
Source of atomic scattering factors	International Tables for Crystallography, (1992, Vol. C, Tables 4.2.6.8 and 6.1.1.4)
Computer programs	
Structure solution	SHELXS97 (Sheldrick, 1990)
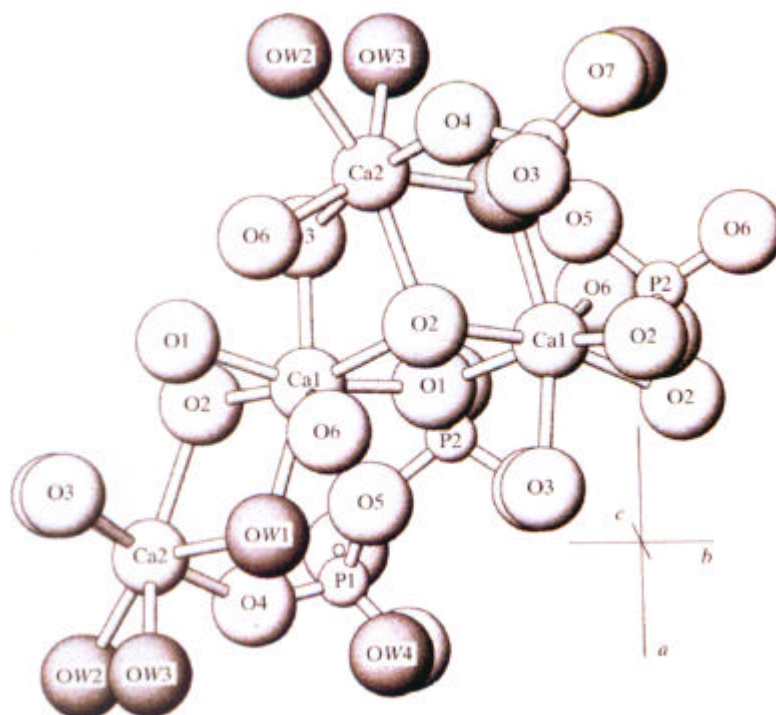
Figure (7.8): Details of atomic coordination

Table (7.9)

Atomic coordination of the CPPT crystals

Ions	x	y	z
Ca1	0.4691	0.0022	0.7271
Ca2	0.2613	0.1473	0.3157
P1	0.7424	0.0268	0.9849
P2	0.5607	0.2385	0.5199
O1	0.5129	0.2410	0.1263
O2	0.4707	0.2434	0.8748
O3	0.6795	0.0141	0.8352
O4	0.2187	0.1544	0.9504
O5	0.6512	0.0938	0.0491
O6	0.6311	0.0693	0.5232
O7	0.8390	0.1595	0.0257
OW1	0.2649	0.0895	0.6711
OW2	0.8827	0.0078	0.6201
OW3	0.0776	0.1621	0.1167
OW4	0.8928	0.1621	0.3290

Four of the O atoms in the asymmetric unit are not bound to P and are supposed to be O atoms of water. The hydrogen bonds are supposed to be oriented towards the closely situated other O atoms of water or `under-bonded' O atoms from the pyrophosphate groups. Table (7.9) gives the final atomic coordination of the CPPT crystals. The OW1 atoms are shared by both Ca1 and Ca2 polyhydra and reside relatively deep inside the layers. Remaining O atoms of water are situated on the surface of layers. OW2 and OW3 are bound to Ca2, while the OW4 atoms do not come close to any Ca atom. The O7 terminal atoms from the pyrophosphate group, which also do not bind to any Ca, reside on the surfaces of layers. The OW3 atoms, which protrude farthest from the surface of one layer face of O7 atoms (distance 2.71), sit deepest on the surface of the neighboring layer. OW2 and OW4, which have equal medium heights on the surface and face each other on neighboring layers (distance 2.90). The other potential hydrogen bonds can be connected to the contacts of water O atoms inside a layer, mutual or with atoms O4, O6 and O7. Brown and Altermat [48] as well as Brese and O'Keeffe [49] have calculated the bond-valance calculations without the consideration of hydrogen bond contributions. OW4 atoms do not coordinate any Ca atom and are thus held in the structure solely by hydrogen bonding to other O atoms. This specific nature of a quarter of the water molecules in the structure is also confirmed by thermal analysis which has shown the loss of one H_2O molecule occurring at 353 K [19].

Figure (7.9) shows the projection of the crystal structure parallel to (001) plane. The main characteristic of the structure is the layers formed by the chains of Ca coordination polyhydra interconnected by pyrophosphate groups. Whereas, figure (7.10) shows the structural layer projected on the (100) plane.
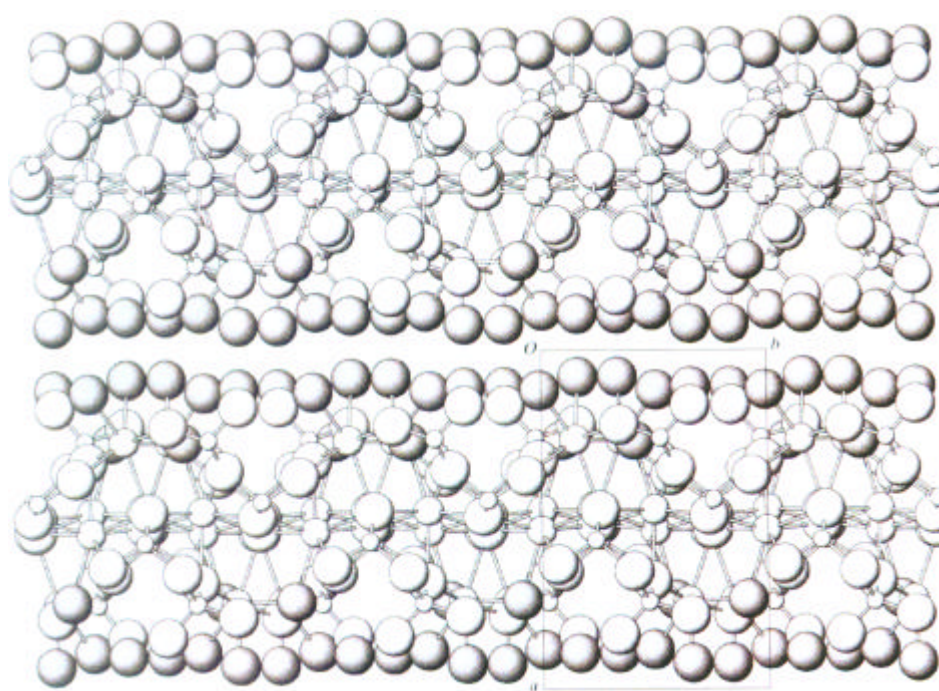
Figure (7.9): **The projection of the crystal structure parallel to (001) plane. Atoms in ascending size are P, Ca, and O, and darker coloring of O is for water.**
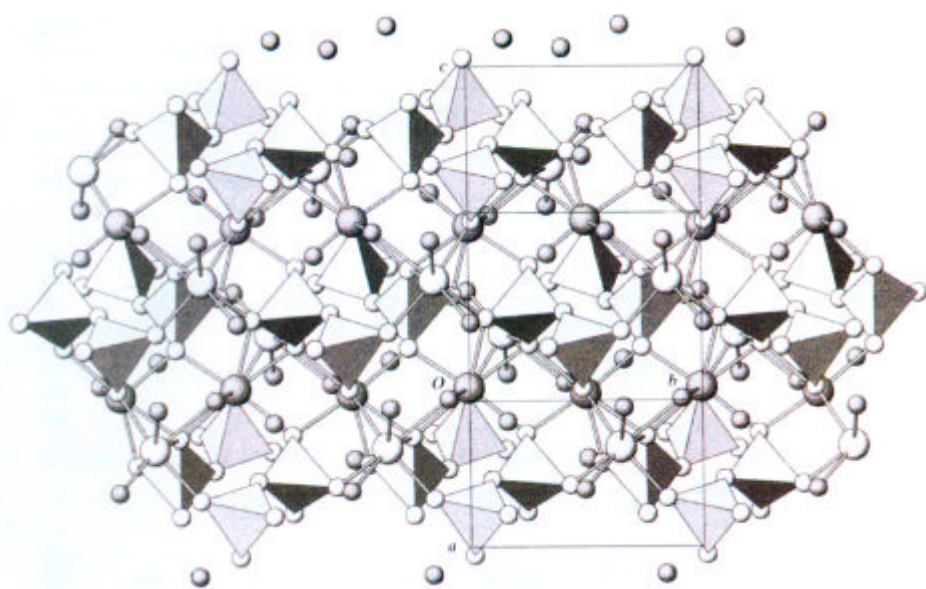
Figure (7.10): The structural layer projected on the (100) plane. Pyrophosphate groups represented as opaque polyhydra. Ca1 as well as water O atoms are colored darker

From the above study, it is confirmed that CPPT crystals are monoclinic having space group $P2_1/c$ and five of the terminal O atoms from a pyrophosphate group bind to Ca atoms, together with O atoms from three of the water molecules. The fourth water molecule forms only hydrogen bonds.

7.4.6   Dielectric Studies of CPPT Crystals:

The dielectric study of pyrophosphate compounds, to the best of the present author's knowledge, is not widely reported. Hitmi et al. [50] have reported the dielectric study of various phosphate compounds, i.e. various apataites, and reported that at high temperatures the dielectric loss occurs due to the dipolar reorientation of ions inside apatite channels. Bian et al. [51] have reported the microwave dielectric properties of the CPP.

In the present study, the values of capacitance were measured using the precession LCR meter, model Agilent *4284A*, at room temperature. The following figure (7.11) shows the variation of dielectric constant with frequency.
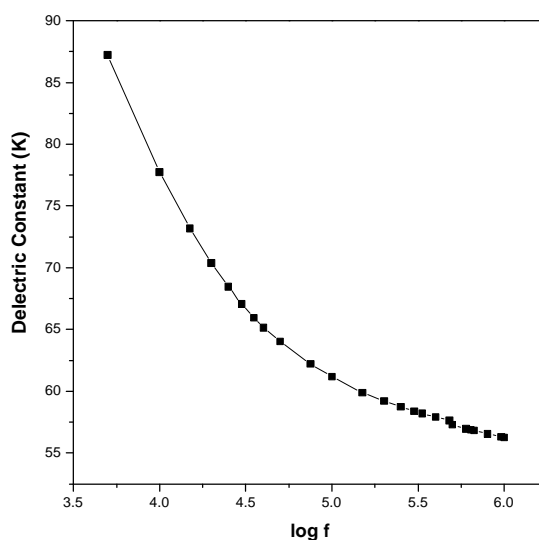
Figure (7.11): Plot of dielectric constant versus *log f*

It can be noticed from the above plot that the dielectric constant decreases as the frequency increase. Initially, the dielectric constant decreases rapidly with increasing frequency and then slowly decreases at higher frequency. This type of behavior

indicates higher space charge polarizability of the material in the low frequency region. As the frequency increases, the dipoles do not comply with the varying external field. Therefore, the polarization decreases and hence the values of dielectric constant decrease as the frequency increases [52]. This behavior is similar to the nature reported by Lopez et al. [53] and Dabhi et al. [54] for zinc tartrate crystals and Arora et al. [55] for strontium tartrate crystals, at room temperature.

Figure (7.12) represents the plot of *tan ä* versus *log f* at room temperature. From this figure it can be noticed that as the frequency increases the loss tangent decreases.
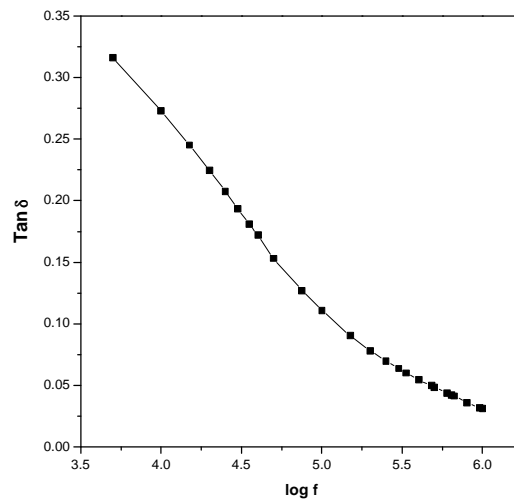
Figure (7.12): Plot of *tan ä* versus *log f*
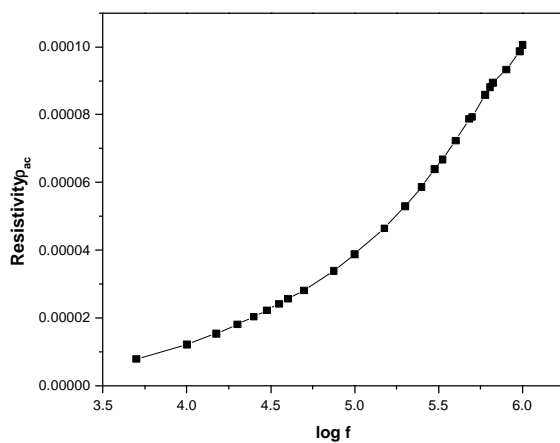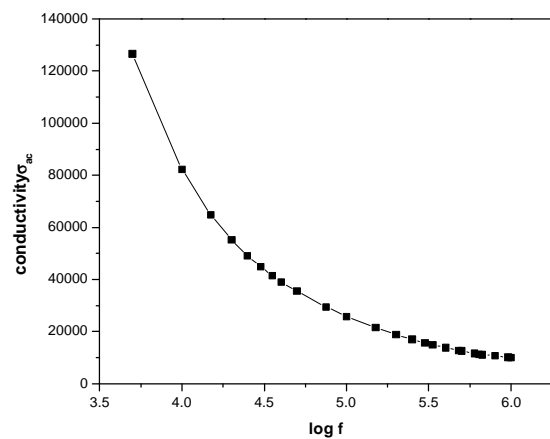
Figure (7.13 a)

Figure (7.13 b)

Figure (7.13 a & b): The plot of a.c. resistivity ($\tilde{n}_{ac}$) and a.c. conductivity ($\acute{o}_{ac}$)

versus *log f*, respectively

Figure (7.13 a & b) shows the plots of a. c. resistivity and conductivity versus frequency. The a.c. resistivity ($\tilde{n}_{ac}$) and a.c. conductivity ($\acute{o}_{ac}$) were calculated using the formulae (5.21 a & b) given in the section 5.4.3 of Chapter-V. From the plots it can be noticed that as the frequency increases, the a.c. resistivity increases and hence the a.c. conductivity decreases.

7.5   *In vitro* **Inhibition Study of the CPPT crystals for Different Extracts:**

Various calcium phosphates and pyrophosphates are associated with different ailments, such as urinary stones and arthropathies. Deposition of CPPD, in articular cartilage in aged humans, can lead to acute arthritic attack with severe pain and inflammation of the affected joints, called pseudo-gout [1-6]. Therefore, many researchers have focused their attention on the growth kinetics, growth mechanism, growth-inhibition and dissolution of CPPD crystals [19, 20]. The inhibitive effect of various metallic ions, for example, ferrous and ferric [56], magnesium and calcium [57] and carboxylate [58], have been studied on CPPD crystals; while, Cheung et al. [59] have reported CPPD inhibition through phosphocitrate. Also, Hunter et al. [60] have reported the effect of glycosaminoglycans on CPPD formation in collagen gels. More recently, Christoffersen et al. [19, 61] have studied the kinetics and mechanisms of growth and dissolution of t-CPPD and m-CPPT crystals. From the study, they concluded that the auto inhibition of crystal growth was found at pH-7.0 for m-CPPT crystals.

In the present study, the single diffusion gel growth technique was used to study the growth and inhibition behaviour of CPPT crystals in the presence of different herbal extracts. Single diffusion gel growth technique provides the simplified model for *in vitro* growth inhibition study of bio-material crystals. The following extracts were used in the present study.

(1)   *Rotula aquatica root*

(2)   *Boerhaavia diffusa root*

(3)   *Commiphora wightii*

The growth of CPPT crystals is already discussed earlier in the section 7.3. In order to study the growth inhibition behaviour of the CPPT crystals, 10 ml of 2% (20mg/ml) concentrated solutions of different extracts were used. A 10 ml of selected extract solution was mixed with calcium nitrate tetrahydrate solution in equal volume. The mixture of selected extract and calcium nitrate tetrahydrate solutions was gently poured on the set gel in respective test tubes. Inhibition study was carried out by considering two parameters, viz. the number of the crystals grown and the total diffusion length in the gel. Figure (7.14) exhibits the growth of CPPT crystals in the presence of different herbal extracts.
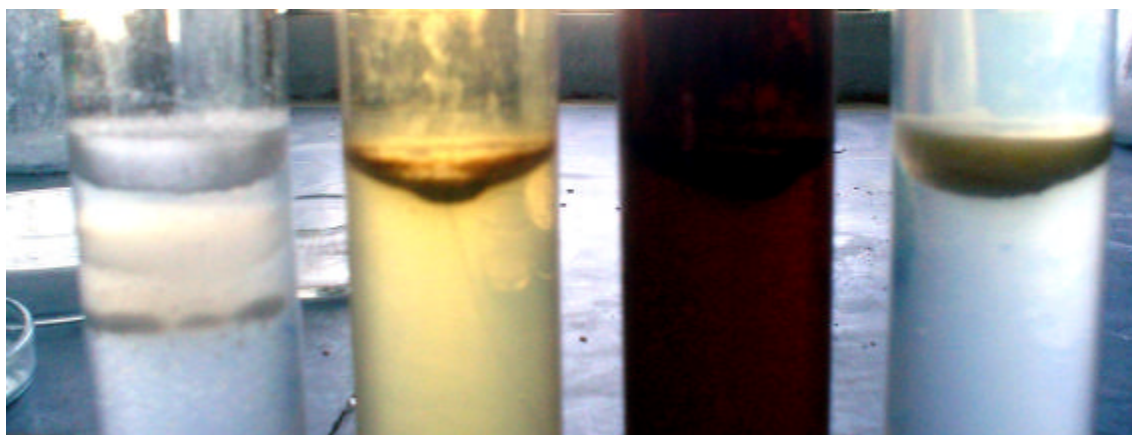
Pure Ca(NO$_3$)$_2$ **B. diffusa**   **R. aquatica**   **C. wightii**

Figure (7.14): Comparative growth-inhibition study of CPPT crystals

When pure calcium nitrate tetrahydrate solution was used, a thick, white particles band of CPPT crystals was observed below the gel liquid interface. Below this a band of tiny, transparent, spherical granules type crystals was observed. The diameter of crystals was of the order of 0.4 mm. The number of grown crystals was

very large. Below this, once again a thin white band of CPPT was observed and, there after, again numbers of tiny crystals were observed. From the gel-liquid interface the total diffusion length in to the gel was 2.8 cm.

In case of aqueous extract of *R. aquatica*, a thick band of CPPT particles was observed within 48 hours of pouring solutions and, thereafter, the band remained the same in thickness. The thickness of the band was 1.2 cm. Interestingly, below this band no crystals of CPPT were grown within 96 hours of pouring solutions. After 120 hours of pouring the solution, three small crystals were grown and six crystals were observed after 168 hours. The diameters of the crystals were of the order of 0.5 mm. From the gel-liquid interface the total diffusion into the gel was 2. 0 cm.

When the solution of aqueous extract of *B. diffusa* was used, a thick band of CPPT particles of 0.8 cm width was observed within 48 hours of pouring solutions. Below this band, only two small crystals were grown after 120 hours and four crystals were observed after 168 hours. It was found that the total diffusion into the gel was 1.6 cm from the gel-liquid interface.

Very encouraging results were obtained in the case of *C. wightii.* No band of CPPT particles was observed, only two tiny crystals were observed after 48 hours of pouring the solutions and four tiny crystals were observed after 168 hours. The diameter of the crystals was of the order of 0.5 mm. The total diffusion length into gel, from the gel-liquid interface, was estimated to be 0.8 cm. Table (7.10) represents the number of crystals grown and the total diffusion length in the presence of different herbal extracts. It is to be noted that calcium nitrate tetrahydrate solution served as a control solution. Whereas, the table (7.11) gives the growth behaviour data of CPPT crystals.

Table (7.10)

Comparative growth inhibition study of CPPT crystals in the presence of different herbal extracts

No.	Supernatant solution	Total number of crystals grown	Total diffusion length
1	Cacium nitrate	Innumerable	2.8 cm
2	Cacium nitrate + *Rotula aquatica*	6	2.0 cm
3	Cacium nitrate + *Boerhaavia diffusa*	4	1.6 cm
4	Cacium nitrate + *Commiphora wightii*	4	No band

Table (7.11)

Growth behaviour of CPPT crystals

No.	Supernatant solution	Number of crystals grown (in hours after pouring the supernatant solutions)			
		48 hr	96 hr (Below Thick band)	120 hrs (Below Thick band)	168 hrs (Below Thick band)
1	Cacium nitrate	Innumerable			
2	Cacium nitrate + *Rotula aquatica*	1.2 cm (Thick band)	Nil	3	6
3	Cacium nitrate + *Boerhaavia diffusa*	0.8 cm (Thick band)	Nil	2	4
4	Cacium nitrate + *Commiphora wightii*	2 crystals	3	3	4
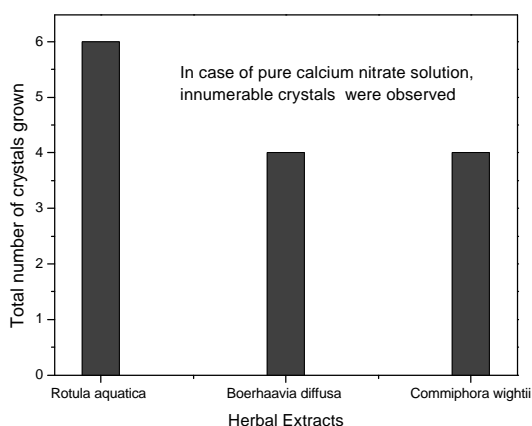
Figure (7.15 a)
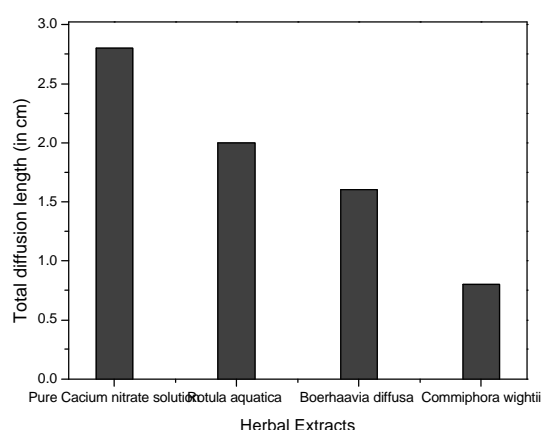
Figure (7.15 b)

Figure (7.15 a & b): Histograms, exhibit the comparison of the number of the crystals and total diffusion length, respectively, in the presence of different herbal extracts.
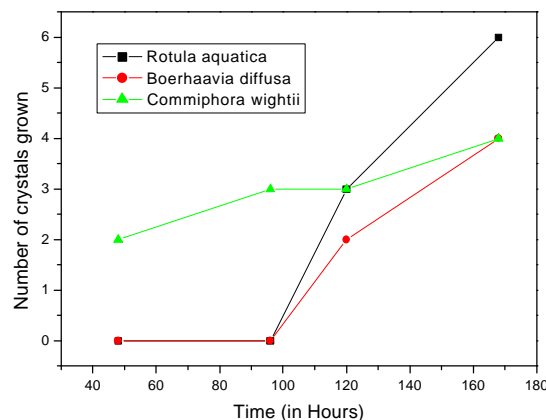
Figure (7.16): Plots of number of crystals versus time (in hours) for different

herbal extracts.

Figure (7.15 a & b) shows the histograms, giving the comparison of the number of the crystals grown and the total diffusion length, respectively, in the presence of different herbal extracts, Moreover, figure (7.16) presents the plots of number of crystals versus time (in hours) for different herbal extracts containing supernatant solutions. Figure (7.16) indicates that the maximum number of crystals was found in the case of *R. aquatica,* while *B. diffusa* and *C. wightii* gave equal number of crystals.

From the above study one can notice that all the three extracts show good inhibition with comparison to the pure calcium nitrate solution. The number of crystals is very large in the pure calcium nitrate solution, but due to competition in the growth between different crystals the average diameter of crystals is comparatively less. However, the best inhibition was observed in the case of *C. wightii* followed by *B. diffusa* and *R. aquatica.*

7.6   Conclusion:

(1)   CPPT crystal growth was carried out by using single diffusion gel growth technique in normal test tubes. Good quality, transparent, spherical granules type crystals were grown. The crystals were very small and the diameter of the crystals was of the order of 0.5 mm. CPPT crystals have also been grown

using the wet chemical process and the size of grown crystals were less than 90.80 micron.

(2)   CPPT crystals showed very high thermal stability. From the calculation, it was noticed that four water molecules were associated with the crystals. Nearly at 110 ^{0}C, CPPT crystal gave up all four water molecules and gradually became anhydrous. Anhydrous sample remained stable up to 900 ^{0}C. Dehydration process started from 80 ^{0}C, because one of the water molecules was attached with the hydrogen bond. Small hump in the thermogram was observed at 280 ^{0}C , which might be due to phase transitions.

(3)   Applying the Coats and Redfern relation to the dehydration stage of the thermogram, the kinetic parameters, such as, order of reaction and activation energy, were evaluated. The values of order of reaction and activation energy were found to be 5/2 and 72.214 kJ Mol^{-1}, respectively.

(4)   The thermodynamic parameters were also evaluated for the dehydration process from the thermogram. The values of the standard change in entropy, enthalpy and Gibbs free energy were found to be 125.32 J mol^{-1}, - 65.013 kJ mol $^{-1}$ and -111.619 kJ mol $^{-1}$, respectively. This suggested the spontaneous type process.

(5)   The FT-IR spectrum confirmed the presence of the O-P-O bending, P-O symmetric and asymmetric stretching, O-H bending and stretching and oxygen-calcium bonds.

(6)   The results of powder X-ray diffraction (XRD) analysis s suggested that CPPT crystal was having monoclinic system with *P2$_1$ / C* space group. The unit cell parameters of CPPT crystals were obtained as follows

a =12.287   *b= 7.511*   *c = 10.675*   and   *â = 113.57^0*

The estimated values of cell parameters were appreciably matching with the values reported by Balic-Zunic et al [24]. In the CPPT crystal structure, five of the terminal O atoms from a pyrophosphate group bind to Ca atoms together with O atoms from three of the water molecules. The fourth water molecule is attached with hydrogen bond.

(7) For CPPT crystals the values of dielectric constant decreased as frequency increased. Initially, the dielectric constant decreased rapidly with increasing frequency and then decreased very slowly. This type of behaviour suggested the presence of higher space charge polarizability of the material in the low frequency region, and as the frequency increased a point was reached where the space charge could not sustain and comply with the varying external field. Therefore, the polarization decreased and hence exhibited reduction in the values of dielectric constant. The variation of *tan ä* versus *log f* suggested that as the frequency increased the loss decreased. The variation of a.c. resistivity with *log f* indicated that as the frequency increased the value of a.c. resistivity increased and hence the value of a.c. conductivity decreased.

(8) Three different medicinal herbal extracts were used to study the growth inhibition of CPPT crystals. The growth-inhibition study of CPPT crystals was carried out by measuring the number of crystals grown and the total diffusion length in the gel column. All the three aqueous extracts studied, namely, *R. aquatica, B. diffusa* and *C.wightti,* were giving good results in terms of less number of crystals grown and less diffusion length in the gel the column, with comparison to pure calcium nitrate solution. The test tubes having pure calcium nitrate were used as a control. However, *C. wightti* showed the best inhibition results for CPPT crystals.

References:

[1]   D. J. McCarty; *"In Arthritis and Allied Conditions"*, W. J. Koopman Ed; Williams and Wilkins: Baltimore, (1997) 81.

[2]   L. M. Ryan and D. J. McCarty; *"In Arthritis and Allied Conditions"* W. J. Koopman, Ed: Williams and Wilkins; Baltimore, (1997) 2103.

[3]   J. Kaplan; *eMedicine J.*, **2** (2001) 5.

[4]   B. M. Rothschild and M. A. Bruno; *e Medicine J.*, **2** (2001) 12.

[5]   N. J. Barkin; *eMedicine J.,* **3** (2002) 1.

[6]   C. Saadeh, and J. Malacara; *eMedicine J.* **3** (2002) 3.

[7]   S. J. Gupta; *J. Ind. Rheumatol. Assoc.*, **10** (2002) 5.

[8]   G. Fam Adel; *Curr. Opin Rheumatol,* **12** (2000) 228.

[9]   K. Rosenthal Anne; '*Crystal Arthopathies'*. P. J. Maddison, D. A. Isenberg, P. Woo & D. A. Glass Eds. Oxford Text book of Rheumatology 2nd Edn. Oxford University Press, (1998) 1567.

[10]   L. M. Ryan and D. J. McCarty; *Ann.Rheum. Dis.,* **54** (1995) 939.

[11]   D. J. McCarty; *Dis. Month,* **40** (1994) 260.

[12]   K. P. H. Pritzker; *J. Am. Geriatr. Soc.,* **28** (1980) 439.

[13]   A. Beutler, S. Rothfuss, G. Clayburne, M. Sieck and H. R. Schumaker; *Arthritis Rheum.* **36** (1993) 704.

[14]   A. Swan, B. Chapman, P. Heap, H. Seward, and P. Dieppe, *Ann. Rheum. Dis.,* **53** (1994) 467.

[15]   A. Swan, B. Heyward, B. Chapman, P. Heap, H. Seward and P. Dieppe; *Ann. Rheum. Dis.,* **54** (1995) 825.

[16]   E. H. Brown, J. R. Lehr, J. P. Smith and A. W. Faizer; *Agri. and Food Chem.* **11(3)** (1963) 214.

[17] A. A. Mirtchi , J. Lemaitre and E. Munting; *Biomaterials,* **10(9)** (1989) 634.

[18] http://www.mercksource.com/pp/us/cns

[19] M. R. Christoffersen, T. Baliæ-Žuniæ, S. Pehrson and J. Christoffersen; *J. Cryst.Growth,* **212** (2000) 500.

[20] M. R. Christoffersen, N. Seierby, T. Baliæ-Žuniæ, and J. Christoffersen; *J. Cryst.Growth,* **203** (1999) 234.

[21] F. H. Lin, C.J. Liao, K. S.Chen, J. S. Sun, and H. C. Liu; *Biomaterials.* **18(13)** (1997) 915.

[22] A. Srinivasan, E. Belanger, J. Woulfe and M. Goyal; *Canad. J Neurol Sci.,* **32(1)** (2005) 109.

[23] '*Merck Index, An Encyclopedia of Chemical and Drugs*', 8th Edition, Ed. Paul G. Stecher, Merck & Co., U.S.A. (1968) p-195.

[24] T. Baliæ-Žuniæ, M. R. Christoffersen and J. Christoffersen; *Acta Cryst.,* **B56** (2000) 953..

[25] http://www.emedicine.com/med/topic1938.htm

[26] Kirk Othmer; *"Encyclopedia of Chemical Technology",* 2nd Ed., Vol.17, Interscience, Division of John Willey & Sons Inc. (1970) p- 456.

[27] N. S. Mandel; *Acta Cryst.* **B31** (1975) 1730.

[28] P. O'Brien and G. Rafelatos; *Crystal Growth and Design,* **3** (2003) 431.

[29] V. S. Joshi and M. J. Joshi; *Cryst. Res. Technol.,* **38 (9)** (2003) 817.

[30] K. V. Shah, V. Sudarsan, M Goswami, A Sarkar, S Manikandan, Rakesh Kumar, B. I. Sharma, V. K. Shrikhande and G. P. Kothiyal; *Bull. Mater. Sci.,* **26-7** (2003) 715.

[31]   R. L. Frost, S. J. Mills and K. L. Erickson; *Thermochimica Acta,* **419(1-2)** (2004) 109.

[32]   M. Ashok, N. Meenakshi Sundaram and S. Narayana Kalkura; *Materials Lett.,* **57** (2003) 2066.

[33]   E. R. Losilla, A. Cabeza, S. Bruque, M. A. G. Aranda, J. Sanz, J. E. Lglesias and J. A. Alonso; *J.l of Solid State Chem.,* **156** (2001) 213.

[34]   M. Weil; *Monatshefte für Chemie / Chemical Monthly,* **134** (2003) 1509.

[35]   L. E. Jackson and A. J. Wright; *Mater. Sci. and Eng.,* **284-286** (2005) 71.

[36]   A. W. Coats and J. P. Redfern; *Nature*, **201** (1964) 68.

[37]   A. Datta, M. Agarwal and S. Dasgupta; *Proc. Indian Acad. Sci.* (*Chem. Sci.*), **114 (4)** (2002) 379.

[38]   B. A. Derfus, S. M. Kurtin, N. P. Camacho, I. Kurup, and L. M. Ryan; *Connect Tissue Res.,* **35(1-4)** (1996) 337.

[39]   D. de Waal and C. Hutter; *Microchimica Acta,* **14** (1997) 243.

[40]   E. C. Victoria and F. D. Gnanam; *Trends. Biomater. Artif. Organs.,* **16** (2002) 12.

[41]   B. Derfus, S. Kranendonk, N. Camacho, N. Mandel, V. Kushnaryov, K. Lynch and L. Ryan; *Calcif. Tissue Int.,* **63** (1998) 258.

[42]   G. S. Gopalakrishna, B. H. Doreswamy, M. J. Mahesh, M. Mahendra, M. A. Sridhar, J. Shashidhara prasad and K. G. Ashamanjari; *Bull. Mater. Sci.*, **28**(1) (2005) 1.

[43]   G. S. Mandel, K. M. Renne, A. M. Kolbach, W. D. Kaplan, J. D. Miller and N. S. Mandel; *J. Cryst. Growth,* **87** (1988) 453.

[44]   K. P. H. Pritzker; *'Calcium Phosphate in Biological and Industrial Systems'*, Edited by: Z. Amjad, Kluwer Academic Publisheres, Boston (1998) 277.

[45]   N. L. Davis, G. S. Mandel, N. S. Mandel and R. E. Dikerson; *J. Crystallogr. Spectrosc. Res.* **15** (1985) 513.

[46]   www.ccp14.ac.uk

[47]   E. Makovicky and T. Balic-Zunic; *Acta Cryst.* **B54** (1998) 766.

[48]   I. D. Brown and D. Altermatt; *Acta Cryst.* **B41** (1985) 244.

[49]   N. E. Brese and M. O'Keeffe; *Acta Cryst.* **B47** (1991) 192.

[50]   N. Hitmi, C. Lacabanne and R. A. Young; *J. Phys. Chem Solids,* **45** (1984) 701.

[51]   J. Bian, D. Kim and K. S. Hong; *J. Euro. Cera. Soc.*, **23(14)** (2003) 2589.

[52]   F. M. Reicha, M. El-Hi-ti, A. Z. El-Sonabati and M. A. Diab; *J. Phys. D; Appl. Phys.,* **24** (1991) 369.

[53]   T. Lopez, J. Stockel, J. Peraza, M. E. Torres and A. C. Yanes; *Cryst. Res. Technol.,* **30** (1995) 677.

[54]   R. M. Dabhi, B. B. Parekh and M. J. Joshi; *Indian J. Phys.* **79(5)** (2005) 503.

[55]   S. K. Arora, V. Patel, B. Amin and A. Kothari; *Bull. Mater. Sci.* **27** (2004) 141.

[56]   P. T. Cheng and K. P. Pritzker; *J. Rheumatol.*, **15(2)** (1988) 321.

[57]   P. T. Cheng and K. P. Pritzker; *J. Rheumatol.*, **8(5)** (1981) 772.

[58]   P. T. Cheng and K. P. Pritzker; *Calcif Tissue Int.,* **42(1)** (1988) 46.

[59] H. S. Cheung, I. V. Kurup, J. D. Sallis and L. M. Ryan; *The Am. Soc. for Biochem. and Mol. Biol.,* **271** (45) (1996) 28082.

[60] G. K. Hunter, M. D. Grynpas, P. T. Cheng and K. P. Pritzker; *Calcif Tissue Int.,* **41(3)** (1987) 164.

[61] M. R. Christoffersen, T. Baliæ-Žuniæ, and J. Christoffersen; *J. Cryst. Growth and Design,* **2(6)** (2002) 567.

Chapter VIII

Growth Inhibition Study of Calcium Hydrogen Phosphate Dihydrate (brushite) Crystals

8.1   Introduction:

Urinary calculi are hard the masses developed from crystals that separate from the urine and build up on the inner surfaces of the kidney or urinary tract [1]. Many factors affect the urinary calculi formation; particularly, different mineral metabolisms are the most important factors in the formation of urinary calculi [2]. Urinary calculi are mainly composed of crystalline components. Multiple steps are involved in the formation of calculi, which are nucleation, growth and aggregation [3]. There are several theories for the formation of the urinary calculi [3-6]. Briefly, the cause of formation of urinary calculi can be due to the one of the following reasons [7].

(1)   By an augmentation of concentration of salts beyond the supersaturation capacity of urine.

(2)   By a decreased supersaturation capacity of urine.

(3)   By the presence of promoter, this promotes the crystallization of   substances responsible for urinary calculi.

More details about the mechanisms and pathophysiology of urinary calculi formation are given in Chapter-II.

Among all the varieties of urinary calculi, 75 % of them are containing calcium salts. Calcium is present in urinary calculi as calcium oxalate (either monohydrate or dihydrate, or a combination of both) and much less commonly

available as calcium phosphate, but mixed calcium calculi (containing both calcium phosphate and calcium oxalate) are more common than calcium phosphate calculi. Calcium phosphate is present in urinary calculi as either calcium apatite $(Ca_{10}(PO_4)_6(OH)_2)$ or calcium hydrogen phosphate dihydrate (CHPD, $CaHPO_4 \cdot 2H_2O$). The CHPD is also known as brushite [3].

Urinary calculi are one of the most painful urological disorders; hence many researchers have reported the growth inhibition study of CHPD as well as calcium oxalate monohydrate (COM) or calcium oxalate dihydrated (COD) type urinary crystals [8-11]. Many compounds have been identified as inhibitors of calcium oxalate as well as CHPD crystal growth, for example, tartrates in natural and artificial urine media [8], some amino acids [9], citrate [10], polyhydroxycarboxylic acids [11].

In the present study, macro size and micro size CHPD crystals were grown by using single diffusion gel growth technique and modified gel growth technique, respectively. The modified gel growth techniques was developed by the present author for achieving rapid crystallization of some bio-materials and study the inhibition effect of different solutions on them. This technique provides results of inhibition study of CHPD crystals very rapidly and *in situ* observations are possible.

Different concentrations of citric acid and tartaric acid were used to study the inhibition or the dissolution of already grown CHPD crystals. It is important to note that tartaric acid and citric acid are available in plenty in certain fruits, such as tamarind, grapes, lemon, etc. Therefore, it has been chosen to study the growth inhibition or dissolution of CHPD crystals using these acids.

8.2   Physical and Chemical Properties of CHPD (Brushite):

Brushite or CHPD, is naturally occurring mineral and it is formed at low pH by reaction of phosphate-rich solutions with calcite and clay [12, 13]. Pettit and

Lemaitre [14] studied the working characteristics of radio-opacified brushite cements. Also, Brendlen et al. [15] have studied the feasibility of dual-paste presentation of injectable brushite cements. Table (8.1) lists the physical and chemical properties of brushite.

Table (8.1)

Physical and chemical properties of CHPD [12, 13]

General Brushite Information	
Chemical Formula:	$CaHPO_4$ $2(H_2O)$
Composition:	Molecular Weight = 172.09 gm
	Calcium 23.29 % Ca 32.59 % CaO
	Phosphorus 18.00 % P 41.24 % P_2O_5
	Hydrogen 2.93 % H 26.17 % H_2O
	Oxygen 55.78 % O
	100.00 % 100.00 % = TOTAL
Empirical Formula:	$Ca(HPO_4)$ $2(H_2O)$
IMA Status:	Valid Species (Pre-IMA) 1865
Locality:	Found on Aves Island, Venezuela, west of Dominica, in the Caribbean Sea.
Name Origin:	To honor Professor George Jarvis Brush (1831-1912), American mineralogist, Yale University, New Haven, Connecticut, USA.
Synonym:	ICSD 16132
	PDF 11-293
Brushite Crystallography	
Cell Dimensions:	a = 5.88 , b = 15.15 , c = 6.37 , beta = 117.467°
Crystal System:	Monoclinic - Prismatic H-M Symbol (2/m) Space Group: I2/a
Physical Properties of Brushite	
Cleavage:	[010] Perfect, [001] Perfect
Color:	Colorless, Yellow, Yellowish white, White.
Density:	2.328
Diaphaniety:	Transparent to Translucent
Hardness:	2.5 - Finger Nail
Optical Properties of Brushite	
Optical Data:	Biaxial (+), a=1.539, b=1.546, g=1.551, bire=0.0120, 2V(Calc)=80, 2V(Meas)=86.
Calculated Properties of Brushite	
Electron Density:	$r_{electron}$=2.38 gm/cc. note: $r_{Brushite}$ =2.33 gm/cc.
Photoelectric:	$PE_{Brushite}$ = 3.72 barns/electron $U=PE_{Brushite}$ x $r_{electron}$= 8.85 barns/cc.
Radioactivity:	GRapi = 0 (Gamma Ray American Petroleum Institute Units) Brushite is Not Radioactive

Characterization of CHPD crystals by TGA, FT-IR and SEM was reported by Joshi and Joshi [16]. They calculated kinetic and thermodynamic parameters of dehydration from thermogram.

Generally, Phosphates of calcium are present in urinary calculi as either apatite $[Ca_{10}(PO_4)_6(OH)_2]$ or brushite $(CaHPO_4 \cdot 2H_2O)$ [3]. Brushite was earlier thought as isomorphous with gypsum. However, it was found [17] that it has structure on the lower symmetry space group C_S^4.

The phosphate tetrahydra are not exactly regular but the P-O separating is lying between 1.34 and 1.69 . Each calcium atom has around it six phosphate oxygen and together with the PO_4 groups they form corrugated sheets between which water molecules are lying. Nevertheless, the positions of hydrogen atoms were not established by X-Ray diffraction data. The lower symmetry of brushite indicates piezoelectricity, which is not there in gypsum crystals. The lattice parameters of brushite are *a = 9.973 , b= 7.288 , c= 6.293 and â= 106.871 ,* indicating monoclinic type crystal structure, the projection along b_o axis is shown in the figure (8.1) [17].
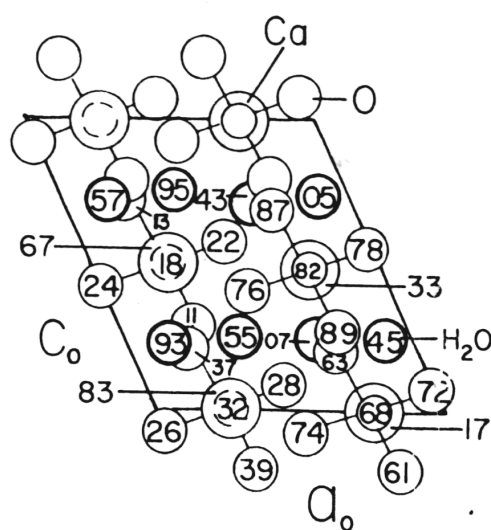
Figure (8.1): The crystal structure of CHPD

As per one assumption, in aqueous solutions the bi-layers of water molecules are for most of the real time exposed at surface of the (010) face, on the other hand, the lateral faces have a mixed ionic character with intercalated water molecules [18]. Because of this kind of ionic structure, CHPD posses a good model crystal for studying several aspects of interaction between additives and crystals. Skiric et al. [19] have summarized the important points as follows for CHPD inhibition:

(a) The importance of molecular size and structure of the additive, i.e., small or macromolecules, number of functional groups in the molecule and overall charge in the growth of CHPD and other related crystals. This may be useful in the selection of inhibiting molecule.

(b) The importance of a structural fit between the organic molecule and the ionic structure of a particular crystal face of CHPD. This decides the order of inhibition or reaction at a particular face.

(c) The influence of the hydration layer exposed on the surface of the crystals.

8.3 Growth of CHPD Crystals:

The growth of crystals in static solution is generally explained with the help of standard laws of physical chemistry. However, normal urine in the human body is not a static solution, but new solutes are added and subtracted from the solution. Moreover, it is difficult to mimic the urinary tract *in vitro*; however, the growth of crystals in a gel medium under static environment helps explain the growth of urinary calculi in a body to a certain extent. Hence the growth of urinary calculi can be simulated in a laboratory by growing crystals in a silica hydro gel medium. The gel framework, though chemically inert, provides a three dimensional matrix in which the crystal nuclei are delicately held and provides a substratum for a gradual supply of nutrients for growth. The growth of urinary crystals in silica hydro gel can be

considered as a simplified *in vitro* model of the highly complex growth of urinary calculi *in vivo*.

The growth of crystals from the gel is the simplest technique under ambient conditions, which is also suitable for the growth of bio-materials crystals, urinary type crystals and certain other compound crystals, which are sparingly soluble and decomposes at low temperatures. The gel density, pH and concentration of the reactants are important factors influencing the growth of good quality single crystals at room temperatures. This technique has been elaborately explained in Chapter-III. This technique has also been employed as a simple technique to grow various urinary type crystals [16, 20-22] and study the role of various inhibitors *in vitro* [23-24].

The macro-size and micro size CHPD crystals have been harvested, in the present study, by using the normal gel growth technique and the modified gel growth technique, respectively.

(a)   **Gel Preparation**:

The stock solution of sodium meta-slicate was prepared as mentioned in the section 5.3 of Chapter V. By adding double distilled water of appropriate volume in to the stock solution, one can prepare solution of the desired specific gravity. The specific gravity was selected as 1.05.

(b)   **Macro Size CHPD Crystal Growth**:

Glass test tubes of 2.5 cm diameter and 15 cm length were used for growing the crystals. As mentioned earlier, sodium meta-silicate solution of specific gravity 1.05 was acidified by adding appropriate amount of orthophospheric acid so that 4.0 and 5.0 pH could be obtained for the mixture, which was subsequently transferred into different test tubes. After gelation took place, 20 ml, 1M, aqueous solution of calcium chloride was carefully poured on the set gels. Crystals were found to be

growing very rapidly within two days from pouring the supernatant solutions. Elongated, platelet type and star shaped crystals were grown in the gel.
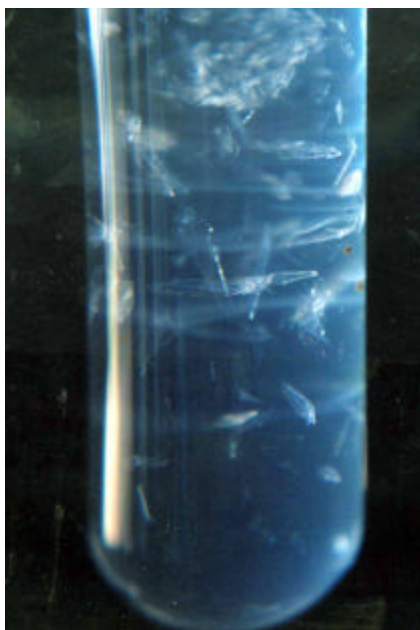
Figure (8.2): Growth of CHPD crystals

The apparent length of growing crystals was measured by traveling microscope of 0.001cm least count, at different time intervals. The figure (8.2) shows the growth of CHPD crystals in a test tube.

(c)   Micro Size CHPD Crystal Growth:

Glass slides with cover slips and Petri dishes were used as micro-crystal growth apparatus. The glass slides were arranged in the Petri dish in the form of a plus sign, where the lower slide was just used for the support and the upper slide was used for micro-crystal growth. To grow the micro-crystals in a silica gel medium, a sodium meta-silicate solution of specific gravity 1.06 was mixed with 1M orthophospheric acid so that pH 5.0 could be set for the mixture. Thereafter, with help of suitable glass dropper a small drop of this mixture was put at the middle of glass slide. A cover slip was then placed on this drop in such a manner that it floated on the mixture and covered almost the area of a cover slip size, without any spillage beyond

the cover slip. To assure that the gelling process occurred properly without drying the solution, the slides were placed in a Petri dish in such a way that water poured in the Petri dish did not touch the cover slip, but remained slightly below the upper surface of the slide. The details of experiments are already discussed Chapter-III. After setting the gel, water was sucked from the Petri dish with the help of suitable dropper. Thereafter, 1M, $CaCl_2$ solution was poured with care using appropriate glass dropper so that it should cover the slide up to the level of cover slip. The poured solution diffused through the gel and reacted with the impregnated orthophospheric acid in the gel medium which resulted into the growth of micro-crystals within 24 hours. The cover slip was having diameter of 18 mm and the total area of 254.34 mm^2. The drop put on the slide to form the gel was of the order of 10 micro-liters, therefore, the thickness of the gel could be estimated to be of the order of 0.039 mm. Figure (8.3 a and b) shows the photographs of the CHPD micro crystals.

The slides were observed regularly by using dissecting microscope and photographs were taken using attached digital CCD color camera (water WAT 2020, Japan) with digital Zipshot twin-driver (Across Inc. Fermount, CA 94538). The lengths of crystals were measured by using software Image tool.

The growth of micro-crystals can be seen in the photographs of Figure (8.3- a-f). Figures (8.3-a and b) show rhombic type platelet crystals without having any leaflet on its surface, but at some places the leaflets are seem to be under development or beginning as it is marked in figure (8.3-a and c). Due to multiple branching the micro-crystal develops in to star shape morphology, which is exhibited in Fig. (8.3-d). The star shape morphology indicates that all leaflets are spreading out from the basic micro-crystal; the dimension of the observed micro-crystals is 60 ìm X 60 ìm. Figure (8.3- c) shows a platelet of 40ìm X 70 ìm is having a leaflet type of structure and like

a mica sheet the new leaflets are getting developed, which is confirming the earlier SEM observations of Joshi and Joshi [16] on CHPD macro crystals.
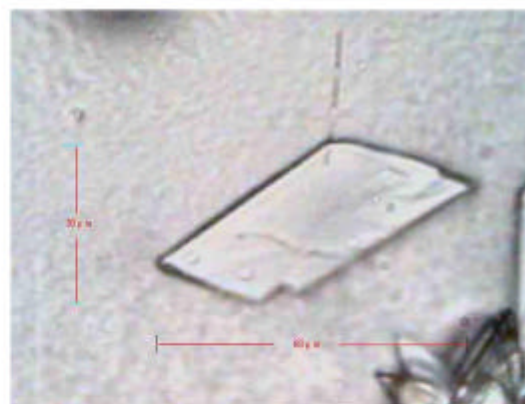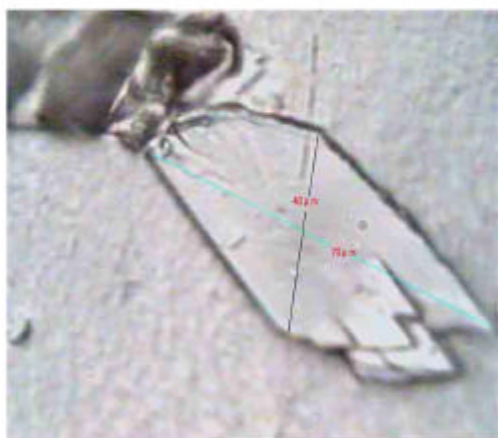

Figure (8.3-a)

Figure (8.3-b)

Figure (8.3-c)

Figure (8.3-d)

Figure (8.3e)

Figure (8.3-f)

Figure (8.3): Micro CHPD crystals with the measurements

However, Figures (8.3-e and f) show a possible formation of another needle, by protruding parts from the needle on different sides and, ultimately, turns in to a star shape morphology with sharp needles coming out from the common center. This type of star shape morphology is different from the star shape morphology obtained from the platelet type crystals. In the case of stars originated from platelets the common center is not observed, whereas in the case of the star originated from the needles the common center is observed.

8.4   Growth-Inhibition Study of CHPD Crystals:

Under steady state conditions the normal urine contains minimal quantities of crystals, which represents a delicate balance of a number of parameters working in opposing direction. Urinary Stone [3] formation should be viewed as an imbalance in these parameters, which is represented in figure (8.4).
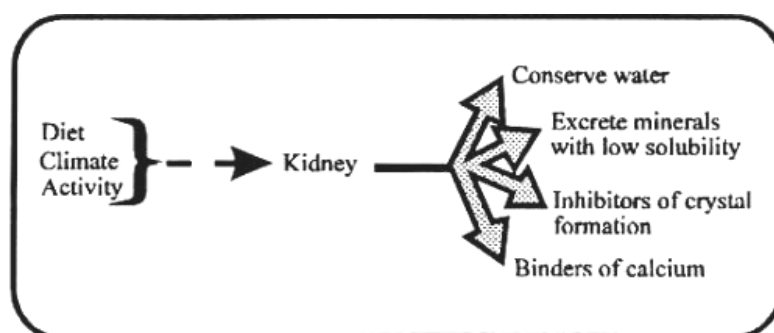
Figure (8.4): Factor affecting the formation of urinary stones

In urine, when the concentration of a substance reaches a point at which the saturation would take place in water, crystallization does not occur as expected. However, the urine has the ability to hold more solute in the solution, than does pure water. Many organic molecules such as urea, uric acid, citrate and complex muco-proteins of urine, naturally, affect the solubility of other substances, which has been discussed by Menon et al. [3]. Hence the saturation and solubility product in water are simple to define, but urine is a more complex solution and it is difficult to define. The point at which saturation is reached and crystallization begins is referred to as the

thermodynamic solubility product K_{SP}. If the concentration of solute increases and a point is reached where it cannot be hold in solution, this concentration is known as K_{FP}, which is the formation of product of urine. Criticality to the formation of a crystal is the saturation state of that solution. This depends on solute concentration, pH, ionic strength and existence of soluble complexes.
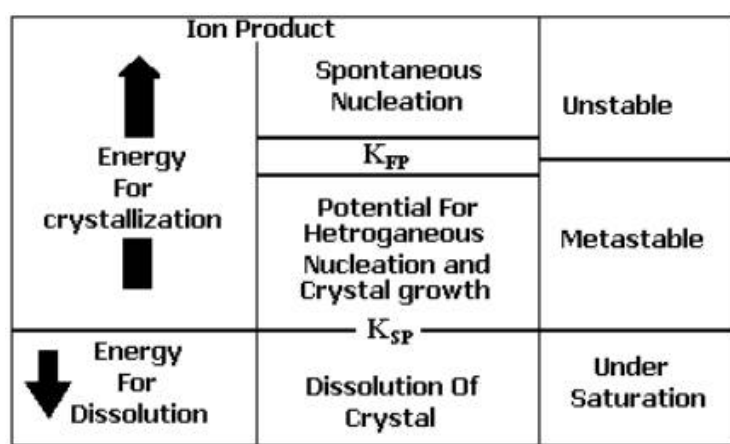

Figure (8.5): Chart of reaction kinetics for precipitation

The simple overview of the problem of crystallization and dissolution is described in the chart of Figure (8.5). Once the concentration of solute exceeds K_{FP}, the solution becomes unstable and spontaneous nucleation occurs (homogeneous and heterogeneous nucleation) and the crystal growth proceeds.

Moreover, an estimation of the state of saturation of urine with the stone-forming salts is of prime importance in clinical practice. Usually, the state-of-saturation indicates the free energy of a given solution, which by entropy tends to decrease, resulting into the precipitation of the super-saturated solid phase [25]. In general, the saturation increases with the concentrations of ionic components and, especially, it depends on the activities of the constituent (non-complexed) free ions. To calculate the state of saturation (â), the free ion concentration must be established from the difference between the measured total concentration and the sum of concentrations of all the relevant complexes [25]

The amount of soluble complexes depends on their stability constants. The free ions in solution interact in such a way that their electrochemical activity decreases by a coefficient that is inversely related to the ionic strength. In other words, in concentrated urine, the activity coefficient tends to decrease and for a given ion concentration the activities are lower at higher ionic strength. The state of saturation ultimately results from the activity product of constituent ions and can be expressed as relative super-saturation, by calculating the ratio between the activity product and the solubility product of a given salt. This has been discussed by Marangella et al. [25] in detail by exemplifying for calcium oxalate. A CD-ROM has been made on O' Turin and Messina model, which offers a computer programme named URSUS, requiring input variables of some cations (Na, K, Ca) and anions (oxalate, phosphate, citrate, etc.). The results obtained include, concentrations of main soluble complexes, state-of-saturation with calcium oxalate monohydrate (COM), brushite, etc., in terms of indications of saturation or super-saturation.

Many chemicals found to be having inhibitive actions on the growth of urinary stones and crystals; for example, tartrates have been found as a good inhibitor in natural and artificial urine media [8]; some amino acids, which show the influence on the spontaneous precipitation of calcium oxalate and depend on the type and the concentration of amino acids used [9]; the citrate compounds, which show the inhibition of nucleation and growth steps of COM crystallization [10]; nephrocalcin and Tamm-Horsfall, glycoprotein are potent inhibitors of COM crystal aggregation [26] and some phosphate derivatives, such as, D fructose-1.6-diphosphate, pyrophosphate methylene diphosphonate and phytate are found to be strongly inhibiting the growth of COM seed crystallization [27]. Magnesium, citrate, pyrophosphate and nephrocalcin make up the most of the inhibitors for the calcium

phosphate crystal system [28]. Natarajan et al. [29] have studied various inhibitors and promoters based on hosts of fruit juices, extracts from vegetables and cereals and natural substances. On the other hand, Joshi [30] as well as Joseph [31] have tested various inhibitors such as certain fruit juices, homogenate solutions of Ayurvedic medicinal plants and different pulses. Recently, Joshi et al. [32, 33] have reported the inhibition of growth of the CHPD and COM crystals by aqueous extracts of Ayurvedic medicinal plants *Tribulus terrestris* and *Bergenia ligulata.*

In the present investigations, different concentrations of citric acid and tartaric acid for growth inhibition or dissolution of macro size CHPD crystals and only citric acid for the same purpose for micro size CHPD crystals have been studied in detail.

8.4.1   Inhibition and Dissolution Study of the Macro size CHPD Crystals:

(a)   Inhibition and Dissolution Study of The Macro CHPD Crystals Using Citric Acid:

Citrate is the important complexer of calcium in urine and reduces ionic calcium concentration [34, 35]. It also inhibits spontaneous and heterogeneous nucleation [33, 36, 37]. The unique citrate complexes formed by iron (III), aluminum, chromium and beryllium have also shown important inhibitive action of mineralization and growth of hydroxyapatite crystals, which are associated with the arthropathy. [38, 39]. Moreover, citrus juices, for instance, orange and lemon, are expected to prevent the stone formation due to their high citrate content [40]. The effect of orange juice consumption on urinary stone risk factor is also studied by Wabner and Pak [41]. Ettinger et al. [42] have reported that potassium magnesium citrate is effective prophylactic against recurrent of calcium associated nephrolithiasis. Joshi et al. [43] have reported the inhibition of the growth of CHPD crystals by lemon juice and citric acid in the presence of human urine and artificial reference urine. A

critical review has recently been written by Mattle and Hess [44] on preventive treatment of nephrolithiasis with alkali citrate. Also, the role of dietary citrate on bio-chemical risk factors of urolithiasis has been studied Marickar [45]. Apart from this, prophylactic and therapeutic properties of a sodium citrate preparation in the management of calcium oxalate urolithiasis have been reported by Allie-Hamdulay and Rodgers [46].

In the present investigation, CHPD crystals were grown by the single diffusion gel growth method. When crystals achieved maximum growth, the inhibitive effects of citric acid solutions having different concentrations were studied by adding them into the supernatant solution. Unlike, in the earlier studies [30, 31, 43] different inhibitive solutions were added in the supernatant solutions right from the beginning of the growth of crystals and compared with the growth of crystals without inhibitor solutions.

In case of pure calcium chloride containing supernatant solution, the nature of growth is exhibited by a plot of figure (8.6-a), which is a plot of apparent length of growing crystals versus time for pH value 4.0. From this plot, it can be seen that after five days of pouring the supernatant solution, the crystals almost acquire the maximum values of length. For the pH value of 4.0, citric acid solutions of different concentrations were added in equal amount to the calcium chloride containing solutions in the respective test tubes. Figure (8.6 b) is a plot of apparent length of growing crystal versus time for 10 ml, 0.2 M citric acid solution; it indicates a slight decrease in length of crystal after pouring citric acid. By adding 10 ml of 0.4 M citric acid solution into $CaCl_2$ solution, it was found that the growth rate decreased rapidly. The crystals dissolved faster than the previous case. This can be seen from figure (8.6 c). Whereas, Figure (8.6 d) is a plot of apparent length of growing crystal versus

time, for adding 10 ml, 0.6 M citric acid solution into the supernatant solution of CaCl$_2$; shows that the growth decreases very rapidly. In case of adding 10 ml of 0.8 M and 1.0 M citric acid solutions into CaCl$_2$ solution, interestingly, crystals dissolved within two days and one day, respectively. This can be verified from the figures (8.6 e and f)
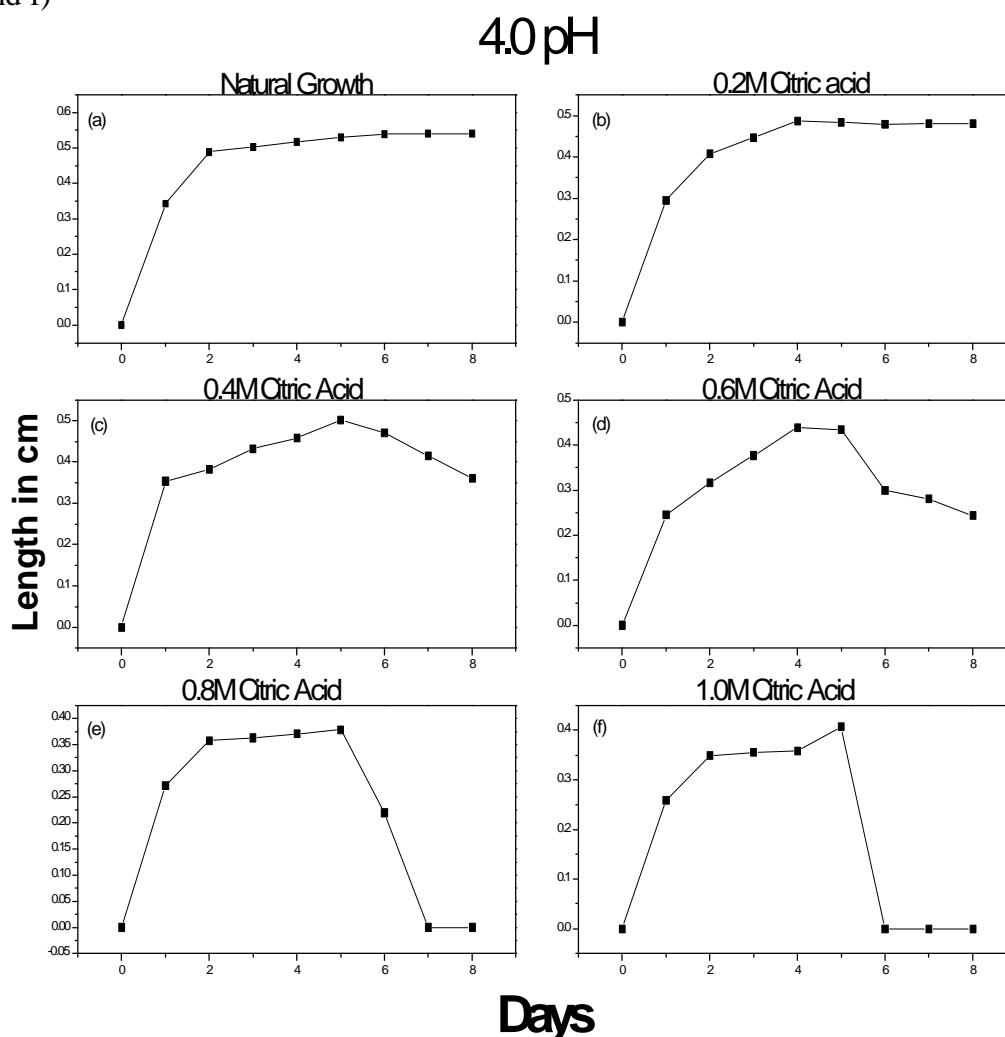

Figure (8.6): Plots of growth observation of CHPD crystals in the presences of different concentration of citric acid

Same types of results were available for 5.0 pH. It also indicates that as the molar concentration of citric acid increases, the crystals dissolve rapidly. For 5.0 pH the length of crystals is less than that of for 4.0 pH, this is because of harder gel and smaller pore size so that the diffusion process becomes slow.

Hypocitraturia, a low amount of citrate in urine, is considered to be an important risk factor for urinary stone formation. Urinary citrate is considered as important inhibitor of the crystallization of stone forming calcium salts. The mean normal urinary citrate excretion is 640 mg/24 hr. However, the hypocitraturia is, generally, considered when the citrate excretion is less than 320mg/24hr. But the severe hypocitraturia is when the citrate excretion is of less than 100 mg/24 hr. The normal urine citric acid level is within 320 to 1240 mg/24 hr. There are many reasons for increase or decrease of urinary citric acid levels. The urine citric acid level may decrease with acidosis, severe muscular activity, hypoparathyroidism, diabetes and chronic renal failure. On the other hand, urine citric acid levels may increase with a high carbohydrate diet, astrogen therapy and vitamin D [47]. In the pathophysiology, the excretion of citrate in urine is a function of filtration re-absorption, peritubular transport and synthesis by renal tubular cell. The proximal tubule reabsorbs most 70-90% of filtered citrate and as a result the citrate secretion is negligible. Altogether, the acid-base status plays the most significant role in the citrate excretion. Alkalosis enhances citrate excretion, where as acidosis decreases it. In acidosis, increased citrate utilization by the mitochondria in the tricarboxylic acid cycle occurs. This results in lower intracellular levels of citrate facilitating citrate re-absorption and hence reducing citrate excretion. Citrate excretion is impaired by acidosis, hypokalemia, high animal protein diet and urinary tract infection [47]. Hence citrate plays predominant roles in the mechanisms of urinary calculi formation. First of all citrate binds with calcium ions in the urine and reduces calcium ion activity, consequently, the lowering of the urinary supersaturation of calcium phosphate and calcium oxalate. Second, citrate has a direct inhibitory effect on the crystallization and precipitation of salts.

Citrate inhibits nucleation and growth steps of calcium oxalate monohydrate (COM) [10] as well as CHPD [43] crystallization. The citrate inhibition suggests that, sodium citrate, citric acid and other citrate compounds are acting as alkalization agents indicated for systemic metabolic acidosis (renal tubular acidosis), while urinary alkalization or hypocitraturia contains di-sodium citrate. Pak et al. [48] reported successful management of uric acid nephrolithiasis with potassium citrate. Potassium citrate reduces urinary saturation of calcium salts by complexing calcium and reducing ionic calcium concentration. Pak [49] preferred potassium citrate because it appears to decrease urinary calcium excretion at least transiently. On the other hand, sodium citrate does not lower urinary calcium excretion; perhaps as the result of the increased sodium load associated with therapy [50] .Sodium-potassium citrate was used by Hofbauer [51], this study did not give any conclusive results on patients. No prospective randomize study has confirmed the superiority of potassium citrate over sodium citrate in prevention of stone recurrence as Menon et al. [3] have noted down. This suggests that as sodium citrate and potassium citrate due to their alkalizing effect have inhibition effect, it is worth to study the effect of citric acid on the growth inhibition of CHPD crystals. This has leaded the present author to verify the growth inhibition of CHPD crystal *in-vitro* condition.

It has been observed by Joshi and Joshi [43] that the supernatant solutions, for the growth of CHPD crystals, containing citric acid, lemon juice, lemon juice and artificial reference urine (ARU) and lemon juice and natural urine in addition to calcium chloride solutions exhibited various degrees of inhibitions. In their study they poured supernatant solutions containing different inhibitors in various test tubes and compared the results with the pure calcium chloride containing supernatant solution. They proved citrate inhibition [35] for CHPD crystals as well as they also proved that

the highest inhibition was in the case of lemon juice, which contains citric acid, plus natural urine, as natural urine also contains some natural inhibitors. The present investigation provides further proof of citrate inhibition of calcium containing urinary crystals, such as CHPD crystals, *in-vitro* condition. The higher concentrations of citric acid in the supernatant solutions dissolved the grown crystal very rapidly by forming soluble salt calcium citrate, whereas in the case of lower concentrations of citric acid, that is, less than 0.2 M concentrations, the inhibition to the growth of CHPD crystals was observed. These results may be useful to investigate the effect of citric acid on the dissolution and inhibition of urinary calculi. Though the level of mean citric acid excretion is very low in human body, this *in-vitro* study may help to understand the inhibition of growth by raising citrate concentration in urine in patients who are prone to stone formations. One has to be aware of side effects and toxicity limit of citrate concentrations in urine.

In conclusion, citric acid is found to be inhibiting the growth of CHPD crystals in the lower concentrations of less than 0.2 M and dissolving CHPD crystals for the higher concentrations of citric acid. As the concentration of citric acid is increased, the dissolution of CHPD crystals becomes more rapid.

(b) **Inhibition and Dissolution Study of the Macro CHPD Crystals Using Tartaric Acid:**

As tartrate forms metal ion complexes with calcium [52], the presence of tartrate in urine may decrease the amount of ionized calcium available for calcium containing urinary calculi. The effect of tamarind and tartaric acid as inhibitors of calcium oxalate crystallization in urine has been discussed by Croft et al. [8]. Recently, Joseph et al. [53] have reported the effect of tartaric acid and tamarind solutions on the growth of CHPD crystals.
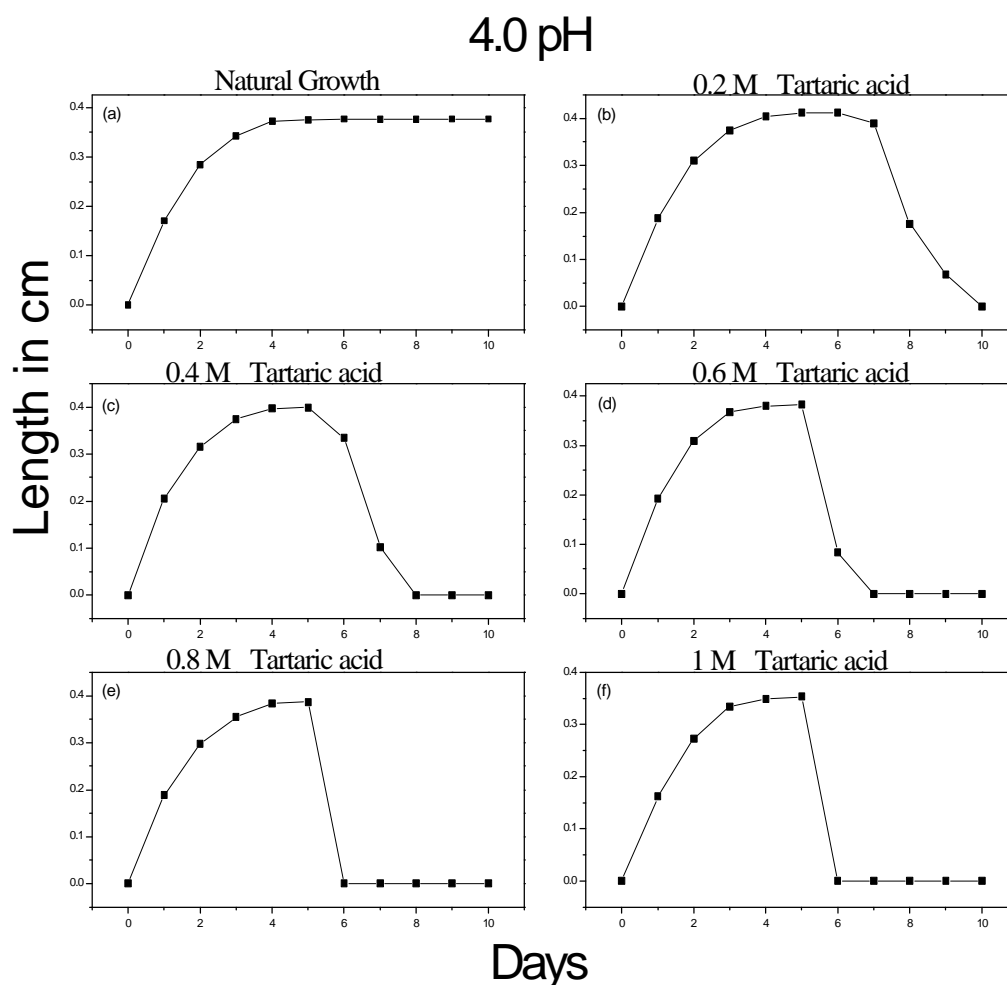
Figure (8.7): Plots of the growth observation of CHPD crystals in the

presences of different concentrations of tartaric acid

In order to investigate the effect of tartaric acid on the already grown crystals, first crystals were allowed to grow up to the maximum size and then tartaric acid solutions of different molar concentrations were added to calcium chloride supernatant solution, in the respective test-tubes. From the measurements of apparent length of growing crystals with time it was observed that the average crystal length reached its saturation level on the fifth day from pouring the supernatant solution. In other words, the crystals achieved maximum average length on the fifth day and then the growth was very slow. The molar concentrations of tartaric acid such as 0.2 M, 0.4M, 0.6M, 0.8 M and 1.0M were selected. Same behavior was observed for 5.0 pH,

but the lengths of the crystals were less, this may be due to the harder gel and smaller pore size of the gel.

The nature of crystal growth patterns is exhibited in fig. (8.6 a-f). Figure (8.6 a) depicts the growth of CHPD crystals without tartaric acid. In case of adding 0.2 M tartaric acid, the inhibition of growth and slow dissolution of crystals is observed, which is shown in figure (8.6 b). It can be observed very clearly from the figures (8.6 c, d, e, and f) that as the concentration of tartaric acid increases the dissolution of crystals become more rapid and for 1M concentration it is the highest one. For the higher concentration of tartaric acid, notwithstanding, the growth of calcium tartrate was initiated at the same time the dissolution of CHPD crystals occurred. Therefore, it is important to arrive at the proper molar concentration of tartaric acid, which dissolves CHPD crystals but does not initiate the growth of calcium tartrate crystals. This had tempted the authors to verify the solubility of CHPD crystals in tartaric acid. A small CHPD crystal was selected and was put in a 1 M tartaric acid solution and it was observed under the traveling microscope. Initially, the surface of selected crystal was heavily etched then eroded due to tartaric acid. It was observed that appreciable amount of dissolution of the crystal took place within a few hours and within a day the crystal was completely dissolved.

Tartrates are expected to form metal ion complexes with calcium [52], which decreased the amount of ionized calcium available for calcium salt precipitation. Tartrates bind with the cations needed for crystal formation and subsequent growth and also function as a crystal growth inhibitor of calcium oxalate by chemical adsorption on the crystallization sites at a growing interface [54]. An evaluation of tamarind and tartaric acid as inhibitors of calcium oxalate crystallization in urine is reported by Croft et al. [8].

Also, Singh et al. [55] have earlier reported the inhibitory effect of tamarind on urolith in urine. Thomas et al. [56] attempted to explore the possibility of using tamarind and tomatoes in controlling crystalluria. Moreover, Anasuya and Sasikala [57] have studied lithogenic properties of urine before and after ingestion of 10g Tamarind daily. They found complete disappearance of calcium oxalate crystal aggregates, fall in density in crystalluria, reduction in crystal size, decrease excretion of oxalic acid, increased excretion of phosphorous and increased inhibitory activity of urine towards crystal growth.

The Food and Agriculture Organization of the United Nation and World Health Organization (WHO) have evaluated tartaric acid and its potassium-sodium and sodium salts for daily intake [58]. When taken by mouth, only about 20% of ingested tartaric acid is eliminated in the urine, inasmuch as it is destroyed in the intestinal tract by bacterial action the remaining one is not absorbed. Finkle [59] suggested that L(+) tartaric acid is inert in the human body. A study was published in which the percentages of both L (+) and D(-) tartaric acid eliminated in urine after intramuscular injection to a man were found only slightly greater than those after oral administration [60].

Tartrate forms metal ion complexes, which are water soluble and help to inhibit or dissolve already grown CHPD crystals. The dissolution time of grown CHPD crystals depends upon the concentration of tartaric acid added in the supernatant solution. As the concentration of tartaric acid increases the dissolution occurs faster.

8.4.2 Inhibition or Dissolution Study of the Micro Size CHPD Crystals:

In the previous sections the author has reported the growth and inhibition of the macro size CHPD crystals. A novel modified gel growth technique for micro crystals

was developed by the present author and its advantages are already mentioned earlier. In the present section, on the basis of micro crystal growth, the inhibition study is reported for different concentrations of citric acid and *in situ* observations with the help of photomicrographs are covered.

The growth of micro-size CHPD crystals is already reported in section 8.3 of the present chapter. The growth inhibition of micro-size CHPD crystals is studied by first conducting the growth experiment of CHPD crystals in several slides and then adding solutions of citric acid in molar concentrations of 0.2, 0.4, 0.6, 0.8 and 1.0 in equal amounts that of $CaCl_2$ solution in the respective Petri-dishes. The growth of micr-crystals was monitored before and after adding the citric acid solutions under optical microscope. For comparison purpose, in each set three Petri-dishes were kept without adding any citric acid solutions, in other words, these served as controls. The observations were made by using Carl-Zeiss (Axioskop 2 plus) microscope in the transmitted light mode with the help of different filters and photographs were taken using CCD camera attached to the microscope with maximum magnification 40X.
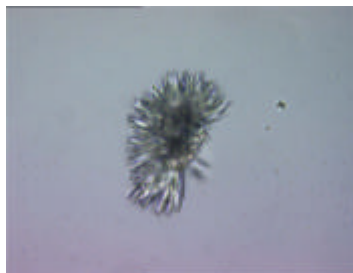
| Figure (8.8-a) | Figure (8.8-b) | Figure (8.8-c) |
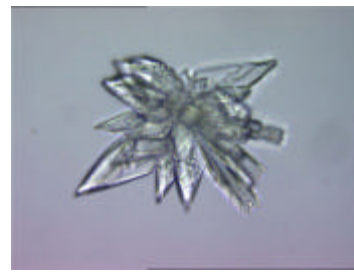
Figure (8.8): various types of CHPD micro crystals

For the control solution, that is, without adding any citric acid solutions, mainly two types of growth morphologies were observed, viz., needle type and star type. The star type morphology can again be considered as of two types, one with broad platelet

type branches and the other with fine needle type branches. The needle type and both star type crystals are shown in Figures 8.8 (a-c), respectively.
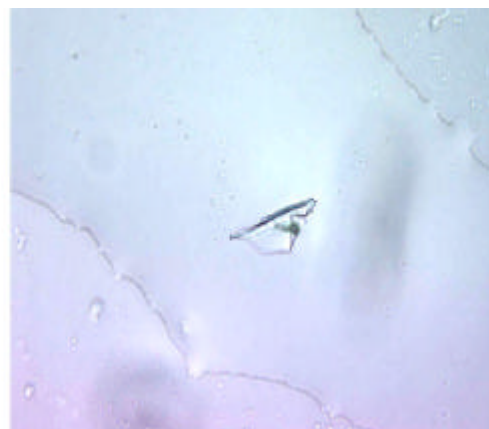

<div style="text-align:center">

Figure (8.9-a)   **Figure (8.9-b)**

Figure (8.9): Inhibition of CHPD crystal using 0.2 M citric acid

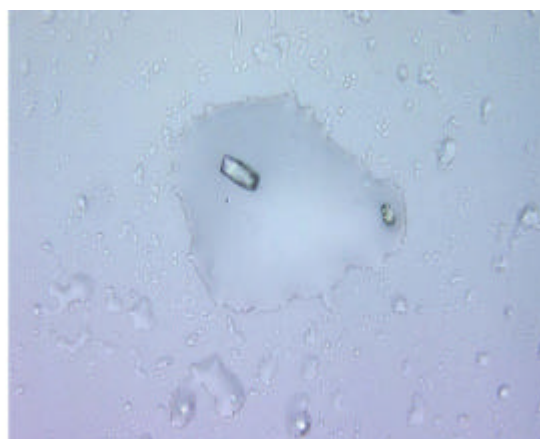</div>

<div style="text-align:center">

Figure (8.10-a)   **Figure (8.10-b)**
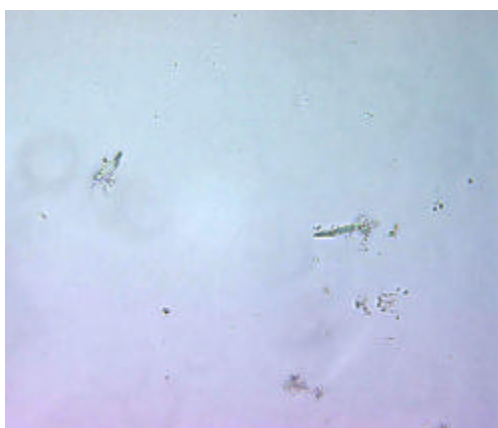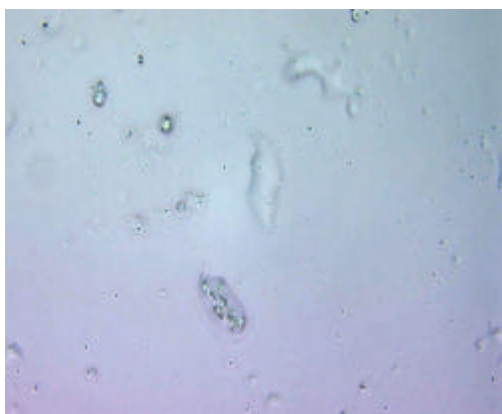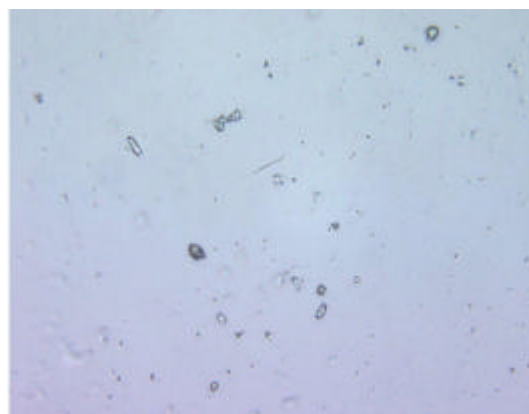
Figure (8.10): Inhibition of CHPD crystal using 0.4 M citric acid

</div>

<div style="text-align:center">

Figure (8.11-a)   **Figure (8.11-b)**

Figure (8.11): Inhibition of CHPD crystal using 0.6 M citric acid

</div>

Figure (8.12-a)   **Figure (8.12-b)**

Figure (8.12): Inhibition of CHPD crystal using 0.8 M citric acid

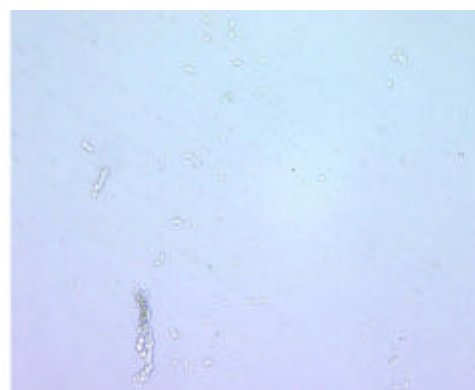

Figure (8.13-a)   **Figure (8.13-b)**

Figure (8.13): Inhibition of CHPD crystal using 1.0 M citric acid

The crystal observed after 2 hours from pouring 0.2M citric acid solution is shown in figure (8.9-a), which is further dissolved in to a small fragment after 12 hours from pouring the citric acid solution as shown in Figure (8.9-b). Figure (8.10-a) shows the dissolution onset on a needle type crystal after 2 hours of pouring 0.4M citric acid solution. Figure (8.10-b) indicates a needle is fragmented after heavy dissolution and a small left over part is visible after 12 hours of pouring 0.4 M citric acid solution. In case of pouring 0.6M citric acid solution, the dissolution of crystals becomes faster. Figure (8.11-a) shows the crystals start dissolving, 2 hours after pouring 0.6M citric acid solution. Figure (8.11-b) shows that the crystals become fragmented into small parts but still its original morphology is vaguely visible. For 0.8

M and 1.0M citric acid solutions, the dissolution of CHPD micro-crystals becomes much more rapid. This is in accordance with the earlier study on inhibition and dissolution of macro size CHPD crystals, which is already reported in section 8.4.1. In case of 0.8 M citric acid solution, just two hours after pouring the citric acid solution the crystals start fragmenting and 12 hours after pouring the solution the crystals are dissolved in majority. The similar results were obtained for 1 M citric acid solution. These results correspond to the earlier results on the macro size CHPD crystals and, further, support the citrate inhibition theory.

8.5   Conclusion:

(1)   The CHPD crystals were grown by the normal gel growth technique and the modified gel growth technique. The normal gel growth technique used conventional glass test tubes and yielded macro size CHPD crystals. In contrast to that the modified gel growth technique used Petri dishes and glass slides and micro size CHPD were harvested. The micro size CHPD crystals were observable under optical microscope.

(2)   The modified gel growth technique provided a tool to observe the development of the crystals *in situ*. This requires comparatively less amount of chemicals and yields comparatively rapid growth of crystals. In the case of normal gel growth, nearly the period of ten days is required for the complete growth- inhibition study, whereas in the modified gel growth technique it is hardly 3 to 4 days. Modified gel growth technique is advantageous for growth inhibition studies.

(3)   For the macro crystals of CHPD, the growth inhibition in the presence of different concentrations of citric acid and tartaric acid was studied. It was found that as the concentration of acid increased the dissolution of crystals

became rapid. For low concentrations of acids the inhibition of crystals was observed, but for higher concentrations the dissolution was observed.

(4)   For the modified gel growth technique, after achievening growth of crystals, different concentrations of citric acid were used to study the growth-inhibition of CHPD micro-crystals. The micro size crystals were observed under optical microscope. It was also found that as the concentration of citric acid increased the dissolution of crystals became faster.

References:

[1]   http://kidney.niddk.nih.gov/kudiseases/pubs/stonesadults/#whatis

[2]   F. L. Coe, M.J. Favus (Eds.); '*Disorders of Bone and Mineral Metabolism'*, Raven Press, New York, (1992).

[3]   M. Menon, B. G. Parulkar and G. W. Drach; '*Urinary Lithiasis, Etiology, Diagnosis, and Medical Management; Campbell's Urology'*, 7th Ed., W. B. Saunders Co., London, (1998) 2261.

[4]   J. S. Wolf and M. L. Stoller; *J. Urol.* **152** (1994) 1609.

[5]   V. Vermotten; *J. Urol.* **48** (1942) 27.

[6]   A. Randall; *New Engl. J. Med,* **214** (1936) 234.

[7]   http://www. About crystals.com

[8]   K. Croft, J. H. Adair, R. Bowyer and J. G. Brockis; *"Urinary Stones",* Proc. of the 11th Interenational Urinary Stone Conference, Singapore 1983. Eds. R.L. Ryall, et. al (Cheurchill Livingstone Co. Melbourne, 1984).

[9]   D. Skrtic, H. Furedi-Milhofer; *J. of Cryst. Growth,* **129** (1993) 449.

[10]   P. A. Antinozzi, C. M. Brown and D. L. Purich; *J. Cryst. Growth,* **125** (1992) 215.

[11]   F. Grases, A. Millan and A. Garcia-Ruso; *J. Cryst. Growth,* **89** (1988) 496.

[12]   http://www.mindat.org/min-793.html

[13]   http://www .Brushite Mineral Data.htm

[14]   C. Pittet and J. Lemaître; *European Cells and Materials*, **3 (1)** (2002) 13.

[15]   D. Brendlen, C. Pittet and J. Lemaître; *European Cells and Materials,* **5(1)** (2003) 1473.

[16]   V. S. Joshi and M. J. Joshi; *Cryst. Res. & Technol.,* **38** (2003) 817.

[17]   W. G. Wyckoff; *"Crystal Structure"*, Inter-science, John Wiley & Sons. (1965) 644.

[18]   D. Haninen, B. Geiger and L. Addadi; *Langmuir, 9* (1993) 1058.

[19]   M. Sikric, S. Sarig and H. Füredi-Milhofer; *Progress in Colloid Polym. Sci.* **110** (1998) 300.

[20]   K. Rajendra Babu, M. Deepa, M. K. Nair and V. K. Vaidyan; *Bull. Mater. Sci.* **21** (1998) 121.

[21]   N. Srinivasan and S. Natarajan; *Indian J. Physics, 70A* (1996) 563.

[22]   G. R. Shivkumar, E. K. Girija and S. N. Kalkura; *Cryst. Res. & Technol*. **33(2)** (1998) 197.

[23]   K. C. Joseph and M. J. Joshi; Abstracts., XIII-Int. Conf. on Crystal Growth, July 30-Aug 4, (2001), Kyoto, Japan, p-602

[24]   V. S. Joshi and M.J. Joshi; Abstracts., XIII-Int. Conf. on Crystal Growth, July 30-Aug 4, (2001), Kyoto, Japan, p-603

[25]   M. Marangella, C. Vitale and M. Petrarulo, C. Bagnis, M. Bruno and A. Ramello; *Nephrol. J.,* **13** (2000) 551.

[26]   J. Asplin, de. Gannellis, Y. Nakagawa and F.L. Coe; *Am. J. Physiol.,* **260** (1991) 569.

[27]   F. Grases and P. March; *J. Cryst. Growth,* **96** (1989) 993.

[28]   H. Ito and F. L. Coe; *Am. J. Physiol.,* **233** (1977) F455.

[29]   S. Natarajan, E. Ramchandran and D. Blissin Suja; *Cryst. Res. and Technol.,* **32** (1997) 553.

[30]   V. S. Joshi; *'Ph.D. Thesis',* Saurashtra University, Rajkot (2001).

[31]   K. C. Joseph; *'Ph.D. Thesis',* Saurashtra University, Rajkot (2005).

[32] V. S. Joshi, B .B. Parekh, M. J. Joshi and A. D. B. Vaidya; *Urol. Res.* **33** (2005) 80.

[33] V. S. Joshi, B. B. Parekh, M. J. Joshi and A. D. B. Vaidya; *J. Cryst. Growth,* **275(1-2)** (2005) e-1403.

[34] J. L. Mayer and L. H. Smith; *Invest. Urol.,* **13** (1975) 36.

[35] C. Y. C. Pak; *J. Urol,* **128** (1982) 1157.

[36] D. L. Kok, S. E. Papapolulos and O. L. M. Bijovet; *Lancet.,* **10** (1986) 1056.

[37] M. J. Niscar, K. Hill and C. Y. C. Pak; *J. Bone. Miner. Res.,* **2** (1987) 215.

[38] J. L. Meyer and W. C. Thomas Jr.; *J. Urol,* **128** (1982) 1372.

[39] W. C. Thomas Jr.; *Proc. of the Soc. Exptl. Biol. and Med.,* **128** (1982) 321.

[40] M. A. Seltzer, R. K. Low, M. McDonald, G. C. Shami and M. L. Stoller; *J. Urol.,* **156** (1996) 907.

[41] C. L. Wabner and C. Y. C. Pak; *J. Urol.,* **149** (1993) 1405.

[42] B. Ettinger, C. Y. C. Pak, J. T. Citron, C. Thomas, B. Admas Huet and A. Van Gessel; *J. Urol.,* **158** (1997) 2069.

[43] V. S. Joshi and M. J. Joshi; *Indian. J. of Pure and Appl. Phys.,* **41** (2003) 183.

[44] D. Mattle and B. Hess; *Urol. Res.* **33** (2005) 73.

[45] F. Marikar; *Abstract. 11th European Symposium on Urolithiasis',* Coburg, Germany, 16-18th June (2005).

[46] S. Allie-Hamdulay and A. L. Rodgers; *Urol. Res.* **33** (2005) 116.

[47] H. H. Woo, Jit Tan Ben; *Hypocitraturia;* Eds. Gomella L. G. et al., www. Emedicine.com/med/topic3030.htm

[48] C. Y. C. Pak, K. Sakhee and C. Fullor ; *Kidney Inst.* **30** (1986) 422.

[49] C. Y. Pak; *Mineral Electrol Metals;* **13** (1987) 257.

[50] K. Shakhaee, J. A. Harvay, and P. K. Padakino; *J. Urol.* **150** (1993) 310.

[51]   J. Hofbauer, R. Hofbarth, N. Szabo and M. Marberger; *Br. J. Urol.,* **73** (1994) 362.

[52]   L. G. Sillen and A. E. Martell; (Eds);*"Stability Constants of Metal Ion Complexes"* Supplement No.1, Chemical Society of London, Burligton House.1971.

[53]   K. C. Joseph, B. B. Parekh and M. J. Joshi; *Curr. Sci.,* **88 (8)** (2005) 1232.

[54]   H. Fleisch; *Kidney Int.,* **13** (1978) 361.

[55]   P. P. Singh, P. Hada, I. M. S. Narula and S. K. Gupta; *Indian J. of Exptl. Biology,* **25** (1987) 863.

[56]   J. Thomas, K. Sachidev, S. Sindhu, R. Vathsala and Y. M. F. Marickar; *Urol. Res.,* **16** (1988) 242.

[57]   A. Anasuya and M. Sasikala; *Nutrition Res.,* **10** (1990) 1109.

[58]   Twenty first Report of the Joint FAO/WHO Experts Committee on Food Additives., Geneva, WHO Technical Report Series no. 617, (1977).

[59]   P. Finkle; *J. Biol. Chem.,* **100** (1933) 349.

[60]   C. W. Bauer and R.W. Pearson; *J. Amer. Pharm. Assoc. Sci.* **46 (**1957) 575.

Chapter IX

Growth and Characterization of

Some Special Interest Crystals

The present chapter deals with the spin off studies, which includes three diverse materials, namely, (1) sodium oxalate, (2) sodium pyrophosphate and (3) 4-(2-hydroxy-phenylamino)-pent-3-one. These crystals have been studied with special interest. The water soluble salts of sodium are found in our body which provides the basis of bio-crystallization when their anions combine with calcium and form calcium oxalate or calcium pyrophosphate crystals, responsible to ailments like urinary stones and arthritis, respectively. The third one is the organic crystal with special interest because of its novel photoconducting behavior and some NLO (non-linear optical) property.

9.1   Growth and Characterization of Sodium Oxalate crystals:

The presence of oxalates is widespread in nature. Many times these minerals are formed as a result of expulsion of heavy metals from fungi, lichens and plants [1-3]. The production of simple organic acids, for example, oxalic and citric acids, have profound implications for metal speciation in biogeochemical cycles [4]. The metal complexing properties of the acids are essential to the nutrition of fungi and lichens and affect the metal stability and mobility in the environment [4]. Lichens and fungi produce oxalates of heavy metals as a mechanism for the removal of heavy metals from the plant [5]. Recently, Macnish et al. [6] have identified intracellular calcium

oxalate crystals in Geraldton wax flowers (*Chamelaucium uncinatum*), which can be viewed as the complexation of oxalic acid with calcium controlling the concentration of heavy metals in the plant. Moreover, minerals like calcium oxalate are also important from the aspect of human physiology because they are found in urinary tracts [7, 8]. Many other divalent oxalates exist in nature. The magnesium based oxalate is known as glushinskite [9, 10]. Whereas, the copper oxalate is known as moolooite [2, 11] and the ferrous oxalate as humboldtine [12, 13]. Two natural univalent oxalates are also well-known. These are the oxalates of sodium and ammonium known as natroxalate and oxammite, respectively [14].

Applications of various metal, mixed metal and non-metal oxalate compounds are well known. Many researchers have studied several synthetic metal and non-metal oxalates such as nickel oxalates, calcium oxalates, ammonium oxalates, etc, and mixed metal oxalate, for instance, dipotassium bisoxalatonickel(II) hexahydrate [15-21]. Many oxalates are predominantly found active in second harmonic generation (SHG) [22, 23]. Moreover, sodium oxalate is one of the many organics present in Bayer liquor (Bayer Process; extraction of alumina from its mineral) [24].

In the present investigation, sodium oxalate crystals have been grown by using single diffusion gel growth technique and characterized by employing various techniques, viz. thermogravimetry, FT-IR and dielectric study.

9.1.1   Growth of Sodium Oxalate Crystals:

(a)   Gel Preparation:

The silica hydro-gel was prepared from sodium meta-silicate solution of desired specific gravity, as mentioned in the section 5.3 of Chapter-V. The stock solution of sodium meta-silicate was prepared as mentioned earlier in section 5.3 of Chapter-V. By adding double distilled water of appropriate volume in to the stock

solution, one can prepare the solution of desired specific gravity. In the present study, the specific gravity was selected as 1.05. This sodium meta silicate solution was acidified by 3 N, acetic acid in such a manner that appropriate pH was obtained. The pH value 5.0 was fixed for the mixture.

(b)   Sodium Oxalate Crystal Growth:

The growth of sodium oxalate crystals has been carried out using the solubility reduction method of the single diffusion gel growth technique. This has been elaborately explained in Chapter –III.

Figure (9.1): Sodium oxalate crystal growth

Glass test-tubes of 25mm diameter and 150mm length were used as crystal growth apparatus. The above mentioned mixture was poured in equal volumes in different test tubes and allowed to set into the gel form. Within 48 hours a good quality neutral gel was set. Thereafter, 1.5 M oxalic acid solution was poured on to the set gel. After a few days good quality, colourless, transparent, prismatic, single crystals of sodium oxalate have been grown, which are shown in figure (9.1).

9.1.2   Characterization of Sodium Oxalate Crystals:

9.1.2.1 Thermogravimetry Analysis (TGA):

Several oxalate compounds have been studied by various researchers [25-27]. Girija et al. [26] have reported the TGA of gel grown calcium oxalate monohydrate (COM) crystals. Recently, Frost and Weier [25] have reported the thermal decomposition of humboldtine (FeC_2O_4 $2H_2O$) using nitrogen atmosphere.

Thermogravetric analysis of the sodium oxalate crystals was carried out using nitrogen atmosphere on STA 409C instrument at SAIF, Chennai. The sample was heated up to 1000 ^{0}C from the room temperature at the heating rate of 28 ^{0}C/ min., the following figure (9.2) shows the thermogram of sodium oxalate crystals.
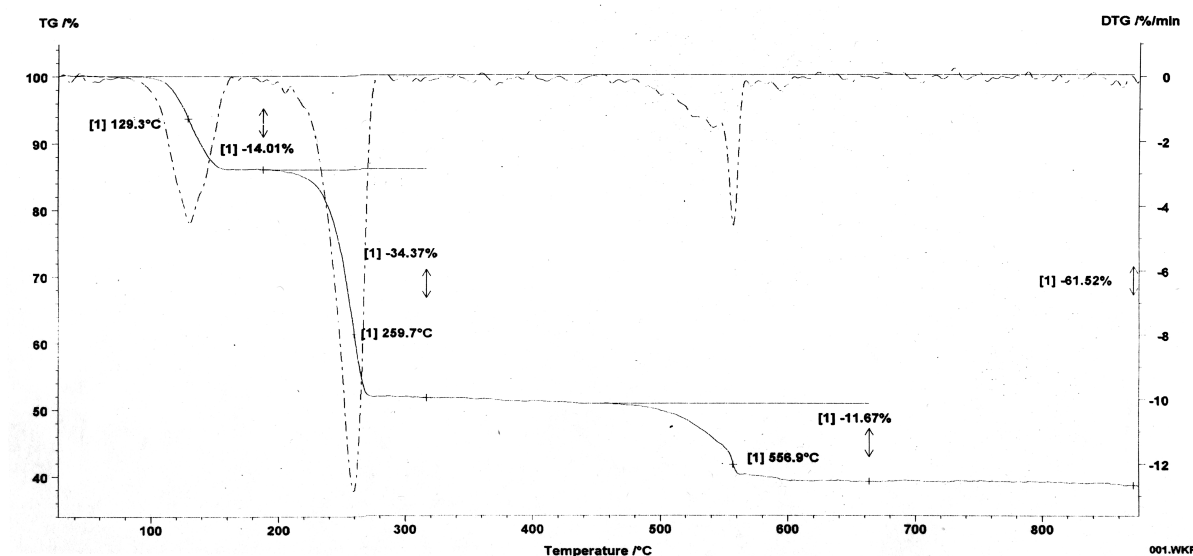
Figure (9.2): Thermogram of the sodium oxalate monohydrate crystals

From the thermogram one can observe that the sample has lost its water molecule at 129.3 ^{0}C and becomes anhydrous. In the second stage, at 259.7 ^{0}C the loss of 2CO is observed and in the third stage the ½ O_2 is lost at 556.9 ^{0}C. However, one water molecule was associated with the sodium oxalate crystal. Table (9.1) represents the decomposition process of the sodium oxalate crystals.

Table (9.1)

The decomposition process of sodium oxalate monohydrate crystals and TG results.

Temperature (^{0}C)	Substance	Theoretical weight (%) (Calculated)	Practical weight (%) (from graph)
Room Temperature	$Na_2C_2O_4 \cdot 1.21\ H_2O$	100	100
129.3 ^{0}C	$Na_2\ C_2O_4$	85.99	85.99
259.7 ^{0}C	Na_2O_2	50.19	51.62
556.9 ^{0}C	Na_2O	39.88	39.95

9.1.2.2 Kinetic Study of Dehydration:

The pyrolysis occurs through many stepped mechanisms. Various kinetic parameters such as the order of reaction, the frequency factor and the activation energy can be calculated from the pyrolysis curve. Kotru et al. [28] reported the kinetics of solid state decomposition of neodymium tartrate. They also calculated various kinetic parameters.

The Coats and Redfern relation [29] was used to calculate various kinetic parameters of decomposition process for sodium oxalate crystals, which are discussed in detail in section 6.4.2 of Chapter-VI. Figure (9.3) represents the best linear fitted plot of Coats and Redfern relation for n=0, where n represents the order of reaction. The values of activation energy and frequency factor are also calculated.
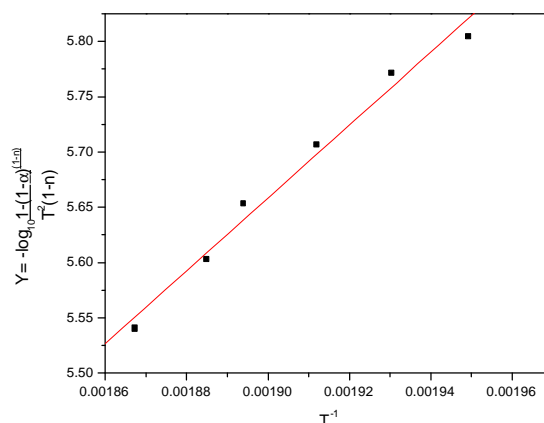

Figure (9.3): Plot of Coats and Redfern relation for sodium oxalate crystals

The values of frequency factor and activation energy are estimated from the equation (6.1) of section 6.4.2 of Chapter-VI, which are estimated to be 2.141 X 10^{17} and 62.414 kJMol^{-1}, respectively.

Table (9.2)

The values of different kinetic parameters obtained from the Coats-Redfern relation.

Samples	Kinetic Parameters
Sodium oxalate monohydrate	Order of reaction (n) = 0
	Activation energy (E) = 62.414 kJMol^{-1}
	Frequency factor (A) = 2.141 X 10^{17}

9.1.2.3 Thermodynamic Parameters: -

The thermodynamic parameters have also been evaluated from the decomposition stage of thermogram of sodium oxalate monohydrate crystals by using formulae given in section 6.4.3 of Chapter-VI. Table (9.3) represents various thermodynamic parameters of decomposition of sodium oxalate crystals.

The standard enthalpy, Ä$^{\#}$H°, is positive, which indicates the reaction is endothermic. The positive value of standard change in entropy, Ä$^{\#}$S°, indicates spontaneous reaction. Also, the positive value of standard change in Gibbs free energy, Ä$^{\#}$G°, suggests spontaneous reaction.

Table (9.3)

The values of different thermodynamic parameters of sodium oxalate crystals

Sodium oxalate monohydrate crystalline sample	Entropy Ä$^{\#}$S° = 82.1696 JMol^{-1}
	Enthalpy Ä$^{\#}$H° = 53.708 kJ Mol^{-1}
	Gibbs free energy Ä$^{\#}$G°=10.684 kJ Mol^{-1}
	Standard change in internal energy Ä$^{\#}$U° = 58.0616 kJ Mol^{-1}

9.1.2.4 FT-IR Spectroscopic Studies: -

Various researchers have studied oxalic acid and oxalate compounds by the FT-IR and Raman spectroscopy [6, 25, and 27]. Frost et al. [30] have studied various natural oxalate compounds using both Raman and Infrared spectroscopy and reported that each oxalate mineral has its own characteristic spectrum. However, the minerals weddellite and whewellite are showing strong similarities in their spectrum, except for the water OH stretching region and the very low wave number region. In another study, Frost and Weier [25] have reported the FT-IR and Raman spectroscopic study of the humboldtine (FeC_2O_4 $2H_2O$). Joshi [27] reported the FT-IR spectroscopic study of the COM crystals.

The FT-IR spectrum of sodium oxalate monohydrate was recorded on a Shimadzu 8400 instrument in KBr disc medium, in the range from 400 cm^{-1} to 4000 cm^{-1}. From this spectrum one can notice that the absorptions between 418 cm^{-1} to 600 cm^{-1} show the presence of oxygen-metal bonds. Broad absorptions at 1741.6 cm^{-1} and 1613.3 cm^{-1} indicate the presence of more than one C=O bond, while the absorptions at 885.3 cm^{-1}, 1029.6 cm^{-1} and 1236.3 cm^{-1} are due to C - C stretching vibrations.
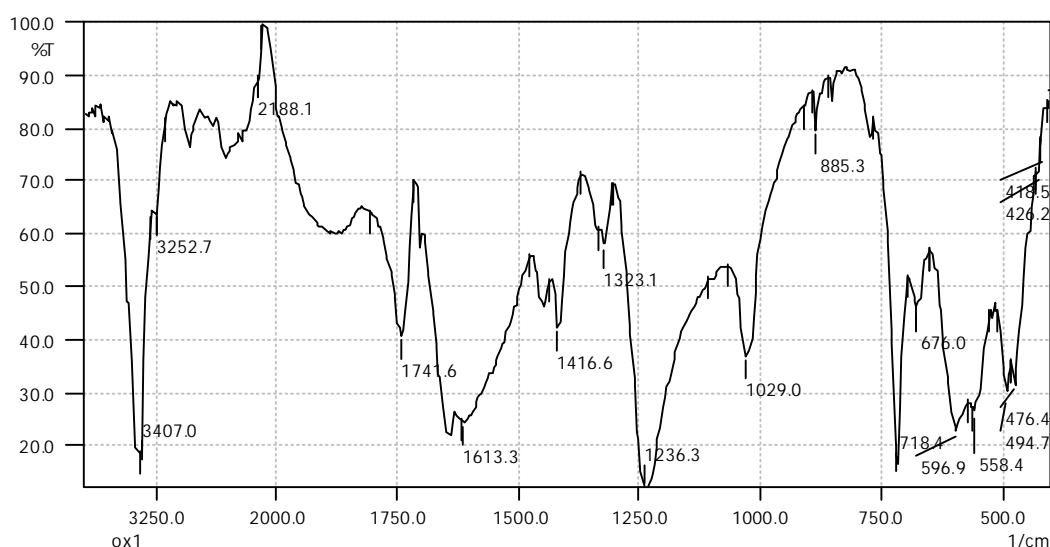

Figure (9.4): FT-IR spectrum of the sodium oxalate crystals

Table (9.4)

Assignments of different absorption bands in the FT-IR

spectrum of sodium oxalate monohydrate crystals

Sodium oxalate monohydrate crystals	
Assignments	Observed frequencies (Cm^{-1})
Metal-oxygen bond	418.5 to 596.9
C= O	1613.3 1741.6
C - C	885.3 1029.6 1236.3
O – H bending	1323.1 1416.6
O-H Stretching	3407.0

The presence of water of hydration is primarily confirmed with the presence of sharp dip at 3407 cm^{-1}, which is regarded due to O-H stretching. The figure (9.4) represents the FT-IR spectrum of the sodium oxalate crystals and Table (9.4) gives the assignments of different bonds in the spectrum.

9.1.2.5 Dielectric Studies of the Sodium Oxalate Crystals:

The variation of capacitance values at different applied frequencies is measured by precision LCR meter at room temperature, using pelletized samples. The values of dielectric constants were calculated using the standard formula.
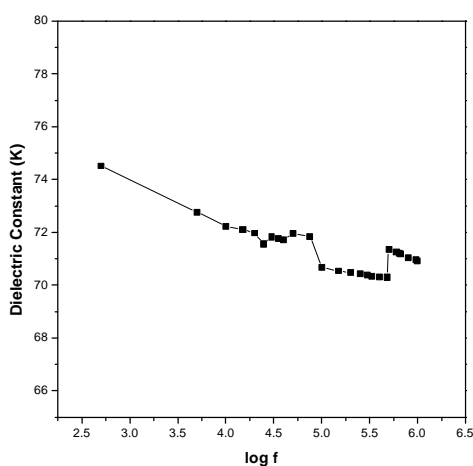
Figure (9.5): Plot of dielectric constant versus *log f*

The variation of dielectric constant with frequency is shown in figure (9.5). The plot suggests that as the frequency increases the dielectric constant decreases with some variations. However, the variation in the dielectric constant is very less, that is, 74.51 maximum and 70.30 minimum, in the range of frequency applied. It can be concluded that the dielectric response of the sodium oxalate monohydrate crystal was very less through out the applied frequency region.

9.2 Growth and Characterization of Sodium Pyrophosphate (SPP) Crystals:

The pyrophosphate ion, $(P_2O_7)^{-4}$, is produced in large quantities in the human body during the synthesis of proteins and other macromolecular substances [31] and is found in low concentrations in blood, saliva, and other body fluids, all of which are natural, aqueous chemical systems. Moreover, certain crystalline pyrophosphates, namely, the monoclinic and triclinic polymorphs of calcium pyrophosphate dihydrate, $Ca_2P_2O_7. 2H_2O$, occur naturally in the cartilage of the joints and under pathological conditions these crystals may be released into the synovial fluid, causing the disease pseudogout or "calcium pyrophosphate crystal deposition disease" [32]. Pyrophosphate ion is also adsorbed onto the surfaces of calcified tissues in the body and may make up as much as 1% of the total inorganic phosphate in bone and dentin [31]. Sodium pyrophosphate is also used to extract the iron and aluminum from the soil organic complexes [33].

The aim of the present study is to grow sodium pyrophosphate (SPP) crystals using the slow evaporation solution growth technique with the help of indigenously developed set up. The FT-IR spectroscopy and dielectric studies have also been carried out for the SPP crystals.

9.2.1 Growth of SPP Crystals:

A necessary condition for the growth of crystals is the acquisition of supersaturation [34]. Supersaturation is defined as $\ddot{A}C = C_{01} - C_{02}$, where C_{01} is the saturation concentration at temperature T_1 of the saturator and C_{02} is the saturation concentration at temperature T_2 of the crystallizer [35]. Supersaturation can be achieved by addition of solute, by evaporation of solvent, by temperature gradient (particularly in hydrothermal method) or by super-cooling. If the temperature is lowered by a constant rate, the constant value of $\ddot{A}C$ can be achieved by knowing the rate of lowering. Also to achieve the required supersaturation, the evaporation of solvent at constant rate and constant temperature is carried in another method. Required supersaturation can also be achieved by continuously lowering temperature in the predetermined programmed manner, which is more difficult than the first two methods. However, the choice of the method is mainly dependent on the shape of the solubility curve and the magnitude of solubility. Recently, Arora and Amin [36] have made an attempt to develop indigenous set up for solution growth.

However, in the present study, indigenously made growth set-up is also developed, which can be easily employed for temperature lowering as well as solvent evaporation techniques.

9.2.1.1 Indigenous Set up for Solution Growth Method:

Indigenous set up for slow cooling technique was designed and developed by the present author, which is shown in figure (9.6). A glass beaker of 2 liter capacity was selected as a crystallizing apparatus. This beaker was placed in another beaker filled with water and the water was constantly stirred with the help of aerator to maintain the homogeneous temperature through out the beaker. Water of the outer beaker could also be stirred by low RPM motors.
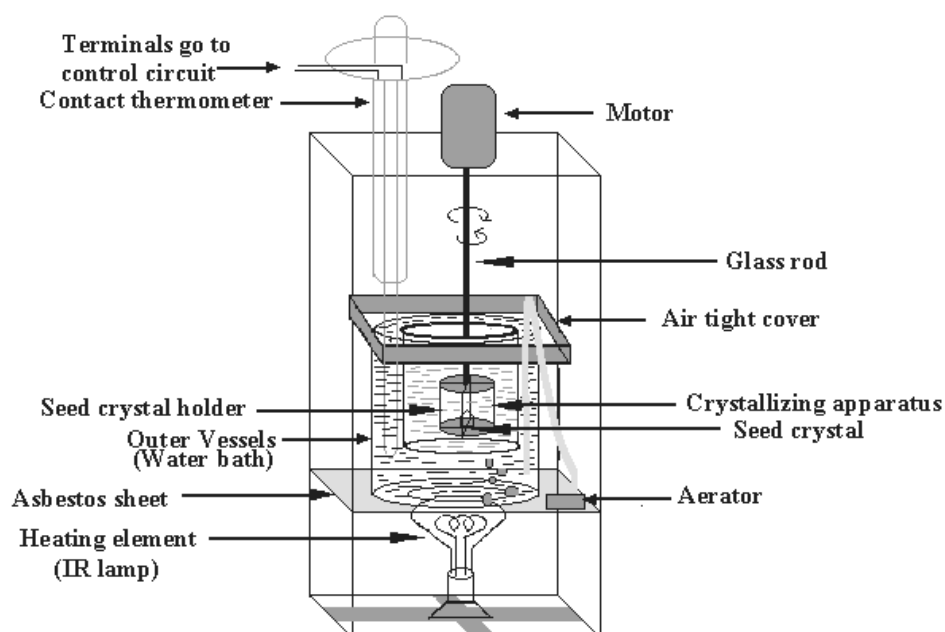
Figure (9.6): The schematic diagram of the indigenously made growth set-up for solution growth

A special kind of seed holder was designed on the basis of earlier design of Dixit et al. [37]. The schematic diagram of the seed crystal holder is shown in figure (9.7). Kinetics of surface processes is strongly dependent on convection driven by crystal and platform rotation; such stirring modes have been successfully used to enhance growth rates in several solutions growth systems [38].
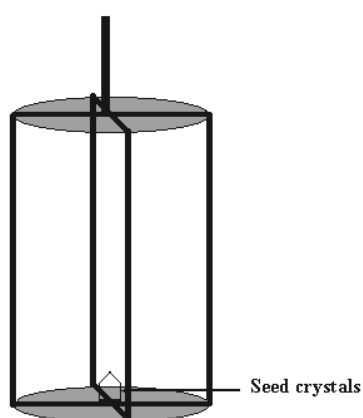

Figure (9.7): Seed crystal holder

In the present case, a disc shape acrylic platform with four acrylic supporting poles, connected to the motor drive, employed as the seed crystal holder. The seed crystal was sticked with suitable non-reacting glue on the platform. The acrylic platform and poles were properly buffed so that no unwanted nucleation occurred at corners and edges. A suitable motor executing back and forth rotations was selected to rotate the seed crystal holder.

9.2.1.2 SPP Crystal Growth:

The seed crystals were grown from controlled evaporation of saturated solution of SPP in water in a small beaker. Good quality seed crystals were picked up for growth. A glass beaker of 2 lit. capacity was used as the crystallizing apparatus. This beaker was kept in a water bath with temperature control of $\pm$ 0.1 ^{0}C. Water in the bath was stirred slowly with the use of aerator. Supersaturated solution of SPP was poured in the crystallizing apparatus and a seed crystal was put carefully in the specially made seed crystal holder. The temperature of the water bath was maintained at 40 ^{0}C and the evaporation rate was carefully controlled.

Figure (9.8): Grown SSP Crystals

Good quality single crystals with maximum dimension 0.75 cm X 0.75 cm were obtained. Figure (9.8) shows the type of crystal grown. The crystals were transparent and prismatic with different faces.

9.2.2   Characterization of SPP Crystals:

9.2.2.1 FT-IR Spectroscopic Studies: -

Phosphate and pyrophosphate compounds are widely studied due to their various applications. Many researchers have studied their FT-IR and other characteristics [39-42]. The FT-IR spectrum of the cadmium calcium pyrophosphate crystals has been reported by de Waal et al. [43]. Recently, Gopalkrinshna et al. [44] have reported the FT-IR spectrum of the hydrothermally grown potassium iron (III) pyrophosphate crystals.

The FT-IR spectrum of SPP crystals has been recorded, using the KBr disc, on Shimadzu 8400 instrument in the range of 400 cm^{-1} to 4000 cm^{-1}. Figure (9.9) represents the FT-IR spectrum of the SPP crystals.
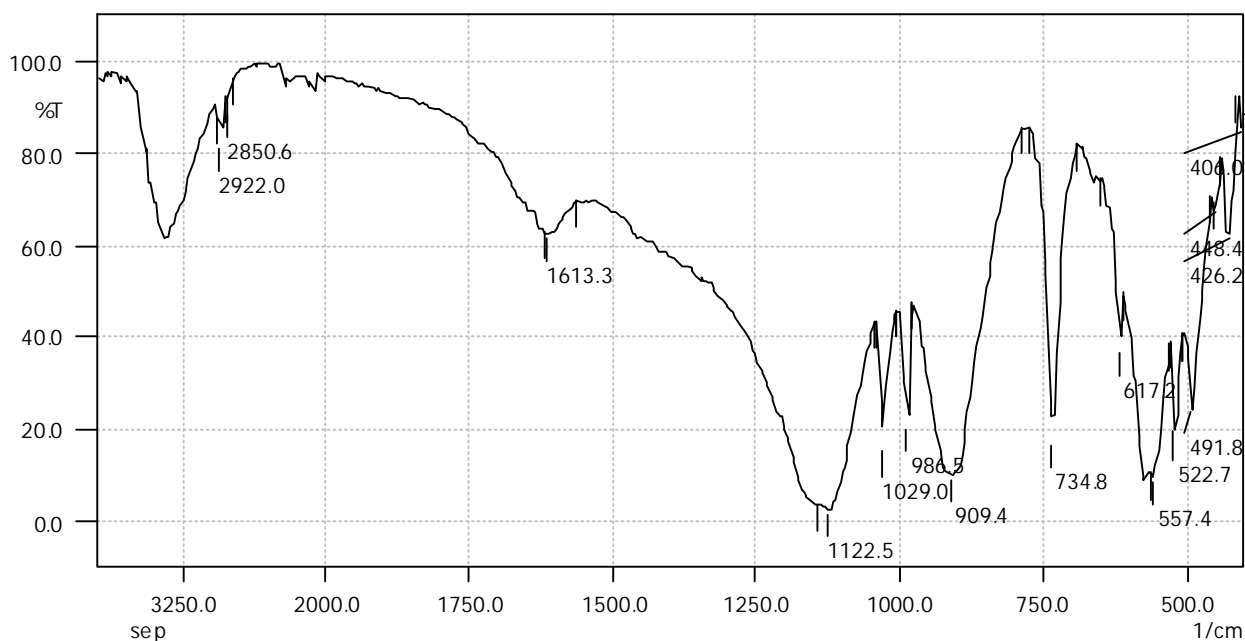

Figure (9.9): FT-IR spectrum of SPP crystals

From the spectrum one can notice the absorptions within 400-491.8 cm^{-1} are due to the presence of metal-oxygen bond. The O-P-O bending was recorded at the 557.4 cm^{-1} and 522.7 cm^{-1}. The P-O symmetric stretching vibrations are observed at 909.4 cm^{-1} and 986.5 cm^{-1}, while the asymmetric stretching vibrations are observed at the

1029.0 cm⁻¹ and 1122.5 cm⁻¹. The absorptions at the 3350 cm⁻¹ and 1613.3 cm⁻¹

correspond to the O-H stretching and bending, respectively. Table (9.5) represents the

assignments of different absorption bands in the FT-IR spectrum of the SPP crystals.

Table (9.5)

Assignments of different absorption bands in the FT-IR spectrum of SPP crystals

Sodium pyrophosphate dehydrate ($Na_4P_2O_7$)	
Assignments	Observed frequencies (Cm^{-1})
O–P–O bending	557.4 522.7
P-O Symmetric stretching bonds	909.4 986.5
P-O Asymmetric stretching bonds	1029.0 1122.5
O-H in plane bending	1613.3
O-H Stretching	3350
Metal-Oxygen bonds	400-600

9.2.2.2 Dielectric Studies of the SPP Crystals:

In this study, the values of the capacitance were measured using the precision

LCR meter; model Agilent 4284A, at room temperature. The pelletized samples were

kept in a specially designed holder for the measurements of values of capacitance at

different applied signal frequencies. The dielectric constant was obtained by using the
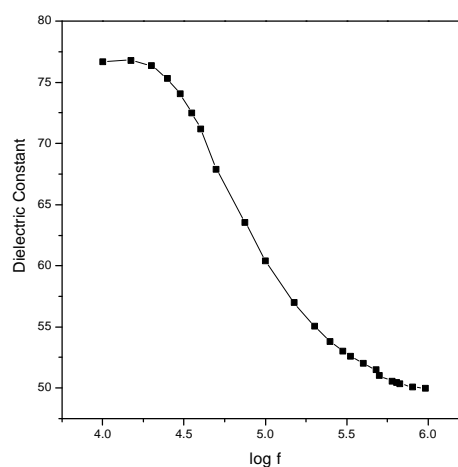
standard formula.

Figure (9.10): Plot of dielectric constant versus *log f*

The figure (9.10) represents the variation of dielectric constant with the frequency. This figure indicates that as the frequency increases the dielectric constant decreases.
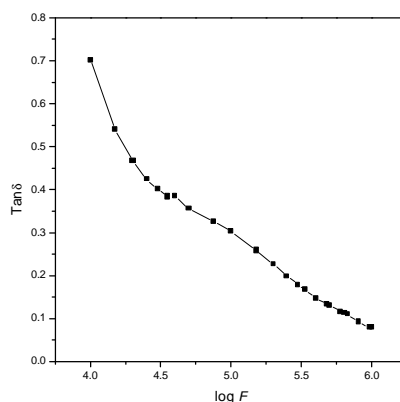

Figure (9.11): Plot of tangent loss versus *log f*

This type of behavior indicates higher space charge polarizability of the material in the low frequency region. As the frequency increases, the dipoles do not comply with the varying external field. Therefore, the polarization decreases and hence the values of dielectric constant decrease as the frequency increases. Figure (9.11) represents the plots of dielectric loss versus frequency, which indicates that as frequency increases the loss tangent decreases. This gives the similar behavior as reported earlier by Dabhi et al. [45] and Arora et al. [46] for various tartrate crystals
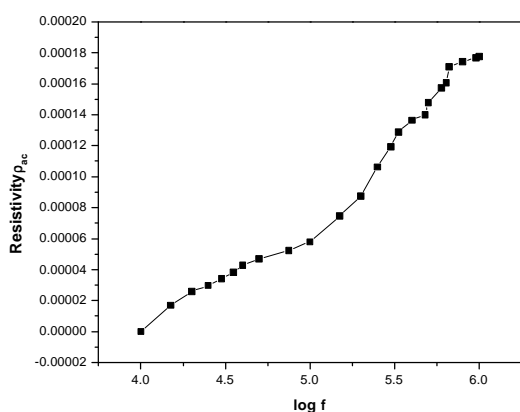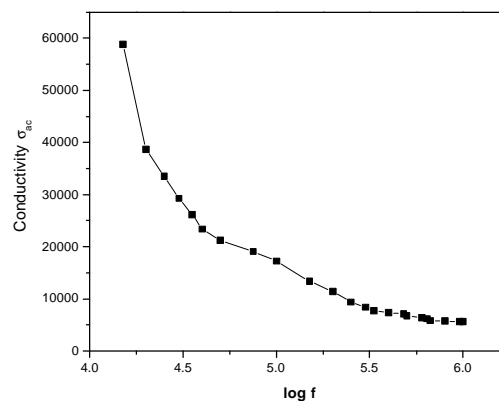

Figure (9.12-a)

Figure (9.12-b)

Figure (9.12 a & b): The plots of a.c. resistivity *(ñ$_{ac}$)* and a.c. conductivity *(ó$_{ac}$)* versus *log f*

The figure (9.12 a and b) represent the plots of a.c. resistivity and a.c. conductivity versus frequency. The a.c. resistivity and a.c. conductivity were calculated using the formulae (5.21 a and b) given in the section 5.4.3. of Chapter-V.

Figures indicate that as the frequency increases the resistivity increases and the conductivity decreases.

9.3 Growth and Characterization of 4-(2-hydroxy-phenylamino)-pent-3-en-2-one Organic Crystal:

N-Phenyl, especially, N-Benzyl amino acids find applications in peptide synthesis and are valuable building blocks for the synthesis of chiral compounds [47]. Such types of compounds effect heterogene catalysts which have been used for arylation trisopropylsilyl [48], tat-butyl demthyl silyl [49] and benzyl protecting groups [50]. The development of 4-(3', 5'-Dibromo 4'-hydroxyphenyl) aminl-6,7-dimethoxy quinazoline [51] has provided the basis for new treatment as well as prevention programs for allergic asthma. Owing to the medicinal properties of (hydroxyl-phenyl amino derivatives), the crystal growth of organic material 4-(2-hydroxy-phenylamino)-pent-3-en-2-one (HPAP) has been carried out. Apart from the crystal structure determination, different characterizations, such as FT-IR, TGA, dielectric studies, photoconductivity measurement and NLO test have also been carried out.

9.3.1 Growth of HPAP Crystals:

The synthesis of HPAP was done by using solution of 2- amino phenol (1.09 gm, 0.01 mole) and acetyl acetone (1.00 gm, 0.01 mole) in methanol (20 ml), which was stirred for 12 hours in presence of a few drops of pyradine at room temperature. The reaction mixture was allowed to stand at room temperature for 24 hours. The

content was then poured into the ice-cold water. The solid separated was filtered and washed with water and recrystallized from methanol.

In the present study, acetone and methanol both were selected as solvents; however, methanol yielded good quality single crystals. The seed crystals were grown from controlled evaporation of saturated solution of HPAP in methanol and good quality crystals were picked up for growth. A glass jar of 4 cm diameter and 7 cm length was selected as a crystallizer. This jar was kept in a water bath with temperature control of $\pm 0.1\ ^0$C. Water in the bath was stirred slowly. Supersaturated solution of HPAP was poured into crystallizer and a seed crystal was hung by using very fine nylon thread. The temperature of the water bath was maintained at $40\ ^0$C and the evaporation rate was carefully controlled.
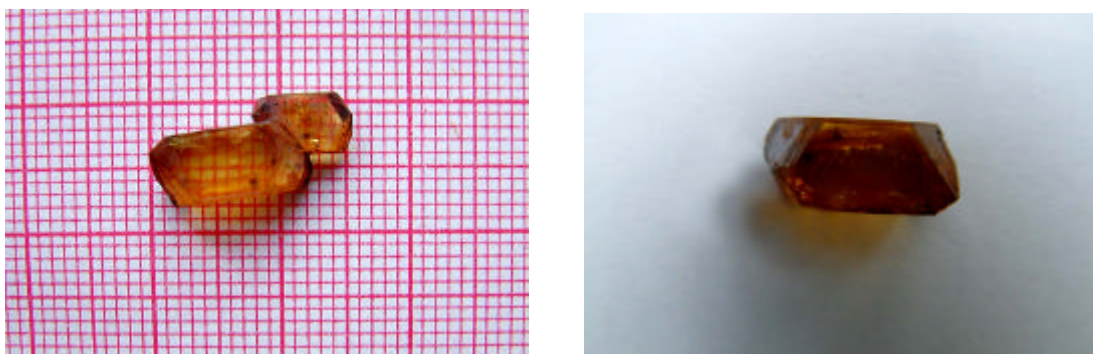

Figure (9.13): Photograph of the grown HPAP crystals

Good quality single crystals with maximum dimension 1.5 cm X 0.75 cm were obtained. Figures (9.13) show the types of crystals grown. The crystals were yellowish brown in color.

9.3.2   Characterization of HPAP Crystals:

9.3.2.1 Single Crystal X-ray Diffraction and Structure Determination:

The three dimensional intensity data were collected on an Enraf-Nonius CAD-4 diffractometer. The reflection data were collected at 293 K and ù/2è scan mode was employed for data collection by using MoK$_á$ radiation (ë = 0.71073 Å). The structure

has been elucidated by direct methods using SHELEX 97 [52]. All non-hydrogen atoms of the molecule were located from the E-map. Isotropic refinement of the structure by least squares methods using SHELEX 97 [53] was followed by anisotropic refinement of all the non-hydrogen atoms. All the hydrogen atoms were fixed stereochemically. Atomic scattering factors were taken from International tables for crystallography (1992 Vol. C Tables 4.2.6.8 and 6.1.1.4). Geometrical and other structural calculations were performed by using PARST [54] programme. The experimental details and other measurement data are given in Table (9.6). The atomic coordinates and anisotropic displacement parameters of the non-hydrogen atoms are given in Table (9.7) and geometry of intra- and intermolecular hydrogen interactions are given in Table (9.8). The bond lengths and bond angles are given in Table (9.9). An ORTEP diagram of the compound with atom numbering scheme is shown in figure (9.14) and figure (9.15) represents the packing diagram of HPAP crystals, which showing the hydrogen-bonding network [55].
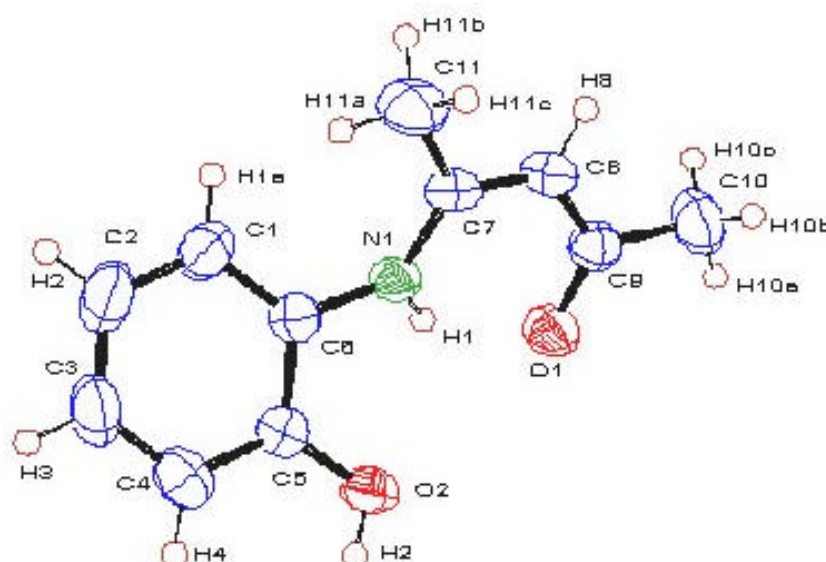

Figure (9.14): ORTEP Diagram of HPAP Crystals

Table (9.6)

Crystal data from single crystal XRD

Crystal data and experimental data.	
Formula	$C_{11}H_{13}NO_2$
Relative formula weight	192.23
Crystal system	Orthorhombic
Space group	$P2_12_12_1$
Cell dimensions	a = 8.839(3)
	b = 10.517(2)
	c = 11.223(3)Å
Z	4
V	1043.4(5)Å^3
T	293(2) K
Dx	1.224 Mg/m^3
ì	0.084 mm^{-1}
è$_{max}$	24.95^o
Radiation (M$_o$ K$_á$)	ë=0.71073 Å
Crystal Size	0.3 x 0.2 x 0.3 mm
F (000)	412
Total no. of reflections	1095
No. of independent reflections	1078
No. of observed reflections	1079
No. of parameters	128
R-value	0.0425
Rw	0.1211
Refinement method	Full- matrix least- squares on F^2
Goodness-of-fit on F^2	1.043
(Ä/ó)$_{max}$	0.005
(Äñ)$_{max}$	0.204 e. Å^{-3}
(Äñ)$_{min}$	–0.179 e. Å^{-3}
Measurement:	ENRAF-NONIUS Detector Program
Program system:	ENRAF-NONIUS Program
Structure determination:	SHELXS97
Structure drawing:	ORTEP III
Refinement:	SHELXL97

Table (9.7)

Atomic coordination of non-hydrogen atom of HPAP crystals

Atomic coordinates (x 10^4) and equivalent isotropic thermal parameters (Å^2 x 10^3) for non-hydrogen atoms				
Atom	X	Y	Z	U_{eq}^*
O1	4531(2)	6847(2)	8517(2)	55(1)
O2	0807(2)	7068(2)	9604(2)	54(1)
N1	1977(3)	5782(2)	7819(2)	40(1)
C1	-0309(4)	4410(3)	7765(3)	57(1)
C2	-1712(4)	4127(3)	8227(4)	70(1)
C3	-2280(4)	4813(3)	9156(3)	65(1)
C4	-1468(3)	5800(3)	9641(3)	55(1)
C5	-0072(3)	6120(2)	9177(2)	41(1)
C6	0517(3)	5424(3)	8216(2)	41(1)
C7	2593(3)	5780(3)	6732(2)	42(1)
C8	4032(3)	6224(3)	6552(2)	46(1)
C9	4953(4)	6765(3)	7444(3)	44(1)
C10	6472(4)	7294(4)	7122(3)	68(1)
C11	1679(4)	5332(4)	5685(3)	66(1)

$U_{eq}^* = (1/3)\sum_i \sum_j U_{ij} a_i^* a_j^* (a_i . a_j)$

Table (9.8)

Geometry of intra- and intermolecular Hydrogen interactions

Geometry of intra- and intermolecular Hydrogen interactions.			
X-H...A	H...A(Å)	X...A(Å)	X-H...A(^{o})
O2–H2…O1	1.831(2)	2.650(1)	176.5(2)
N1–H1…O1[(i)]	1.934(1)	2.639(3)	138.4(1)
Equivalent position: (i) -x-1/2, -y+3/2, -z+2			

Table (9.9)

Various bonds and bond length of HPAP crystals

| Bond lengths (Å) and bond angles (°)			
Bond Lenghts (Å)			
O1-C9	1.263(3)	C3-C4	1.375(5)
O2-C5	1.352(3)	C4-C5	1.381(4)
N1-C7	1.336(3)	C5-C6	1.403(4)
N1-C6	1.416(4)	C7-C8	1.370(4)
C1-C2	1.377(5)	C7-C11	1.502(4)
C1-C6	1.389(4)	C8-C9	1.410(4)
C2-C3	1.363(5)	C9-C10	1.498(5)
Bond Angles (°)			
C7-N1-C6	131.2(2)	C1-C6-N1	124.7(3)
C2-C1-C6	120.1(3)	C5-C6-N1	116.2(2)
C3-C2-C1	120.4(3)	N1-C7-C8	120.9(2)
C2-C3-C4	120.7(3)	N1-C7-C11	119.7(3)
C3-C4-C5	120.1(3)	C8-C7-C11	119.4(3)
O2-C5-C4	124.0(3)	C7-C8-C9	124.6(3)
O2-C5-C6	116.4(2)	O1-C9-C8	122.3(3)
C4-C5-C6	119.6(3)	O1-C9-C10	118.0(3)
C1-C6-C5	119.1(3)	C8-C9-C10	119.7(3)
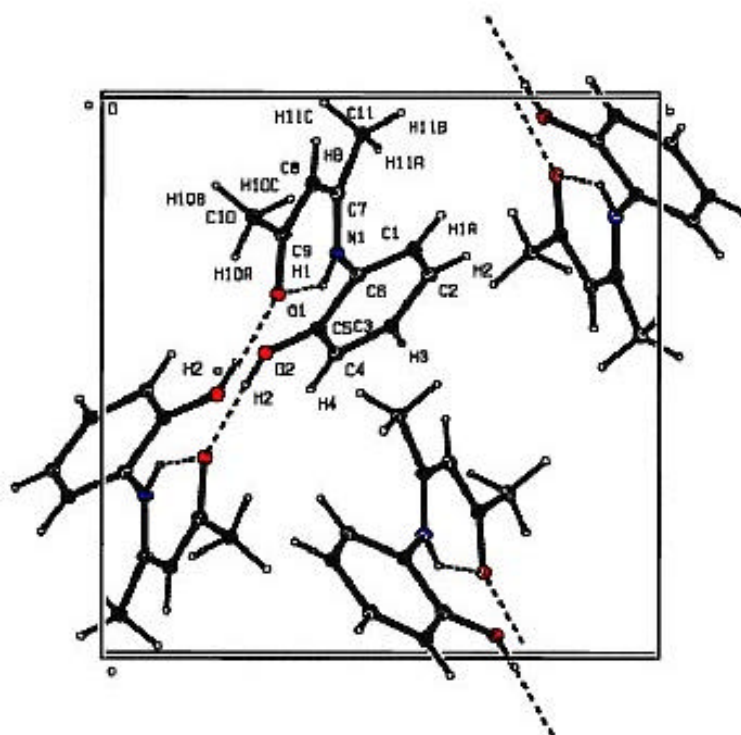
Figure (9.15): Packing diagram 4-(2-hydroxy-phenylamino)-pent-3-en-2-one showing the hydrogen-bonding network

9.3.2.2. Description of the Crystals:

The phenyl ring has geometry, which is more or less similar to its standard values [56-57]. The bonds distances, O1-C9 and N1-C7, are shorter than the normal expected values and the variation of this kind in the value of bond distances has been observed in case of some analogous structures [56-59]. The small value of N1-C7 [1.336(3) Å] in comparison to C6 [1.416(4) Å] results into significant variation in C7-N1-C6 bond angle [131.2 (2)^0]. The difference in C-N bond distances could be due to presence of carbonyl group located at C9 position. Shorting of C7-N1 bond length and a large value of the C-N-C bond angle leads to the existence of N1-H1…O1 intramolecular H- bond [60]. The magnitude of torsion along C6-N1 bond is 35. 3^0. The torsional deformation in other bonds of the side chain is insignificant. The oxygen atom O2 is deviated significantly below the plane of phenyl ring [deviation being -0.823 (2) Å] and it results in the formation of O2-H2…O1 intermolecular interaction. The crystal structure is stabilized by an Intramolecular N1-(amino)-H1…O1 (one) and intermolecular O2-H2…O1 hydrogen bond which falls in the range of 'intermediate hydrogen bonds' as proposed by Desiraju and Steiner [60]. Both kinds of interactions are depicted in the unit cell-packing diagram figure (9.15) in which the molecules are held together through a hydrogen-bonded network. The intramolecular bond results into a virtual six membered ring thus making the present molecule look like as two ring structure. The molecules exhibit typical orthorhombic symmetry. In both the interactions, O1 acts as a bifurcated acceptor atom whereas O2 and N1 act as donors. The details of hydrogen bonding is shown in Table (9.8).

Using compiled data for a large number of O-H…O and N-H…O contacts, Desiraju and Steiner [60] have found significant statistical directionality and

concluded that these are legitimately viewed as 'intermediate' hydrogen bonds, with a greater contribution to packing forces than simple van der Waal interactions.

9.3.2.3 Thermal Studies of HPAP Crystals:

TGA and DSC were performed to know the thermal behaviors of the crystals. Figure (9.16) is the thermogram of the HPAP crystals, which suggests that the crystals give up moisture below 100 ^{0}C and remain stable up to 156.08 ^{0}C, thereafter, decompose rapidly and give up almost 100 percent weight at 350 ^{0}C. A minor weight loss at 89.56 ^{0}C is observed, which may be due to release of moisture from the surface.
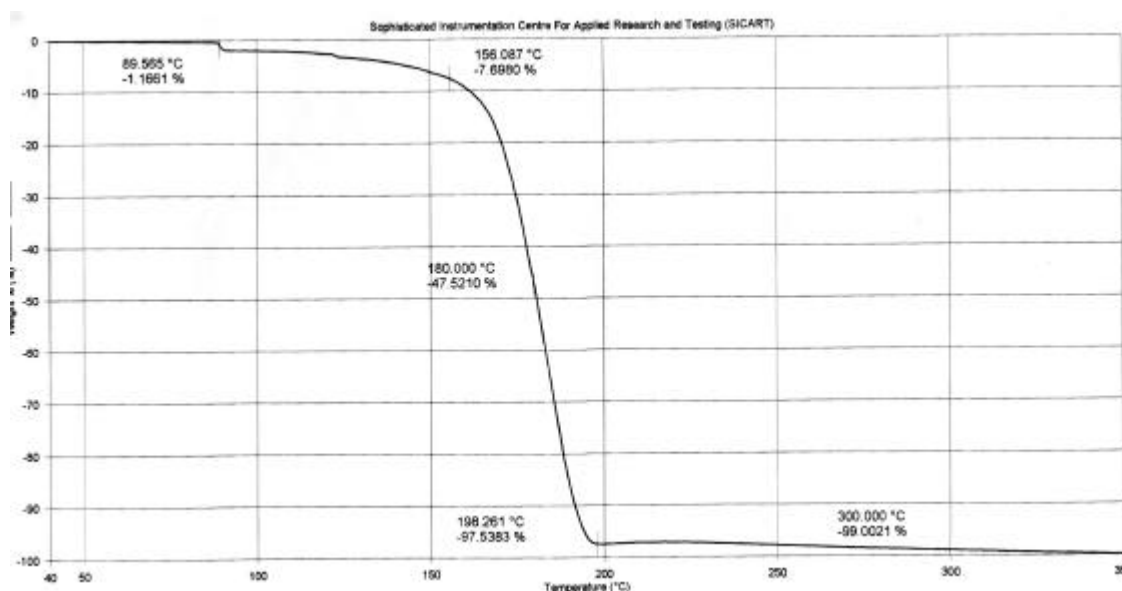

Figure (9.16): Thermogram of the HPAP crystals

The compound remains stable up to 156.08 ^{0}C and then decomposes in a single step to almost zero weight. Figure (9.17) shows DSC trace of the compound, which indicates strong endothermic reaction at 193.296 ^{0}C on set values. This corresponds to decomposition of the compound.
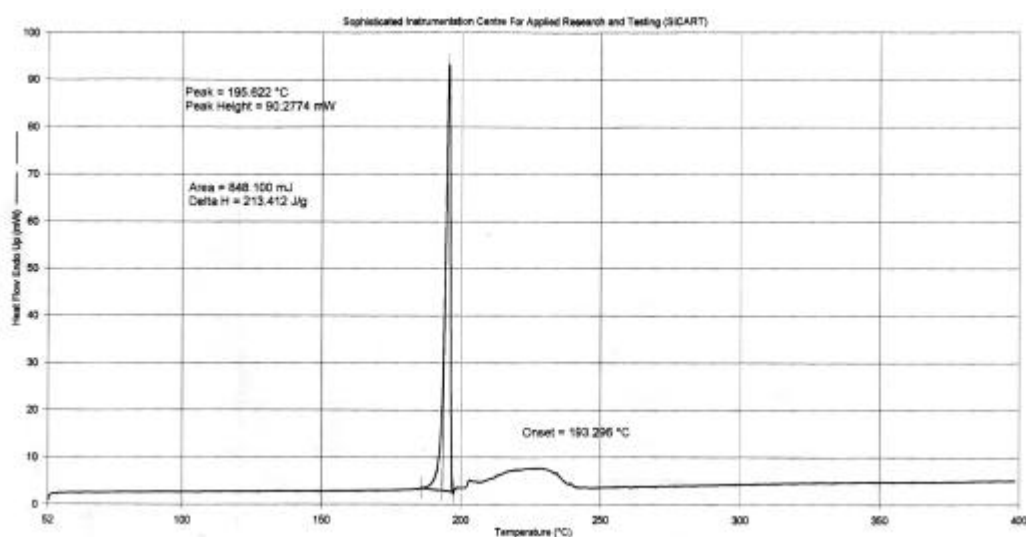
Figure (9.17): DSC curve of the HPAP crystals

9.3.2.4 FT-IR Study of HPAP Crystals:

FT-IR spectrum of HPAP crystals was recorded on the Shimadzu 8400 instrument in the range of 400 cm^{-1} to 4000 cm^{-1}. Crushed powder of pure HPAP crystals was mixed with KBr powder and pelletized for FT-IR spectroscopy. Figure (9.18) represents the molecular structure of the HPAP and figure (9.19) represents the FT-IR spectrum of the HPAP crystals.
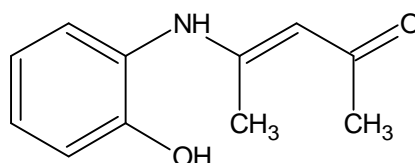

Figure (9.18): Molecular structure of the HPAP

The absorptions taking place within 3440 cm^{-1} to 3250 cm^{-1} are due to –OH and –NH stretching vibrations. The absorption at 2725 cm^{-1} is due to –CH stretching of alkane. Whereas, the absorptions at 1689 cm^{-1} and 1614 cm^{-1} are due to –C=O and –C=C-, respectively. The ring skeleton is identified by the absorption at 1434 cm^{-1}. Moreover, the absorptions occurring at 1174 cm^{-1} and 750 cm^{-1} are responsible to –C-O-C- and orthosubstitution, respectively. Table (9.10) represents various bonds of the HPAP crystals and their absorbed radiation frequencies.
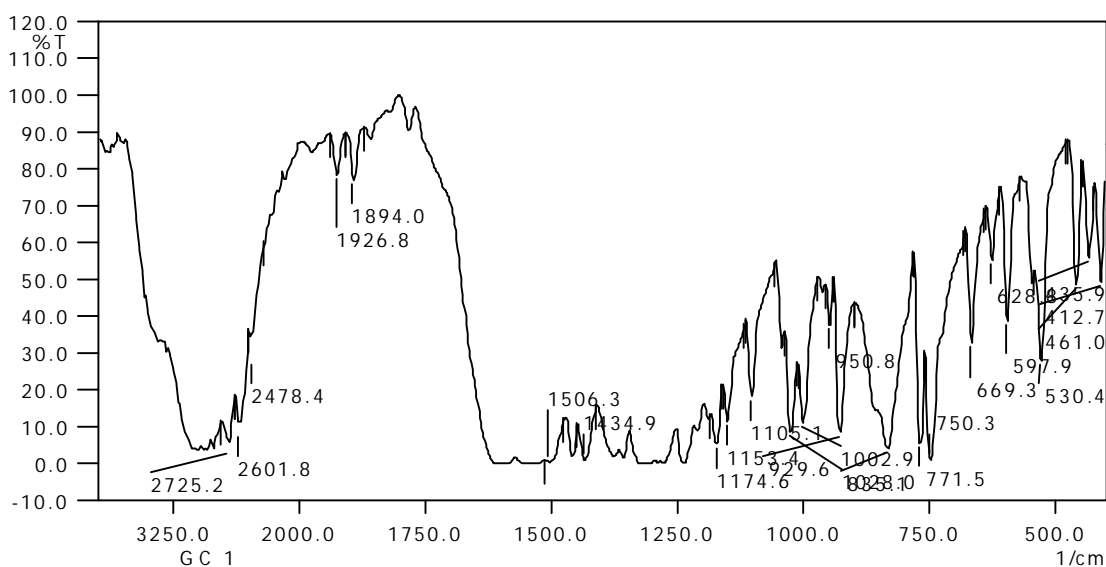
Figure (9.19): FT-IR spectrum of the HPAP crystals

Table (9.10)

Assignments of different absorption bands in

the FT-IR spectra of HPAP crystals

4-(2-hydroxy-phenylamino)-pent-3-en-2-one	
Assignments	Observed frequencies (Cm^{-1})
O – H Stretching	3440.8
N –H Stretching	3250
-CH str. of alkane	2725.2
C= O	1689.5
C = C	1614.3
	1506.3
Ring Skeleton	1434.9
C – O – C	1174.6
Orthosubstitution	750.3

9.3.2.5 Dielectric Studies:

The variation of dielectric constant with frequency has been studied. The dielectric constant was calculated using the formula from section 4.7 of Chapter IV. The variation of dielectric constant with frequency is shown in figure (9.20).
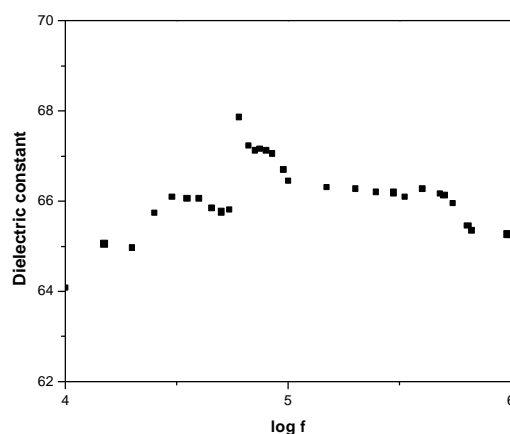
Figure (9.20): Plot of dielectric constant versus *log f*

From the plot it can be notice that the variation in the dielectric constant is very less but haphazard, that is, 70.242 is the maximum value and 65.252 is the minimum value, in the range of frequency from 10 kHz to 1MHz; which suggests that the crystal is very small responsive to the variations in the applied a.c. current.

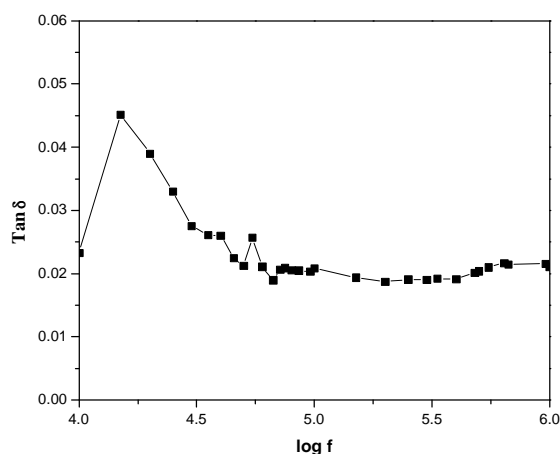**Figure (9.21): Plot of *tan ä* versus *log f***

A typical behavior is observed for the dielectric loss with frequency, which is shown in figure (9.21). Very small variation in the value of dielectric constant with frequency corresponds to the results obtained by other workers on lead phthalocyanine [61]. There are several contributions to the dielectric constant, which

are (1) ionic polarizability (2) interstitial polarizability (3) electronic polarizability (4) lattice polarizability (5) molecular polarizability and (5) ferroelectric transition. It may be conjectured that the molecular polarizability variations are very small with applied frequency of a.c. current. The details are discussed elsewhere [45, 61].

9.3.2.6 Photoconductivity and NLO Studies of HPAP Crystals:

Polished sample of the HPAP was attached to a microscope slide and two electrodes of thin copper wires were fixed by the use of silver paint. The distance (d) between the electrical contacts was 0.112 cm. The sample was connected in series to a d.c. power supply and a picoammeter (Keithley 480). The details of the experimental set-up used in the present study are reported elsewhere [62]. The applied voltage was increased from 0 to 300 V in the steps of 20 V and the corresponding dark current was recorded. The sample was then exposed to the radiation from a 100 W halogen lamp containing iodine vapour and tungsten filament. The emission spectrum of the halogen lamp was observed to be a continuous one with wavelengths ranging from 300 to 1000 nm. The photocurrent was recorded for the same range of the applied voltage. The details of the set-up are discussed in Chapter IV. Figure (9.22) shows the field dependence of dark and photo currents of HPAP crystals and Table (9.11) gives the data of dark current and photocurrent for HPAP crystals.
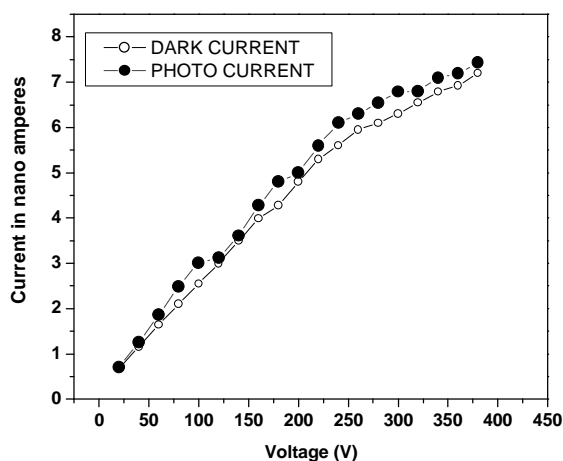

Figure (9.22): Field dependent conductivity of the HPAP crystals

Table (9.11)

Photoconductivity Studies of HPAP Crystals

Voltage (V)	Dark Current (nA) I_d	Photo Current (nA) I_p
20	0.68	0.71
40	1.16	1.25
60	1.64	1.87
80	2.1	2.49
100	2.55	3.01
120	3	3.12
140	3.5	3.61
160	3.99	4.28
180	4.28	4.8
200	4.8	5.0
220	5.3	5.6
240	5.6	6.1
260	5.95	6.3
280	6.1	6.55
300	6.3	6.79
320	6.55	6.8
340	6.79	7.1
360	6.92	7.12
380	7.2	7.23

It can be noticed from figure (9.22) that both dark and photo currents increase almost linearly for HPAP crystals but the dark current is less than the photocurrent, which is known as *positive photoconductivity*. Photoconductivity is explained in detail by Joshi [63]. Photoconductivity was also reported in pure and doped L-argenin phosphate (LAP) crystals by Pragasam [64]. This type of behavior of photoconductivity is due to the increasing number of charge carriers or their life time.

Non-Linear Optics (NLO) is the experimental set-up or the apparatus in which the linear input results in *non-linear output*. Before the advent of lasers, transparent optical materials were assumed to be passive, that is, unaffected by light traveling through them. The high powers of Laser beams made it possible for the first time to observe that the presences of light can, in fact, affect the medium. Intense light can change the refractive index of absorption of the material. When this happens, the light

itself is affected by the change, in a nonlinear way. This can convert Laser in to harmonics of higher orders, i.e. into different colors. This was first observed by Franken et al. [65] in 1961.

In the case of linear optical transitions an electron absorbs a photon from the incoming light and does a transition to the next higher unoccupied allowed state.
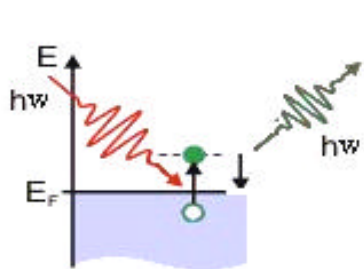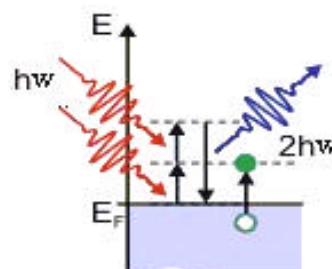

Figure (9.23-a)   **Figure (9.23-b)**

Figure (9.23): Formation of SHG from the crystals

When this electron relaxes it emits a photon of frequency less than or equal to the frequency of the incident light (Fig. 9.23-a). Second harmonic generation (SHG), on the other hand, is a two photon process where this excited electron absorbs another photon of same frequency and does a transition to yet another allowed state at higher energy. This electron, on having transition back to its original state, emits a photon of a frequency which is two times that of the incident light (Fig. 9.23-b). This results in the frequency doubling in the output [66].

The non-linear optics is traditionally introduced by considering that the dielectric susceptibility $\div$ can be expanded in a Taylor series in terms of oscillating optical field. The term $\div_1$ is the dielectric susceptibility measured at low powers. The term $\div_2$, linear in the field, multiplies the incident optical field, generating second harmonic frequencies. The term $\div_3$ is quadratic in the field, producing third harmonic frequencies or introducing a change in the index of refraction. There is a close relationship between $\div_2$ and electro-optic effect. In that phenomenon, an applied

electric field multiplied by the optical field creates an index change through the $\div_2$ term, so that the index of refraction is controlled by an external applied field. [67] Chelma and Zyss [68] have compiled detailed information on this phenomenon and materials observing that.

Materials, which possess optical nonlinearities, have been studied extensively for their possible applications in various fields, for example, telecommunication, optical computing, optical data storage and optical information processing [69-71]. Organic NLO materials are, generally, more versatile than their inorganic counterparts due to their more favorable nonlinear response, but these substances are often formed by weak van der Waals and hydrogen bonds and hence possess a high degree of delocalization [72]. Many organic crystals are well known for their potential NLO applications, such as p-hydroxyacetophenone [73], benzoyl glycine [74], hippuric acid [75], etc. Recently, Dhanuskodi and Vasantha [76] and Dhanuskodi and Manikandan [77], have reported the growth of semi-organic NLO materials, L-aluminium oxalate and methyl-p-hydroxy benzoate, respectively. However, these crystals have inherent limitations such as increased optical absorption, narrow transparency window and poor mechanical and thermal stability. On the other hand, the inorganic NLO crystals have excellent mechanical and thermal properties but possess relatively modest optical nonlinearties because of the lack of ð - electron localization. Potassium dihydrogen phosphate (KDP) [78], ammonium dihdrogen phosphate (ADP) [79], lithium niobate [80], potassium penta borate [81] etc., are well known inorganic NLO materials. Combining the high optical nonlinearity and chemical flexibility of organics with temporal and thermal stability as well as excellent transmittance of inorganics, a new class of semiorganic materials has been developed, which is attracting a great deal of attention in the nonlinear optical field [82, 83]. L-Histidine

tetrafluoroborate (L-HFB) is a semiorganic NLO material, having SHG efficiency five times greater than KDP [84]. There are many other semiorganic materials with potential SHG efficiency, for example, amino-acid salts; L-arginine phosphate monohydrate [85], and zinc cadmium thiyocynate (ZCTC) [86].

In the present study, NLO properties of the HPAP crystals were measured by measuring the second harmonic generation (SHG) efficiency. The crystal was evaluated by the Kurtz and Perry powder technique using a Q-switched, mode locked Nd:YAG laser. A microcrystalline material of KDP was used for the comparison purpose with HPAP sample in the SHG measurements. The fundamental laser beam of 1064 nm was used as a source. For a laser input pulse of 6.2 mJ, the second harmonic signal (532 nm) of 23 to 24 mV and 275 mV were obtained through HPAP and KDP crystal, respectively. Thus the SHG efficiency of HPAP crystal was nearly one tenth of KDP crystals. But the NLO properties can be increased either by proper doping of the suitable material or by making the proper inorganic salt of HPAP.

9.4 Conclusion:

(1)   The growth of sodium oxalate crystals was carried out using the single diffusion gel growth technique in the test tubes. Good quality, colourless, transparent, prismatic, single crystals of sodium oxalate were harvested.

(2)   Sodium oxalate crystal decomposes into the three stages. In the first stage, at 129.3 ^{0}C, the sample gives up its water molecule and becomes anhydrous. In the second stage, at the 259.7 ^{0}C, the loss of 2CO is observed; in the third stage, the ½ O_2 is lost at 556.9 ^{0}C and the final product di-sodium oxide remain stable up to 1000 ^{0}C. One water molecule was associated with the sodium oxalate crystal.

(3)   Applying the Coats and Redfern relation to the decomposition stage of the pyrolysis curve of sodium oxalate crystals, the kinetic parameters, such as, the order of reaction and activation energy, were evaluated. The values of order of reaction and activation energy were found to be zero and 62.414 kJ Mol^{-1}, respectively.

(4)   The thermodynamic parameters were also evaluated for the decomposition stage of the pyrolysis curve of sodium oxalate crystals. The values of the standard change in entropy, enthalpy and Gibbs free energy were found to be 82.169 J mol^{-1}, 53.708 kJ mol^{-1} and 10.684 kJ mol^{-1}, respectively. The reaction was suggested as spontaneous type from the thermodynamic parameters.

(5)   The presence of metal-oxygen bond, C=O bond, C-C bond and O-H bending and stretching were confirmed from the FT-IR spectrum of the sodium oxalate crystals.

(6)   As frequency increased the dielectric constant decreased for sodium oxalate crystals. However, sample showed very less response to frequency change.

(7)   SPP crystals were grown by using the indigenously developed crystal growth set up, which can be used for both slow evaporation and slow cooling methods. However, SPP crystals were grown by the slow evaporation technique. Good quality single crystals with maximum dimensions of 0.75 cm X 0.75 cm were grown.

(8)   The P-O symmetric and asymmetric stretching, O-P-O bending, O-H bending and stretching and metal oxygen bonds were confirmed form the FT-IR spectrum of the SPP crystals.

(9)   Dielectric constant decreased as the frequency increased for the SPP crystals. This suggested the high polarizability of the material in the low frequency region. The loss tangent and the conductivity also decreased as the frequency increased and, in contrast, the resistivity increased as the frequency increased.

(10)   The growth of HPAP crystals was carried out using the slow evaporation technique. Good quality, transparent, yellowish brown colour crystals of maximum 1.5 cm X 0.75 cm dimensions were grown.

(11)   From the single crystal XRD it was confirmed that the HPAP crystal was having orthorhombic crystal structure with space group $P2_12_12_1$. The cell parameters were estimated as follows,

$a = 8.839(3)$, $b = 10.517\,(2)$, $C = 11.223\,(3)$, $á = â = ã = 90^0$

(12)   The HPAP crystals exhibited very poor thermal stability. Pyrolysis curve suggested that the crystals gave up moisture below $100\,^0C$ and remained stable up to $156.08\,^0C$, thereafter, it decomposed rapidly in one stage and lost almost 100 percent weight at $350\,^0C$. A minor weight loss at $89.56\,^0C$ was observed, which might be due to the release of moisture from the surface.

(13)   FT-IR spectrum of HPAP crystals confirmed the presence of C=O, C=C, C-N, N-H stretching and rocking vibrations, O-H bond and ring skeleton.

(14)   Dielectric study suggested very poor response to the frequency change. However, the dielectric constant versus frequency gave the haphazard behavior, within the maximum 70.242 and the minimum 65.252 values of the dielectric constant.

(15)   The photoconductivity study suggested that the value of the dark current was less than the photocurrent, indicating the positive photoconductivity.

(16)   The NLO properties of the HPAP crystals were carried by Kurtz and Perry powder technique using a Q-switched, mode locked Nd:YAG laser. With comparison to a well-known NLO material, potassium dihydrogen phosphate (KDP), it showed one tenth of second harmonic generation (SHG) efficiency. Hence, sample gave very poor NLO behavior but it could be increased by proper doping of different suitable materials.

References:

[1]   H. J. Arnott and M. A. Webb; *Scanning Electron Microsc.,* (1983) 1747-1758.

[2]   J. E. Chisholm, G. C.Jones, and O.W. Purvis; *Mineralogical Magazine,* **51** (1987) 715.

[3]   A. Frey-Wyssling; *Am. J. Bot.,* **68** (1981) 130.

[4]   G. M. Gadd; *Mineralogical Society Series,* **9** (2000) 57.

[5]   T. Wadsten and R. Moberg; *Lichenologist,* **17** (1985) 239.

[6]   A. J. Macnish, D. E. Irving, D. C. Joyce, V. Vintage, A. H. Wearing, R. I. Webb and R. L. Frost; *Austr. J. of Botny,* **51** (2003) 565.

[7]   J. P. Pestaner, F. G. Mullick, F. B.Johnson and J. A. Centeno; *Archives of Pathology & Laboratory Medicine,* **120** (1996) 537.

[8]   J. Dubernat and H. J. Pezerat; *Appl. Crystallogr.,* **7** (1974) 387.

[9]   H. Pezerat, J. Dubernat, and J. P.Lagier; *C. R. Acad. Sci.,* Paris, Ser. C*,* **288** (1968), 1357.

[10]   M. J. Wilson and P. Bayliss; *Mineralogical Magazine,* **51** (1987) 327.

[11]   R. M. Clarke, and I. R. Williams; *Moolooite, Mineralogical Magazine,* **50** (1986) 295.

[12]   K. Rezek, J. Sevcu, S. Civis, and J. Novotny; *Casopis pro Mineralogii a Geologii,* **33** (1988) 419.

[13]   E. Manasse; *Rend. accad. Lincei,* **19** (1911) 138.

[14]   H. Winchell and R. J. Benoit; *Taylorite, , Am. Mineralogist,* **36** (1951) 590.

[15]   R. I. Bickley, H. G. M. Edwards, and S. J. Rose, *J. of Mol. Struc.,* **243** (1991) 341.

[16]   H. Chang, and P. J. Huang; *Analytical Chem.,* **69** (1997) 1485.

[17]   D. Duval, and R. A. Condrate, Sr.; *Appl. Spectroscopy*.**,** **42** (1988) 701.

[18]   H. G. M. Edwards, D. W. Farwell, R. Jenkins and M. R. D. Seaward; *J. of Raman Spectr.,* **23** (1992) 185.

[19]   I. I. Kondilenko, P. A. Korotkov, N. G. Golubeva, V. A. Klimenko and A. I. Pisanskii; *Optika i Spektroskopiya,* **45** (1978) 819.

[20]   O. I. Kondratov, E. A. Nikonenko, I. I. Olikov and L. N. Margolin; *Zhurnal Neorganicheskoi Khimii,* **30** (1985) 2579.

[21]   T. A. Shippey; *J. of Mol. Structure,* **63** (1980) 157.

[22]   H. L. Bhat; *Bull. Mater. Sc*i., **17** (1994) 1233.

[23]   S. Dhanuskodi and K. Vasantha; *Cryst. Res. Technol.* **39(3)** (2004) 259.

[24]   Sipos, Gabriella, *Ph. D. Thesis,* School of Applied Chemistry, Curtin University of Technology, (2003).

[25]   R. L. Frost and M. L. Weier; *Thermal Analysis and Calorimetry,* **75(1)** (2004) 277.

[26]   E. K. Girija, S. ChriticLatha, S. N. Kalkura, C. Subramanian and P. Ramasamy; *Mater Chem. and Phys.* **52** (1998) 253.

[27]   V. S. Joshi, *Ph .D. Thesis,* Saurashtra University, Rajkot (2001).

[28]   P. N. Kotru, K. K. Raina and M. L. Koul; *Indian J. Pure and Appl. Phys*., **25** (1987) 220.

[29]   A. W. Coats and J. P. Redfern; *Nature*, **201** (1964) 68.

[30]   R. L. Frost, J. Yang, and Z. Ding; *Chinese Sci. Bull.,* **48(17)** (2003) 1844.

[31]   R. G. G. Russell; *Arthritis and Rheumatism*, **19** (1976) 465.

[32]   D. S. Howell; *'Diseases Due to The Deposition of Calcium Pyrophosphate and Hydroxyapatite' Textbook of Rheumatology;* In W.N. Kelley, E.D. Harris, S. Ruddy, and C.B. Sledge, Eds., (2nd edition) W.B. Saunders, Philadelphia., (1985) 1398.

[33] A. Mijovilovich, C. Saragovi, S.G. Acebal, E.H.Rueda and M.E. Aguirre; *Hyperfine Interactions,* **C3** (1998) 336.

[34] M. S. Joshi and K. Baby Paul; *J. Cryst. Growth,* **22** (1974) 321.

[35] G. M. Loiacono, J. J. Zola and Kostecky; *J. Cryst. Growth,* **62** (1983) 545.

[36] S. K. Arora and B. Amin; *Prajna,* **13** (2005) 169.

[37] V. K. Dixit, B. V. Rodrigues and H. L. Bhat; *Bull. Mater. Sci.,* **24** (2001) 455.

[38] W. L. Wilox, *J. Cryst. Growth,* **65** (1983) 133.

[39] V. S. Joshi and M. J. Joshi; *Cryst. Res. Technol.* **38 (9)** (2003) 817.

[40] M. Ashok, N. Meenakshi Sundaram and S. Narayana Kalkura, *Mater. Lett.,* **57** (2003) 2066.

[41] A. Datta, M. Agarwal and S. Dasgupta; *Proc. Indian Acad. Sci.* (*Chem. Sci.*), **114 (4)** (2002) 379.

[42] B. A. Derfus, S. M. Kurtin, N. P. Camacho, I. Kurup, and L. M. Ryan; *Connect Tissue Res.,* **35(1-4)** (1996) 337.

[43] D. de Waal and C. Hutter; *Microchimica Acta,* **14** 243-244 (1997).

[44] G. S. Gopalakrishna, B. H. Doreswamy, M. J. Mahesh, M. Mahendra, M. A. Sridhar, J. Shashidhara Prasad and K. G. Ashamanjari; *Bull. Mater. Sci.*, **28(1)** (2005) 1.

[45] R. M. Dabhi, B. B. Parekh and M. J. Joshi; *Indian J. Phys.* **79(5)** (2005) 503.

[46] S. K. Arora, V. Patel, B. Amin and A. Kothari; *Bull. Mater. Sci.* **27** (2004) 141.

[47] G. M. Coppola and H. F. Schuster; *'In Asymmetric Synthesis: Construction of Chiral Molecules Using Amino Acids',* Wiley; New York, (1987).

[48] R. S. Coleman and W. Chem; *Org. Lett.,* **3** (2001) 1141.

[49]   M. K. Lakshman, J. C. Keeler, J. H. Hilmer and J. Q. Marten; *J. An. Chem. Soc.,* **121** (1999) 6090.

[50]   O. J. Plante, S. L. Buchwald and P. H. Seeberger, *J. An. Chem. Soc.,* **1222** (2000) 7148.

[51]   R. Malaviya, C. L. Chen, C. Navara, R. Malaviya, X. P. Hu, M. Keena,, B. Waurzyniak and M. Faith; *The J. of Pharmacol. & Expt. Therapeutics,* **295(3)** (2000) 912.

[52]   G. M. Sheldrick, SHELX97, '*Program for Crystal Structure Determination',* University of Gottingen, Germany, (1997)a.

[53]   G. M. Sheldrick, SHELX97, '*Program for Refinement of Crystal Structure',* University of Gottingen, Germany, (1997)b.

[54]   M. J. Nardelli; *Appl. Cryst.*, **28** (1995) 659.

[55]   L. J. Farrugia, Molecular Graphics-ORTEP-3 for windows, *J. Appl. Cryst.* **30** (1997) 565.

[56]   J. Jean-Claude Bertrand, F. B. James and J. George; *Acta Cryst.,* **C49,** (1993) 1070.

[57]   Q. Yang, Y. Tang, W. Yang and H. Chen; A*cta Cryst.,* **C54** (1998) 1532.

[58]   K. Chinnakali, Hoong-Kun Fun, K. Sriraghavan and Vaylakkavoor and T. Ramkrishnan; *Acta Cryst.,* **C54** (1998) 955.

[59]   C. C. Ersanli C. Albayrak, M. Odabasoglu and A. Erdonmez; *Acta Cryst.,* **C59** (2003) 6012.

[60]   G. J. Desiraju and T. Steiner; '*The Weak Hydrogen Bond',* IUCr, New York (1999).

[61]   K. D. Patel and A. T. Oza; *Bull. Mater. Sci.,* **19** (1996) 731.

[62] F. P. Xavier, A. R. Inigo and G. J. Goldsmith; *J. Prophyrins Phthalocyanines,* **3** (1999) 679.

[63] V. N. Joshi, '*Photoconductivity',* Marcel Dekker, New York, 1990.

[64] A. Joseph Arul Pragasam, *Ph. D. Thesis,* University of Madras, Chennai, India (2004).

[65] P. A. Franken, A. E. Hill, C. W. Peters, and G. Weinreich; *Phys. Rev. Lett.,* **17** (1961) 118.

[66] http://physik.uni-graz.at/~sas/NLO/node1.html

[67] E. Garmire, *Physics Today,* (1994) 23.

[68] D. S. Chelma and J. Zyss; *"Non-linear Optical Properties of Organic Molecules and Crystals',* **Vol. 1-2.** Academic Press, Orlando.

[69] S. Chenthamarai, D. Jayaraman, P. M. Ushasree, K. Meera, C. Subramanian and P. Ramasamy; *Mat. Chem. Phys.*, **64** (2000) 179.

[70] M. S. Wong, C. Bosshard, F. Pan and P. Gunter; *Adv. Mater.*, **8**, (1996) 677.

[71] V. G. Dmitriev, G. G.Gurzadyan and D. N. Nicogosyan; '*Handbook of Nonlinear Optical Crystals',* Springer- Verlag, New York, (1999).

[72] M. N. Bhat, and S. M. Dharmaprakash; *J. Cryst. Growth,* **236** (2002) 376.

[73] N. Vijayan,, R. Ramesh Babu, M. Gunasekaran, K. Gopalkrishnan, R. Kumaresan, P. Ramasamy and C. W. Lan; *J. Cryst. Growth,* **249** (2003) 315.

[74] H. S. Nagaraja, V. Upadhyaya, P. Mohan Rao, A. P. Sreeramana and A. P. Bhat; *J. Cryst. Growth,* **193** (1998) 674.

[75] M. Narayan Bhat and S. M. Dharmaprakash; *J. Cryst. Growth,* **243** (2002) 526.

[76] S. Dhanuskodi and K. Vasantha; *Cryst. Res. Technol.*, **39 (3)** (2004) 259.

[77] S. Dhanuskodi and S. Manikandan; *Cryst. Res. Technol.*, **39 (7)** (2004) 586.

[78]   F. Zernike, and J. E. Midwinter; *'Applied Nonlinear Optics,'* John Wiley and Sons, New York (1973).

[79]   P. D. Maker, R. W. Terhune, M. Nynenoff and C.M. Savage; *Phys. Rev. Lett.,* **8** (1962) 21.

[80]   R. C. Miller G. D. Boyd and A. Savage; *Appl. Phys. Lett.* **6** (1965) 77.

[81]   S. A. Rajasekar, K. Thamizharasan, A. Joseph, Arul Pragasam, J. Packiam Julius and P. Sagayaraj; *J. Cryst. Growth,* **247** (2003) 199.

[82]   Y. J. Ding and X. D. Mu, and X. Gu; *J. Nonlinear Opt. Phys.& Mater.,* **9** (2000) 21   .

[83]   X. W. Wang, D. Xu, M. K. Lu, D. R. Yuan, and S. X. Xu, *Mater. Res. Bull.,* **36** (2001) 879.

[84]   M. D. Aggarwal, J. Choi, W. S. Wang, K. Bhat, R. B. Lal, A. D. Shields, B. G. Penn,   and D. O. Frazier; *J. Cryst.Growth,* **204** (1999) 179.

[85]   D. Eimerl, S. Velsko, L. Davis, F. Wang, G. Loiacono and G. Kennedy; *IEEE J. Quan. Electron.* **25** (1989) 179.

[86]   K. V. Rajendran, D. Jayaraman, R. Jayavel, and P. Ramasamy; *9th National Seminar on Crystal Growth',* Chennai, (2003).

Chapter X

General Conclusions

Ruby, amethyst, emerald diamond,

 Sapphire, sarddonyx, fire, ide, carbuncle,

Jancinth, jasper, crystal-a-shine,

 Topaz, turquoise, tourmaline, opal,

Beryl, onyx and aquamarine,

 Marvel oh mortal- their hue, luster, loveliness,

Pure as a flower when its petals unfurl,

 Peach re carnelian, apple green chrysoprase,

Amber and Coral and pearl!!

         - Walter De La Mare

In this poem archeologist and poet Walter De La Mare (1873-1966) describes numerous sparkling natural crystals with wonderful facets, brilliant colors and perfect transparencies; which have remained the cynosure of aristocrats and nouveaux riches of various civilizations since many ages. The crust of the *mother Earth* remained the main source of crystals until different crystal growth techniques were developed to grow crystals in the laboratory. To understand the nature and properties of different natural crystals, geology has gained importance and, of course, with a multidisciplinary approach [1].

The discipline of bio-mineralogy arose from the realization that inorganic compounds in the human body are also well known natural minerals in the earth [2].

Some twenty seven minerals in the human body are identified and analyzed. There are several examples of bio-mineralization processes. Magnetite is important mineral of iron oxide having magnetic properties. Studying the brain tissues of the dead people suffering from Alzeimer's disease by employing the SQUID megnatometry, the detection of high amount of magnetite in brain can be linked to early diagnosis of the disease [3]. Calcite crystal is also very useful mineral of calcium carbonate with important optical properties. A transformation of amorphous calcium carbonate into calcite during sea urchin larval spicule growth has been reported by Beniash et al [4].

The solid solutions in hydroxyapatite, the principal calcium phosphate mineral that constitutes bones, are pertinent to the strength and flexibility of limbs. The substitution of F^- for OH^- in the mineral greatly increases the strength of bones; hence the fluoroapatite is a critical member of the solid solution. The most common is the efficacy of fluoride bearing toothpaste that is clearly related to the apatite crystal chemistry. Abnormality in bone formation leads to *Paget's disease* (high rate of formation) or *rickets* (low rate of formation). The nucleation of hydroxyapatite in the organic matrix of collagen is a challenge for both mineralogists and organic chemists. Particularly, a fascinating set of bones in the ear, called *otoliths* or *ear stones*, are attached to the hair- like nerve fibers that respond to the action of gravity. The clusters of ear stones in four cavities help the human maintain the equilibrium. [1].

In the present thesis, out of the well known minerals in the human body three minerals; hydroxyapatite, calcium pyrophosphate and brushite are studied. Hydroxyapatite and calcium pyrophosphate are also responsible for the arthritis in the human body. Monosodium urate monohydrate is responsible for the gouty arthritis, which is also studied in the present research work. There are certain oxalate salts

found in a body, which either directly or indirectly play important role. Sodium oxalate is studied and characterized by the present author. Similarly, sodium pyrophosphate, a water soluble salt, is also important in many respects. This has also been grown and characterized. Organic molecular solids encompass wide varieties of materials having diverse applications ranging from pharmaceuticals, confectionaries, explosives, bio-materials to recently developed NLO materials. The organic molecular crystals of HPAP are synthesized, grown and characterized to identify their novel applications.

The general conclusions can be broadly drawn as follows:

(1)   Hydroxyapatite (HA) crystals were grown by the gel growth technique. The crystals were formed in the Liesegang ring formation having monoclinic crystal symmetry and the unit cell parameters were determined. Generally, HA has hexagonal crystal structure and in the rare cases it is formed in the monoclinic form, which may be due to low temperatures of the crystal formation. Usually, the HA crystals are grown by the hydrothermal method or the sol-gel method at higher temperatures. The grown crystals, in the present study, were characterized by different techniques. The FT-IR study confirmed that the HA crystals were not having any CO_2 inclusion. The dielectric study indicated that the value of dielectric constant decreased as the frequency increased. This suggested higher space charge polarizability in the low frequency region and a relaxation behavior.

       The growth inhibition study of HA crystals in the presence of different herbal extracts revealed that *R. acquatica* and *B. diffusa* were giving promising results in terms of comparatively lesser periodic precipitation and lesser diffusion length, respectively. However, *B. serrata* and

C. wightti did not show significant inhibition. Hydro-ethnolic and ethanolic extracts did not give good inhibition in comparison to the aqueous extracts. The particle size was found to be largest in the hydro-ethnolic extracts followed by the ethanolic and at last the aqueous ones. The diffusion coefficients were calculated and it was confirmed that *R. acquitica* exhibited minimum value of diffusion coefficient. *R. acquitica* was found to be much promising herbal extract for inhibition of HA.

(2) It is difficult to grow monosodium urate monohydrate (MSUM) crystals due to very low solubility of uric acid in any known solvent. Very thin, transparent, needle type crystals of MSUM were grown by the gel technique as well as by the wet chemical technique. The crystals were characterized by different techniques. Thermogravimetry suggested that crystals were thermally unstable and the dehydration began at 130 ^{0}C by liberation of water molecules. The kinetic and thermodynamic parameters for dehydration were evaluated. The positive value of standard change in Gibbs free energy and standard change in entropy suggested spontaneous type reaction. The positive value of standard change in enthalpy suggested the endothermic process. The FT-IR study suggested the presence of O-H, N-H, C=C, C=O, and C-N bonds. The cell parameter data of MSUM are yet not available in the literature. The powder XRD (X-ray diffraction) study confirmed the crystalline nature of the grown samples. The dielectric study suggested that as applied frequency increas the value of dielectric constant decreased suggesting higher space charge polarizability in the low frequency region and a relaxation behavior. The a.c. conductivity and a.c. resistivity behaviors were also studied. The growth inhibition study of MSUM in the presence of different herbal extracts revealed

that *R. acquitica* and *A. lanata* extracts gave good inhibition results, whereas, *B. serrata, B. diffusa* exhibited comparatively less inhibition.

(3)   Calcium pyrophosphate tetrahydrate (CPPT) crystals were grown by the single diffusion gel growth technique. Good quality, transparent, spherical granules type crystals were harvested. The thermal stability of the crystals was estimated by thermogravimetric analysis, which suggested that the crystals became anhydrous at 110 ^{0}C temperature. The kinetic and thermodynamic parameters of dehydration were evaluated. The value of standard change in Gibbs free energy is negative suggesting spontaneous process. The negative value of standard enthalpy and positive value of standard entropy suggested the spontaneous type of nature under all conditions. The FT-IR study indicated the presence of P-O and O-H types of bonds along with the metal-oxygen bond. The powder XRD data suggested the monoclinic crystal structure, which was matching with the reported values. The dielectric study suggested a relaxation behavior and higher space charge polarizability in the low frequency region. The growth inhibition study of CPPT, in the presence of different herbal extracts, suggested good inhibition in *R. acquatica,, B. diffusa* and *C. wightti*. However, *C. wightti* gave best results among all.

(4)   Brushite or calcium hydrogen phosphate dihydrate (CHPD) crystals were grown by the conventional single diffusion gel growth technique for macro-size crystals as well as the modified gel growth technique for micro crystals. Tartaric acid and citric acid are found in many fruits and natural products. There are theories on citrate inhibition of urinary calculi. Effect of citric acid and tartaric acid on already grown crystals was verified in their natural

growth environment in the gel medium. It was observed that as the concentration of tartaric acid as well as citric acid increased the inhibition increased and, finally, the dissolution of crystals took place.

A modified gel growth technique was developed to grow the micro size CHPD crystals and observe their formation *in situ*. This technique gave the crystals very rapidly and the growth inhibition study was performed within a short time of a few hours rather than a few days in the conventional technique.

(5) In general, it was observed that *R. acquatica* gave good inhibition in all the three types of crystals growth, viz, HA, MSUM and CPPT.

(6) This *in vitro* studies may be helpful to *in vivo* studies and, subsequently, for animal models and, ultimately, to develop preclinical formulations.

(7) Oxalate salts are observed commonly in living organisms. Sodium oxalate crystals were grown by the gel growth technique. Good quality, colorless, transparent, prismatic, single crystals were harvested. The thermal stability was evaluated by thermogravimetry analysis, which suggested that the crystals became anhydrous at 129. 3 ^{0}C, by giving up the water of hydration. The kinetic and thermodynamic parameters were estimated for the dehydration process. The positive values of standard change in entropy, enthalpy and Gibbs free energy suggested spontaneous type of reaction. The presence of metal-oxygen bond, C=O, C-C and O-H bonds were confirmed through the FT-IR spectroscopic study. The dielectric study suggested very poor response to the frequency changes; however, at lower frequency region it showed comparatively higher dielectric constant values.

(8)   Sodium pyrophosphate crystals were grown by the indigenously developed solution growth set-up using slow evaporation technique. The maximum dimension of the grown crystal was 0.75 cm X 0.75 cm. The FT-IR spectroscopy suggested the presence of O-P, O-H and metal-oxygen bonds. The dielectric constant decreased with the increase in value of frequency suggesting higher space charge polarizability in the low frequency region and a relaxation behavior.

(9)   Organic molecular crystal of 4-(2-hydroxy-phenylamino)-pent-3-en-2-one (HPAP) was grown by using slow evaporation technique. Good quality, transparent, yellowish brown color crystals of the maximum dimension of 1.5 cm X 0.75 cm were grown. From the single crystal XRD the lattice parameters, molecular packing in the unit cell, bond lengths and ORTEP diagram of the HPAP molecule were obtained. The HPAP crystals exhibited thermal stability up to $100\ ^{0}C$ and then decomposed. The FT-IR spectrum confirmed the presences of C=O, C=C, C-N, N-H and O-H bonds. The dielectric study suggested that crystals were giving poor response to the changes in the frequency. The photoconductivity study indicated a positive photoconductivity. The NLO properties were verified and it was found that the crystals were poor NLO material with comparison to potassium dihydrogen phosphate (KDP).

Scope for the Future Work:

Attempts are required to be made to grow nano-crystalline forms of all the three compounds and study their properties as well as how they react with different chemicals and extracts in the nano form. Also, it is important to develop a bio-ceramic form of monoclinic hydroxyapatite crystals, which can be tested for bone substitution. Also, it is required to verify the bio-compatibility of the monoclinic hydroxyapatite crystals.

To explore the micro crystal growth technique to all other crystals and apply it to the growth inhibition study.

To develop semiorganic NLO material from HPAP crystal, which can be envisaged, for better performance, either from doping or reaction with proper substitute.

References:

[1]   H. T. Yoder Jr; *Proc. Am. Philos. Soc.,***146** (2002) 37.

[2]   H. C. W. Skinner, *Minerals and Human Health* in *Environmental Mineralogy,* Eds D.J. Vaughan and R.A. Wogelius, Vol.2, Chap.11, p-383.

[3]   S. Bhattacharya, *New Scientist*, April 2003.

[4]   E. Beniash, J. Aizenberg, L. Addadi, S. Weiner, *Proc. Royal. Soc. London,* **B264** (1997) 461.